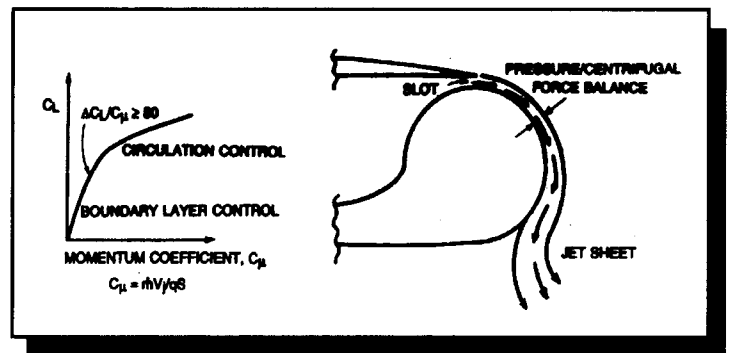Final Report –Summary of Research

GTRI Report A5928/2003-1

# Application of Circulation Control Technology to Airframe Noise Reduction



**K. K. Ahuja, L. N. Sankar, R. J. Englar, Scott E. Munro, Yi. Li, and R. J. Gaeta**

Georgia Institute of Technology, GTRI/ATASL

Aerospace and Acoustics Technologies Branch

Atlanta, Georgia 30332-0844

31 May 2003

# FOREWORD

This final summary progress report was prepared by Georgia Institute of Technology, Atlanta, Georgia, for NASA Langley Research Center, under Grant NAG-1-2146. The report provides a summary of the work done during the period March 1999 - March 2003. The work described here was funded under NASA Langley Research Center's Breakthrough Innovative Technologies element of the Airframe Systems Base Research and Technology program to study the feasibility of applying Circulation Control Technology to Airframe Noise Reduction.

For NASA Langley, Dr. Richard R. Antcliff was the program manger during the first year. Thereafter, Dr. Robert E. McKinley of NASA Langley Research Center was the NASA program manager.

Dr. Krish Ahuja, Dr. L. Sankar, and Mr. Robert E. Englar of Georgia Tech were the COPIs.

Two Doctoral dissertations were produced under this effort. Dr. Scott Munro carried out much of the experimental effort for steady blowing. Dr. Yi Li carried out all of the computational effort. GTRI Research Engineer Dr. Richard Gaeta was responsible for conducting all experiments using pulsed blowing. He also carried out flap-egde blowing experiments near the end of the program.

The assistance of the following individuals is gratefully acknowledged: Steve Williams, who skillfully built many of the test models; Warren Lee who carried out trailing edge blowing experiments; undergraduate students Barry Hellman, Robert Combier, Brian Cook and Ben Murdock and other undergraduate students who assisted in the experiments.

Georgia Tech's the program manger for this effort was Dr. Ahuja. Any questions concerning this report should be addressed to Dr. Krish K. Ahuja (tel: 770-528-7054, email: krishan.ahuja@gtri.gatech.edu).

# NOMENCLATURE

AR     Aspect Ratio

a     Speed of sound

c, C     Chord

$c_l$     Airfoil lift coefficient

CCW     Circulation control wing

$C\mu$     $\dfrac{\dot{m}V_j}{qS}$

$C_{\mu 0}$     Average Momentum Coefficient for pulsed jet

D     Drag of the Wing

f     Pulsed jet Frequency when used with pulsed jet, equal to acoustic frequency when used with noise spectra

h     Slot height

I     Sound Intensity

L     Lift of the Wing

$L_{eq}$     Characteristic length for the HARN, $L_{eq} = h^{3/4}w^{1/4}$

$M_c$     Convection Mach number

$M_l$     Jet centerline Mach number

OASPL – Overall Sound Pressure Level

PIV     Particle image velocimetry

$P_{ref}$     Reference acoustic pressure, 20 $\Box$Pa

q     Dynamic pressure

R     Radial distance from jet exit to measurement location

$R_x$     Space-correlation

$R_{x\tau}$     Cross-correlation

r     Radius of CCW surface

Re     Reynolds number

SPL     Sound Pressure Level

T     Temperature

V     Velocity

w     Width of rectangular nozzle (large dimension)

$\alpha$     Angle of attack

$\Theta$     Polar angle (with respect to the flow axis)

<u>Subscripts</u>

s     Associated with slot

T     Associated with tunnel freestream

j     Associated with jet

o     Ambient condition

$\ell$     Associated with local measurements

# EXECUTIVE SUMMARY

This report is a summary of the work performed by Georgia Tech Research Institute (GTRI) under NASA Langley Grant NAG-1-2146, which was awarded as a part of NASA's Breakthrough Innovative Technologies (BIT) initiative. This was a three-year program, with a one-year no-cost extension. Each year's study has been an integrated effort consisting of computational fluid dynamics, experimental aerodynamics, and detailed noise and flow measurements.

Year 1 effort examined the feasibility of reducing airframe noise by replacing the conventional wing systems with a Circulation Control Wing (CCW), where steady blowing was used through the trailing edge of the wing over a Coanda surface. It was shown that the wing lift increases with CCW blowing and indeed for the same lift, a CCW wing was shown to produce less noise.

Year 2 effort dealt with a similar study on the role of pulsed blowing on airframe noise. The main objective of this portion of the study was to assess whether pulse blowing from the trailing edge of a CCW resulted in more, less, or the same amount of radiated noise to the farfield. *Results show that a reduction in farfield noise of up to 5 dB is measured when pulse flow is compared with steady flow for an equivalent lift configuration.* This reduction is in the spectral region associated with the trailing edge jet noise. This result is due to the unique advantage that pulsed flow has over steady flow. For a range of frequencies, more lift is experienced with the same mass flow as the steady case. Thus, for an equivalent lift and slot height, the pulsed system can operate at lower jet velocities, and hence lower jet noise. The computational analysis showed that for a given time-averaged mass flow rate, pulsed jets give a higher value of $C_l$, and a higher L/D than equivalent steady jets. This benefit is attributable to higher instantaneous jet velocities, and higher instantaneous $C_\mu$ values for the pulsed jet. Pulsed jet benefits increase at higher frequencies. However, these advantages are somewhat offset by the unsteadiness in the loads, which will cause structural vibrations and fatigue. Additional studies must be done, perhaps with multiple jets on the upper and lower surfaces, to smooth out the fluctuations in lift while retaining the benefits.

The rest of the effort was devoted to examining ways of reducing flap edge noise by blowing air through a Coanda nozzle over a rounded tip of the flap. In this case, we were successful in moving the tip vortex away from the tip, but the device producing the blowing was noisy and we were unable to examine the noise benefits, although we believe that the movement of the tip vortex far from the tip should provide noise benefits.

It should be noted that in an effort to understand the fluid dynamics and the aeroacoustics of a jet blowing over a Coanda surface, we also carried out a very extensive study of the high aspect ratio slot jets. A first-ever set of far-field noise spectra were measured for jets exhausting from slots with aspect ratios in the range 100 to 3000. Parallel measurements of velocity profiles, length scales and convection velocities were measured to understand the noise generation of high aspect ratio jets. Attempts were also made to develop jet noise prediction schemes for such jets.

Much of the work done under this effort has been described in five conference papers and two doctoral theses. The first year's work on the use of steady blowing was described in two AIAA papers presented at the 2001 AIAA Aerospace Sciences Meeting in Reno. Subsequent work was presented at the 9th AIAA/CEAS Aeroacoustics Conference and Exhibit held at Hilton Head May 12-13. Another paper is to be presented at the 2004 AIAA Aerospace Sciences Meeting in Reno in January 2004. All six papers are included with this report as Appendices. The bulk of the experimental work done in an effort to produce a pulsed flow that is free of upstream noise is also attached as an Appendix.
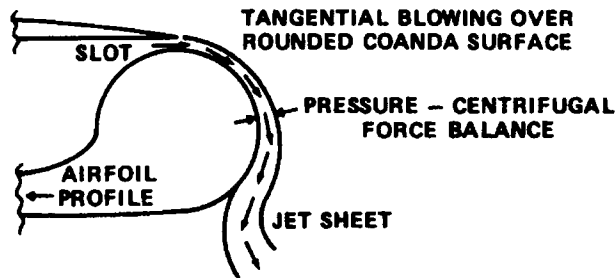
# TABLE OF CONTENTS

# 1.0 INTRODUCTION

## 1.1 Background

Circulation Control (CC) is a recently maturing pneumatic aerodynamic technology that offers significant improvements over the well-known jet flap and blown-flap concepts of blown lift augmentation. The jet sheets or the tangentially-blown flaps of these two concepts are replaced by the non-moving round or near-round CC trailing edge slot or slots, Figure 1. The blown sheet remains attached to the CC curved trailing edge by a balance between the negative pressure differential across the jet and the centrifugal force acting on the curving jet. The resulting flow entrained into the curving jet sheet initially acts as a boundary-layer control (BLC) at very low momentum (blowing) coefficients

**Figure 1. Circulation Control.**

to prevent separation. At slightly higher blowing, the jet adheres to the round trailing edge, moving the airfoil's stagnation point and streamline well onto the lower surface and acting as a pneumatic circulation control. This greatly augments the airfoil lift well beyond that of mechanical conventional high-lift flap systems, and into the region of Supercirculation (i.e., well beyond BLC). Because this dramatically changes the airfoil static pressure distribution, the concepts can also be used to modify the aerodynamic moments as desired, as well as increase/decrease the drag and the downstream wake.

Although the noise benefits of Circulation Control have never been shown by anyone through experimentation, it has high potential for reduction of airframe noise and was the subject of this study. This study was motivated by the expectation that pneumatic circulation control wing (CCW) like devices for high lift operation will reduce noise by significantly reducing the impact of flow separation, high angle of attack operation, large complex components exposed in the freestream such as jet/flap interactions, trailing edge and flap edge vortices, large wakes behind the airfoil, etc., associated with conventional high lift devices of today. Also, short ground roll distances plus steep approach and climbout offered by this technology can dramatically reduce the ground noise footprint. In addition, this method offers considerable weight reduction. This will reduce the fuel requirements per flight, thus reducing the emission impact.

One could question: What about the noise produced by the blowing jets used for CCW? Fortunately, the width of the jet slot used for Circulation Control even in a full-scale system is expected to be of the order of a fraction of an inch. This will produce dominant noise in the high and ultrasonic frequency region and will have little noise impact on community noise. Also, short distances plus steep approach and climbout offered by this technology can dramatically reduce the ground noise footprint. In addition, this method offers considerable weight reduction. This will reduce the fuel requirements per flight, thus reducing the emission impact.

## 1.2 Study Objective

The objective of this program was to utilize pneumatic or Circulation Control technology for reducing airframe noise. This investigation was accomplished through a highly integrated effort consisting of (a) detailed aerodynamic measurements of lift and drag in a wind tunnel equipped

with a 6-component balance, (b) acoustic measurements in an anechoic flight simulation facility, (c) CFD analysis of selected configurations.

A three-year program was originally proposed. Due to facility issues a one-year no-cost extension was exercised.

During the first year, a test configuration that had produced significant lift improvement and had displayed a drag-control capability in our previous work was selected for noise testing in Georgia Tech's Anechoic Flight Simulation Facility. For the sake of comparison, another test configuration consisting of an airfoil and a conventional flap was also tested. A parallel task on CFD of pneumatic flow control was also carried out. Based upon the results of the CFD analysis and the initial acoustic tests, an optimized pneumatic configuration was tested for its noise reduction capabilities.

The second year's effort concentrated on a similar investigation of pulsed blowing to control airframe noise. The third and the fourth year were spent in investigating tangential blowing as well as flap-edge blowing to control trailing edge and flap edge noise.

Two doctoral students, Mr. Scott Munro and Mr. Li, worked on this program and received their Doctorates. Mr. Munro's dissertation[1] concentrated on the experimental portion of the effort and his academic advisor was Dr. Krish Ahuja. Mr. Li's dissertation[2] concentrated on the computational effort and his academic advisor was Dr. L. Sankar. Both students had Mr. Robert J. Englar available for additional advice and consultation on various aspects of the circulation control technology because of Mr. Englar's experience in this area for over 25 years. Dr. Richard Gaeta, who has extensive experience with engine cycles through his work at GE, also made himself available for technical consulting.

Finally, a total of six technical papers documenting the results of this effort were prepared. Two papers[3,4] were presented in 2001 at the AIAA Reno Meeting and three papers[5,6,7] were presented at the 2003 AIAA/CEAS Aeroacoustics meeting at Hilton Head. Abstract for another paper has been sent for a presentation at the 2004 Reno meeting. All papers are being modified for submission to a journal.

---

[1] Munro, S., *Jet Noise of High Aspect-Ratio Rectangular Nozzles with Application to Pneumatic High-Lift Devices*, Ph.D Thesis, Georgia Institute of Technology, 2002.

[2] Liu, Yi., *Numerical Simulation of the Aerodynamic Characteristics of Circulation Control Wing Sections*, Ph.D Thesis, Georgia Institute of Technology, 2003.

[3] Munro, S., Ahuja, K., and Englar, R., "Noise Reduction Through Circulation Control Technology," AIAA Paper 2001-0666, Jan. 2001.

[4] Liu, Y., Sankar, L. N., Englar, R. J. and Ahuja, K. K., "Numerical Simulations of the Steady and Unsteady Aerodynamic Characteristics of a Circulation Control Wing Airfoil," AIAA paper 2001-0704, January 2001.

[5] Munro, S. and Ahuja, K. K., "Aeroacoustics of a High Aspect-Ratio Jet," AIAA paper 2003-3323, 2003, presented at the 9th AIAA/CEAS Aeroacoustics Conference and Exhibit, Hilton Head, South Carolina, 12-14 May 2003.

[6] Munro, S. and Ahuja, K. K., "Fluid Dynamics of a High Aspect-Ratio Jet," AIAA paper 2003-3129, 2003, presented at the 9th AIAA/CEAS Aeroacoustics Conference and Exhibit, Hilton Head, South Carolina, 12-14 May 2003.

[7] Munro, S. and Ahuja, K. K., "Development of a Prediction Scheme for Noise of High-Aspect Ratio Jets," AIAA paper 2003-3255, 2003, presented at the 9th AIAA/CEAS Aeroacoustics Conference and Exhibit, Hilton Head, South Carolina, 12-14 May 2003.

## 1.3    Report Outline

The study described here is a very fundamental study of the fluid dynamics and aeroacoustics of Circulation Control jets. The program has been very intense and many original results have been generated. A complete presentation of the work would be very lengthy and difficult to follow. Therefore, the most significant results, which have already been distilled into technical papers, are presented in an extended Appendix to this report. A summary of the key achievements is provided in the next section.

Likewise, should the reader desire to obtain further details, they should refer to the two doctoral dissertations alluded to above.

## 2.0 KEY ACCOMPLISHMENTS TO DATE

Significant accomplishments have been made during the first year. This section includes a summarized set of highlights, some in the form of PowerPoint images.

### 2.1 Aeroacoustics of the CCW Configuration with Steady Blowing

Figure 2 provides an executive summary of the program with bullets for the historical perspective of why circulation control technology type configuration needs to be investigated for reduced airframe noise along with the planned approach, accomplishments and future plans. It also shows schematics of the type of wing used in the present study.

Figure 3 provides a list of disadvantages of multi-flap conventional wing and the advantages of a pneumatic circulation control wing (CCW). This figure also shows a photograph of an actual full-scale Navy aircraft A-6 Intruder where the circulation control technology was demonstrated to be a viable concept.

Figure 4 further elaborates the points made in Figure 3 and includes acoustic data obtained from the present investigation for steady blowing. Clearly, the spectra shown here point out that for the same lift, reduced noise levels can be obtained for a system equipped with circulation control.

Finally, Figure 5 provides photographic views of the reference conventional wing and the circulation control used in the present investigation. The conventional wing was operated with a gap in its flap, which is representative of cut outs provided in actual wings due to structural constraints or to prevent engine exhaust from impinging on an extended flap in the case of wing-mounted engines. Typical noise spectral comparison for the two wings mounted in GTRI's flight simulation facility is provided on the right hand side of this figure. Spectrum of the background noise obtained by operating the empty tunnel background is also shown. Data for a flight velocity of 220 ft/s at a microphone located in the flyover plane directly below the trailing edge at a distance of 11.5 ft from the slot center is shown here. The CCW flap angle was set to 30°. The slot velocity was adjusted to provide the same lift as produced by the conventional wing. The lift data was obtained in our earlier studies using the same two wings in another wind tunnel equipped with a six-component balance. Clearly, the CCW shows significant noise benefit in the main audio range of frequencies. Actually, even if the two spectra were identical, CCW configuration should be considered better because of its simple design and lightweight.

Appendix A contains details of the aeroacoustics of the CCW.

### 2.2 Computational Study of the CCW Configuration with Steady Blowing

Figure 6 shows a selected result of our computational study. The wing model used for the experiments was modeled for the CFD analysis. Velocity vectors with and without pneumatic blowing are shown in this figure with a superimposed forward velocity. It can be seen that without blowing, a well-defined vortex shedding is obtained downstream of the small flap used in the circulation control slot. This vortex shedding is absent with the blowing. This is reflected in our acoustic measurements as seen in the typical noise spectra shown on the right hand side of the same figure. Without blowing, a well-defined discrete tone associated with the vortex shedding is seen at a frequency of about 1600 Hz. This tone completely disappears on using the blowing through the circulation slot. This is a powerful result in that it indicates that not only can we potentially reduce broadband noise associated with airframe spectrum, but also the vortex

4

shedding noise produced by various bluff bodies in a stream can potentially be controlled using circulation control technology.

An unsteady three-dimensional compressible Navier-Stokes solver was developed. This solver is capable of handling isolated wing-alone configurations. Both finite wings and 2-D airfoils may be simulated with the same solver. The boundary conditions have been coded in a general form so that the researcher may specify the slot location, slot size, blowing velocity, and the direction of blowing. The effects of turbulence were modeled using either a Baldwin-Lomax eddy viscosity model, or using the Spalart-Allmaras one-equation model.

A 3-D grid generation code was also developed that can model wings of general plan form. Figure 7 shows the body-fitted grid at a typical control station.

The flow solver was validated by computing viscous subsonic flow over a small aspect-ratio wing made of NACA 0012 airfoil sections at an angle of attack of 8 degrees. The freestream Mach number was 0.12, while the Reynolds number based on wing chord was $1.5 \times 10^6$. Surface pressure data for this wing are available from experimental studies done by Bragg et all. Figure 8 shows typical surface pressure distributions at three span stations. A good agreement with measurements is observed.

Following the code validation, the 3-D Navier-Stokes solver was applied to the CCW wing configuration shown in Figure 7. Simulations were done both for a no-blowing case, and a case where blowing was applied near the trailing edge, on the upper surface. Figure 9 shows the velocity vectors indicative of the flow pattern in the trailing edge region. For the no-blowing case, a region of separation was present upstream of the flap, and downstream. The flow downstream of the flap exhibited a periodic vortex shedding. With blowing, this recirculation region and the unsteady vortex shedding were completely eliminated.

The primary benefit of the circulation control through blowing was in the lift coefficient. While the wing in the no-blowing case produced a lift coefficient of 1.22, the same wing, with a blowing coefficient $C\mu$ of 0.15, produced a lift coefficient of 2.6. Such as large lift coefficients can presently be realized on conventional wings only with the use of high lift systems such as flaps and slats.

The coordinates of an airfoil tested for the acoustic measurements are shown in Figure 10. The aft region of this airfoil may be rotated, simulating an integral flap as in Figure 7. A series of aerodynamic calculations were carried out for various flap settings, with and without blowing. The blowing slot locations, height, and the blowing coefficient were parametrically changed. The resulting flow characteristics were stored in the form of pressure fields, vorticity fields, and force coefficients for comparisons with the experimental studies, and for the evaluation of the noise characteristics of the wing.

It became quite clear that the circulation control has two primary benefits: very large lift coefficients without the use of high lift devices, (b) elimination of separation in the aft regions of the wing. Both these benefits may be expected to have attendant noise reduction benefits.

Additional details of the progress on the computational task appear in Appendix B.

## 2.3 Need to Study a High Aspect Ratio Nozzle flow and Noise Defined

Considerable amount of acoustic data was acquired for the CCW configuration. After initial examination of this data, it became clear that identifying individual noise sources in the entire

5

CCW system as tested will be difficult without examining the noise field of an isolated thin slot of a span comparable to that used in the CCW itself. Much value will be added if individual noise components can be studied and used to determine how much each part affects the noise of the entire system. Possible individual contributors are the jet flow from the slot, the changed directivity due to curvature, or perhaps the jet impinging on freestream flow. Although much work has been done in the area of jets, no one has extensively looked at the properties of extremely high aspect-ratio jets, similar to the CCW slot. In the current study, aspect ratios range from 1,200 to 10,000. There has been acoustic work on rectangular jets, but the aspect ratios have rarely been greater than 10. Thus, to study the unique characteristics of a CCW slot-like high aspect-ratio jets, a high aspect ratio nozzle (HARN) was fabricated. The HARN was mounted in the Anechoic Chamber at GTRI where it was used to study the effect of aspect ratio on the farfield jet noise. Acoustic measurements were taken for several jet Mach numbers, slot heights, and aspect ratios with microphones located in the acoustic farfield at several angles relative to the jet flow.

Attachments to the HARN also allowed for investigation of jet turning on the directivity of the noise. A variety of curved surfaces were fabricated to simulate the CCW cylindrical surface that creates the jet turning. Acoustic measurements were taken in a similar fashion to the aspect ratio tests discussed above. This nozzle is shown schematically in Figure 11.

The HARN was fabricated at GTRI in order to perform jet noise studies on very high aspect ratio jet flows. The primary focus was to provide a similar jet flow model to the CCW wing, in scale and flow, separate from the other aerodynamic influences incurred in the CCW system. Because of the interest in maintaining similarity between the HARN and the CCW being tested, the HARN was designed to be 30" wide (see Figure 11). The HARN mounts to a round-to-rectangular transition duct section (2.75" square exit) that mounts directly to the 4" opening on the plenum of an available jet rig. It gradually contracts to the desired slot height in one dimension and expands to the 30" width in the other. Both of these dimensional changes occur over about 30 inches of axial length. The HARN was designed with exit plates that are adjustable. This allowed the slot to have potentially an infinite number of slot heights within the bounds of fully closed to 0.25". For the current study, most of the heights were kept similar to those in the CCW tests, ranging from 0.003" to 0.020".

The HARN was fabricated out of aluminum with an intended maximum pressure of about 25 psig, enough to produce a slot exit Mach number slightly over 1.2. The external surface of the HARN is sloped towards the exit, so that the entrained flow is more nozzle-like rather than a wall-jet. A curved attachment piece to provide a Canada surface was fabricated, again maintaining the shape and size of the CCW system being tested in the Flight Simulation facility of GTRI. It was attached to the HARN via a piece that allowed it to change angles similar to deflecting the flap on the CCW.

Results from both of these studies were compared to ascertain whether or not the noise from these unique aspects of the CCW technology could be predicted by existing jet mixing noise theory or by some correction to existing theory.

Note that noise spectra obtained with HARN configuration for most operating conditions was expected to be independent of any potential internal noise that might limit understanding of the data from the circulation control wing for some conditions. This is because the HARN was mounted on a jet noise facility that had been calibrated for its acoustic cleanliness and past data from which has been used extensively by the aeroacoustics community to validate jet noise theories. This data thus also helped us identify the bounds of the acoustic cleanliness of the

6

CCW test configuration and provided further confidence in that the CCW data was not contaminated by any upstream noise associated with slot air supply tubes. The results of HARN study are presented in Appendices C, D, and E. Appendix C describes the farfield characteristics of high aspect ration jets and compares them with those of a round jet. Appendix D describes the fluid dynamics of jets issuing from such jets. Finally, Appendix E provides a description of some schemes of predicting jet noise from high aspect ratio jets. A summary of the results of this extensive study of HARN is provided below:

## 2.4    Aeroacoustics of Jets Issuing from a High Aspect Ratio Nozzle  (HARN)

A large amount of acoustic data was collected for the HARN. This included a range of aspect ratios from 100 to 3000, well above the range of rectangular jet noise data found in the literature. The jet velocities tested ranged from 400 to 1100 ft/s and data were recorded at 9 different polar angles.

The HARN acoustic data were compared with trends expected from Lighthill's theoretical predictions and those that are commonly used to collapse and scale round jet noise data and low-aspect-ratio rectangular jet noise data. An initial comparison of sample HARN and round nozzle data showed some general similarities, but also some distinct differences. The general shape of the spectra at various polar angles seemed to be similar. The directivity of the HARN noise seems to have a peak at about $\Theta = 20°$, similar to what has been found for round jets. The HARN data also appeared to have a significant amount turbulent absorption and scattering of high frequency noise at low polar angles evidenced by lower SPL levels at high frequencies and higher SPLs at low frequencies for low polar angles.

From the HARN acoustic data, parameters for scaling acoustic data from a high aspect-ratio nozzle were found. The largest width data was found to vary with $h^2$ while the data for the two smaller nozzle widths were proportional to $h^{3/2}$. The width had only a moderate effect on the jet noise. Although no exact scaling relationship was extracted from the data, a best fit to the data was found to be $I \sim V_j^8 L_{eq}^2$, where $L_{eq} = h^{3/4} w^{1/4}$. The frequency was found to be weakly dependent on the nozzle height and width. Again, using a best-fit approach, and using the defined equivalent length as a normalizing parameter, the frequency was converted to Strouhal number by $f L_{eq}/V_j$. This definition came from the examination of the data and determining a best fit scaling law, while consistency with round jet noise theories and prediction schemes were used as a constraint, i.e., the sound intensity had to remain proportional to a characteristic length squared.

No direct relationship was found that provided reasonable scaling as a function of the polar angle. A first attempt to scale the data as a function of polar angle as it appears in the convective amplification term in Lighhill's formulation and subsequently modified by Ffowcs-Williams. This formulation did not work well at smaller polar angles. However, this result was similar to what other researchers have found when applying it to round jet noise data. It is believed that this is due to scattering and absorption of turbulence that must pass through the shear layer of the jet on its path to a microphone at a low polar angle.

Further description of this portion of the study is given in Appendix C.

## 2.5    Fluid Dynamic Behavior of Jets Issuing from a High Aspect Ratio Nozzle

In order to support the acoustic data, fluid dynamic measurements were made on the HARN. These included PIV measurements, single hot-wire measurements, and two-wire hot-wire measurements.

7

The PIV data did not provide a wealth of quantitative information, however much was gained by simply examining the flow visualization images. The jet emerged from the exit in what appeared to be a laminar-like condition. In most cases there was a visible instability that developed and eventually seemed to cause the jet to break down into a distinctively turbulent jet. The instability was still visible in some cases even in this highly turbulent region. The breakdown point seemed to be Reynolds number dependant as it appeared to vary with jet velocity, although this was difficult to confirm due to the extremely small size of the jet before the breakdown.

Single hot-wire measurements were made to characterize the general behavior of the high aspect-ratio jet. Velocity profiles and turbulence intensities appeared similar to those that would be expected for a jet of this type. The centerline velocity decay confirmed that the jet behaved similar to a 2-d turbulent jet over a large streamwise distance. The breakdown of the jet seen in the PIV was noted in the sudden change in the spreading rate of the jet. A marked change in the spread rate occurred at about the same x/h location where the bursting of the jet seemed to occur in the PIV images.

Global length-scales were found using the method first published by Davies, Fisher, and Barratt[8]. Convection velocity was also extracted from the data using a method described in the same paper. The global length-scales calculated tended to support the acoustic data acquired in the accompanying acoustic study in reference [1]. The length-scale seemed to scale with $h^{3/4}w^{1/4}$ for a constant frequency. Unfortunately only a few data points were calculated due to the immense amount of data required to find one length-scale point.

Another piece of valuable information that can be calculated from the cross-correlation measurements is the convection velocity of the turbulent eddies. This was calculated for each wire separation location. The convection velocity was found to vary with distance downstream from the nozzle exit. It was determined to be related to the centerline velocity. The convection velocity was approximately 0.6 of the local centerline velocity, not 0.6 of the jet exit velocity as is often assumed.

Convection velocity was also calculated as a function of frequency using the phase of the cross-power. It was found that the convection velocity varies with frequency, spanning a range from about 0.4 $V_l$ to 0.8 $V_l$ over a frequency range that is dependent on the streamwise location more than the nozzle height. (Here $V_l$ is the local velocity.) This is important since convection velocity is often assumed to be about 0.65 $V_j$. Thus, $V_c$ is most likely over estimated since downstream of the core $V_l < V_j$.

Another possible method of measuring the length-scale was also evaluated. Since the coherence was readily available it was used to find a coherence-length. Using this method, the length-scale is found as a function of frequency rather than a global value found using cross-correlation data. Coherence-length as a function of frequency was calculated for all the two-wire correlation data. The calculated coherence-lengths scaled with the $L_{eq}$ defined in the acoustic study at measurement locations far from the nozzle exit. Measurements near the nozzle exit did not appear to scale with $L_{eq}$.

Further description of this portion of the study is given in Appendix D.

---

[8] Davies, P.O.A.L, Fisher, M.J., and Barratt, M.J., "The Characteristics of the Turbulence in the Mixing Region of a Round Jet." Journal of Fluid Mechanics, Vol. 15, No. 3, pp. 337-367, 1963

## 2.6 Development of a Prediction Scheme for High Aspect-Ratio Jet Noise

From the HARN acoustic and fluid dynamic data there were some basic trends that had been identified. The acoustic data was found to vary with $V_j^8$. An equivalent length was also defined to parallel round jet scaling based on Lighthill's equation, which contains a length dimension squared. No direct relationship was immediately apparent between $L_{eq}$ and h and w. A "best-fit" to the data was used to define $L_{eq}$ making the sound intensity proportional to $L_{eq}^2$. The relationship found was $L_{eq} = h^{3/4}w^{1/4}$.

Since this was a rather unlikely scaling-parameter, a more in-depth examination of the OASPL data's variation with h and w was carried out. The prediction scheme was re-arranged into a form containing area and aspect ratio rather than $L_{eq}$ ($I \sim (A\ (AR)^{-1/2}$, note $A(AR)^{-1/2} = L_{eq}^2$). This provided a direct way of scaling both round jet noise and HARN jet noise using the same scaling equation.

In addition to the scaling parameter associated with the geometry, the fluid dynamic data revealed that the convection Mach number was not necessarily $0.65\ M_j$. In fact, $M_c$ varied with distance downstream of the nozzle and actually was found to be proportional to the local centerline velocity of the jet, $V_r$. Thus, over much of the noise-producing region of the jet, the average $M_c$ is much lower than $0.65M_j$.

In addition, it was found that $M_c/M_t$ was also a function of frequency. Other researchers have shown that different frequencies are generated at different downstream locations in the jet flow. These facts were used to generate an improved convection Mach number estimation. These changes to the estimates from Lighthill's equation improved the collapse of HARN acoustic data, particularly at low polar angles where the convection Mach number has the greatest effect.

This data was also compared with classic round jet acoustic data using the same modifications in order to make the comparison using a common prediction scheme. The two very different nozzles produced similar results in many ways. Both jets follow the $V_j^8$ law and have a similar spectral shape and were found to have similar amplitudes when scaled by the developed prediction scheme. The amount of agreement was surprising since the geometries were so vastly different. However, the modified convection Mach number did not improve the collapse of the round jet data used in the comparison. This is believed to be due to the fact that the high frequency noise from the round jet is produced near the jet exit, thus a significant portion of the spectra actually is associated with a convection Mach number of $0.65\ M_j$. However, in the case of the HARN, collapse was improved because it is believed that the noise generated close to the exit of the HARN had such high frequencies that it was beyond the capabilities of the data acquisition system. Thus, the majority of the noise recorded in the spectra is associated with turbulence with much lower convection Mach numbers downstream of the core region of the jet.

The HARN acoustic data was also compared with Tam's generic jet noise spectra. Tam's generic curves predicted the shape of the spectra quite well. In general, the HARN data was found to collapse using a modified version of the round jet scaling parameters derived from Lighthill's equation.

Further description of this portion of the study is given in Appendix E.

## 2.7 Effect of Pulsed Blowing on Farfield Noise

The main objective of this study was to assess whether pulse blowing resulted in more, less, or the same amount of radiated noise in the farfield. *Results show that a reduction in farfield noise*

*of up to 5 dB is measured when pulse flow is compared to steady flow for an equivalent lift configuration.* This reduction is in the spectral region associated with the trailing edge jet noise. This result is due to the unique advantage that pulsed flow has over steady flow. For a range of frequencies, more lift is experienced with the same mass flow as the steady case. Thus, for an equivalent lift and slot height, the pulsed system can operate at lower jet velocities, and hence lower jet noise.

At low frequencies (below 1 kHz), the pulsed flow configuration generated more noise in the farfield. This is most likely due to the pulsing mechanism itself. Since the high pressure air feeding the pulsing mechanism was first passed through a high performance muffler, it is likely that this increase in not due to upstream valve noise. Most likely, the impulsive component of the air that periodically fills the plenum causes a broadband source that reaches the farfield. Although the benefit of a pulse trailing edge jet is evident from a mass flow usage and jet noise perspective, attention should be paid towards the design of a viable pulsing system. Future research program in this area should concentrate on the development of a "quiet" pulsing device.

Further details of this portion of the study are provided in Appendix F.

## 2.8 Effect of Pulsed Blowing on CCW Fluid Dynamics- CFD Results

Unsteady Reynolds-averaged Navier-Stokes calculations were carried out for a supercritical airfoil equipped with a 30-degree dual-radius CCW flap. The predicted values of lift coefficient, when the airfoil is operating using Circulation Control are in excellent agreement with measurements. Calculations were also done for a pulse jet configuration. It was found that the pulse jet configuration gave larger increments in lift compared to the steady jet, at a given time-averaged mass flow rate. This was attributed to the fact that the pulsed jet had larger instantaneous momentum coefficients leading to enhanced Coanda effect. Finally, pulsed jet performance improved at higher pulse frequencies due to the fact that the airfoil had not shed the circulation into the wake before a new pulse cycle began.

While these simulations are very encouraging, additional calculations are needed to further define the optimum placement of slots, and to establish the minimum mass flow rates needed to achieve lift coefficients comparable to conventional high-lift systems.

Further details of this portion of the study are provided in Appendix G.

## 2.9 Streamwise and Spanwise Tangential Blowing

Circulation Control has a number of other uses. It may be used to modify the spanwise lift distribution of wing sections, effectively altering the span loading of lift forces. Since the trailing vortex structures are directly affected by, and related to the bound circulation, one can modify the strength (or spatial distribution) of trailing vortex structures, including the strong vortex that forms at the wing tips.

Attempts were made to study the benefits of 3-D Circulation Control. Two cases were studied. The first is a streamwise tangential blowing on a wing-flap configuration. The second is a spanwise tangential blowing over a wing with a rounded wing tip. Some interesting results have been obtained for both cases, demonstrating that there are many potential practical applications for the Circulation Control technology, beyond high lift applications. Much of the work done under this program was based upon the CFD analysis. Selected experiments were also performed.

10

### 2.9.1 Streamwise Blowing on a Wing-flap Configuration

The flap edge vortex is always a strong source of the airframe noise, especially when high lift devices are fully deployed during take-off or landing. According to Prandtl's classic lifting-line theory, a trailing vortex will be generated whenever there is a change in the bound circulation over the wing. For a wing-flap configuration, the lift and hence the bound circulation is much higher over the flap than on the main wing. Thus the circulation will not be continuous at the interface between the wing and the flap, and a very strong vortex will be generated here. These vortices have been seen in many experiments and flight tests. This vortex, due to its interaction with the flap gap, will generate a strong noise, commonly labeled as "flap-edge noise".

A number of approaches have been proposed to eliminate this noise source. Vortex fences and serrated flap edges have been proposed and tested. These devices add to the weight and cost of manufacturing of the wing. Because these are passive devices, they can be at best optimized for a single operating condition (e.g., a specified flap angle, flow angle of attack, and free-stream velocity), and cannot be expected to work for all conditions.

The purpose of this portion of the present program was to determine if the Circulation Control technology may be used to modify the lift distribution along the span, thereby weakening or eliminating the flap-edge vortex. Figure 12a shows a sketch of this concept – a wing-flap configuration with tangential blowing over the main wing. Only the left half of this wing-flap configuration has been simulated, and the flow has been assumed symmetric. In this region, the wing section within the first five chord-lengths from the central boundary has a 30-degree flap, and there is a weak jet blowing ($C_\mu \cong 0.01$) over the flap to suppress the vortex shedding. The other part of the wing has no flap, but a scheduled CC blowing is put in this section of the wing to generate high lift that is comparable with the lift generated by the 30-degree flap.

Three cases were studied computationally. In the first case, there is no blowing on the main wing, so it is just a regular wing-flap configuration. In the second case, there is a constant blowing, which means the $C_\mu$ is constant along the span, over some sections of the main wing (from 15C to 20C). Finally, a gradual blowing case has been studied, where the $C_\mu$ is gradually increased along the span over some sections of the main wing (from 10C to 20C). Figure 12b shows the lift coefficient distribution along the span of this wing-flap configuration for these three cases. When there is no blowing, a steep jump in lift coefficient is found at the interface between the main wing and the flap. It is expected because the sectional lift generated in the vicinity of the 30-degree flap is much higher than the main wing. In the second case, when a constant blowing is put over a section of the main wing, the lift at these stations will be greatly increased due to the Coanda effect. Thus the difference of lift between the blowing section of the main wing and the flap will be reduced, but a jump in the lift is still found at the interface between the blowing section of the main wing and the unblown section. In the third case involving the gradually blowing, it is seen that the lift is smoothly increased along the span, from 0.25 to 1.4 over the flap without a sudden change. This is due to the gradual increase in the blowing momentum coefficient, $C_\mu$.

In summary, the preliminary conclusions for the 3-D tangential streamwise blowing over the wing-flap configuration are: 1) the flap-edge vortex is generated by the suddenly increase in the lift along the flap-edge interface; 2) CC blowing with a constant momentum coefficient can not eliminate the flap-edge vortex, but can weaken and move the location of this vortex from the flap-edge towards the main wing; 3) a gradually varying CC blowing can totally eliminate the vortex. It should be noted that this is just a preliminary simulation, and that the model used here

11

is very simple. To fully understand the effect of the CC blowing on the flap-edge vortex, more detailed simulations are recommended.

For Results see Chapter 5 of Yi Liu's PhD Dissertation[2].

We attempted to setup an experiment to confirm these findings, but established that they were too expensive within the budget constraints of current grant.

### 2.9.2 Spanwise Blowing over a Rounded Flap Edge

Tip vortex is generated by the pressure differences between the upper and lower surface of the lift wing. Since in general, the pressure at the lower surface is much higher than that at the upper surface, the vorticity of the fluid particles within the boundary layer at the lower surface will flow around the wing tip, roll-up, and form a tip vortex. The tip vortex formation may be drastically altered by generating a flow in a direction opposite to that of the boundary layer. To investigate the feasibility of this concept, a wing-tip configuration was studied computationally. Selected experiments were also carried out.

Figure 13 shows a sketch of this concept for a rounded wing tip. The wing is a simple rectangular wing with NACA 0012 airfoil sections, but the wing tip is round. The angle of attack was 8 degrees, giving rise to sufficient lift and a strong tip vortex. The jet slot is located above the rounded wing tip edge, and the jet is coming in the spanwise direction.

Three cases have been studied. In the first case, there is no blowing, simulating a rectangular wing with a rounded wing tip. In the second case, there is a small amount of blowing with $C_\mu$ = 0.04. In the third case, there is a stronger blowing with $C_\mu$ = 0.18. Figures 14 shows the vorticity contours around the wing tip region at three different streamwise locations, which are x/c = 0.81, 1.0 and 1.50, respectively. From those figures, it is seen that there is a strong tip vortex if there is no blowing, which is expected. If there is a small amount of blowing over the wing tip in the opposite direction, the tip vortex will be pushed away from the wing tip, but the vortex could not be eliminated. Even when the blowing is increased, the tip vortex is just pushed down and far away from the wing. Another weaker vortex with an opposite rotation direction has been generated. Figure 15 shows the velocity flow field around the wing tip region at x/c = 0.81. It shows the same qualitative behavior as the vorticity contour.

The preliminary conclusions for the 3-D spanwise blowing over a rounded wing tip configuration is that the jet blowing around the rounded wing tip can modify and change the location of the tip vortex. It cannot totally cancel or eliminate the tip vortex, but can change or increase the vertical clearance between the wing and the vortex. Since the blade vortex interaction of rotors is strongly influenced by the clearance between the following blades and the tip vortex, this approach does have the potential of reducing BVI noise also. It can also slightly reduce the drag of the whole wing tip configuration by pushing the tip vortex away from the wing, and increasing the aspect ratio. Details of this can also be seen in the PhD dissertation of Yi Liu[2].

Attempts were also made to carry out an experimental study to reduce flap edge noise by blowing compressed air over flap-edge tip to reduce flap-edge noise, an important component of airframe noise. Initially, A rounded tip was provided at the tip with a small plenum chamber suitably built to provide blowing air so as to blow in a direction counter to the tip vortex. Unfortunately, much of this air appeared to eject approximately perpendicular to the flow direction. This might have been due to a very small span of blowing at of the tip of the model flap. This configuration was also thought to be beneficial as blowing through the tip was expected to displace the tip vortex away from the flap edge, which in return was expected to

12

reduce flap edge noise. Utilizing a Coanda surface installed at the flap edge, steady blowing was used in an attempt to diminish the vortex resulting from the uneven lift distribution. The strength of this lifting vortex was augmented artificially by steady blowing over the deployed flap.

The test article for this study was the same 2D airfoil that was used in the steady blowing program reported earlier (also used in pulsed blowing tests, see Appendix G), however its trailing edge geometry was modified. An exact duplicate of this airfoil shape was made out of fiberglass with no flap, and in the "clean" configuration. It was attached to the existing airfoil to make an airfoil that has half of its flap deployed and half un-deployed. Figure 16 shows a schematic of the planform showing the two areas where steady blowing was introduced. The flap-edge blowing or the auxiliary blowing was in the direction normal to the freestream velocity vector. Slot heights for the blowing chambers were on the order of 0.014 inches. Figure 17 shows this airfoil installed in GTRI's Anechoic Free Simulation Facility.

Flow visualization of the vortex indicated that the effect of increasing the main flap blowing was a "strengthening" of the lift vortex. The strengthening was only assumed and not quantified. The vortex became more "vigorous" and intuitively, wing lift was increasing on the deployed flap, the vortex should have become more intense. The effect of blowing on the flap edge was observed to "push" the vortex further towards the trailing edge span. This was observed clearly with tufts. This can be seen clearly in Figure 18. This picture was taken with the camera pointed at the underneath of the wing/flap system. With no blowing from the flap edge, the tuft at the flap edge follows the vigorous motion of the tip vortex. As soon as the flap edge blowing is turned on, the vortex moves to the right in the picture from tuft labeled 1 to tuft labeled 2. The strength of the shifted vortex was not quantified but the effect on the farfield acoustics was to increase the high frequency content of the radiated noise, most likely due to the issuing air jet, while mildly affecting the low frequency content. Thus no noise benefits were observed. Additional work needs to be done on the effect of tip blowing on flap-edge noise.

The results of this portion of the study are documented in Appendix H.

## History

- Airframe noise & engine noise compete during aircraft approach phase.
- High-lift devices contribute significantly to airframe noise.
- No alternatives to mechanical, high-lift devices investigated.

## Alternative

- Circulation Control Technology.
- Significant potential in reducing airframe noise.

## Studies, Modeling and Assessment

- Conduct study using CCT to control noise.
- Model flow physics.
- Conduct assessment of lift using conventional wing and circulation control.

## Accomplishments

- CFD analysis carried out with blowing and without.
- Lift and blowing increased concurrently.
- Noise Reduction obtained in audio range
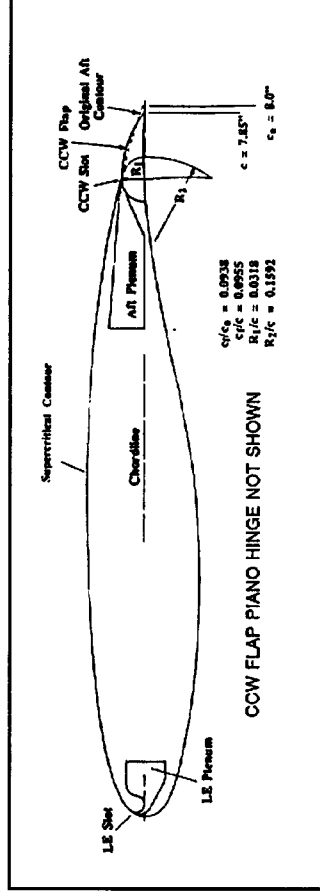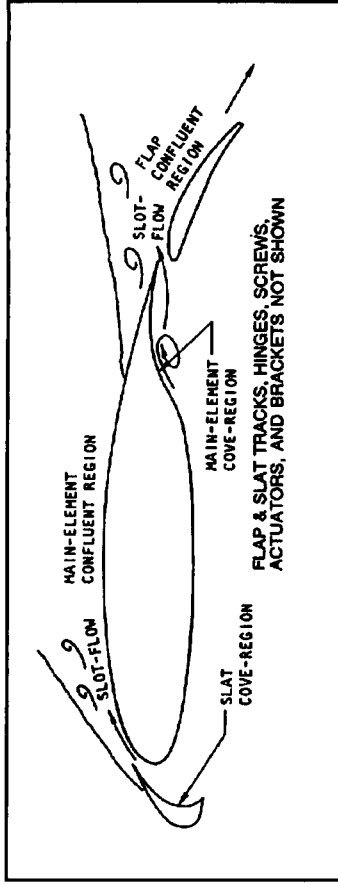
## Future Plans

- Understand conditions which produce noise reduction for same lift.
- Understand drag implications.
- Extend investigation to pulsed blowing and tangential blowing.

SLOT-FLOW
FLAP CONFLUENT REGION
MAIN-ELEMENT CONFLUENT REGION
SLOT-FLOW
MAIN-ELEMENT COVE-REGION
SLAT COVE-REGION
FLAP & SLAT TRACKS, HINGES, SCREWS, ACTUATORS, AND BRACKETS NOT SHOWN

Supercritical Camber
Chordline
LE Slot
LE Plenum
CCW Flap
CCW Slot
Original Aft Contour
Aft Plenum
$c = 7.85"$
$\varepsilon_0 = 8.0°$
CCW FLAP PIANO HINGE NOT SHOWN
$c_f/c_a = 0.0938$
$c/c = 0.0955$
$R_1/c = 0.0318$
$R_2/c = 0.1592$

**Figure 2. Application of Circulation Control Technology to Airframe Noise Reduction.**

14

## Mechanical Multi-Slotted Flaps

- Heavy
- Complex
- Draggy

## Pneumatic CCW

- Light
- Simple
- Variable CD
- Less Noise
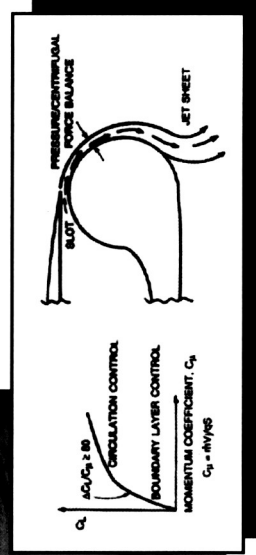
**Figure 3. Comparison of Existing High-Lift Systems: Mechanical vs. Pneumatic.**

15

- Mechanical high-lift configurations can employ 3 or more trailing-edge flap elements plus one or more leading-edge elements. They also employ many tracks, actuators, and support mechanisms to deploy/retract the devices, plus mechanical spoilers and ailerons. These devices are Noisy and cause compromises to be made in terms of weight, structure, complexity, reliability, wing sizing, and overall performance.

- Clearly, a system that can do away with most of the mechanical components, reduce the wake width, reduce noise significantly, improve performance and yet keep the aircraft flight-worthy is needed. One way to accomplish this is to replace mechanical components responsible for lift by pneumatic or Circulation Control technology.



- Potential for noise reductions is very high.

- Shorter runway

- No nose droop

- Simple design, smaller wings, less weight

- Circulation Control Wing (CCW) can generate more lift due to blowing at zero degrees incidence than the maximum $C_l$ of mechanical airfoils.

- Our current results show reduction in broad band noise, as well as vortex shedding noise.



- Circulation control is an innovative flow control technology that can dramatically improve aerodynamic performance and simplify mechanical complexity through pneumatic means.

- Circulation control technology has previously been developed and flight-demonstrated for civilian and military aircraft (for example, A-6/CCW).
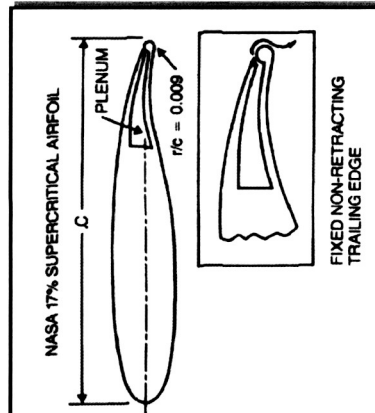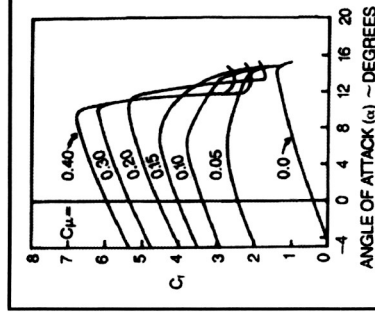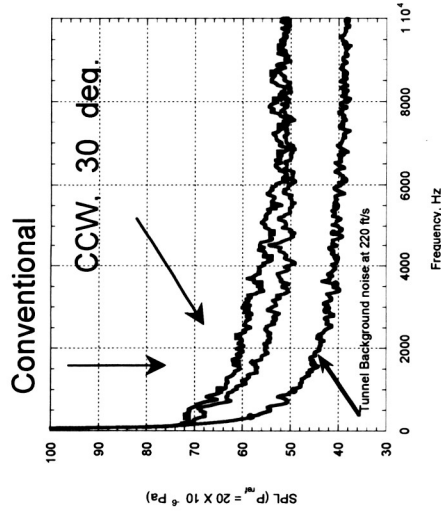
Highly Improved Lift of a CCW Configuration

**Figure 4. Noise Reduction through Circulation Control Technology.**

16
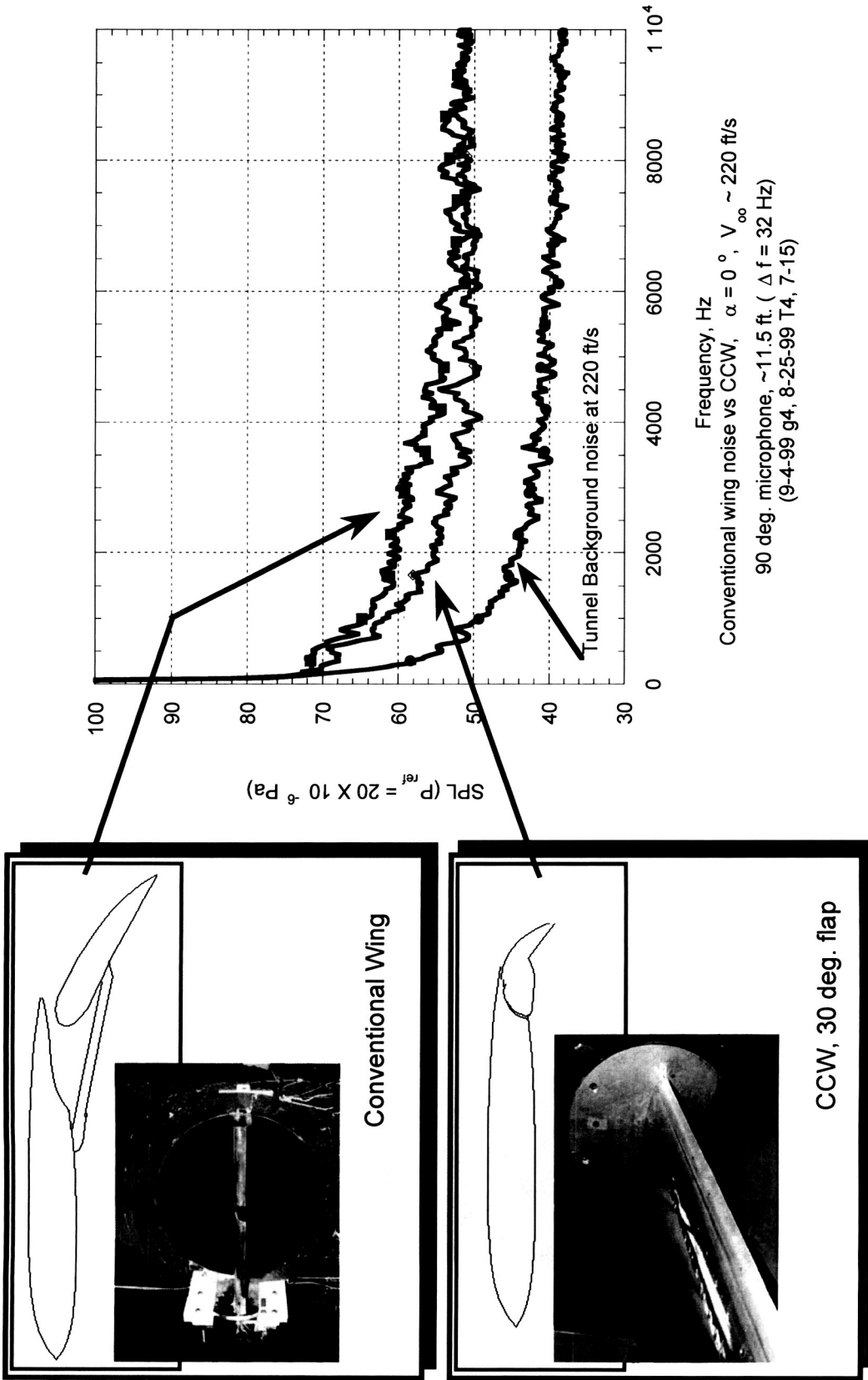
**Figure 5. Noise Reductions at Constant Lift (Conventional Wing vs. CCW Wing).**

17

No Blowing, $C_\mu = 0.0$

Blowing, $C_\mu = 0.025$

CCW, 30 deg. flap

Frequency, kHz

SPL ($P_{ref} = 20 \times 10^{-6}$ Pa)

Trailing edge flap noise, V = 240 ft/s, CCW 30 degree flap, $\alpha = 0°$, h ~ 0.003
90 deg. microphone, ~11.5 ft. ($\Delta f = 2$ Hz)
(8-26-99, junk, junk1)

Flow Field, $C_\mu = 0.15$

Flow Field around the Airfoil $C_\mu = 0$ Case

18
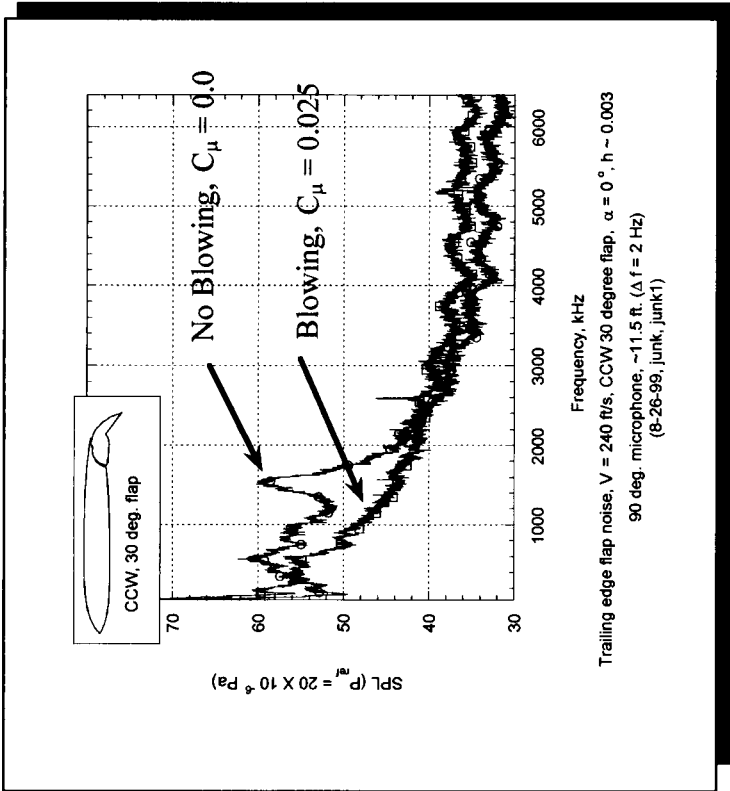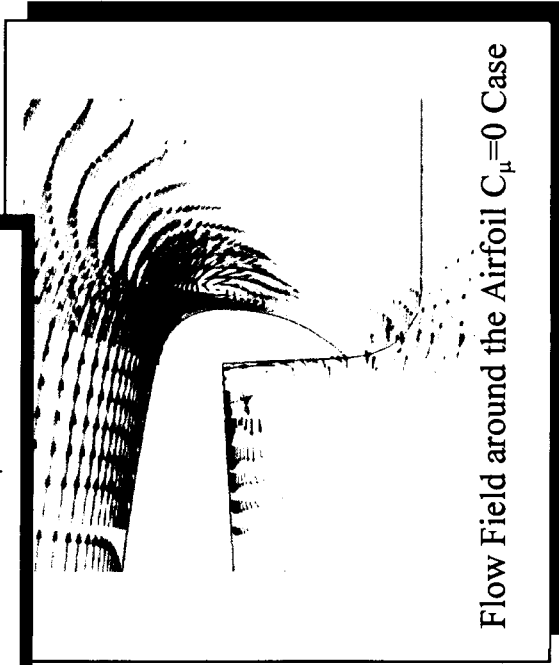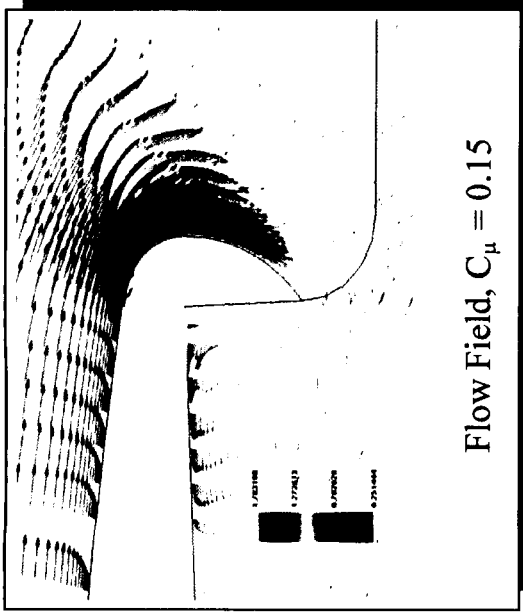
Figure 6. Suppression of Vortex Shedding Noise by Blowing.
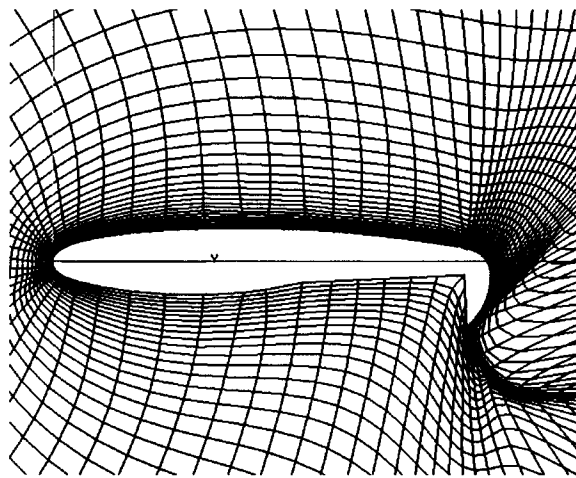
**Figure 7. Body-Fitted Grid at a Typical Span Station for a Circulation Control Wing.**
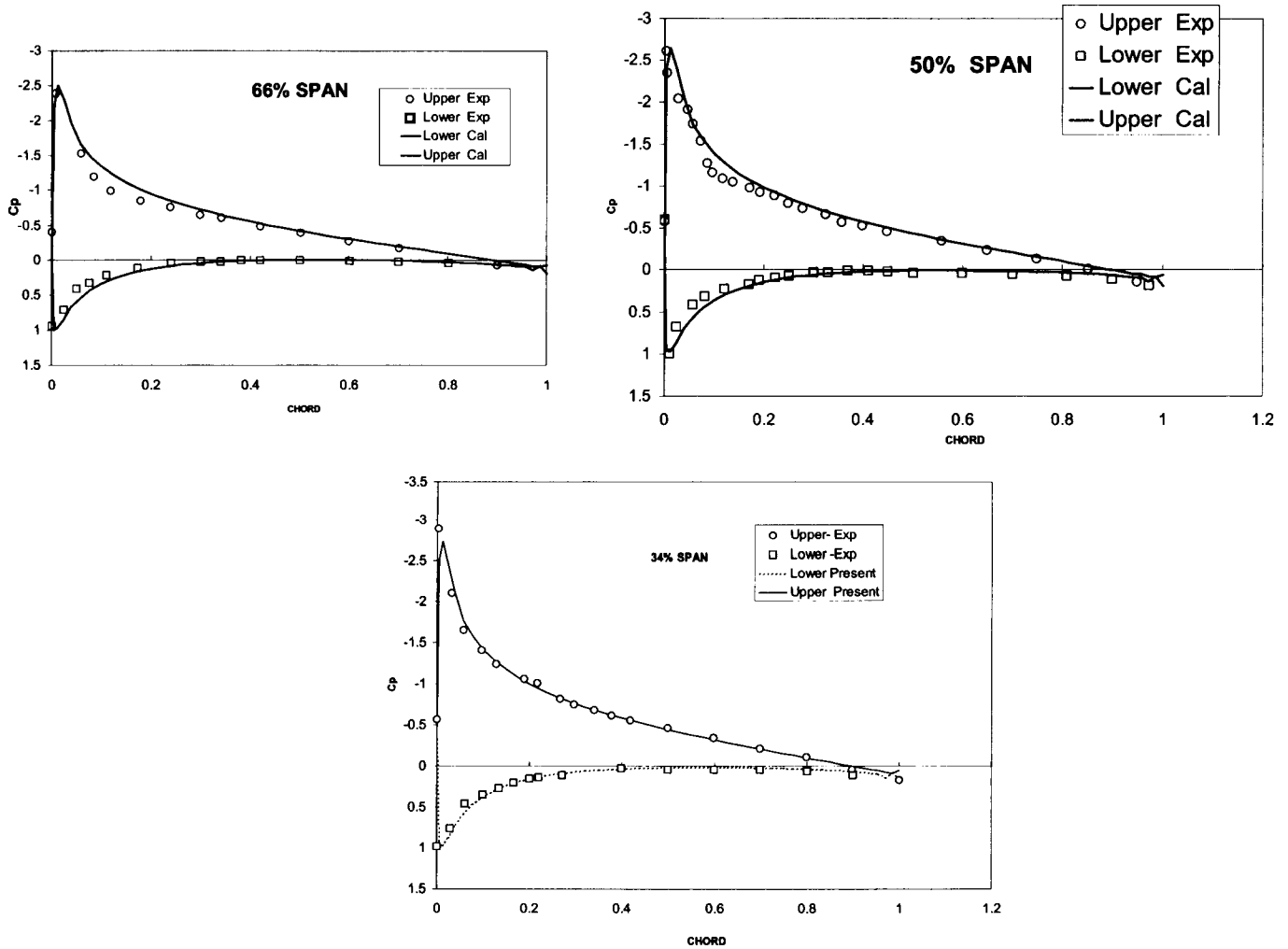






**Figure 8. Computed and Measured Surface Pressure Distributions over an Unswept Wing.**
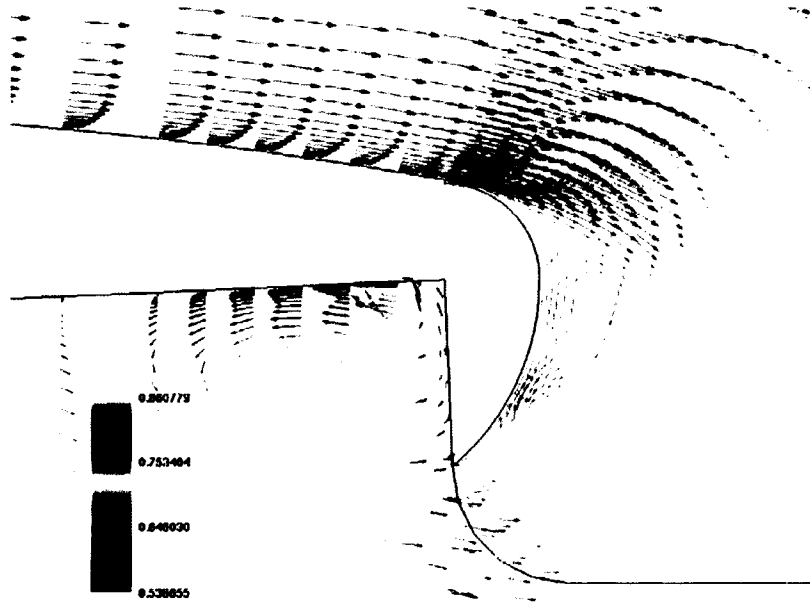
**Figure 9a. Velocity Field in the Vicinity of the CCW Wing Trailing Edge (No-Blowing Case).**
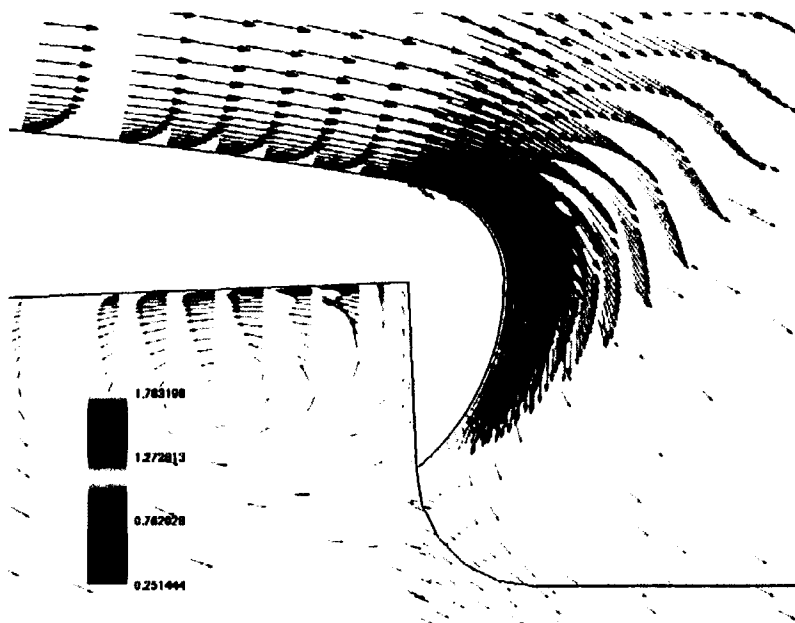


**Figure 9b. Velocity Field in the Vicinity of the CCW Wing Trailing Edge (Blowing Case).**
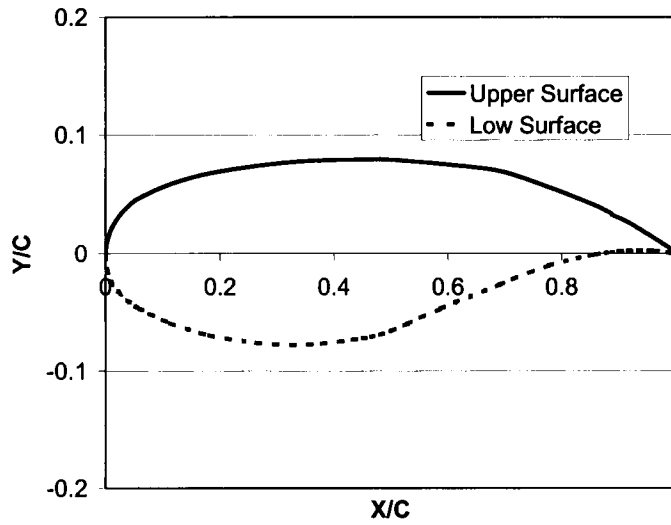
**Figure 10. The coordinates of the airfoil currently being tested.**
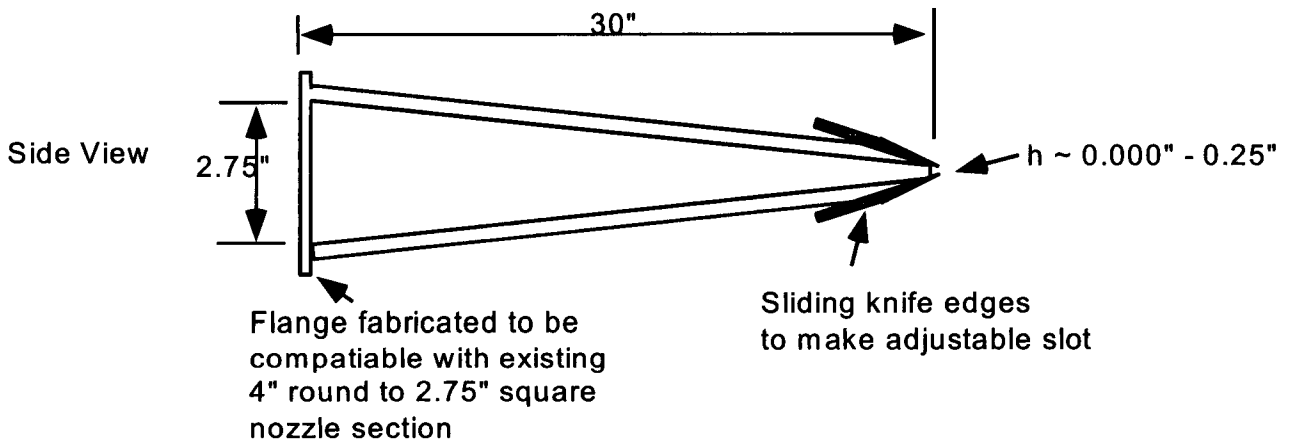


**Figure 11a. Schematic of high aspect ratio nozzle (HARN).**
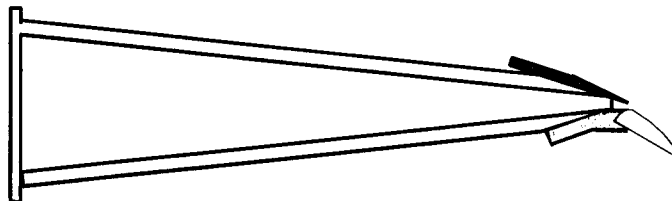


**Figure 11b. Side view of HARN with CCW flap.**

21
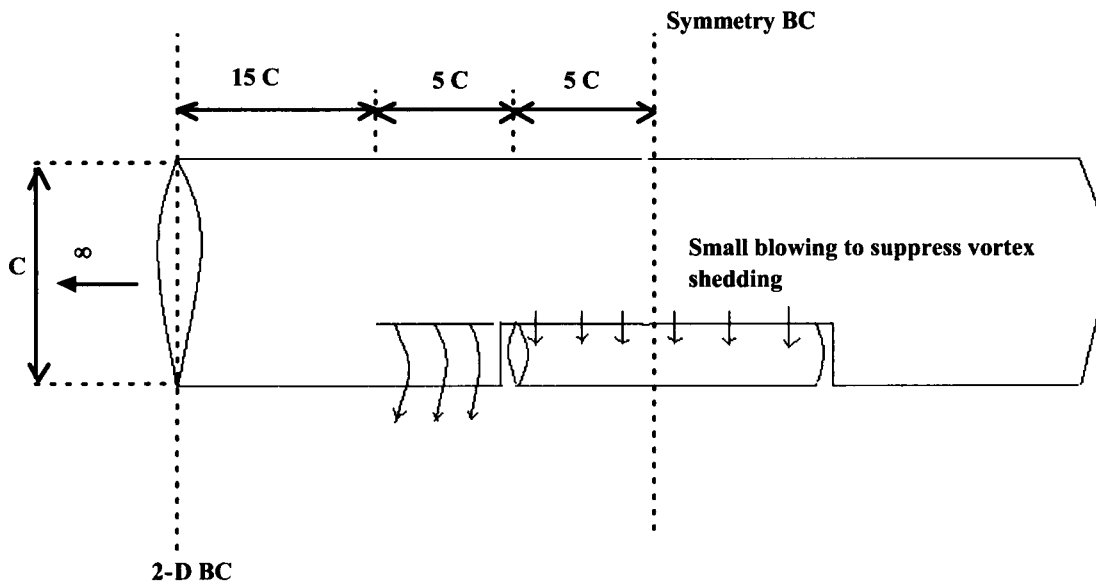
**Figure 12a. The Wing-flap Tangential Blowing Configuration.**
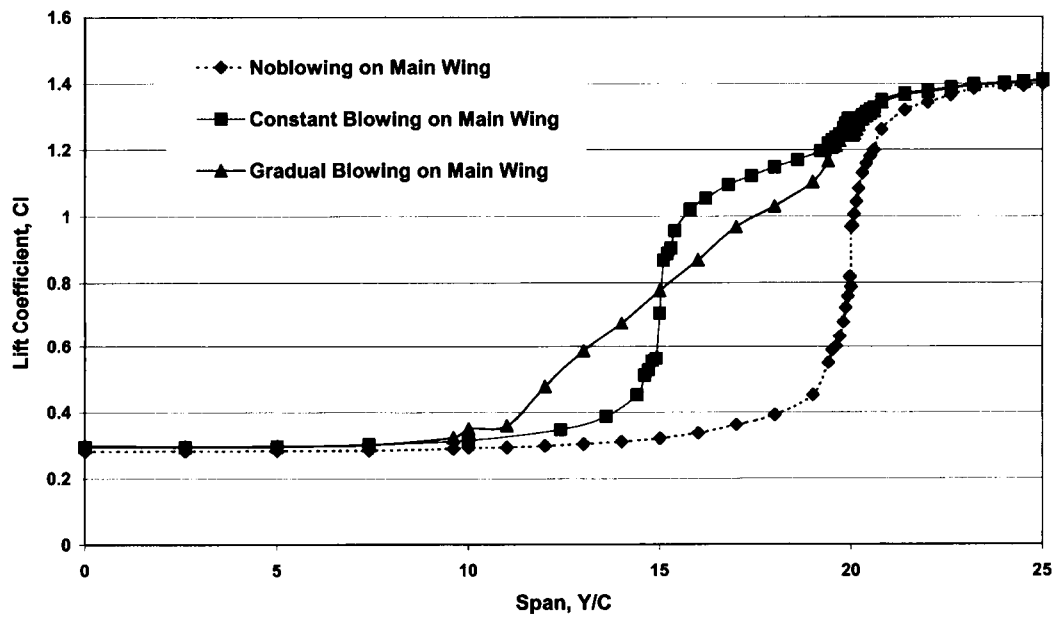


**Figure 12b. The Lift Coefficient Distribution along Span for the Wing-flap Configuration.**

22
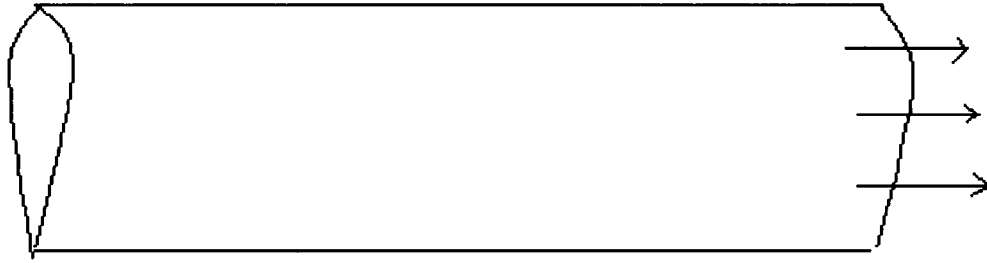
**Figure 13: The Wing Tip Configuration.**

**No-Blowing Case**

**Less Blowing Case ($C\mu = 0.04$)**

**More Blowing Case ($C\mu = 0.18$)**
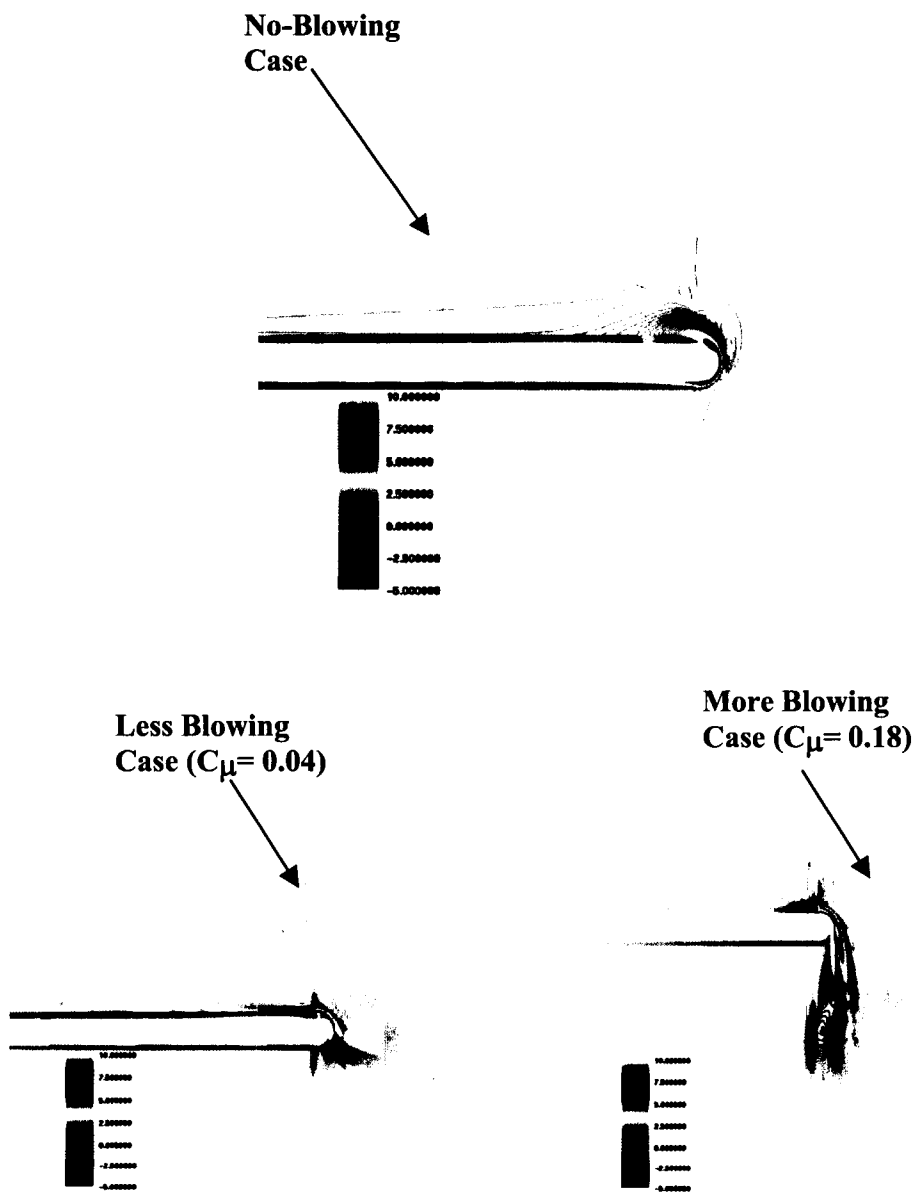
Figure 14. The Vorticity Contours around the Wing Tip (x/C = 0.81).

**No-Blowing Case**

**Less Blowing Case (C$\mu$= 0.04)**

**More Blowing Case (C$\mu$= 0.18)**
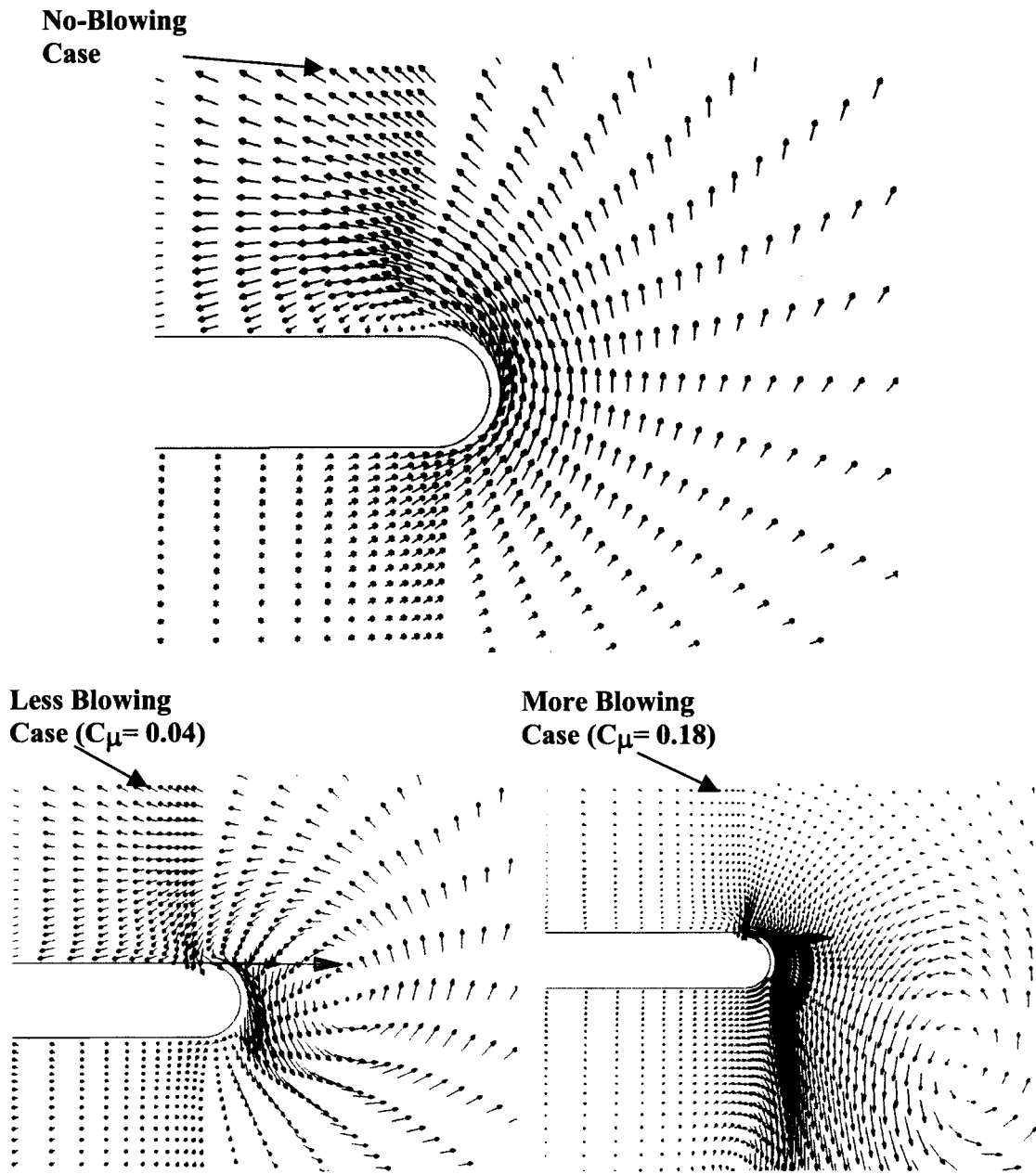
Figure 15. The Velocity Vectors around the Wing Tip (x/C = 0.81).

25

┌─────────────────────────────────────────────────┐
│                                                 │
│              2D Wing Planform                   │
│                                                 │
│         ┌──────────────────────┐ →              │
│         │ Deployed Flap Blowing │ →              │
│         │                      │ →              │
│         └──────────────────────┘                │
└─────────────────────────────────────────────────┘
     ↓     ↓     ↓     ↓     ↓   ↖
                              Flap-Edge Blowing [Coanda Surface]
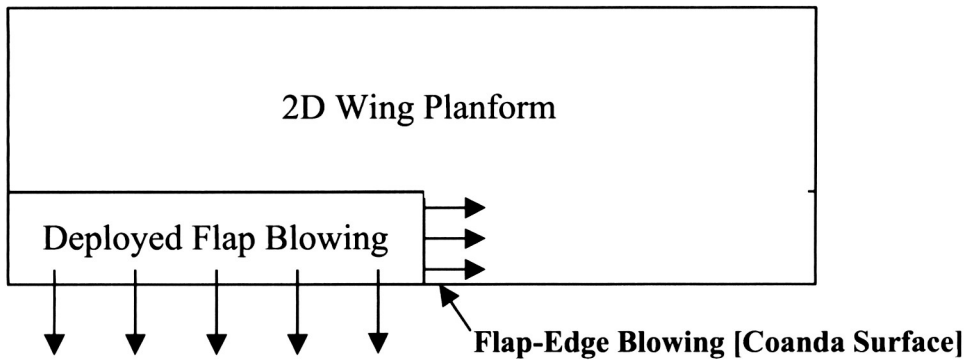
**Figure 16.  Schematic of Flap-Edge Blown 2D airfoil.**
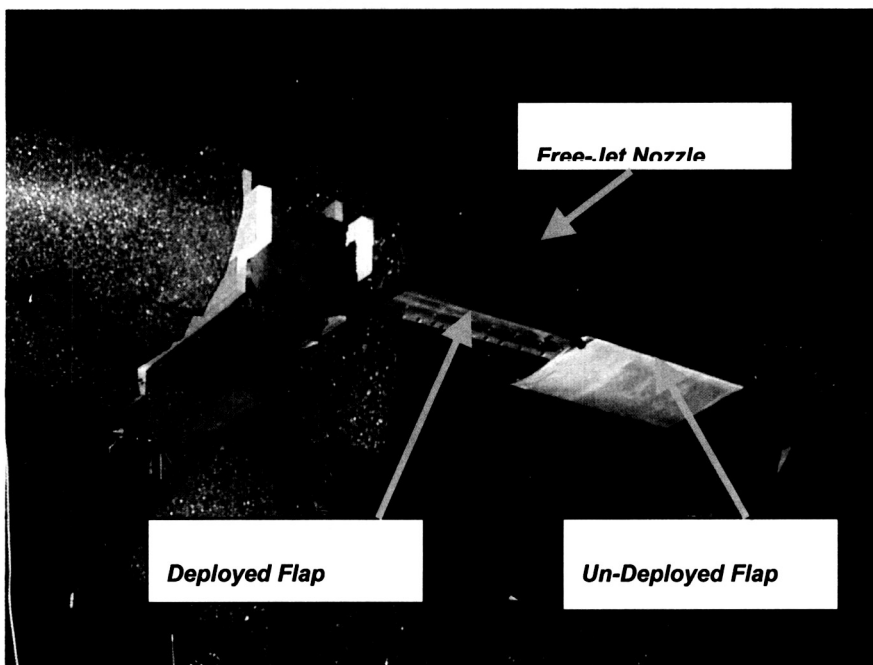


**Figure 17.  Test article installed in Anechoic Flight Simulation Facility.**

**No Blowing**　　　　　　　　　　**Flap-Edge Blowing**
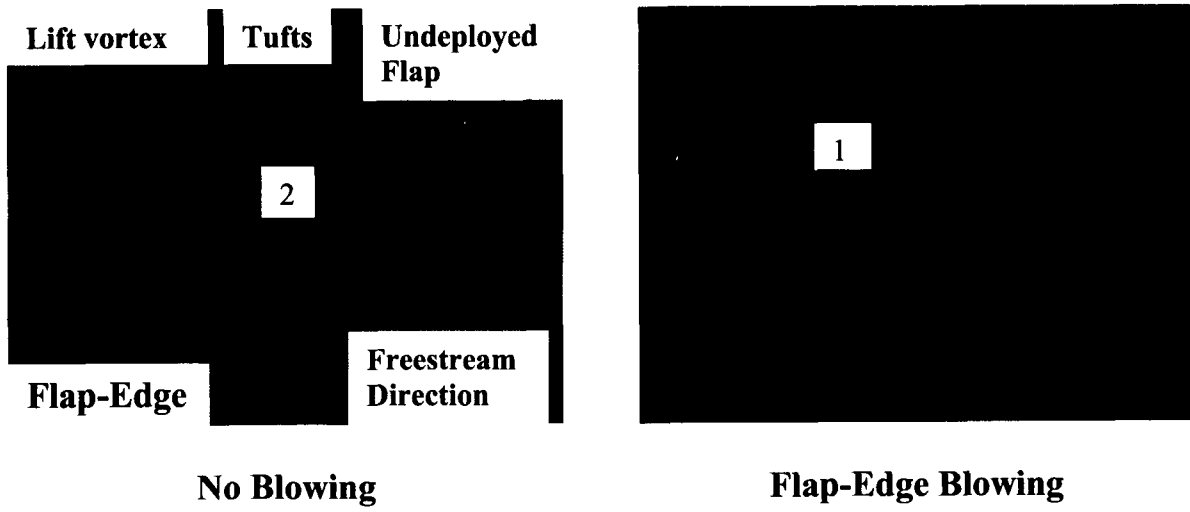
**Figure 18.** **Vortex moves from tuft 1 to tuft 2 on blowing from the tip of the flap edge.**

# APPENDIX A

# Noise Reduction Through Circulation Control

# APPENDIX A

# NOISE REDUCTION THROUGH CIRCULATION CONTROL

Scott E. Munro, K.K. Ahuja, Robert J. Englar

Georgia Institute of Technology

GTRI/ATASL

Atlanta, GA 30332-0844

## Abstract

Circulation control technology uses tangential blowing around a rounded trailing edge or a leading edge to change the force and moment characteristics of an aerodynamic body. This technology has been applied to circular cylinders, wings, helicopter rotors, and even to automobiles for improved aerodynamic performance. Only limited research has been conducted on the acoustic of this technology. Since wing flaps contribute to the environmental noise of an aircraft, an alternate blown high lift system without complex mechanical flaps could prove beneficial in reducing the noise of an approaching aircraft. Thus, in this study, a direct comparison of the acoustic characteristics of high lift systems employing a circulation control wing configuration and a conventional wing flapped configuration has been made. These results indicate that acoustically, a circulation control wing high lift system could be considerably more acceptable than a wing with conventional mechanical flaps.

## Nomenclature

a - Speed of sound

c - Chord

# APPENDIX A

$c_\ell$ - Airfoil lift coefficient

CCW - Circulation control wing

$C\mu$ - $\dfrac{\dot{m}V_j}{qS}$

h - Slot height

$\dot{m}$ - Mass flow

p - Pressure

q - ½ $\rho V^2$ (dynamic pressure)

R - Radial distance from jet exit to measurement location

r - Radius of CCW surface

Re - Reynolds number

SPL - Sound Pressure Level

T - Temperature

V - Velocity

$\alpha$ - Angle of attack

$\Theta$ - Polar angle (with respect to the flow axis)

$\rho$ - Density

Subscripts

s - Associated with slot

T - Associated with tunnel freestream

j - Associated with jet

o - Ambient condition

# APPENDIX A

## Introduction

One of the major environmental dilemmas facing today's aircraft industry is noise pollution from aircraft, especially around the airport. There is a large emphasis on minimizing community noise due to operation of aircraft at and around the airport. Thus, airlines, aircraft manufacturers, NASA and the FAA have made reducing aircraft noise a priority. NASA has proposed a goal of lowering total aircraft noise emissions by 20 EPNdB by year 2020.

In order to meet this goal, NASA and other organizations have been encouraging innovative research to help reduce aircraft noise. Since a major contributor to aircraft noise on approach is airframe noise (or perhaps even on takeoff if the engine noise is eliminated), reducing this noise would be helpful in reaching the industry goals. The major airframe noise contributors are the landing gear, the slats, and the flaps. Much work has been done in these areas in the last five years in an effort to reduce their noise emissions. Of course, the best solution would be to have an aircraft without these protrusions into the flow field. Obviously an aircraft without landing gear would have serious drawbacks, but there are alternate high-lift systems that could replace conventional wing flaps and slats which have shown great promise in maintaining and even surpassing the lifting benefits of conventional flaps.

Circulation control wings (CCW) have been researched and developed extensively, primarily for the purpose of increasing performance and reducing or replacing the conventional flap system of an aircraft.[1] Over the years the CCW systems have gone through many configuration designs for many different applications, including versions for rotorcraft, fighter aircraft, and short haul transports.[1] However, there has been limited research conducted investigating the possible acoustic benefits provided by such a system, other than occasional

# APPENDIX A

references to smaller noise footprints due to shorter take-off and landing distances. The only known work on acoustics of CCW is that of Salikuddin, Brown and Ahuja[2] where they evaluated the noise field of an upper surface blown wing with circulation control. That study, however, did not provide an indication of the acoustic benefits of a circulation control wing versus a conventional wing for the same lift.

Since CCW systems have already been shown as an adequate replacement for conventional flap systems in the aerodynamic realm,[1] they are immediately a candidate for reducing airframe noise since they eliminate much of the structure of the conventional flap system that protrudes into the flow. However, there are many issues that need to be resolved before the claims of lower noise are validated. Since the CCW system has never been evaluated on an acoustics basis, it must be optimized for this, while maintaining, at a minimum, the lift characteristics of a conventional system. The acoustic impact of several parameters must be investigated, such as the blowing slot height, slot velocity, and CCW geometric configuration (i.e., flap type and deflection angle). In order to correctly define the best combination, new areas of research will have to be investigated, including jet noise of extremely high aspect ratio nozzles, and the effects of jet turning on its noise propagation. These many issues are the motivation of the present study. The current work involves both experimental and computational efforts. Only experimental results are presented in this paper. Computational results are presented in Part II of this article and in Reference [3].

## Background

# APPENDIX A

The circulation control wing (CCW) concept has been researched since the1960s. The CCW uses a rounded trailing edge (figure 1).[1] Air is blown tangentially along the upper surface from a plenum supply inside the wing through a slot just upstream of the rounded trailing edge. Blowing moves the upper surface separation point around the trailing edge, thus changing the trailing edge stagnation point location, and hence the circulation for the entire wing. The higher-speed air moving along the surface also causes a suction peak in this region and contributes to increased lift.

The slot flow remains attached to the surface due to the so-called Coanda effect.[4] At low blowing velocities, the tangential blowing behaves similar to a boundary layer control device by adding energy to the slow moving flow near the surface. At higher blowing rates, the lift is increased by the change in circulation described above. A CCW can be designed without any mechanical moving elements if desired. This is achieved using a rounded trailing edge, where the amount of lift is controlled by the pressure valve to the supply plenum. This eliminates the need for flaps with hinges, tracks, screw drives and hydraulics.

The increment in lift generated is controlled by the non-dimensional parameter $C\mu$, defined using slot and freestream properties.

$$C_\mu = \frac{\dot{m}V_s}{q_\infty S} \quad \text{or} \quad C_\mu = \frac{\dot{m}V_s}{q_\infty c}$$

With a wing, the non-dimensionalizing area is the wing surface, S. For an airfoil, typically $C\mu$ is given in $C\mu$/ft since the chord is the only available reference length. In general, a given $C\mu$ will provide a given increment in the lift coefficient over the entire range of angles of attack below stall. The exception to this is when the slot jet velocities or slot heights are large enough to cause

the jet to separate prematurely. Thus, $C\mu$ is used extensively in the literature when discussing circulation control.

The large circular trailing edges used in many of the early experiments evolved into a dual-radius hinged flap, mainly because the non-sharp trailing edge greatly increased drag.[1,6, 7, 8] The hinged flap was a compromise of several desired features. The flap had a curved upper surface, like the cylindrical trailing edge, but a flat lower surface. This overcame the problem of high drag in cruise associated with the non-sharp trailing edge of the early designs. Overall, the hinged flap dual-radius design still maintained most of the circulation-control lift advantages but greatly reduced the drag problem associated with the circular trailing edge system.

The flap itself has several mechanical advantages compared to conventional Fowler flap systems. The flap is about ¼ to 1/3 the size of a conventional flap. This means lower flap weight, and thus fewer structural components are required to hold it in place.[8] The flap is also a simple hinged flap, rather than a complex Fowler type flap that requires complex gearing, tracks, and through gaps, which most likely contribute to airframe noise on their own. The reduced size and simplicity of the CCW system even with a small flap clearly offers some advantage over a conventional system.

There are many potential uses for circulation control. However, the two applications that have received the most research attention have been circulation control rotors (CCR) and CCW applied to an aircraft for short take-off and landing (STOL) capability. The reader is referred to references [1] and [5] where further details and citations on CCW research can be found. Some research pertinent to the present work is briefly mentioned below.

The Navy sponsored a full-scale flight test program on an A-6/CCW in the late 1970s. The design, tests and results are documented in references [9, 10 and 11]. Research has also

been done to investigate applying the circulation control system to a Boeing 737 type of aircraft. A summary of the effort is documented in reference [6]. The only known acoustic work on CCW configurations was performed by Salikuddin, Brown and Ahuja.[2] There are other potential uses for circulation control, including automotive applications[1,12] and helicopters[1,13] where noise reduction may also be appropriate. The acoustic benefits shown in this paper should be applicable to other areas also.

## Facilities and Instrumentation

The anechoic flight simulation facility (AFSF) was used in the experiments. It is located at Georgia Tech Research Institute (GTRI) located at its Cobb County Research Facility in Smyrna, GA. The AFSF operates in an open jet wind tunnel configuration. It is an anechoic facility that allows acoustic measurements to be made in the presence of a freestream (see figure 2). The tunnel inlet has a square inlet which converges down to a 28-inch round duct. The duct terminates in an anechoic room as an open jet. Protruding out from the downstream wall is the collector, which is 4 ft. wide by 5 ft. high. The collector duct extends outside the building and ends at a centrifugal fan powered by a diesel engine. The facility is open circuit, drawing air from outdoors. The details of the facility can be found in references [14 and 15].

In the current experiments, the wings are mounted via mounting brackets to the open jet. This locates the wing across the jet opening immediately downstream of the end of the duct. Figure 3 shows one of the conventional wings mounted at the exit of the open jet. The ambient pressure in the chamber, the plenum pressure for the slot, pressures in the air supply line venturi

mass flow meter, and pressure in the inlet (for freestream velocity) were monitored on individual pressure transducers and manually recorded for each test point.

Acoustic measurements were made with B & K, 4135, ¼" microphones. One microphone was mounted on a traverse system that translated the microphone from angles of 30° to 90° (where 0° is the freestream direction). This system was arranged to make all measurements in the fly-over plane. The microphone was connected to a multi-channel digital frequency analyzer, which is run by software on a PC.

Figure 4 shows a schematic of the blowing system for the CCW. It consists of high-pressure ¾ inch tubing, a mass flow venturi, pressure gauges, and a muffler. On the upstream end, the tubing is connected to an existing high-pressure line with a control valve upstream. The flow passes through a mass flow venturi, and then goes through more tubing to an in-house built muffler which absorbs the upstream valve noise. Downstream of the muffler, the air passes through more tubing to inlets for the CCW plenum.

## Test Models

The test model wing used in reference [6] was used as the test model for this study. This CCW model, shown in figure 5, has a supercritical baseline airfoil shape, but has many different detachable CCW trailing edge configurations. These included different sized flaps and cylindrical trailing edges. Based on past aerodynamic studies, the best overall aerodynamic characteristics were obtained with the small CCW flap configurations. The small deflectable flap allowed for low drag during cruise, but by blowing over the curved upper surface with the flap deflected, significant flow turning could still be achieved when desired. The highest lift

configuration was found to be with the flap deflected 90°. This was used as the starting configuration for the current acoustic tests.

The conventional wing had the same general shape as the CCW over most of the chord. However, its trailing edge was altered with a cut-out for a stowed flap. A single-slotted Fowler flap was attached. Two different flaps were tested. The flap was deflected 30° or 40° from the chord line to simulate a landing configuration. Both flaps spanned the entire wing, but one flap had a cut-out in at the mid-span point. Figure 6 shows the airfoil profile of the model and a drawing depicting the flap cut-out. Figure 3 is a photo of the model installed in the AFSF. The cut-out is to simulate the cut-outs on a real aircraft. Cut-outs are often present for structural reasons or to prevent engine exhaust from impinging on a lowered flap.

## Technical Approach

The current work focused on optimizing a CCW system for low noise impact while maintaining aerodynamic performance sufficient for direct comparison to a conventional flapped wing configuration. The first step was to determine if and how a CCW configuration can have lower noise than a conventional system. This step involved side-by-side comparison of representative configurations under the same conditions, i.e., the same freestream flow and lift conditions. Since there are several variations of CCW systems that have been researched, a basic study of different CCW configurations was done. Since the test models were used in other aerodynamic experiments, this also allowed the use of this data when making the acoustic comparisons.

**APPENDIX A**

The optimized blowing configuration was compared with a conventional wing system. Basic noise spectra of the CCW and conventional wing configurations were acquired at several mean flow velocities and angle of attack. Specific cases where the different configurations had the same lift coefficient were then compared directly. Lift data from previous studies were used for this comparison.

## Results and Discussion

### Acoustic Optimization of Existing CCW State-of-the-Art Configurations

Since the CCW concept has been around for nearly 40 years, there have been many advances, changes, and modifications to the basic concept to improve its overall performance. To attempt to acoustically test all the different configurations would be unreasonable, since many of the changes were made to improve the system. There is little reason to acoustically test a system that is technologically surpassed by a better version. Thus, the goal of the current study is to investigate two or three of the best performing CCW configurations.

Based on previous aerodynamic work, the CCW with its flap deflected 90° was chosen as the beginning point for the study (a possible high-lift configuration for landing approach). This had the best overall high-lift aerodynamic performance of several configurations tested in previous studies. The flap was eventually adjusted to 30° deflection to prevent flap-edge vortex shedding noise that was present in the 90° case.

Six slot heights were chosen for the optimization study ranging from 0.003" to 0.020" These dimensions were chosen because they were typical slot heights used in earlier aerodynamic studies.[6] A wide range of slot Mach numbers was evaluated, ranging from 0.3 to

**APPENDIX A**

1.2. The acoustically optimized CCW test configuration was compared with a conventional flap configuration. The conventional model had the same generic airfoil shape as the CCW, except near the trailing edge to accommodate the conventional flap. The flap chord was about 30% of the wing chord and deflected 40° to simulate a landing configuration. Data were acquired for each test configuration at freestream speeds of 100, 150, 200, and 250 ft/s (nominal) and at geometric angles of attack of 0°, 7°, and 14.°

The majority of the data presented in this section was acquired at a geometric angle of attack of 0° and at the highest freestream velocity of about 240 ft/s unless otherwise noted. Figure 7 shows acoustic spectra for several slot velocities with no freestream flow for the CCW with the 90° flap configuration. It shows a similar trend to the basic jet velocity scaling property developed for round jets. For the measured velocities, $V^8$ scaling of jet noise theory[16] predicts about a 19 dB increase between the two most extreme cases, which is similar to that measured (about 16 dB) above 2 kHz. Some noise due to scrubbing of the slot jet over the flap surface is likely to be present as well.

It appears that the majority of the noise is associated with the jet noise from the slot and not due to internal model and facility noise associated with the blowing system above 2 kHz. However, below 2 kHz the scaling is not followed in the data. This is most likely due to internal noise that is generated from the flow into the wing on its way to the slot. This contaminates the signal making the noise higher for the lower slot velocities, but not affecting the higher velocities where the jet mixing noise is expected to be dominant. Thus, the difference between the data is less than predicted by the theory. This is supported by figure 8.

Figure 8 shows the spectra out to a frequency of 60 kHz. These figures show two slot heights, and hence two slot areas, at the same slot velocity. However, inside the wing the areas

# APPENDIX A

in the flow path remain the same. Since the mass flow into the wing must be the same as the mass flow out, the doubling of the exit area roughly causes a doubling of the mass flow at the exit, and hence a doubling of the mass flow inside the wing. However, since all the areas inside the wing are constant, the velocity must double inside the wing in order to double the mass flow. Thus, if noise is dominated by the internal noise it should follow a sixth power law of the internal velocity, as this noise is expected to be dipole like in nature. If so, the data should reflect an 18 dB increase. However if the noise is dominated by externally produced jet mixing noise, then it will change only to the extent that the exit area has changed. Based upon the available experience/theory on round jets[16] this will provide for the jet mixing noise intensity proportional to slot exit area. This translates into a 3 dB increase in noise after shifting the spectrum for h = 0.006" to the left over the spectrum for h = 0.012" by a factor of one octave to allow for the shift in the noise frequencies proportional to a characteristic length. This number is somewhat smaller than the observed difference in the SPL's of the two spectra in figure 8. All of these arguments assume that we can apply the lessons learned from round jets to very high aspect-ratio jets. Yet, since the noise increase is of the order of 3 dB, it can be said that internal noise is not significant in this case. The fact that the observed difference in spectral SPL's is more than the expected 3 dB could also be associated with the scrubbing noise of the CCW slot jet moving over the rounded edge. If so, it is genuinely produced outside and is not contaminated by any internal noise. Obviously, some clarification of the data is needed. To fully understand the jet noise characteristics of extremely high aspect-ratio jets without the internal noise concerns discussed here, we have fabricated a high aspect ratio nozzle (HARN). We reserve our full judgment until additional studies have been carried out on the HARN, which is being tested by the authors in an acoustically clean facility

# APPENDIX A

We believe that, the data may be contaminated by noise generated internal to the wing below about 2 kHz. A muffler was built and installed in the supply line downstream of all valves to eliminate as much upstream noise as possible. However, due to the small thickness of the wing, inlets into the wing plenum are smaller than desired. This results in a relatively high velocity flow entering into the plenum with no space to absorb the noise generated.

It is believed that these noise sources may be causing a majority of the noise below 2 kHz where the noise is not following the typical $V^8$ jet noise scaling. For the time being, this will be noted and data below 2 kHz will be disregarded as either somewhat corrupted by internal noise or not understood until HARN data becomes available.

Figure 9 shows the noise spectra for several slot jet velocities at a constant freestream velocity and constant slot height of 0.003" There are several things to note. First, with no blowing there is a large-amplitude well-defined tone. It is also important to note that in general the very low frequency noise ( $f \sim< 4$ kHz) is much greater compared to the data in figure 7. Some of this is from the tunnel noise itself ( below about 500 Hz) but most of it is flow noise associated with the freestream flow around the wing. The tone is believed to be due to the shedding of vortices off the bluff trailing edge of the deflected flap. Notice that blowing, even at low slot jet velocities, significantly reduces the magnitude of the tone. However in this case it is not completely eliminated, in fact it dominates the spectra at all blowing velocities.

The tone mentioned above was unexpected. This presented a problem since the tone dominated the spectrum at all blowing conditions, thus any acoustic benefit derived from using the CCW over a conventional wing would be lost if the flap were deflected to 90°. Because of this, it was decided that reducing the flap deflection might produce a less dominant tone, but still provide enough lift with the right amount of blowing to equal that of a conventional wing.

# APPENDIX A

Figure 10 shows two curves with the flap set to 30°. In this case notice that the tone is completely eliminated with a small amount of blowing. The computational study also produced the same result, and is presented in reference [3]. Not only is this advantageous for the current study, but this result could be used in other applications where similar shedding produces a distinct tone.

Data for test conditions similar to those for the 90° deflection are shown in figure 11. Again, with no blowing the tone is present. However, with small amounts of blowing the tone is completely eliminated. Since this configuration showed more promise, the remaining parameters were optimized using the 30° flap configuration. Both slot height and slot jet velocity were examined.

The effect of slot height was investigated next. Figure 12 shows data with similar freestream conditions but different slot heights. It is important to note that this figure compares different CCW configurations with the same lift. For the same $C\mu$ at different h, the slot velocity will be different since $C\mu$ is dependent on mass flow from the slot. Since the goal is to compare the same lift, it is best to look at the data where $C\mu$ is constant since the same $C\mu$ will give the same lift in most cases. There is some variation of lift with h for high $C\mu$, but in the $C\mu$ range of interest here, h does not have an independent affect on the results. Thus, the data in figures 12 shows that there is a lower noise from the larger slot heights for a given lifting condition. This makes sense since $C\mu$ is proportional to mass flow through the slot. By increasing the slot height but maintaining the same mass flow (and hence same $C\mu$) the jet velocity of the slot is lower. At this point it appeared that the most appropriate conditions for comparing a CCW system to a conventional system had been found. Maximize the slot height so that jet velocity is minimized.

# APPENDIX A

Unfortunately it was found that above a slot height of about 0.012" the noise began to increase (for constant Cμ). Since this was contrary to the logical trend associated with what should be happening, some attention was given as to why this was happening. If one looks more closely at Cμ it contains a mass flow term. Initial results indicated that reducing the slot velocity reduced the noise. In the equation this means that $V_s$ would decrease. If one defines the mass flow term based on the mass flow "in" rather than "out" the problem becomes evident.

$$C_\mu = \frac{\dot{m}_s V_s}{qC} = \frac{\dot{m}_{in} V_s}{qC} = \frac{(\rho_{in} A_{in} V_{in}) V_s}{qC}$$

Density will vary with the pressure in the plenum, ($\rho$ = P/RT), but it varies proportionally to slot velocity (as $V_s$ decreases, P decreases, and hence $\rho$ decreases). Area is constant in the plenum regardless of slot height. Thus, in order to offset the decrease in $V_s$ and $\rho$, $V_{in}$ must increase. When this occurs, the internal noise associated with internal velocities will also increase. Figure 13 shows OASPL plotted versus h for constant Cμ. If it is assumed that the highest slot velocity is dominated by external jet noise, the decrease in noise due to falling $V_s$ can also be plotted. In the figure the highest $V_s$ occurs at the smallest h. The drop in OASPL should follow the $V^8$ scaling law. However, in this case keep in mind that the slot velocity drops due to an increase in slot area. Thus the final estimated curve shows dropping OASPL due to slot velocity, but at a lower rate than $V^8$ because of an increase in slot area.

Notice that the experimental data follows $V^8$ scaling for some time but eventually increases away from the estimated drop off. It is believed that this increase is due to the increasing dominance of internal noise as the slot velocity is reduced while the internal velocity is increased.

Although this finding was unfortunate it was not terribly detrimental to the study as long as one keeps in mind that proper design of the internal system will decrease the CCW noise further (in essence it should continue to drop along the estimated slot velocity curve in figure 13 as the slot velocity is decreased). Thus, any benefit found will be enhanced with careful design of the internal system.

## Determining an "equal lift" condition

The next step was figuring out how to compare the two lift augmentation systems. Aerodynamic data from previous studies was used for this (specifically that in reference [6]). Aerodynamic data was available for both conventional wing configurations and the CCW in the form of lift curves ($c_l$ vs $\alpha$ curves). This was convenient since for a CCW, a given $C\mu$ will generally provide a $\Delta c_l$ over the entire angle of attack range (not including the extreme high jet velocities and large slots where the jet separates from the surface). Thus, once the lift for the unblown CCW was found, this could be compared to the $c_l$ for the conventional airfoil and the needed $\Delta c_l$ was be calculated by subtracting the two values. This $\Delta c_l$ was then used to determine the $C\mu$ needed to match lift provided by the conventional wing flap system. Essentially each $C\mu$ is analogous to a flap setting which shifts the baseline lift curve by a given amount. For the particular CCW configuration (CCW with flap at $30^\circ$), a $C\mu$ of about 0.04 produced about the same amount of lift as the conventional wings used in the experiments.

## CCW versus Conventional Wings

Two conventional wing configurations were tested. One configuration with a $30^\circ$ flap spanning the entire span of the wing, and one with a flap deflected $40^\circ$ spanning the entire wing

except for a cut-out region in center span (figure 6 for a drawing figure 3 for a photo of it installed in the AFSF). These wings are the same basic airfoil shape as the CCW. The wings were tested at the same flow conditions as the CCW.

Initially, the conventional wing with the 30° flap was tested. Figure 14 shows a comparison between the conventional wing with the 30° flap and the CCW configuration with lowest noise for the equivalent lift case. Since the h ~ 0.012" data was the minimum CCW noise condition, it is presented in the figure. In the range between 1 kHz and 10 kHz, the CCW has noise levels similar to those of the conventional system. Unfortunately, this was not the desired result, although it does provide assurance that using the CCW system does not increase the noise to the environment in its minimum noise configuration.

However, many aircraft have a cut-out in flaps across the span. This difference contributes a fair share of noise to a conventional wing system since flap edge noise has been identified as a major contributor to airframe noise. Thus, this wing was missing a noise source that would most likely be greatly reduced in a CCW system. Since the CCW flap is much smaller, there is no need for a gap in the flap to avoid engine exhaust. Its small size would also in many cases reduce the need for gaps due to structural concerns. Thus the CCW system with a full span flap is not unreasonable.

Acoustic tests were performed on the new configuration similar to the previous tests. Figure 15 shows the comparison of the wing with the cut-out flap with the CCW. As expected, the cut-out in the flap increased the noise on the conventional system significantly and shows a significant advantage to using a CCW system in the region below 10 kHz and some advantage up to 40 kHz. Beyond 40 kHz the two systems have similar noise levels. The data in this figure and following figures have different frequency ranges to emphasize the areas in the frequency

spectrum where there are differences between the two systems. Similar results can be seen at other freestream velocities and angles of attack, however, the magnitude of the difference varies some depending on the conditions.

Up to this point, only data from a microphone at $\Theta = 90°$ has been shown. This is only part of the noise picture, the changes in directivity of the noise between the two systems must be compared as well. Data were acquired at $30°$, $60°$, and $90°$. It should be noted that there are some differences depending on the angle. Note that the $60°$ and $90°$ positions do not actually have a line-of-sight path to the slot exit which is located on the top surface of the wing. It is also worth noting that the jet from the slot leaves the trailing edge of the wing at about $\Theta = 56°$. Even with freestream velocity, the jet stays relatively close to that angle for some time beyond the trailing edge of the wing.

Figure 16 compares the data for the two wing systems at $\Theta = 30°$ and $\Theta = 60°$. At $30°$ the CCW system produces no real advantage over a conventional system. However there is still some noise reduction in favor of the CCW system at $60°$, similar to the $90°$ data shown earlier. These results indicate that a CCW system certainly has potential for reducing airframe noise. The results also show some trends of high-aspect-ratio jets, however there is still much left to study and resolve before all the aspects of the circulation control wing noise issues are solved and helpful to the design of a practical low noise CCW system.

In order to resolve some of the questions brought up by the CCW and to eliminate the possibility of internal noise contamination, a high aspect-ratio nozzle has been designed and fabricated. This nozzle is presently being tested by the authors in an anechoic facility and the intent is to produce a database of quality high aspect-ratio jet noise data that can be used to verify the speculations about internal noise in the experiments presented here. In addition this data will

be used to augment the present results by demonstrating the even greater benefits possible for a CCW high lift configuration in reducing airframe noise.

## Conclusions

Due to the great interest in reducing aircraft noise, an innovative concept for eliminating a conventional flap system has been tested for its possible acoustic advantages. Previous studies have shown that the circulation control wing is an aerodynamically viable alternate for conventional mechanical flaps. This study shows that there is also a substantial advantage in the acoustic realm. The results presented showed a lower noise spectrum for a CCW system compared to a conventional system for the same lifting condition. It should be noted that even if the CCW produces noise comparable to that of a conventional wing it is an advantage. This is because a CCW is expected to be much lighter than a conventional wing.

It was also noted that the internal noise of the CCW blowing system of the model inhibited finding the full possible advantage a CCW system can offer. It is believed that careful design of a CCW blowing system, including internal details, could further improve the results shown here.

Tests are also ongoing on a very high aspect ratio nozzle to verify the characteristics and scaling of high aspect ratio rectangular nozzles similar to what is found in a CCW blowing slot. These results will provide a greater understanding of this type of jet.

## Acknowledgments

# APPENDIX A

## References

1. Englar, Robert J., "Cicrulation Control Pneumatic Aerodynamics: Blown Force and Moment Augmentation and Modification;, Past, Present & Future." AIAA Paper 2000-2541, Fluids Conference, Denver, CO, June, 2000.

2. Salikuddin, M. Brown, W.H., and Ahuja, K.K. "Noise from a Circulation Control Wing with Upper Surface Blowing," Journal of Aircraft, Vol. 24 No. 1, January, 1987.

3. Liu, Yi, Sankar, Lakshmi N., Englar, Robert J., Ahuja, Krishan K. "Numerical Simulations of the Steady and Unsteady Aerodynamic Characteristics of a Circulation Control Wing." AIAA paper 2001-0704. January, 2001.

4. Dunham, J. "A theory of circulation Control by Slot-Blowing Applied to a Circular Cylinder," Journal of Fluid Mechanics, Vol. 33 Part 3, pp 495-514, 1968

5. Englar, Robert J., Applegate, Constance A. "Circulation control - A Bibliograhpy of DTNSRDC Research and Selected Outside References: January 1969 through December 1983," David W. Taylor Naval Ship Research and Development Center, DTNSRDC-84/052, 1984

# APPENDIX A

6. Englar, Robert J., Smith, Marilyn J, Kelley, Sean M. and Rover, Richard C., III. "Development of Circualtion Control Technology for Application to Advanced Subsonic Transport Aircraft," AIAA Paper 93-0644, presented at AIAA Aerospace Sciences Meeting, January, 1993.

7. Englar, R.J. and Huson, G.G. "Development of Advanced Circulation Control Wing High Lift Airfoils," AIAA paper 83-1847, presented at AIAA Applied Aerodynamics Conference, July, 1983.

8. Englar, Robert J. "Low-Speed Aerodynamic Characteristics of a Small, Fixed Trailing-Edge Circulation Control Wing Configuration Fitted to a Supercritical Airfoil," David W. Taylor Naval Ship Research and Development Center, DTNSRDC/ASED-81/08, March 1981.

9. Nichols, J.H. Jr, Englar, R.J., Harris, M. J., Huson, G.G. "Experimental Development of an Advanced Circulation Control Wing System for Navy STOL Aircraft," AIAA paper 81-0151, presented at AIAA Aerospace Sciences Meeting, January, 1981..

10. Pugliese, A. J., and Englar, R. J. "Flight Testing the Circulation Control Wing," AIAA paper 79-1791, presented at AIAA Aircraft Systems and Technology Meeting, New York, August, 1979.

11. Nichols, J.H., Jr. et al. "Development of High Lift Devices for Application to Advanced Navy Aircraft," Report DTNSRDC-80/058, AD A084-226, April, 1980.

12. Lane, Paul Jr. "Ground Controls," Racecar Engineering, Vol. 9 No. 8, pp 20-23, October 1999.

13. Reader, Kenneth R. "Hover Evaluation of the Circulation Control High Speed Rotor," David W. Taylor Naval Ship Research and Development Center, Report 77-0034, June 1977

# APPENDIX A

14. Ahuja, K.K., Tanna, H.K., and Tester, B.J. "An experimental Study of Transmission, Reflection and Scattering of Sound in A Free Jet Flight Simulation Facility and Comparison with Theory," Journal of Sound and Vibration, 75 (1), pp 51-85, 1981

15. Ahuja, K. K., Tester, B. J., and Tanna, H. K., "The Free Jet as a Simulator of forward Velocity Effects on Jet Noise." NASA Contractor Report # 3056, 1978.

16. Ahuja, K.K., and Bushell, K.W. "An Experimental Study of Subsonic Jet Noise and Comparison with Theory," Journal of Sound and Vibration, 30 (3), pp 317-341. 1973..

17. Tam, C.K.W. and Zaman, K.B.M.Q., "Supsonic Jet Noise from Non-Axisymmetric and Tabbed Nozzles." AIAA Paper 99-0077, 1999.

18. Tam, Christopher K.W., Auriault, Laurent, "Jet Mixing Noise from Fine Scale Turbulence." AIAA Paper 98-2354, 1998.

19. Tam, C.K.W., Golebiowski, M. and Seiner, J.M., "On the Two components of turbulent Mixing Noise from Supersonic Jets." AIAA Paper 96-1716, 1996.

20. Tam, Christopher K.W., "Influence of Nozzle Geometry on the Noise of High Speed Jets." AIAA paper 98-2255, 1998.

21. Ahuja, K.K. "Correlation and Prediction of Jet Noise," Journal of Sound and Vibration, 29 (2), pp 155-168, 1973.

# APPENDIX A

POSSIBLE LEADING EDGE BLOWING

TANGENTIAL BLOWING OVER ROUNDED TRAILING EDGE SURFACE

PRESSURE/CENTRIFUGAL FORCE BALANCE

SLOT

JET SHEET
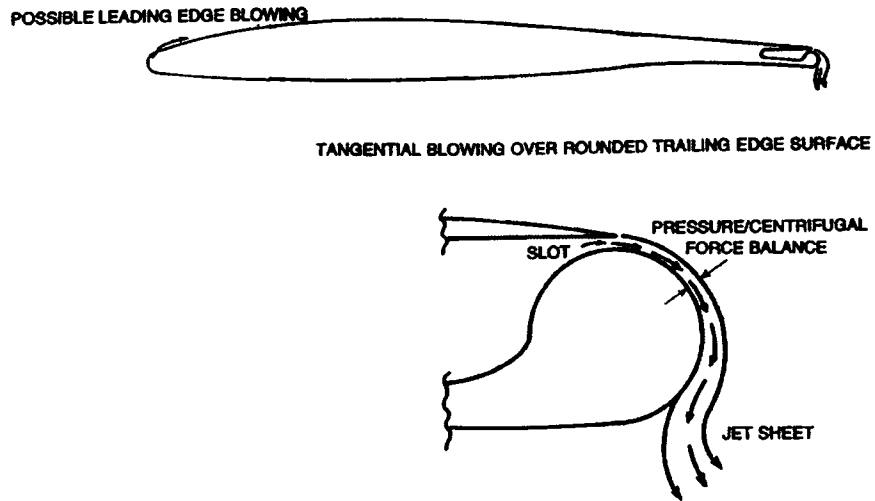
Figure 1: Schematic circulation control wing concept.
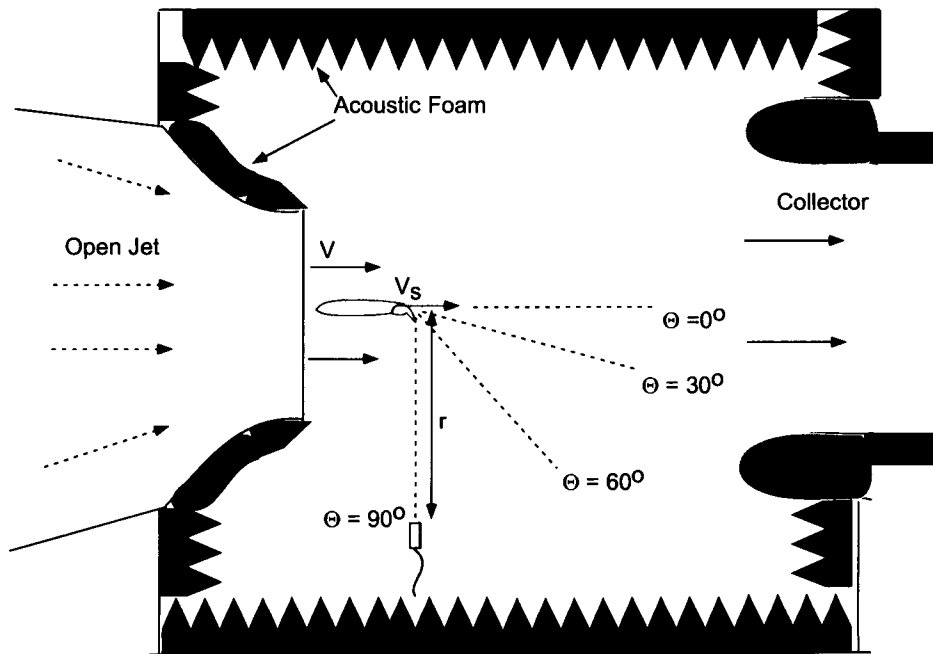
Figure 2: Schematic of Anechoic Flight Simulation Facility (AFSF).
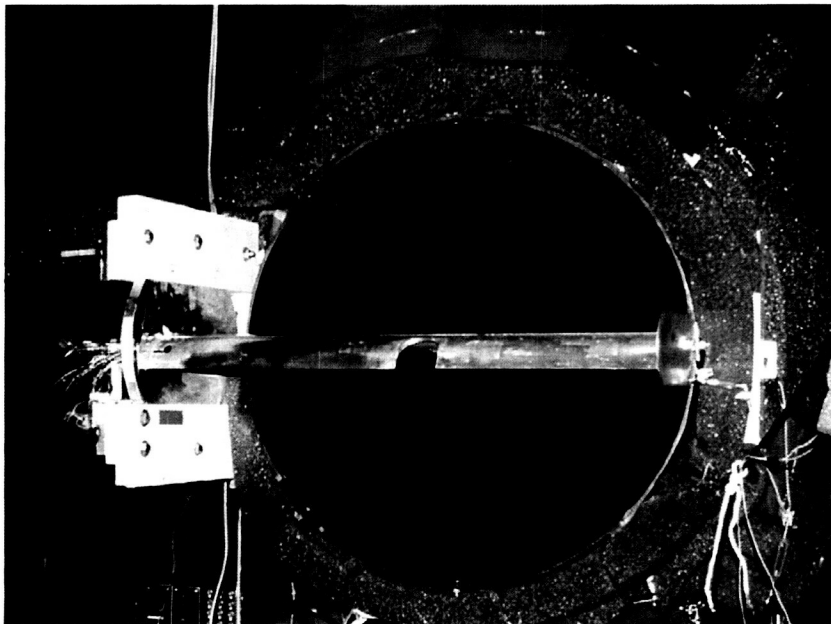
Figure 3: Photo of a conventional wing mounted in AFSF.
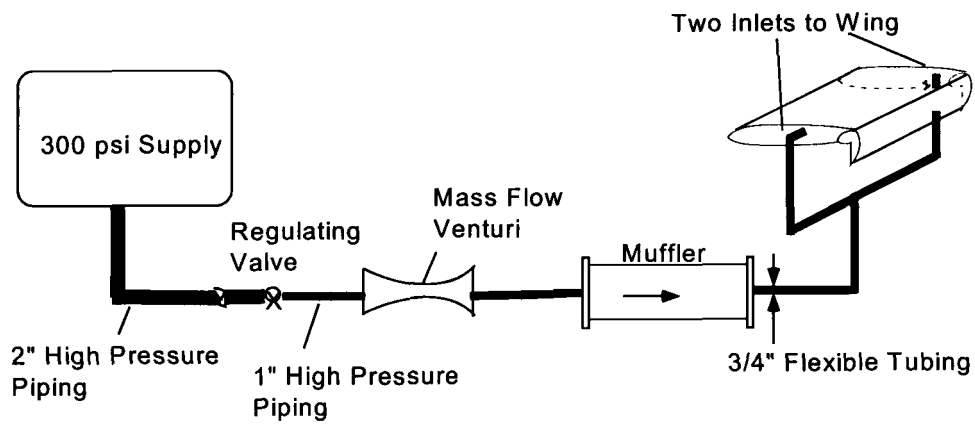
Figure 4:  CCW blowing system configuration.
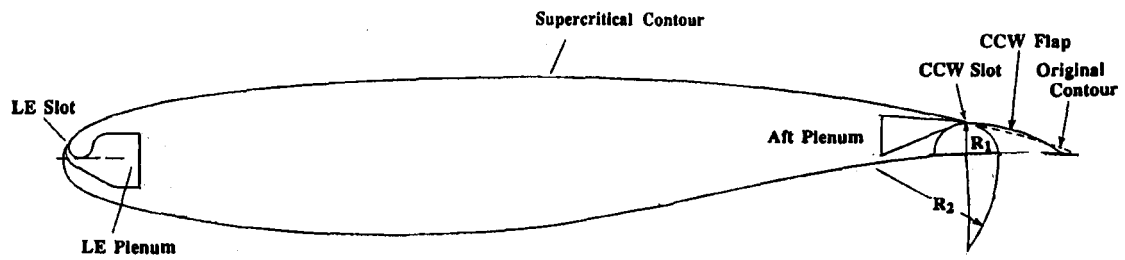
Figure 5: Schematic of CCW flap-wing configuration, generic supercritical airfoil shape..

17 % Thick Supercritical Airfoil

Flap Cove

Flow-Thru Gap

Stored Flap

Actuators

Tracks

Single-Slotted Fowler Flap

(a)

c = 8.0 "

3"

Mounting plate

2"

30"

(b)
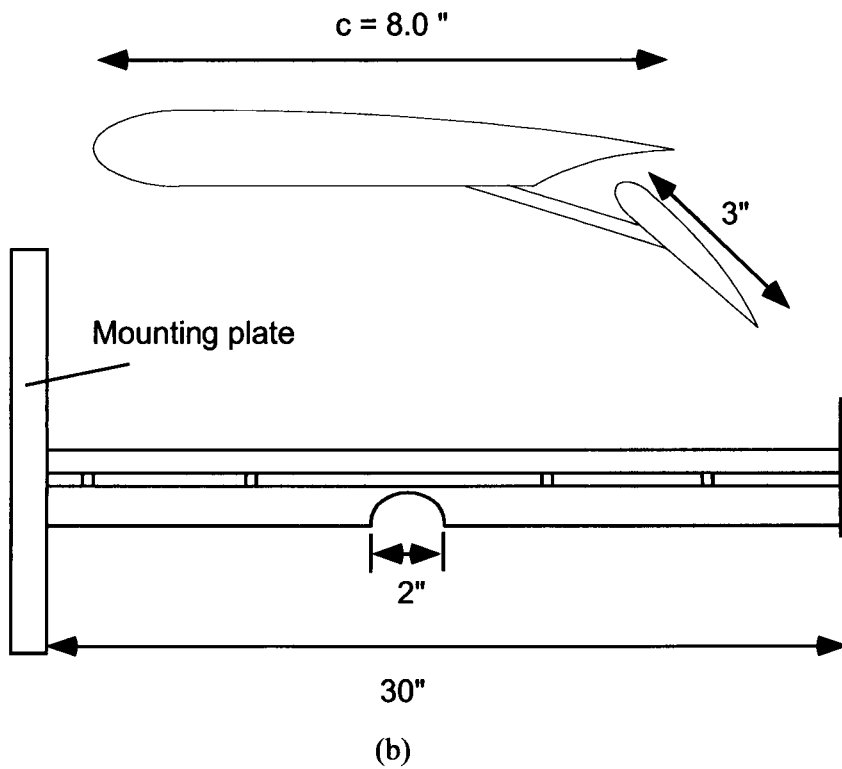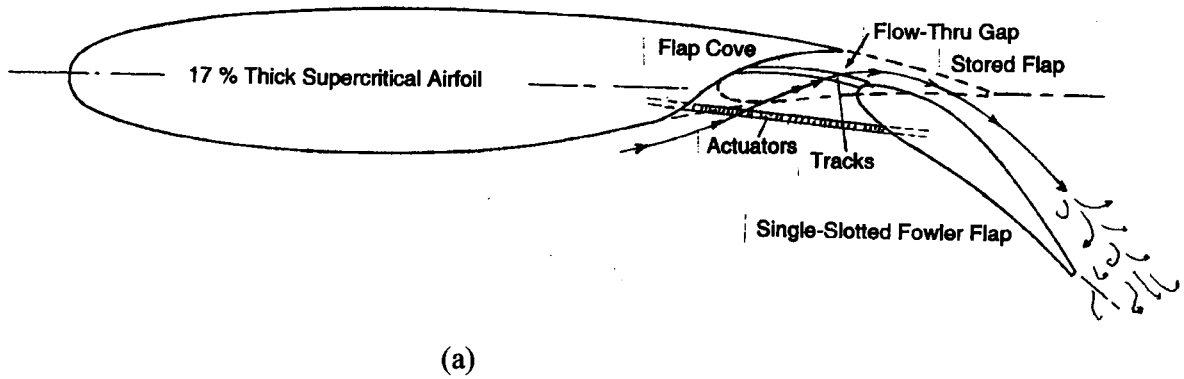
Figure 6: (a) Schematic of conventional flap-wing configuration, generic supercritical airfoil shape (b) Drawing of conventional wing with flap with cut-out.
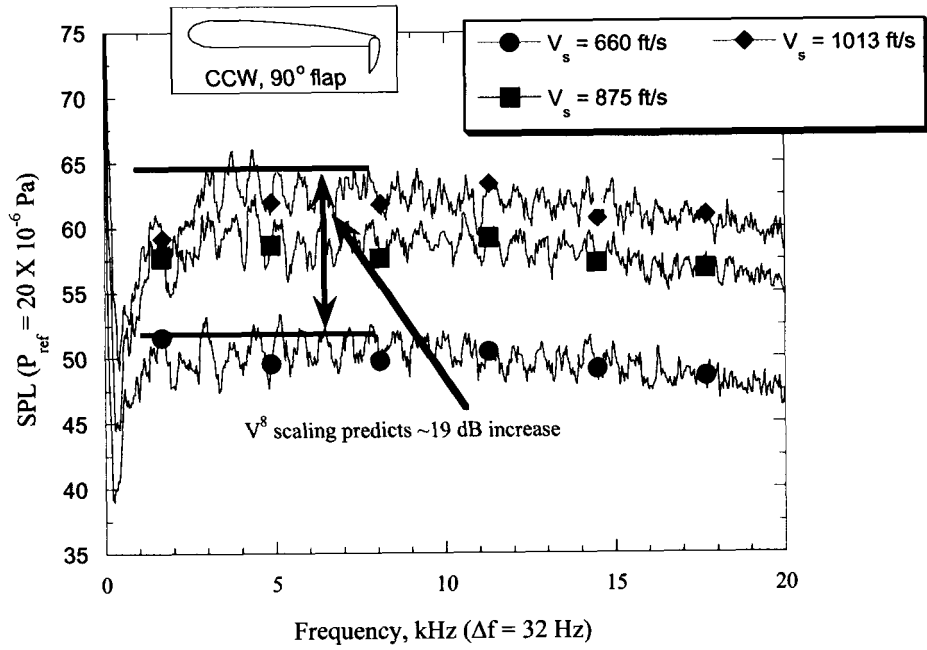
Figure 7: CCW blowing system noise spectra with no freestream flow.
$V_T = 0$ ft/s, h = 0.006"
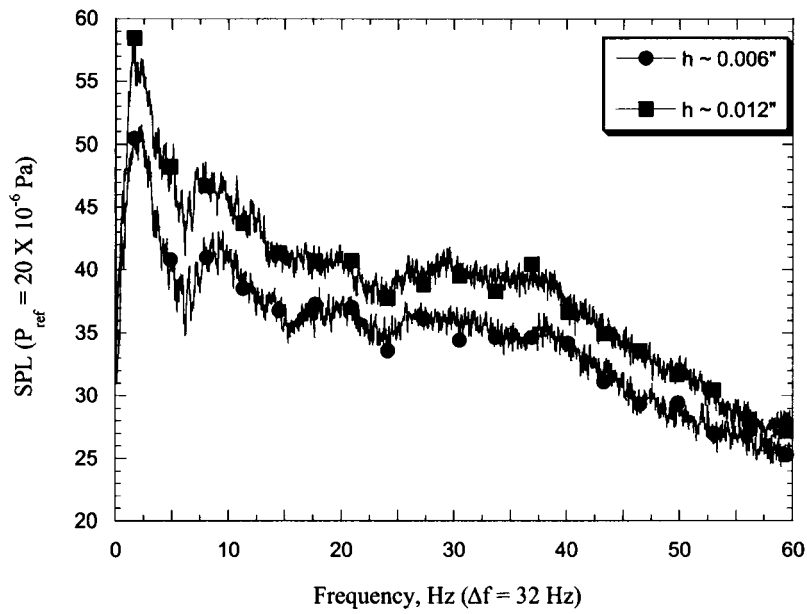
Figure 8: SPL of CCW with different h and the same $V_s$.
$\Theta = 90^\circ$, $V_s = 660$ ft/s, $V_T = 0$ ft/s.

(a)



(b)
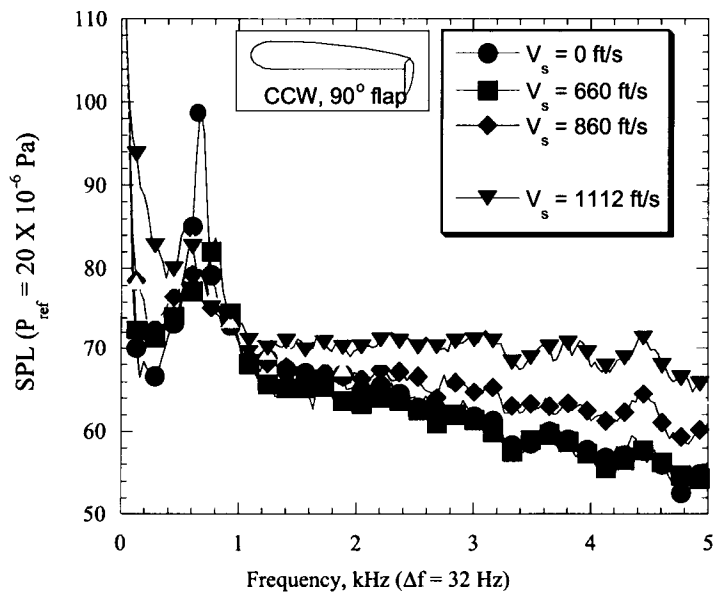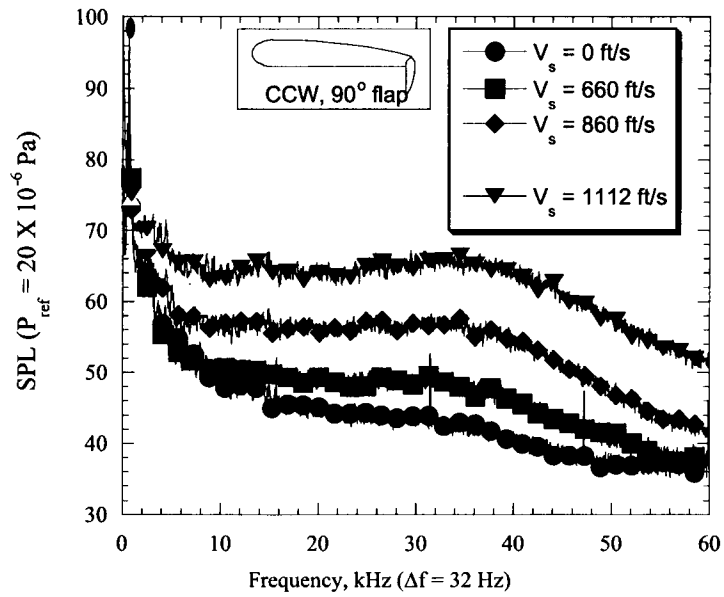
Figure 9: CCW with 90° flap and freestream velocity,
$\Theta = 90°$, $V_T = 220$ ft/s, (a) f = 0 – 60 kHz, (b) f = 0 – 5 kHz.
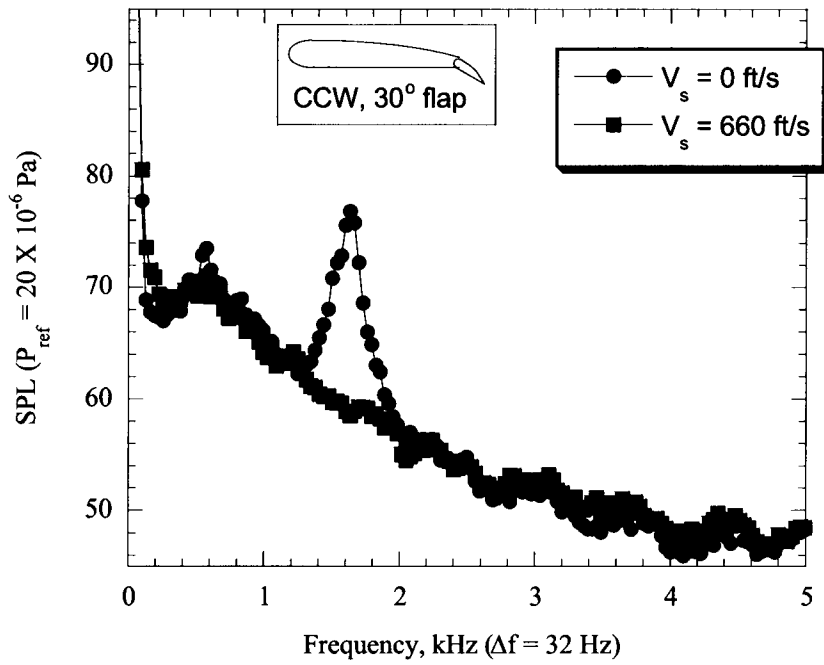
Figure 10: CCW with 30° flap and freestream velocity,
$\Theta = 90°$, $V_T = 220$ ft/s, f = 0 – 5 kHz.
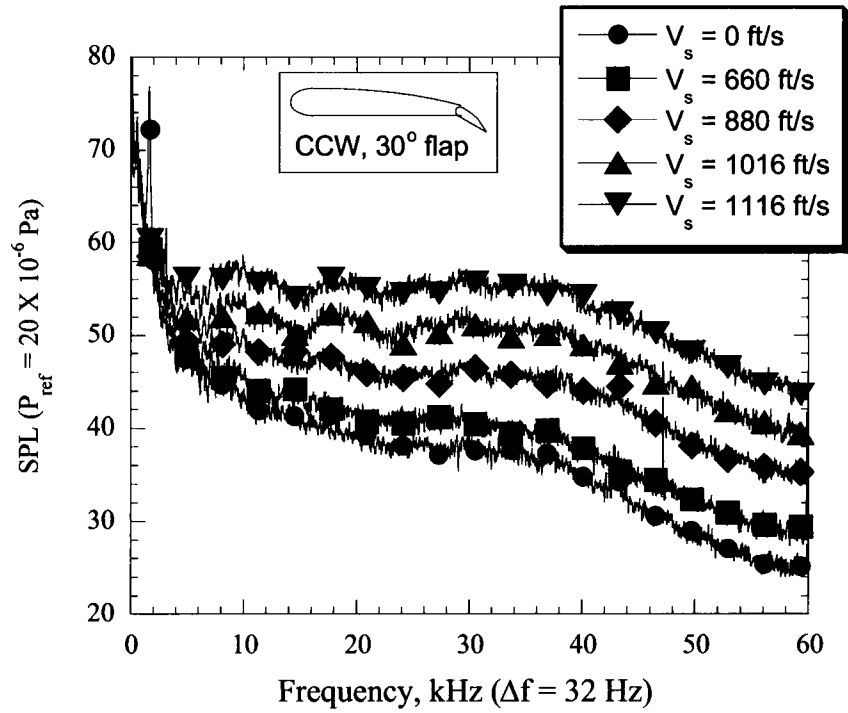
Figure 11: CCW with 30° flap and freestream velocity,
$\Theta = 90°$, $V_T = 220$ ft/s, f = 0 – 60 kHz.

Figure 12: CCW with 30° flap at 3 different h, $C_\mu = 0.04$,
$\Theta = 90°$, $V_T = 220$ ft/s, f = 0 – 60 kHz.

**APPENDIX A**
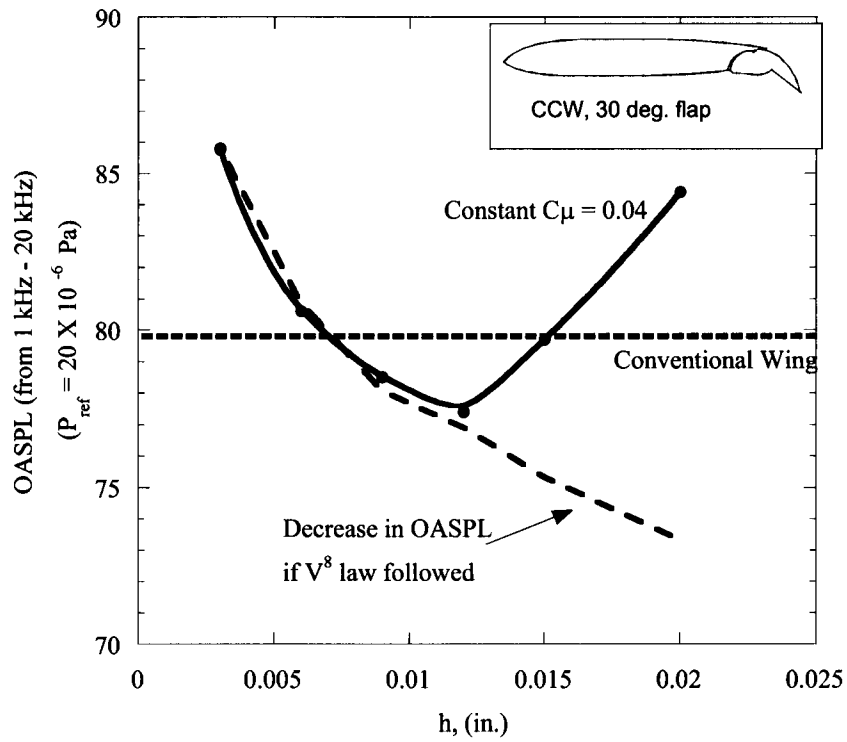


Figure 13:  OASPL for various $C_\mu$ = constant
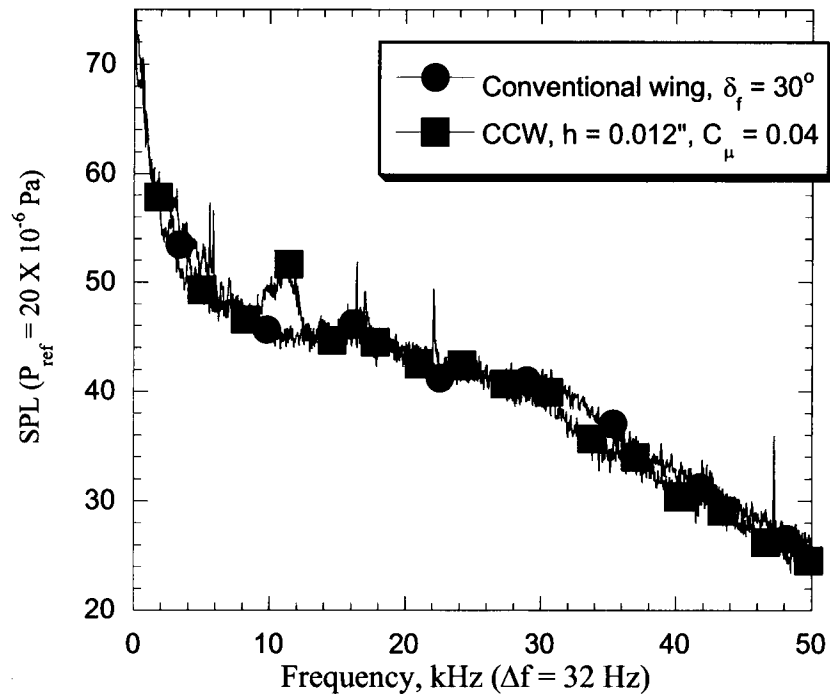
Figure 14: CCW and conventional wing 2-d flap at similar lift condition.
$\Theta = 90°$, $V_T = 220$ ft/s

Figure 15: CCW and conventional wing with cut-out at similar lift condition.
$\Theta = 90°$, $V_T = 220$ ft/s
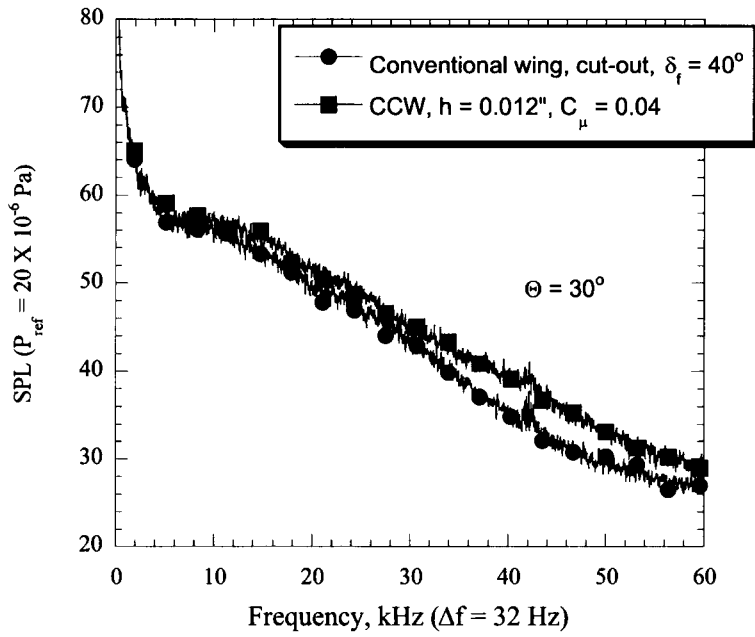
(a)
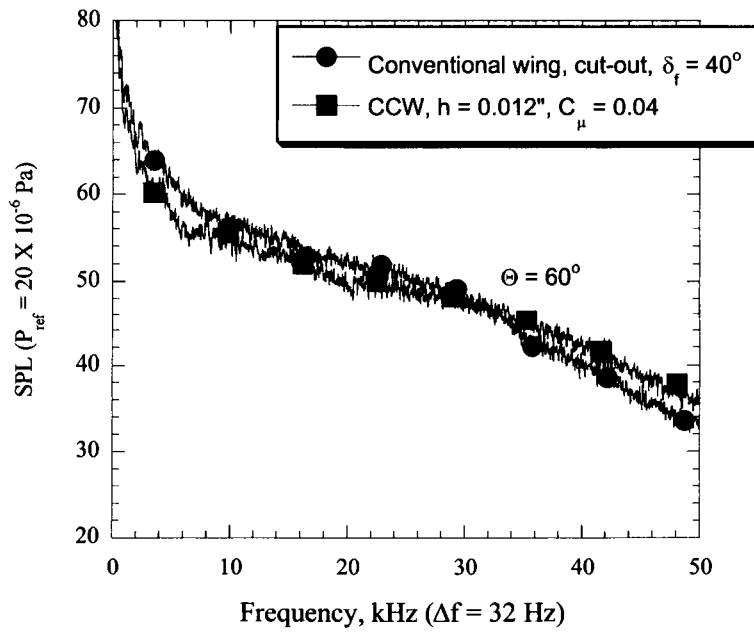


(a)

Figure 16: CCW and conventional wing with cut-out at similar lift condition. $V_T = 220$ ft/s, (a) $\Theta = 30°$, (b) $\Theta = 60°$.

# APPENDIX B


# Numerical Simulations of the Steady and Unsteady Aerodynamic Characteristics of a Circulation Control Wing Airfoil

# APPENDIX B

# Numerical Simulations of the Steady and Unsteady Aerodynamic Characteristics of a Circulation Control Wing Airfoil

Yi Liu, Lakshmi N. Sankar, Robert J. Englar, Krishan K. Ahuja
Georgia Institute of Technology, Atlanta, GA 30332-0150

## ABSTRACT

The aerodynamic characteristics of a Circulation Control Wing (CCW) airfoil have been numerically investigated, and comparisons with experimental data have been made. The configuration chosen was a supercritical airfoil with a 30 degree dual-radius CCW flap. Steady and pulsed jet calculations were performed. It was found that the use of steady jets, even at very small mass flow rates, yielded a lift coefficient that is comparable or superior to conventional high-lift systems. The attached flow over the flap also gave rise to lower drag coefficients, and high L/D ratios. Pulsed jets with a 50% duty cycle were also studied. It was found that they were effective in generating lift at lower reduced mass flow rates compared to a steady jet, provided the pulse frequency was sufficiently high. This benefit was attributable to the fact that the momentum coefficient of the pulsed jet, during the portions of the cycle when the jet was on, was typically twice as much as that of a steady jet.

## NOMENCLATURE

| | |
|---|---|
| $A_{jet}$ | = Area of Jet Slot |
| C | = Chord of Airfoil |
| $C_L$ | = Lift Coefficients, L/qS |
| $C_D$ | = Drag Coefficients, D/qS |
| $C_\mu$ | = Momentum Coefficient |
| $C_{\mu 0}$ | = Average Momentum Coefficient for Pulsed Jet |
| D | = Drag of the Wing |
| f | = Pulsed Jet Frequency |
| L | = Lift of the Wing |
| $\dot{m}$ | = Mass Flow Rate of Jet Blowing, slugs/sec |

| | |
|---|---|
| P | = Pressure |
| q | = Dynamic Pressure |
| S | = Area of the Wing |
| $V_\infty$ | = Free Stream Velocity |
| $V_{jet}$ | = Jet Blowing Velocity |
| $\rho_\infty$ | = Free Stream Density |
| $\rho_{jet}$ | = Jet Blowing Density |

## INTRODUCTION

In recent years, there has been an increasing demand for very large aircraft. At the same time, stringent restrictions on aircraft noise are being proposed by international aviation agencies. Noise pollution from the aircraft, especially around the airport, has becomes a major problem that needs to be solved. Airline operators, aircraft manufacturers, NASA, and FAA have all made noise reduction a priority.

These large aircraft will require sophisticated high-lift systems in order to use existing runways. A major source of airframe noise during take-off and landing is expected to be the high-lift system — namely the flaps, slats, and the flap-edges and gaps. These high-lift systems add to the weight of the aircraft, and are also costly to build and maintain.

An alternative to conventional high-lift systems is Circulation Control Wing technology. This technology and it aerodynamic benefits has been investigated over many years through experiment work[1,2] and numerical analyses[2,3,4]. A limited amount of work has also been done on the acoustic characteristics of Circulation Control Wings[5].

From these studies, it is known that very high $C_L$ values (as high as 8.5 at $\alpha$=0°) may be achieved with CCW airfoils. Because many mechanical components associated with high-lift systems are no longer needed, the wings can be lighter and less expensive to build. Major airframe noise sources, such as flap-edge noise, flap-gap noise, and flow-separation noise can all be eliminated with the use of CCW systems.

In view of the potential of CCW configurations, a coordinated research effort is underway at Georgia Tech involving wind tunnel tests, aeroacoustic tests, and CFD modeling. One of the goals of this research is to compare the aerodynamic and acoustic characteristics of a CCW configuration to that of a conventional high-lift system. A systematic study is also being done on the effects of slot size and placement on the wing lift, drag and noise characteristics. A third goal of this effort is to explore the use of pulsed jets for lift enhancement on CCW airfoils. A supercritical airfoil with a simple hinged dual-radius CCW flap shown in Figure 1 is used in much of this research. From existing experimental data[2], it is known that this CCW hinged flap design with lower flap angle of 30° can maintain most of the Circulation Control high lift advantages, while greatly reducing the drag that arises from

CCW airfoils with a rounded trailing edge and/or larger flap angles.

This paper is limited to the exploration of Circulation Control characteristics of the airfoil shown in figure 1. Two-dimensional study has been done, and preliminary comparisons with experimental data are presented. Preliminary unsteady simulations have also been done to understand the stall and vortex shedding characteristics of the wing/airfoil at high angles of attack and low levels of blowing. Companion studies for a 3-D finite wing may be found in Ref. 6.

## MATHEMATICAL AND NUMERICAL FORMULATION

### Computational Grid

A hyperbolic three-dimensional C-H grid generator is used in all the calculations. The three-dimensional grid is constructed from a series of two-dimensional C-grids with an H-type topology in the spanwise direction. The grid is clustered in the vicinity of the jet slot and the trailing edge to accurately capture the jet behavior over the airfoil surface.

### Unsteady Navier-Stokes Solver

An Unsteady three-dimensional compressible Navier-Stokes solver is being used. The solver can model the flowfield over isolated wing-alone configurations. Both 3-D finite wings and 2-D airfoils may be simulated with the same solver.

The grid generation and the surface boundary condition routines are general enough so that one can easily vary the slot location, slot size, blowing velocity and direction of blowing. The effects of turbulence are modeled using either a Baldwin-Lomax eddy viscosity model, or a Spalart-Allmaras one–equation model. For a detailed discussion of the numerical solution procedure and the turbulence model, the reader is referred to Ref. 7.

### Jet Boundary Conditions

In Circulation Control Wing studies, the driving parameter is the momentum coefficient, $C_\mu$, defined as follows.

$$C_\mu = \frac{V_{jet} * \dot{m}}{S * \frac{1}{2}\rho_\infty V_\infty^2}$$

(1)

Here, the jet mass flow rate is given by:

$$\dot{m} = \rho_{jet} V_{jet} * A_{jet}$$

(2)

In the present study, the jet is subsonic, and the following boundary conditions are specified at the slot exit: the total temperature of the jet, the momentum coefficient $C_\mu$ as a function of time, and the flow angle at the exit. In this simulation, the jet was tangential to the airfoil surface at

the exit. All other parameters were computed using ideal gas law, and through an extrapolation of the Riemann variables (carried by upstream traveling acoustic waves) that enter the subsonic jet slot from the exterior. It may be noted that in the experiment, the flow conditions were such that the exit static pressure at the slot equals the ambient static pressure.

## RESULTS AND DISCUSSION

The initial studies were for a 2-D configuration to understand the high-lift, stall, and vortex shedding characteristics of the airfoil with and without blowing. Some comparisons have been made between the CFD results and the measured data. In parallel with this study, a finite aspect ratio wing was also analyzed to determine its $C_{Lmax}$ with and without Circulation Control. Figure 1 shows the configuration studied. The CCW flap setting may be varied both in the experiments and the simulations. The studies presented here are all for the 30 degree flap setting.

In these studies, the free stream velocity was approximately 94.3 ft/sec at a dynamic pressure of 10 psf and an ambient pressure of 14.2 psia. The free stream density is about 0.00225 slugs/ft$^3$. These conditions translate into a free stream Mach number 0.0836 and a Reynolds Number of $3.95*10^5$, and were chosen to match the experiments done by Englar et al (Ref. 2).

### Steady Jet Results:

Figure 2a shows the computed $C_l$ vs. $\alpha$ curve, for a number of $C_\mu$ values. The calculations correctly reproduce the decrease in the stall angle observed in the experiments at high momentum coefficients, attributable to leading edge stall (Englar, unpublished results). Figure 2b shows the variation of $C_L$ with respect to $C_\mu$ at a fixed angle of attack ($\alpha=0$ degrees). Excellent agreement with measured data from Reference 2 is evident.

These simulations also give some insight into the physics of the flow. For example, consider a typical case at $\alpha = 0°$. Without any blowing, trailing edge separation and vortex shedding occurred and the lift coefficient varied from 0.768 to 0.854. The measured data had an average of 0.878. When Circulation Control was applied with a $C_\mu$ of 0.1657, the 2-D lift coefficient increased to a value of 3.07. This is in excellent (less than 1%) agreement with the measured value of 3.097. As will be discussed below, these values can be attained in conventional wings only with the use of complex flaps, which would considerably increase the mechanical complexity and weight of the wing. For comparison, a 30° Fowler flap on this same airfoil experimentally yielded $C_L =1.8$ at $\alpha = 0°$.

Figure 3 shows the lift coefficient variation with time. It is seen that the variation is periodic with a dimensional frequency around 400Hz for the flow conditions stated earlier. Figure 4 shows the streamlines around the airfoil for the blown and unblown cases. At a

typical instance in time, it is clearly seen that the trailing-edge vortex shedding, a potential source of noise, has been eliminated by Circulation Control.

<u>Pulsed Jet Studies</u>

During the past five years, there has been increased interest in the use of pulsed jets, and "massless" synthetic jets for flow control and performance enhancement. Wygnansky et al.[8, 9], Lorber et al.[10], and Wake et al[11] have studied the use of directed synthetic jets for static separation and dynamic stall alleviation. Hassan[12] has studied the use of synthetic jets placed on the upper and lower surfaces of an airfoil surface as a way of achieving desired changes in lift and drag, offsetting vibratory airloads that otherwise would occur during blade-vortex interactions. Pulsed jets and synthetic jets have also been used to effect mixing enhancement, thrust vectoring, and bluff body flow separation control. Pulsed blowing of blown flap configurations has also been investigated experimentally (Ref. 13). A combined CFD, experimental aerodynamics, and aeroacoustics study has been initiated at Georgia tech to understand and explore this very promising technology.

The present computational studies were aimed at answering the following questions: Can pulsed jets be used to achieve desired increases in the lift coefficient at lower mass flow rates relative to a steady jet? What are the effects of the pulsed jet frequency on the lift enhancement, for a given time-averaged $C_\mu$? What is the optimum wave shape for the pulsed jet, i.e. how should it vary with time?

In the calculations below, the mean flow angle was set at zero, and the dual-radius CCW flap angle was fixed at 30 degree. The free stream Mach number, slot height, chordwise location of the slot, and angle of attack were all, likewise, held fixed. The pulsed jet characteristics are defined by the instantaneous momentum coefficient $C_\mu$, which varies with time as follows:

$$C_\mu(t) = C_{\mu,0} + C_{\mu,0}F(f,t)$$

(3)

A set of preliminary calculations were done using a sinusoidal function form - F(t) equal to cos(2πft). It was found that this was not an effective wave shape to use. The computed $C_l$ values simply oscillated about the mean value, so that the time averaged $C_l$ values were no higher than the steady state values achieved with a fixed jet operating at the mean $C_{\mu0}$ value. However, improved results were obtained when the function F(t) was chosen to be a square shape wave form with a 50% duty cycle. Under this setting, F(t)=1 for half the cycle, and F(t)=-1 for the other half of a cycle, as shown in Figure 5. The frequency "f" indicates the number of times the jet was turned on and off per second. Note that the instantaneous coefficient is thus zero during one half of the cycle, and equals 2 $C_{\mu0}$ during the other half of the cycle, so that the time-averaged value is $C_{\mu0}$.

Figure 6a and 6b show the variation of the time-averaged incremental lift coefficient $\Delta C_l$ over and above the base-line unblown configuration, at three frequencies, 40

Hz, 120 Hz and 400 Hz. These three frequencies correspond to Strouhal numbers f*C/ $V_\infty$ equal to 0.2828, 0.8484 and 2.828 respectively. Figures 7a and 7b show the corresponding behavior of the time-averaged lift-to-drag ratio $C_l/(C_d+C_{\mu0})$. Here, the drag coefficient has been corrected for the u-momentum imparted by the jet into the wake. For comparison, corresponding variations with a steady jet are also shown.

For a given value of $C_\mu$, a steady jet gives a higher value of $\Delta C_l$ compared to a pulsed jet. This is to be expected because the pulsed jet is operational only half the time during each cycle where as the steady jet is continuously on. The benefits of the pulsed jet are more evident in figures 6b. At a given mass flow rate, it is seen that the time-averaged values of lift are higher for the pulsed jet case compared to the steady jet case, especially at higher frequencies. This superior performance of the pulsed jet can be explained as follows. The momentum coefficient is proportional to the square of the jet velocity, where as the mass flow rate is proportional to jet velocity $V_{jet}$. As a consequence, doubling the instantaneous momentum coefficient $C_\mu$ to twice its average value increases the instantaneous mass flow rate only by 40% (1.414 to be exact) compared to a steady jet. The Coanda effect, on the other hand, is dependent on the jet velocity squared, and greatly benefits from these brief increases in the momentum coefficient. This leads to higher lift, compared to a steady jet as seen on figure 6b. The L/D ratio for the steady jet is, however, still better compared to the pulsed jet case as seen on figures 7b, partly because the $C_\mu$ values of the steady jet case with same mass flow rate are lower than the pulsed jet case.

Pulsed jet calculations have also been done at a fixed time averaged value of $C_{\mu0}$ equal to 0.04, while parametrically changing the pulse jet frequency, f. Figure 8 shows these results. It is seen that higher frequencies are, in general, preferred over lower frequencies. Our simulations indicate that the airfoil needs to travel 4 to 6 chord lengths after the jet has been turned off before all the beneficial circulation attributable to the Coanda effect is completely lost. If a new pulse cycle could begin before this occurs, the circulation will almost instantaneously reestablish itself. At high enough pulse frequencies, as a consequence, the pulse jet will have all the benefits of the steady jet at considerably lower mass flow rates.

It should be noted here that $C_\mu$ was varied with time in a square wave at CFD simulation. In practice, it is more convenient to vary the plenum pressure, which controls $C_\mu$, jet velocity and mass flow. If plenum pressure were varied in a square wave form (for pressure values from 0 to two times the average) it is expected that Figure 6a would also show increased $\Delta C_l$ over the steady state value, as shown in Ref. 13.

# APPENDIX B

## CONCLUDING REMARKS

Unsteady Reynolds-averaged Navier-Stokes calculations have been carried out for a supercritical airfoil equipped with a 30-degree dual-radius CCW flap. The predicted values of lift coefficient, when the airfoil is operating using Circulation Control are in excellent agreement with measurements. Calculations have also been done for a pulse jet configuration. It was found that the pulse jet configuration gave larger increments in lift compared to the steady jet, at a given time-averaged mass flow rate. This was attributed the fact that the pulsed jet had larger instantaneous momentum coefficients leading to enhanced Coanda effect. Finally, pulsed jet performance improved at higher pulse frequencies due to the fact that the airfoil had not shed the circulation into the wake before a new pulse cycle began.

While these simulations are very encouraging, additional calculations are needed to further define the optimum placement of slots, and to establish the minimum mass flow rates needed to achieve lift coefficients comparable to conventional high-lift systems. The noise penalty associated with a pulsed jet system must be assessed, and compared to the noise characteristics of conventional high-lift systems. These studies are now in progress.

## REFERENCES

1. Englar, R.J. and Huson, G.G. "Development of Advanced Circulation Control Wing High Lift Airfoils", AIAA Paper 83-1847, presented at AIAA Applied Aerodynamics Conference, July, 1983.

2. Englar, Robert J., Smith, Marilyn J., Kelley, Sean M. and Rover, Richard C. III., "Development of Circulation Control Technology for Application to Advanced subsonic Transport Aircraft", AIAA Paper 93-0644, presented at AIAA Aerospace Sciences Meeting, January, 1993.

3. Shrewsbury, George D., "Analysis of Circulation Control Airfoils using an Implicit Navier-Stokes Solver", AIAA Paper 85-0171, January, 1985.

4. Shrewsbury, G. D., "Dynamic Stall of Circulation Control Airfoils", Ph.D Thesis, Georgia Institute of Technology, November 1990.

5. Salikuddin, M., Brown, W. H. and Ahuja, K. K., "Noise From a Circulation Control Wing with Upper Surface Blowing", Journal of Aircraft, Vol.24, Jan 1987, p55-64.

6. Yi Liu, "Numerical Solution of the Aerodynamic and Aeroacoustic Characteristics of Circulation Control Wings", Ph.D Proposal in preparation.

7. Wake, B.E., "Solution Procedure for the Navier-Stokes Equations Applied to Rotors", Ph.D. Thesis, Georgia Institute of Technology, Atlanta, GA 1987.

8. Seifert, A., Darabi, A. and Wygnanski, I., "Delay of Airfoil Stall by Periodic Excitation", AIAA Journal of Aircraft, Vol. 33, No. 4, 1996.

9. Wygnanski, I, "Some New Observations Affecting the Control of Separation by Periodic Excitation", AIAA 2000-2314, FLUIDS 2000 Conference and Exhibit, Denver, CO, 19-22 June, 2000.

10. Lorber, P.F., McCormick, D., Anderson, T., Wake, B.E., MacMartin, D., Pollack, M., Corke, T., and Breuer, K., "Rotorcraft Retreating Blade-Stall Control," AIAA 2000-2475, FLUIDS 2000 Conference and Exhibit, Denver, CO, 19-22 June, 2000.

11. Brian Wake and Elizabeth A. Lurie, "Computational Evaluation of Directed Synthetic Jets for Dynamic Stall Control," to appear in the American Helicopter Society Annual Forum, 2001.

12. Hassan, A., and Janakiram, R. D., "Effects of Zero-Mass Synthetic Jets on the Aerodynamics of the NACA 0012 Airfoil", Journal of the American helicopter Society, Vol. 43, No. 4, October, 1998.

13. Oyler, T.E. and W.E. Palmer, "Exploratory Investigation of Pulse Blowing for Boundary Layer Control," North American Rockwell Report NR72H-12, January 1972.
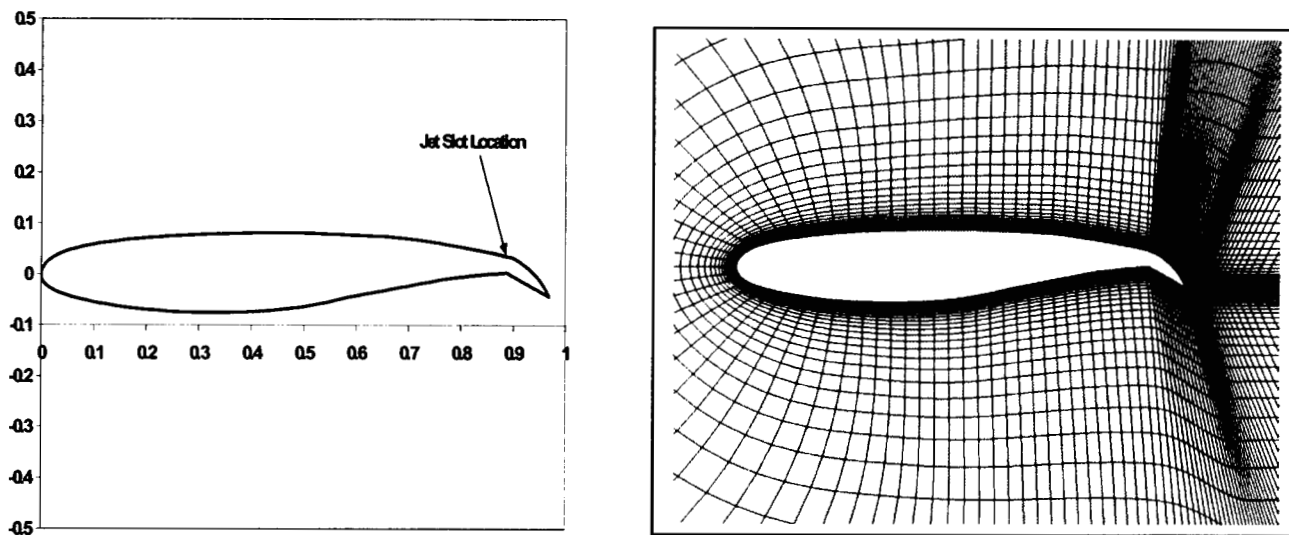
Figure 1. Circulation Control Wing Airfoil (with 30° dual-radius CCW flap) and the Body-Fitted Grid
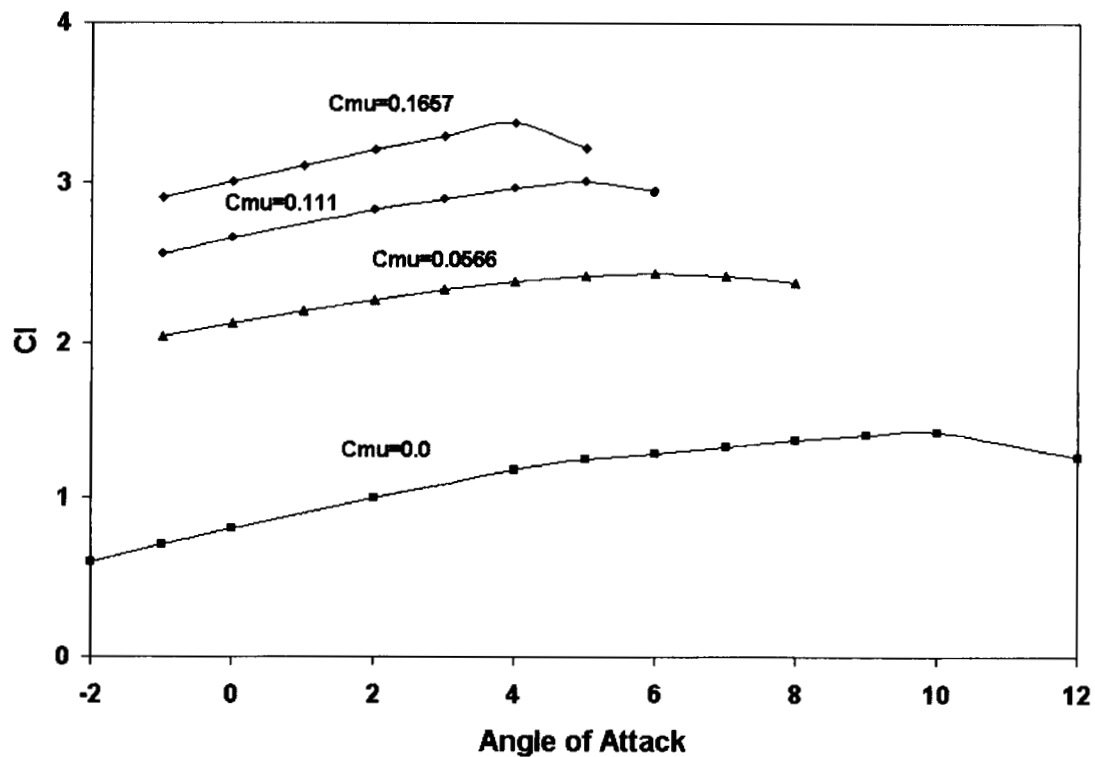


Figure 2a. The CFD-Computed Variation of Lift Coefficient with the Angle of Attack for the 30-degree CCW Flap Case

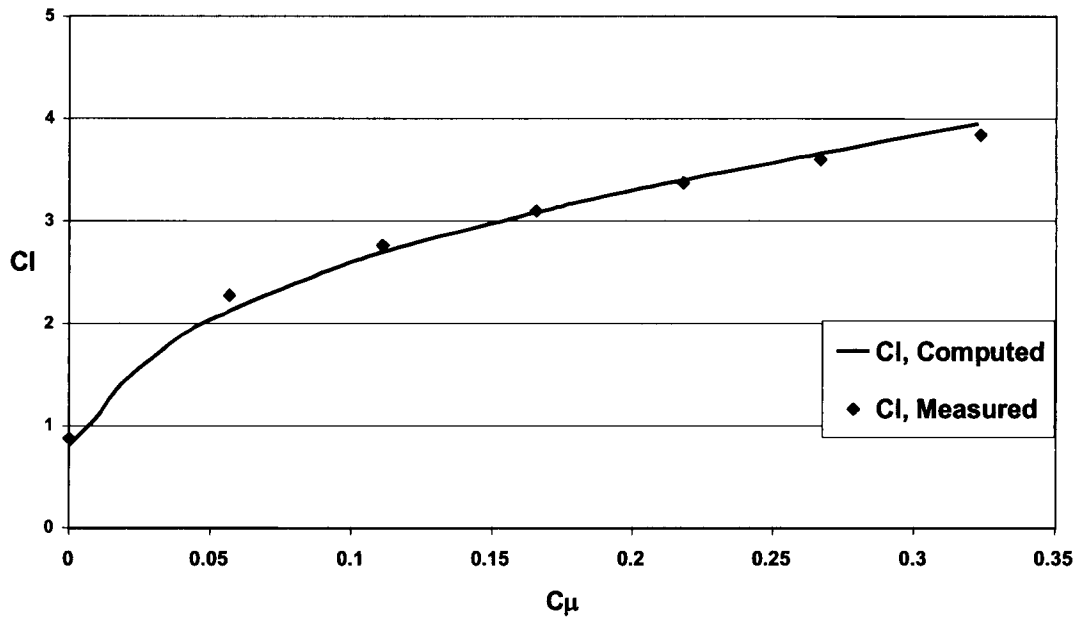**Computed vs. Measured Variations of Lift Coefficient with Momentum Coefficient**



Figure 2b. Variation of the Lift Coefficient with Momentum Coefficient at $\alpha=0°$ and 30° Flap angle (For comparison, a comparable Fowler Flap system with 30-degree flap setting will have a $C_l$ of 1.8)
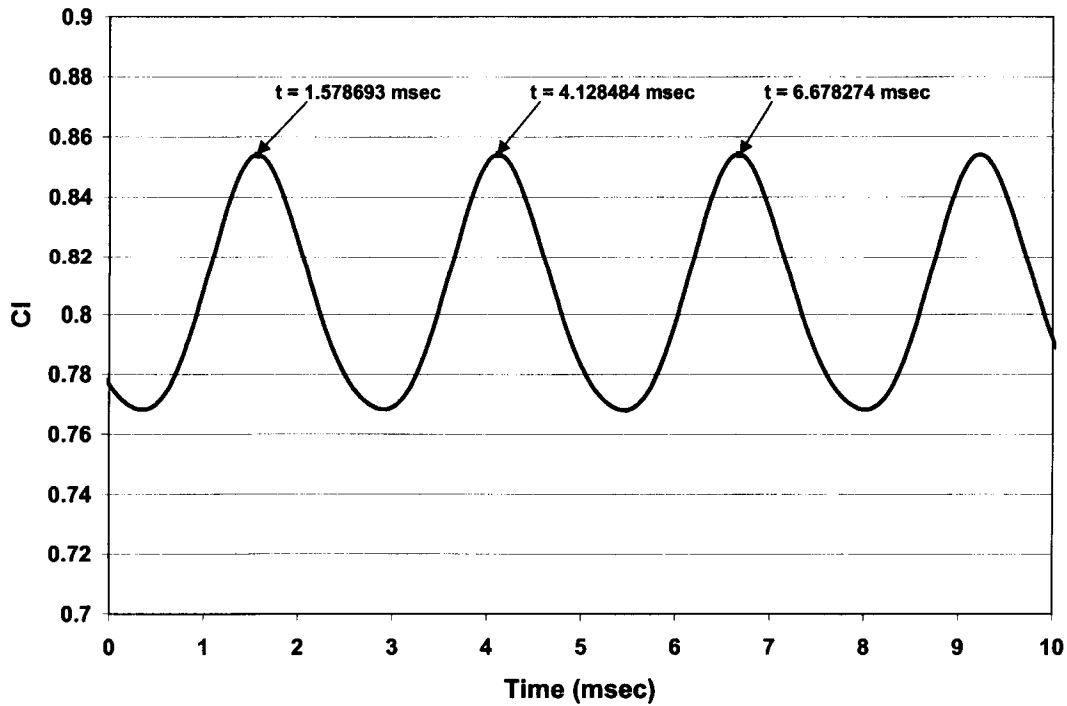


Figure 3. Lift Coefficient Variation with Time for the Unblown Case with a 30-degree Flap Setting (The Shedding Frequency is about 400 Hz)
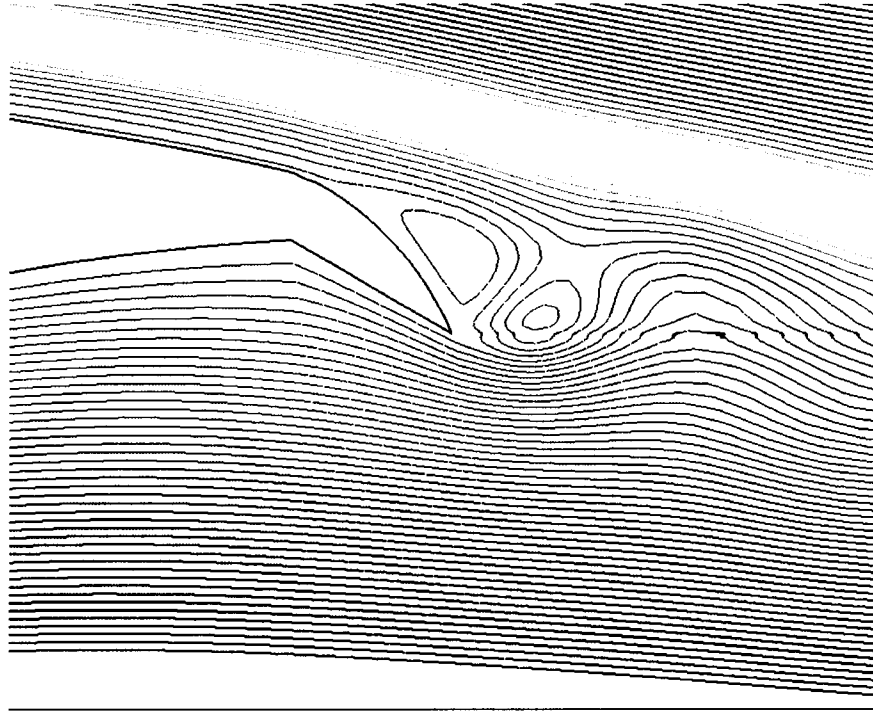
Figure 4a. The Stream Function Contour for the Unblown Case at 30 Degree Flap Setting
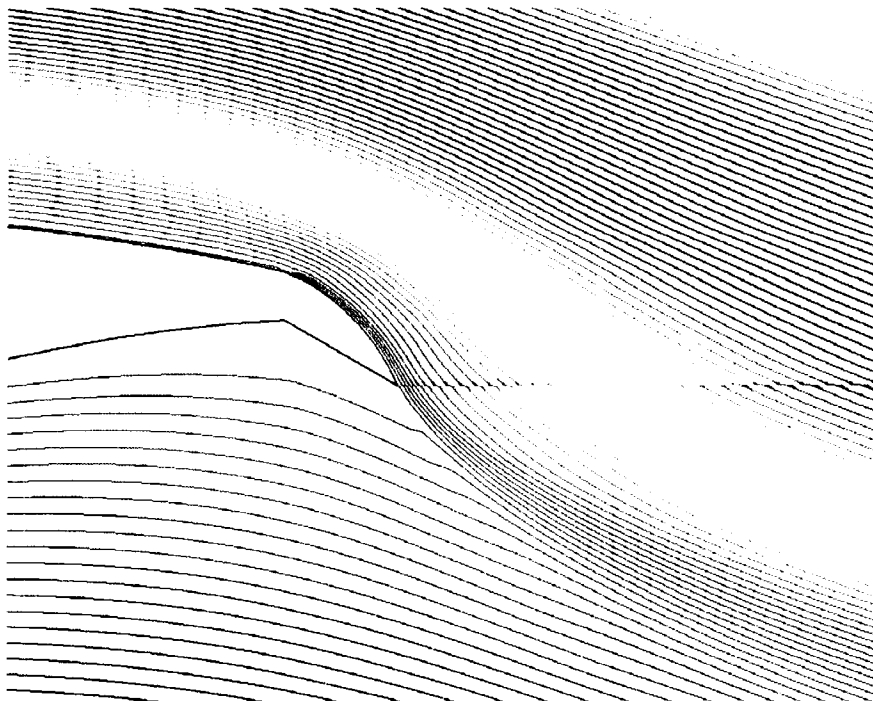
Figure 4b. The Stream Function Contour for the Blowing Case at 30 Degree Flap Setting, $C_\mu=0.1657$

**Momentum Coefficient Variation with Time for Pulsed Jet
Square Wave Form, Frequency = 40 Hz**
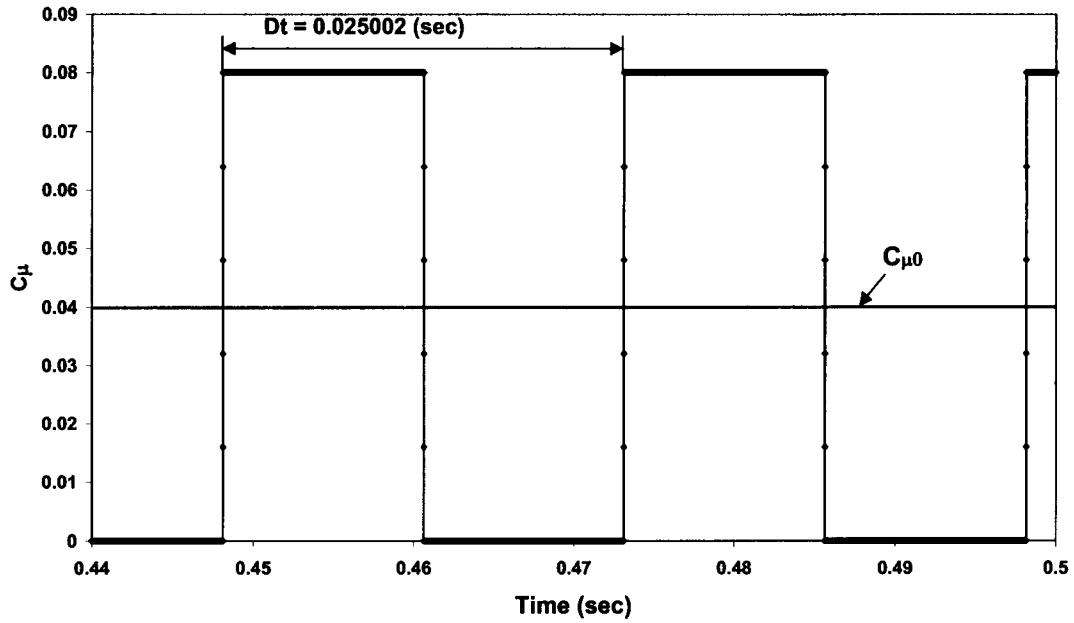


Figure 5. Variation of Momentum Coefficient with Time, Square Wave Form

**Variations of Incremental Lift Coefficient with Time-Averaged Momentum Coefficient
Comparison of Steady Jet with Pulsed Jet**
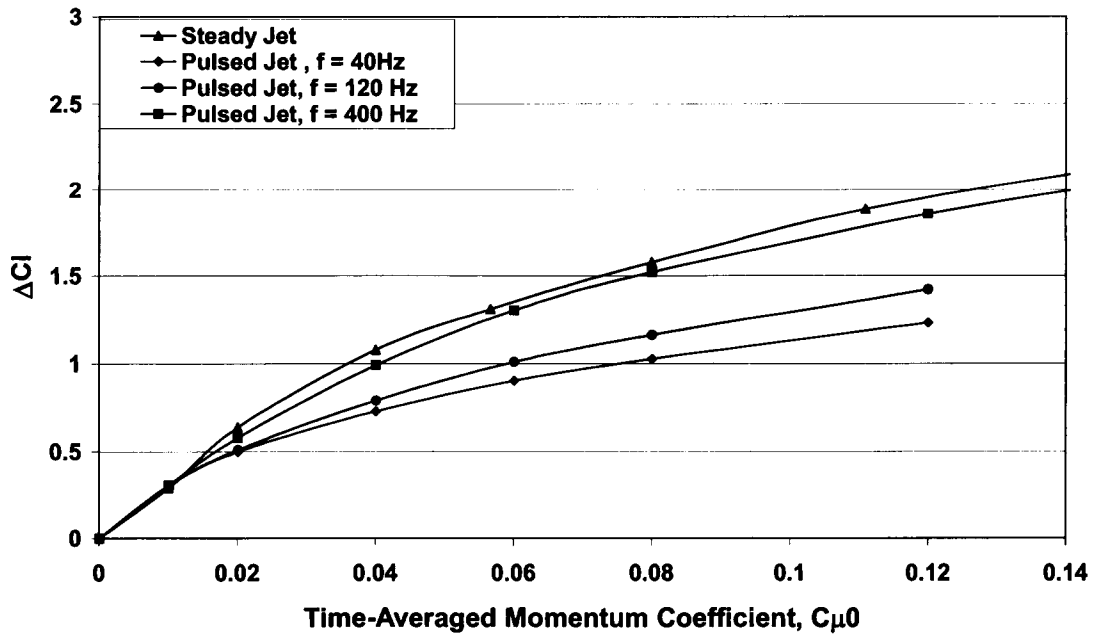


Figure 6a. Variation of Incremental Lift Coefficient with Time-Averaged Momentum Coefficient

**Variations of Incremental Lift Coefficient with Time-Averaged Mass Flow Rate**
**Comparison of Steady Jet with Pulsed Jet**



Figure 6b. Variation of Incremental Lift Coefficient with Time-Averaged Mass Flow Rate

**Variation of Efficiency (Cl/(Cd+Cμ)) with Time-Averaged Momentum Coefficient**
**Comparison of Steady Jet with Pulsed Jet**
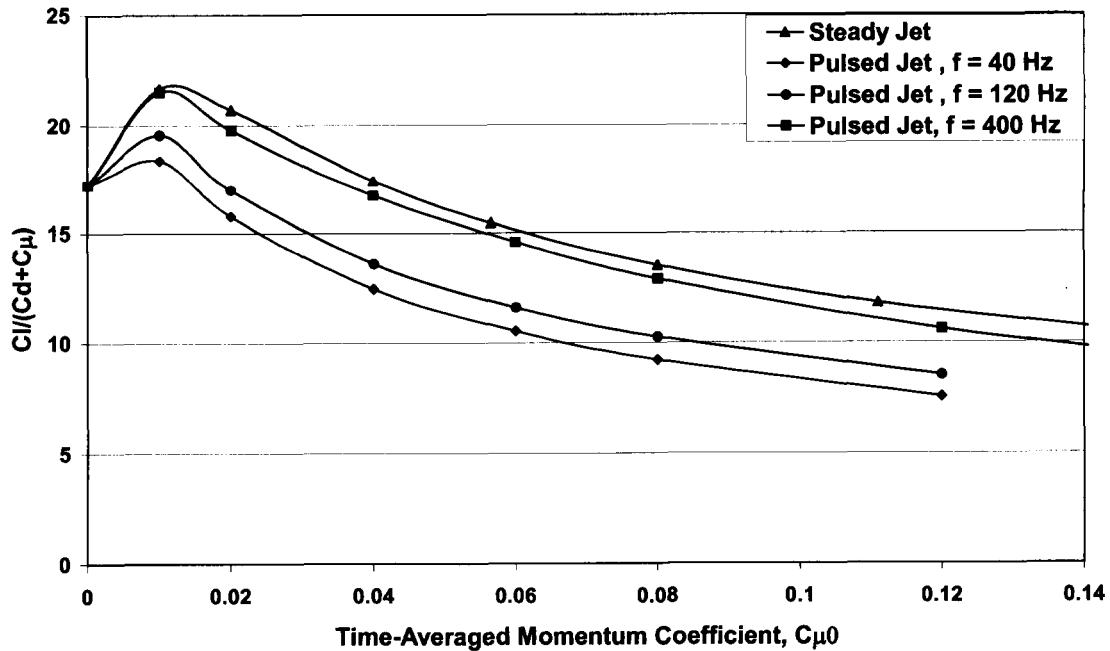


Figure 7a. Variation of Lift-to-Drag Ratio with Time-Averaged Momentum Coefficient

**Variation of Efficiency (Cl/(Cd+Cμ) ) with Time-Averaged Mass Flow Rate**
**Comparison of Steady Jet with Pulsed Jet**



Figure 7b. Variation of Lift-to-Drag Ratio with Time-Averaged Mass Flow Rate

**Average Lift Coefficient Vs. Frequency For Pulsed Jet**
**Vinf=94.3 ft/sec, Chord=8 inch, Minf=0.0836**
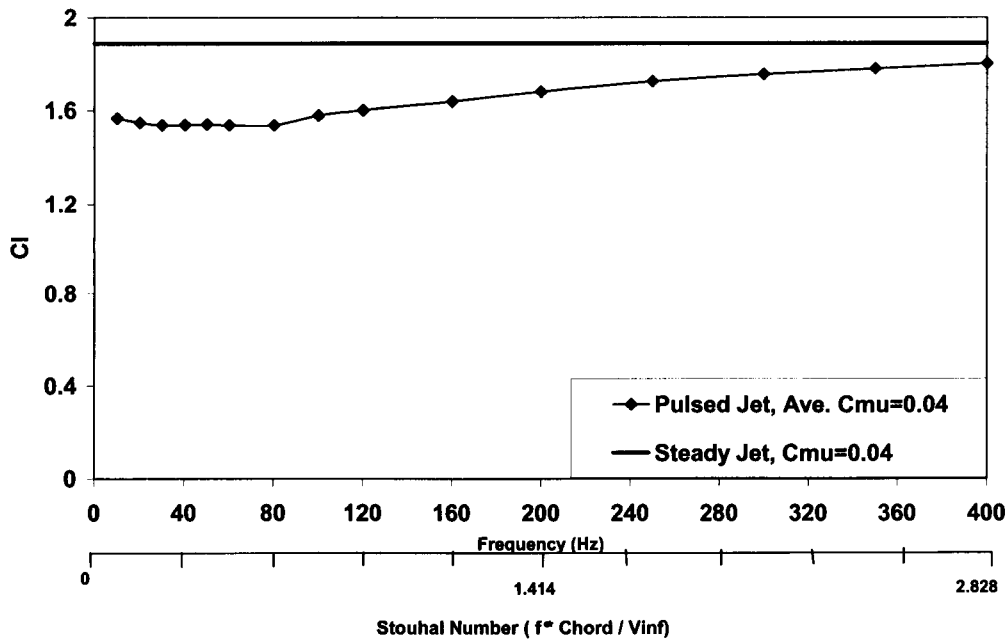


Figure 8a. Variation of $C_l$ with Pulsed Jet Frequency at fixed Time-Averaged Momentum Coefficient

**Average L/D (Efficiency CL/(CD+Cμ)) Vs. Frequency For Pulsed Jet**
**Vinf=94.3 ft/sec, Chord=8 inch, Minf=0.0836**



Figure 8b. Variation of L/D with Pulsed Jet Frequency at fixed Time-Averaged Momentum Coefficient

# APPENDIX C

# Aeroacoustics of a High Aspect-Ratio Jet

# APPENDIX C

## Aeroacoustics of a High Aspect-Ratio Jet

Scott E. Munro[*]
and
K. K. Ahuja
Georgia Institute of Technology
GTRI/ATASL
Atlanta, GA, 30332-0844

## Abstract

Circulation control wings are a type of pneumatic high-lift device that have been extensively researched as to their aerodynamic benefits. However, there has been little research into the possible airframe noise reduction benefits of a circulation control wing. The key element of noise is the jet noise associated with the jet sheet emitted from the blowing slot. This jet sheet is essentially a high aspect-ratio rectangular jet. Thus, to fully understand the noise of a circulation control wing, the noise of high aspect-ratio rectangular jets must also be understood. A high aspect-ratio nozzle was fabricated to study the general characteristics of high aspect-ratio jets with aspect ratios from 100 to 3000. The jet noise of this nozzle was proportional to the 8th power of the jet velocity. It was also found that the jet noise was proportional to the slot height to the 3/2 power and slot width to the 1/2 power.

## Nomenclature

A -- Area (typically of nozzle)
AR -- Aspect ratio
a -- Speed of sound
$a_o$ -- Ambient speed of sound
D -- Diameter of round jet exit
$d_{eq}$ -- Equivalent diameter, $2(A/\pi)^{1/2}$
f -- Frequency
HARN -- High aspect-ratio nozzle
h -- Slot height or rectangular nozzle height (small dimension)
I -- Sound intensity
L -- Characteristic length
$L_{eq}$ -- Characteristic length for the HARN, $L_{eq} = h^{3/4}w^{1/4}$
$M_c$ -- Convection Mach number
P -- Sound power
$P_{ref}$ -- Reference acoustic pressure, 20 μPa
p -- pressure
R -- Radial distance from jet exit to measurement location
Re -- Reynolds number
SPL -- Sound Pressure Level
w -- width of rectangular nozzle (large dimension)

$V_j$ -- Jet exit velocity (fully expanded)
$\Theta$ -- Angle of measurement with respect to the flow axis
$\rho$ -- density

## Introduction

### Motivation

Circulation control wings (CCW) have been researched and developed extensively, primarily for the purpose of greatly increasing lift while reducing or replacing the conventional flap system of an aircraft. More recently CCW have been considered as a possible option for reducing airframe noise. However, there are many issues that need to be resolved. The acoustic effects of many parameters must be investigated, such as the slot height and width, and slot blowing velocity. In order to correctly define the best combination, new areas of research will have to be investigated, including high aspect-ratio rectangular jet noise. This was the motivation of the present study.

The CCW slot jet essentially creates a high aspect-ratio jet, but little research has been performed on high aspect-ratio jet noise, particularly on the very high aspect ratio of a CCW. Thus, this study was devoted to determining the general acoustic characteristics of high aspect-ratio rectangular jets, providing a basic level of understanding that could then be extended to other applications, in particular the CCW case.

## Background

Since there has been little work on high aspect ratio rectangular jet noise, particularly aspect ratios applicable to a CCW, the following sections highlight literature on jet noise for both round and rectangular nozzles.

### Jet Noise from Round Nozzles

As soon as jet and rocket engines began making their way into the aircraft designs, the noise from these new types of engines became an issue. In some cases it was more for controlling damage, such as in the case of a rocket launch, where the launch

area is subjected to a large amount of noise from the rocket motors during the launch. The other major issue came with increased jet travel and jet aircraft activity around airports. The new jet aircraft were much louder and more annoying to the surrounding population.

Thus, research into jet noise soon began to emerge. Much of the early theoretical gains in jet noise prediction came from Lighthill's work on round jets. Various versions of this work are found in references [1- 3]. Lighthill suggested that the noise associated with a particular eddy could be represented by a quadrupole source. From this physical model, several relationships were derived, including 'Lighthill's eighth power law' relationship for the sound intensity[1-4]

$$I \sim \frac{\rho_m^2 V_j^8 D^2}{\rho_0 a_0^5 R^2}(1 - M_c \cos(\Theta))^{-5} \qquad (1)$$

There are important relations that are shown, specifically that the sound intensity is proportional to the eighth power of velocity and inversely proportional to the square of the radius between the source and observer. In the equation, $\Theta$ is the angle of the observer with respect to the downstream jet axis.

The frequency of the noise is also affected by test conditions. Near the exit of the nozzle where the mixing region is small, the turbulence is dominated by small eddies, thus higher frequency noise is associated with the small length scale. As the shear layer grows, the larger eddies further downstream are believed to be responsible for lower frequency jet noise.[4-6] But notice that these characteristics are dependent on the geometry and mixing characteristics of the jet. Thus, the frequencies must also scale in order to be able to predict the entire spectrum of jet noise. The frequency scaling is taken into account by non-dimensionalizing the frequency into a Strouhal number and accounting for the moving sources. This non-dimensional frequency is typically expressed as:

$$\frac{fD}{V}(1 - M_c \cos\Theta) \qquad (3)$$

Most of Lighthill's theory has been experimentally verified for unheated, subsonic, round jets. One key study in this area was performed by Lush[4] and another by Ahuja, and Ahuja and Bushell.[5,6] Ahuja made careful measurements of jet noise for 3 different diameter round jets. Ahuja verified the data by scaling all his data to the same condition, which would collapse all the data if Lighthill's theory were correct. Converting to SPL and normalizing by "standard" conditions, equation (1) becomes

$$"s \tan dard" SPL = SPL - 10 \log\left(\frac{V}{V_s}\right)^8 - 10 \log\left(\frac{D}{D_s}\right)^2$$

$$+ 10 \log\left(\frac{R}{R_s}\right)^2 - 10 \log(1 - M_c \cos\Theta)^{-5}$$

$$(3)$$

where the variables with an 's' subscript signify conditions of the "standard" case. Thus, any SPL measurement from a jet could be transformed, or scaled to the SPL for this standard case. In the reverse, the 'Standard SPL' data could be scaled using a geometry, distance, or velocity to predict what the noise would be in that case. Bushell and Ahuja's experimental data for unheated jets agreed with many of Lighthill's predictions but did not match in all cases.[5,6] It should be noted that all of this work was done for a round jet and therefore is limited in its ability to predict noise only for round nozzles.

Recently Lighthill's theories have come under much scrutiny and some other jet noise theories have come to the forefront. One of those theories has been put forth by Tam and several other researchers.[7-10] They suggest that there are two different noise mechanisms, one that is associated with the large scale turbulence and one with the fine scale turbulence.[7-9] Tam and Auriault also claim that these two mechanisms dominate the acoustic jet noise spectra in different regions of the polar arc. Specifically, large-scale turbulence noise dominates the spectrum at small polar angles, while the fine scale turbulence dominates the spectrum at higher polar angles.[7-9] References [7 and 8] describe two generic noise spectra, one for each type of noise. These generic spectra have been applied to a wide variety of jet noise data with reasonable success.[7-10]

It is apparent that even in the case of the well-studied round jet, there is still discussion of the appropriate theory and scaling. This is also true of other jet noise from non-round nozzles and more complex suppressor nozzles. This is particularly true in the case of rectangular jets where there has not been nearly the focus given to round jets. The following section discusses in some detail the differences found between the round jet case and rectangular jet case.

## Jet Noise From Rectangular Nozzles

Although round nozzles dominated most of the applications where jet noise was of interest, there have always been some applications where a rectangular nozzle is more appropriate. Thus, there has also been some work on the topic of rectangular jet noise.

Almost all work on jet noise was conducted on round jets until there were applications where a

non-axisymmetric shape had advantages over an axisymmetric nozzle. The first rectangular nozzle work strictly for noise reduction appears to be performed by Tyler, et al.[11] Other applications were more thrust related. Rectangular nozzles produced better performance at higher Mach numbers in military aircraft tests.[12,13] However, the rectangular nozzles in these applications typically had aspect-ratios from 2 – 7.[14] These early studies were typically also limited to higher subsonic or supersonic Mach numbers.[15] Other examples of very early studies are Maglieri and Hubbard's work on jets of different aspect-ratio,[16] and Cole's work on high aspect-ratio slot-noise.[17] Maestrello and McDaid investigated slot jets with aspect-ratios from 5 to 20.[18] Gruschka and Schrecker[19] and Schrecker and Maus[20] investigated the noise emitted from high aspect-ratio slot jets with aspect-ratios similar to 100. One of the major motivations behind this work was the fact that jet velocity of rectangular jets decayed at a higher rate compared with round jets, thus resulting in a lower sound energy.[21] However, in all these works, high aspect-ratio referred to aspect-ratios typically at least an order of magnitude lower (sometimes two orders of magnitude) than the CCW jet of interest in the present work.[14,19,20]

The research on rectangular nozzles has produced some differing results. The acoustic power dependence of $V_j^8$ for round jets has been found by some researchers[18] while $V_j^7$ has been found by others.[15,20,22] The work documented in references [18,19] found that the jet velocity dependence was actually a function of the aspect ratio of the jet. The range of aspect ratios tested was from 30 to 120, and the velocity scaling function ranged from $V_j^6$ to $V_j^7$.

Ffwocs-Williams suggested in reference [22] that the exit geometry can affect the noise by an additional component he termed "lip noise." The lip noise radiates as a fluctuating force dipole source. Typically, the dipole source radiates noise proportional to $V_j^6$. Reference [14] speculated that this noise combined with the turbulent mixing noise produced the $V_j^7$ relationship found in their investigation.

Kouts and Yu[15] also noted that the peak frequency of the spectra only had a weak dependence on jet velocity. They also found that the rectangular jet seemed to have more high frequency content than circular jets. Also in contrast to round jets, researchers found that the peak frequency has a weak dependence on the nozzle height.[15,19,20] This was unexpected since round jet noise has a strong dependence on jet diameter and the nozzle height is considered the appropriate scale for the initial mixing region in rectangular jets.[15]

The region where the highest levels of noise are produced in a jet is in the mixing layer around the core region.[21] This is where the shear is very high, and the associated velocities are also at their highest. Well downstream, the flow evolves into a round jet flow, however the flow velocities are much lower than the exit condition and therefore do not radiate jet noise at comparable levels to the near exit region.[21] However, as with round jets there are many theories that have been proposed. In addition to studying round jets, Tam has investigated other nozzle shapes including rectangular jets. In his studies, he has limited his research to low aspect-ratio nozzles. His results indicate that rectangular jets are actually similar to round jets.[9,24-27] References [24-27] show Tam's fits do indeed agree well with the experimental data. This indicates that round jet noise and rectangular jet noise are actually very similar since both can be fit to one set of generic spectral curves.

As is evident by the variation in data and theories, there is still much to be investigated in the area of rectangular jet noise. The aspect ratios considered 'high' in the above discussion are typically one or two orders of magnitude lower than the typical aspect ratio of the nozzles of the present study. Thus, there is definitely a need to generate some clean, systematic very high aspect-ratio noise data so that theories can be extended to this realm.

**Experimental Set-up**
High Aspect-ratio Nozzle Design and Fabrication

The major design consideration used to develop the HARN was to minimize the internal noise that could propagate outside and contaminate the pure jet noise that was the object of the study. The most important step one can take to reduce internal noise is to keep the internal velocities low, and make smooth transitions in the flow path so there is no separated flow. In order to utilize the high-pressure air supply systems of the acoustic facilities at GTRI, the HARN had to be attached to a 4" diameter pipe flange face. Since it was desired to keep the exit geometry of the nozzle similar to that of the CCW model used in references [28 and 29], the 4" diameter inlet pipe was connected to a round-to-rectangular transition section with an exit area of 2.75" X 2.75". This had to expand to the exit geometry of 30" wide by 0.003" to 0.020" high. This produced a contraction ratio of 20-150 depending on the slot height. A contraction ratio on the order of 10 is usually adequate to maintain plenum-like conditions in most wind tunnels.[30] Thus, the upstream portion of the HARN was considered to be an adequate plenum for the slot nozzle. The low flow velocity associated with a plenum would ensure low levels of internal noise. Considerable care was taken

to ensure minimum internal noise in the design of the HARN. Further details of design considerations can be found in reference [29]

Due to a combination of many factors, including cost, the weight of the finished product, and machinability of the material, the HARN was fabricated from 5/8" thick aluminum plate. Figure 1 shows a schematic and photo of the HARN. The exit of the HARN was 30" X 0.25". The top and bottom of the exit were cut back at a 30-degree angle and drilled-and-tapped to receive screws to hold down knife-edge blades. These make the final opening of the HARN slot exit. Shims were placed underneath the knife-edges to vary the height of the slot exit.
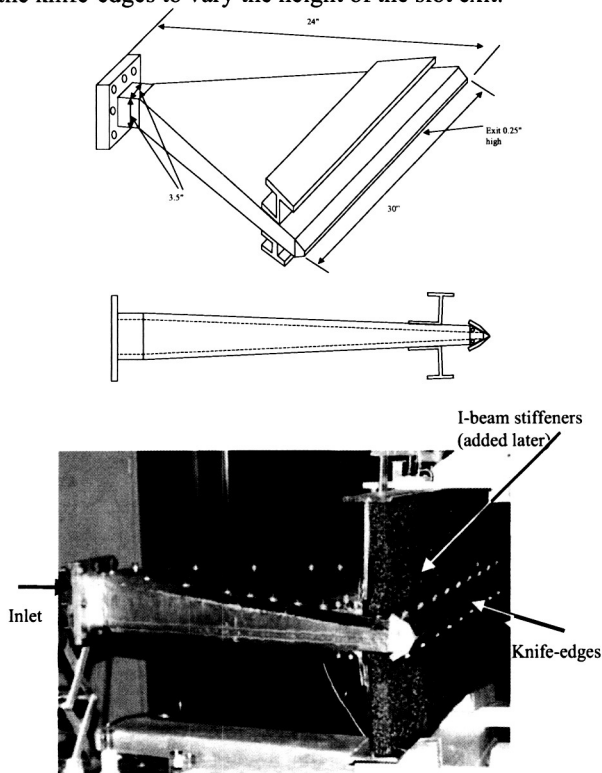


Figure 1: HARN Nozzle

The knife-edges were machined from steel for maximum strength. They were designed to create a converging nozzle for the flow and did not have a straight section parallel to the jet centerline. A straight section machined into the knife-edges would be a constant length. However, since the slot height varied greatly, the non-dimensional length of the straight section would vary significantly. Although it was believed that this would not change the acoustic characteristics of the flow, it was decided to eliminate any straight section to keep the flow characteristics similar for all nozzle heights.

Since one of the initial goals was to minimize internal noise, it was desirable to have no protrusions into the flow that might shed vortices and generate noise. Thus, no tie-down rods were used to help the HARN retain its shape under pressure. Under initial testing it was found that the top and bottom plates of the HARN would bow enough to generate as much as a 1/8" increase in nozzle exit height. This was unacceptable since this is an order of magnitude increase in the height. There were only two ways to resolve this issue, either add tie-down rods through the plenum interior to help carry some of the pressure load, or stiffen the top and bottom plates by adding stiffeners. It was felt that the risk of generating internal noise was too great to add tie-down rods to solve the problem. Thus, the decision was made to stiffen the top and bottom plate with stiffeners placed on the outside surface. Figure 1 shows the stiffeners installed on the HARN.

Some extra parts were also fabricated for additional tests. These included blanking plates that fit inside the HARN to block off portions of the nozzle, in order to test other jet widths. Three sets were made. These could be inserted inside the nozzle to reduce the width from 30" to 14.75" or 6.5". A much more detailed description of the HARN is provided in reference [29].

Instrumentation

The Cobb-County facilities of GTRI house two anechoic chambers, the anechoic static jet facility (ASJF) and an anechoic flight simulation facility (AFSF). The Acoustic data for the HARN could have been acquired in either of these facilities. However, due to scheduling with other projects the AFSF was used. Figure 2 shows a schematic of the HARN set-up in the AFSF. The facility itself has been described in detail references [28 29, and 31]. The facility consists of a converging duct that terminates as a 28-inch diameter round duct in an anechoic chamber. A collector extends out of the chamber on the opposite wall. Freestream flow is provided by a diesel powered fan on the downstream end of the collector. High-pressure air can be piped in through the center of the converging duct allowing for jet-flow and noise studies in the presence of a freestream. For these tests, the wind tunnel feature of the AFSF was not used, essentially making the facility a static test facility.
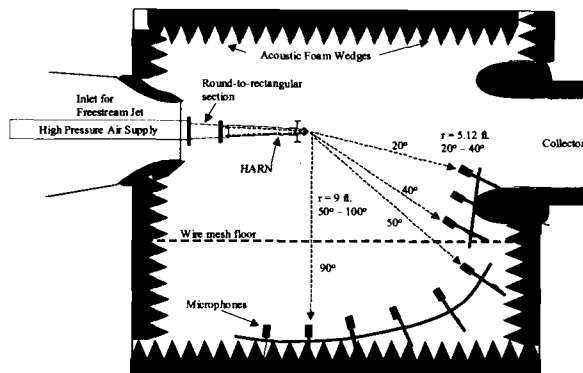
Figure 2: Schematic of HARN installed in AFSF.

Several microphones were placed on a polar arc at fixed angles. The microphone layout is shown in figure 2. More details can be found in reference [29]. Experience has shown that the response of the microphone system (microphone, pre-amplifier and extension cable) changes as the system ages. The microphones are commonly calibrated at one frequency, essentially to establish the conversion from output voltage to pressure amplitude. Unfortunately this assumes that the factory frequency response curve can be used to adjust this calibration over the entire frequency range. The only way to truly compare signals from different microphones is to calibrate the entire system over the entire frequency range of interest. The calibration was accomplished by using a noise source and a newly acquired microphone system as a reference at a reference location. The reference microphone signal was compared to the signal from each microphone. A frequency response correction was then generated for each microphone based on the difference between the reference and the corresponding microphone. More details about the frequency response calibration can be found in reference [29].

For the HARN acoustic tests, microphones were mounted at several angles with respect to the downstream jet axis, specifically, from 20° to 100° at 10° increments (0° being the jet axis in the downstream direction). Due to constraints of the facility (see figure 2), microphones at 20°, 30° and 40° had to be placed 5.12 feet from the nozzle exit, while the rest of the microphones were placed 9 feet from the nozzle exit.

All the microphones used in the tests were B & K type 4135 or type 3939 (replacement of 4135) microphones, with either B & K type 2669 or type 2619 preamplifier. The microphone/pre-amplifiers were connected to an HP 35650 Spectral Analyzer via B & K microphone extension cables and B & K NEXUS power supplies (with built-in conditioning amplifiers). Software based on a PC computer controlled the acquisition process and produced as outputs SPL versus frequency for each channel.

Critical flow and atmospheric parameters were monitored and recorded as necessary. The ambient pressure, temperature and humidity were recorded for each test point in order to make atmospheric absorption corrections to the acoustic data. The total and the ambient pressures were used to set specific exit pressure ratios, and hence jet exit Mach number. The total and static pressures and reservoir temperature were used to find the internal flow velocity. Details of these measurements and how the atmospheric absorption correction was applied are given in reference [29].

Acoustic Measurements Test Matrix

For each nozzle geometry, an attempt was made to acquire acoustic data at jet velocities of 500, 675, 785, 920, 1000, and 1100 ft/s. These corresponded to increments in total pressure that were relatively easy to achieve with the flow controls of the HARN.

A problem encountered when attempting to vary only one variable was that the slot height changed with increasing internal pressure. The knife-edges are attached only at one end and that the pressure exerted on the knife-edge causes a moment about the attachment point. Obviously, as the pressure is increased, the moment is increased and the tip deflects. It turned out that the deflection was even across the span, and seemed to be independent of the initial slot height. The increase in slot height due to this was found to be about 0.0015 in/psi. Unfortunately, for some of the smaller slot heights, this could double or even triple the height of the slot over the range of velocities tested, while causing a 50% increase in height for the larger initial slot heights. This caused a problem when trying to compare data for a constant slot height since the height changed for each velocity condition.

The nozzle width was changed by using blanking plates inside the nozzle. The width was variable from the full width of 30" to 15" and 6.5". These were installed by removing the top plate of the HARN and inserting blanking plates to the desired width.

Due to the extremely small nozzle heights and exit areas, precise jet velocities and slot heights were difficult to attain; however, a nominal test matrix was set. At each of the three nozzle widths mentioned above, a matrix of 4 slot heights and 5 jet velocities were tested. The initial slot heights were nominally 0.015", 0.030", 0.045", and 0.065". This produced aspect-ratios from as low as 100 to as high as 3000. At each slot height and width setting, acoustic data was acquired at 5 nominal jet velocity

conditions 500 ft/s, 675 ft/s, 785 ft/s, 920 ft/s, 1000 ft/s, and 1100 ft/s. At each test point (a particular w, h, and $V_j$) acoustic data were measured at 9 polar angles (20° – 100°) and the supporting pressure and temperature values were recorded as well.

## Acoustic Measurements
### Notes on Acoustic Measurements

High aspect-ratio jet noise data were acquired for several configurations of the HARN. The goal of the acoustic study was to try to determine the general acoustic characteristics of the very high aspect-ratio jet. An attempt was made to vary only one parameter at a time. However, as discussed in the previous sections, that often was not possible. Data will be presented as much as possible with only one parameter varying, and each variable's effect on far field noise spectra and overall sound pressure levels (OASPL) will be discussed. This enables an easy determination of a scaling factor for each variable. First however, it is beneficial to examine the general noise spectra associated with the HARN.

It should be noted that all acoustic data presented will be shown in 1/3-octave spectra or as OASPLs. The data were acquired in narrowband out to 80 kHz ($\Delta f = 64$ Hz) but the data were converted to 1/3 octave bands in order to make comparisons and references to the classic experiments[4-6] on subsonic round jets, which are only available in 1/3-octave bands. Also, all data presented here are corrected for several different factors to render the data lossless. These include corrections for the microphone grid, the presence of the microphone in the free-field, the absorption of sound due to the atmosphere, and the individual microphone frequency response correction. All of the corrections, except for the individual frequency response correction, were applied at the power spectral density levels. This was done to standardize the application of corrections that can vary depending on the bandwidth in which they are applied. These corrections are only mentioned here, details of the corrections and how they were applied to the data can be found in reference [29].

### Typical Acoustic Data

The goal of the HARN acoustic test was to determine the general acoustic characteristics of an extremely high aspect-ratio nozzle. To accomplish this task, acoustic data were acquired at several jet velocities for a given nozzle geometry. There were a total of 72 test conditions, each with acoustic data at 9 polar angles. Since there is such a large amount of data, typical data for several conditions and polar angles will be presented in this section. Data at polar angles of 30°, 60° and 90° will be shown. Data at other polar angles can be found in reference [29].

One-third octave spectra will be presented for all velocities for a given nozzle condition.

Figure 3 shows the acoustic spectra for the 30" nozzle width. The figure shows typical data for the three polar angles for the initial slot height of 0.026". As with round jets, the lower polar angles have a more distinct peak in their spectra. There are also significant increases in the amplitude over the entire frequency spectrum as the velocity is increased. However, one cannot directly extract the velocity relationship from these plots since the slot height also increases as the velocity increases. It should also be noted that there is a small peak below 1 kHz in most of the spectra. This is believed to be associated with internal noise and this portion of the spectra will most likely not follow the trends associated with pure jet noise. The reader is advised to keep this in mind when examining the HARN data.

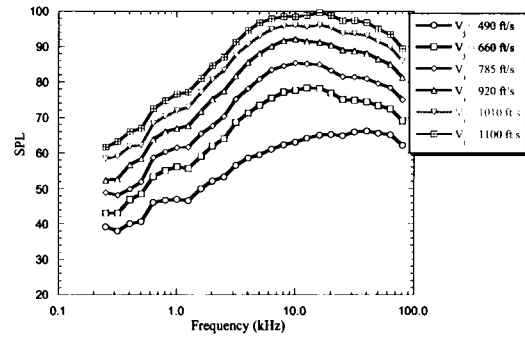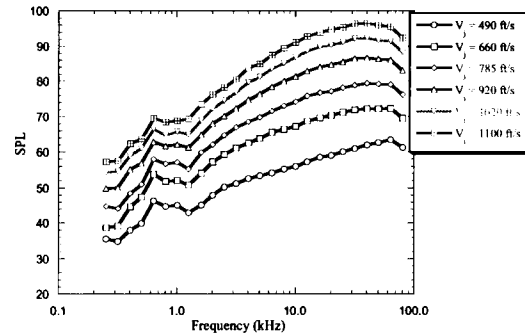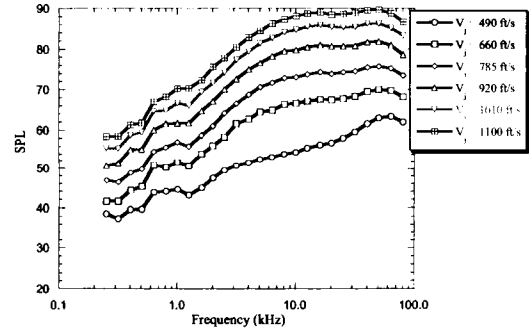is most likely due to internal noise, and should be ignored when using the HARN data. The data presented here are typical examples of the acoustic data for the HARN nozzle and are shown to present the general characteristics of the data.
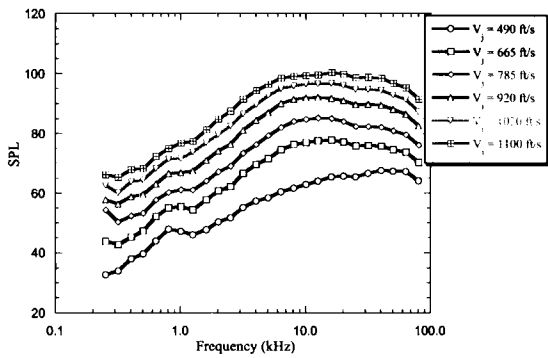


(a)
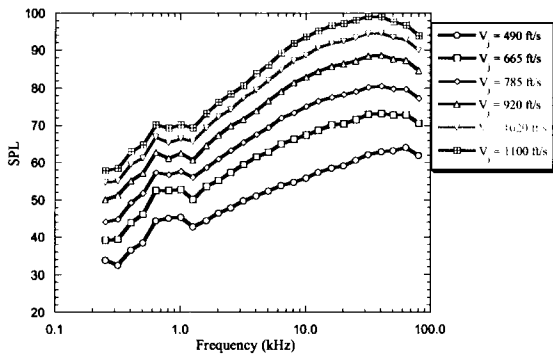


(b)
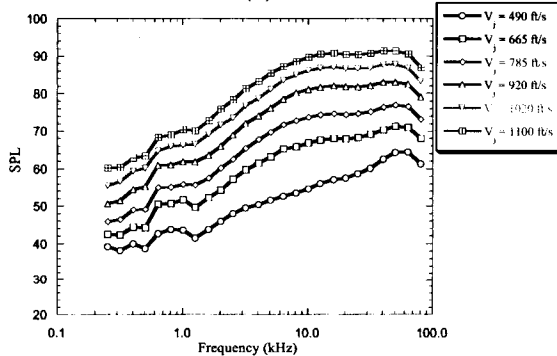


(c)

Figure 3: HARN acoustic data for $h_o$ = 0.026", w = 30", (a) $\Theta$ = 30°, (b) $\Theta$ = 60°, (c) $\Theta$ = 90°.

Figures 4 and 5 show the data for the nozzle with widths set to 14.75" and 6.5", respectively. The corresponding initial slot heights were 0.039" and 0.048". Again, there is a more distinct peak for the 30° data, while the 90° data appear to have more of a flat spectrum. As with the 30" data, increased velocity causes large increases in the amplitude of the data. The 30° data peak frequency seems to increase with increasing velocity. The low frequency peak is also present in these figures. The low frequency peak



(a)



(b)



(c)

Figure 4: HARN acoustic data for $h_o$ = 0.039", w = 14.75", (a) $\Theta$ = 30°, (b) $\Theta$ = 60°, (c) $\Theta$ = 90°.
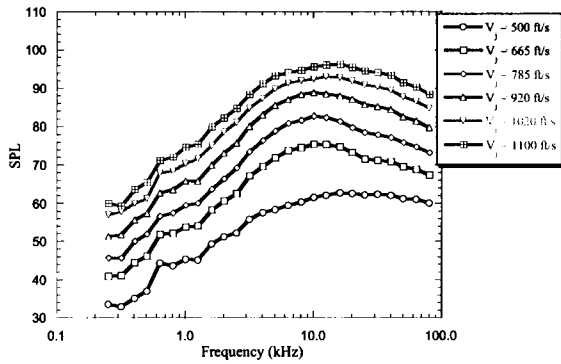
(a)
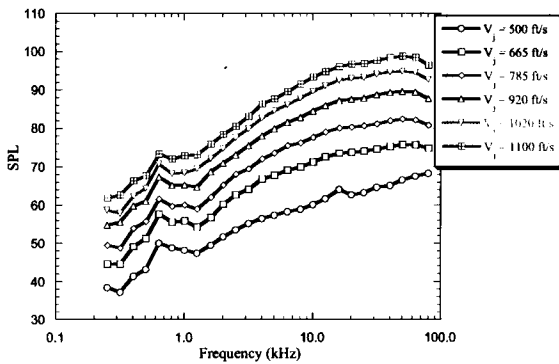


(b)
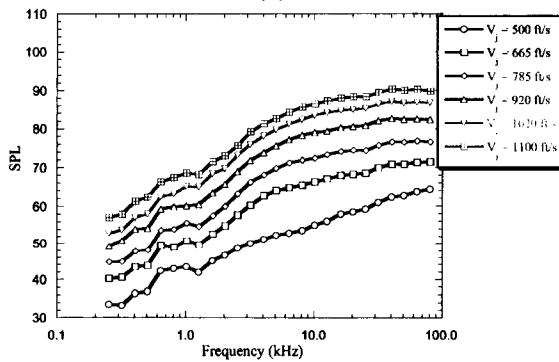


(c)

Figure 5: HARN acoustic data for $h_o$ = 0.048", w = 6.5", (a) $\Theta$ = 30°, (b) $\Theta$ = 60°, (c) $\Theta$ = 90°.

In addition to variations in the spectra with nozzle geometry and jet velocity, the acoustic spectra varies depending on the polar angle where the data are acquired. Figure 6 shows acoustic spectra for a round jet from reference [6]. Notice that the SPLs increase at angles closer to the jet axis. There also is a larger amount of low frequency noise and there is some refraction of high frequency noise as well.

These results are well established for the round nozzle.[5,6]
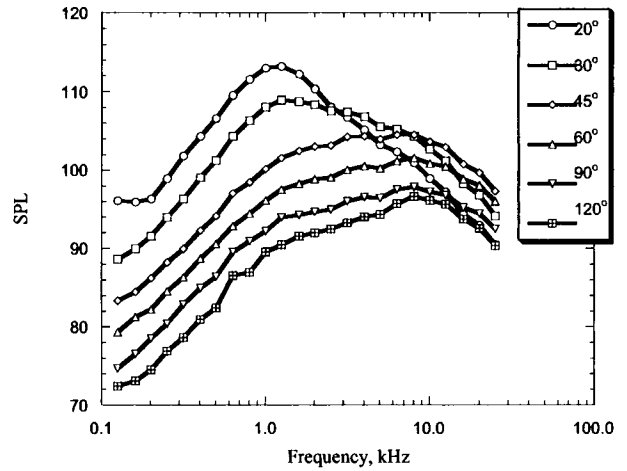


Figure 6: Round jet noise data for D = 2.4", $V_j$ = 1000 ft/s, from reference [6].

Figure 7 shows similar data for the HARN. There are several differences that are noticeable. At first glance it appears that the spectral peak is at $\Theta$ = 40° for the HARN while it is closer to 20° for the round nozzle. However, if the low frequency data are closely examined, the 20° data are higher, indicating that in fact the peak directivity is closer to 20°. The lower spectral peak is most likely due to absorption and scattering of the noise due to turbulence. This effect was well documented in references [4], [5] and [6].

These spectra will be compared to acoustic data from other experiments later in this document. However, first it is desirable to determine how the acoustic amplitude changes due to changes in slot height, width, jet velocity and polar angle. An initial examination of these relationships will be performed in the next section using the OASPLs calculated from the data presented here.
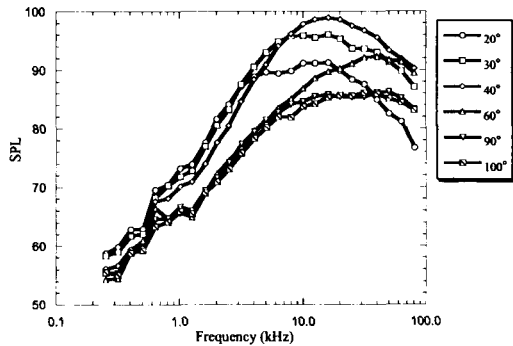
Figure 7: HARN jet noise data for w = 14.75",
h = 0.057", $V_j$ = 1010 ft/s.

## Comparison of HARN Acoustic Data with Established Trends.

There has been very little experimentation with nozzles of high aspect-ratios. Most of the rectangular jet noise data available has been acquired for nozzles with aspect ratios below 20, while there is virtually no acoustic data available for nozzles with aspect ratios greater than 100. Lower aspect-ratio jet noise data has been compared successfully to round jet data by using an equivalent diameter as the geometric parameter.[9,26,27,32,33] There has been some discrepancy associated with the relationship between the SPL amplitude and the jet velocity. Some data has indicated a $V^7$ relationship while other data has shown a $V^8$ or even $V^9$ relationship.[15, 20, 32, 33]

Since round jet noise is essentially considered to be the standard to compare against and there is no accepted method for scaling rectangular jet noise, round jet noise data will be used as the standard for comparison and scaling of the HARN data. It has been well established that the OASPL for round a jet is proportional to $V_j^8$ and $D^2$ (if other variables are kept constant, such as density, speed of sound, etc.).[1, 2, 4, 5, 6, 34]

In addition to the geometry and the jet velocity, the amplitude of the acoustic spectra is dependent on the polar angle. Round jet theory shows that $SPL \sim (1-M_c\cos\Theta)^{-5}$. Experiments on round nozzles have found that this term alone is insufficient to completely collapse round jet noise data. It is believed that this is due to refraction and scattering of high frequency noise by the jet flow. This difference between the theory and the experimental data is shown in figure 8 where round jet noise from reference [6] is presented. Notice that the theory and the experimental data agree well at low jet velocity at all polar angles.

However, the theory over-predicts the OASPL at higher jet velocity, especially in the rear arc.
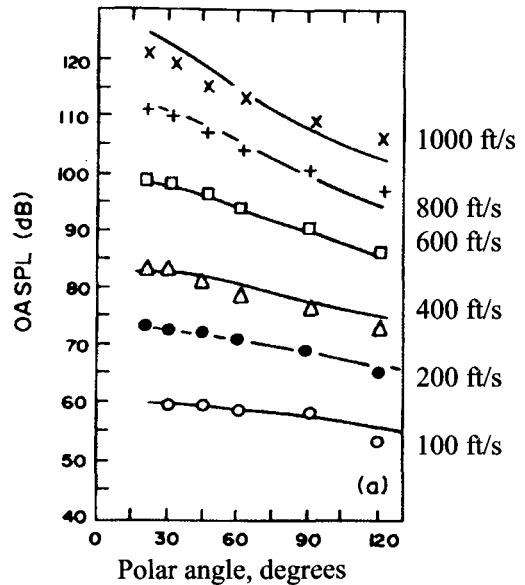


Figure 8: Directivities of OASPL's for round jet noise, D = 2.84", from reference [5].

OASPL was calculated for the HARN spectra over a frequency range from 1 kHz to 75 kHz. OASPL data are seen in figure 9 for the HARN. Notice that there is a greater difference between the theory and the data. At low jet velocities the theory predicts the amplitude reasonably well for angles greater than 40°. However, at very low polar angles there are significant differences and it is clear that the directivity does not follow the directivity given by $(1-M_c\cos\Theta)^{-5}$, even at low jet velocities. It is clear from figure 9 that the directivity given by $(1-M_c\cos\Theta)^{-5}$ does not appropriately represent the data. Thus, the following discussion will concentrate on data at the 90° polar angle to avoid the added complications of a polar angle effect.
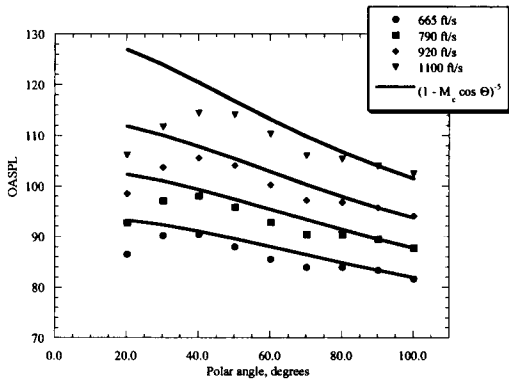
Figure 9: Directivities of OASPL's for HARN jet noise, w = 30", $h_o$ = 0.04".

The equivalent diameter was also calculated using the measured slot height and width for each HARN test condition. The equivalent diameter is defined as

$$D_{eq} = (4A/\pi)^{1/2} = (4hw/\pi)^{1/2}$$

(4)

Thus, $D_{eq}$ is dependent on square root of h and w. Figure 10 shows OASPL for HARN acoustic data plotted against the corresponding $D_{eq}$ for constant jet velocity test conditions. As is obvious in the plot $D_{eq}$, is not the only parameter that determines the amplitude of the OASPL.
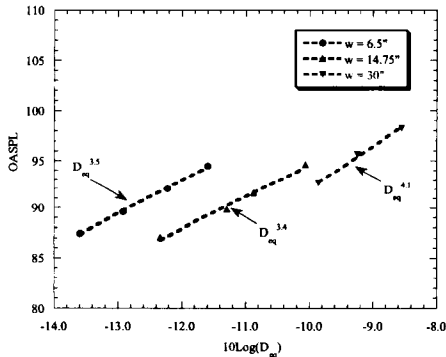


Figure 10: OASPL versus equivalent diameter for all the HARN data for constant $V_j$ = 920 ft/s, $\Theta$ = 90°.

Figure 11 is a plot a plot of several HARN test conditions. Curves are shown for several nozzle widths. The OASPL change for a change in h only is shown since velocity and w are held constant for the points along each curve. As can be seen, the relationship between OASPL and h is not constant

for all w, but a best fit to the data appears to be around $h^{3/2}$.
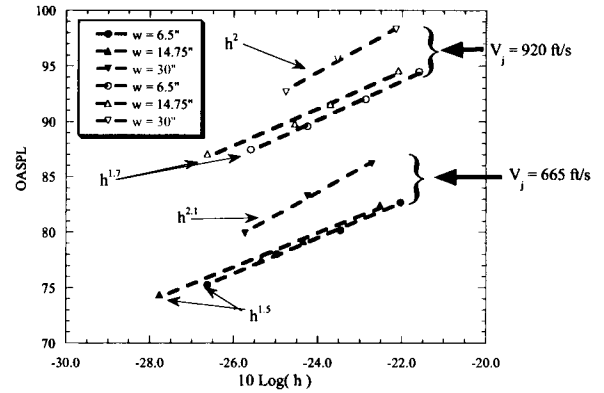


Figure 11: OASPL versus h for constant $V_j$ and w, $\Theta$ = 90$_o$.

The OASPL data is plotted versus the jet velocity in figure 12. There are two things that can be quickly gained from this plot. First, the relationship between the OASPL and the jet velocity seems to be close to $V_j^8$. It should also be noted that the width also has a contribution to the OASPL. This can be seen by the fact that the h correction does not completely collapse all the data, only the data for constant w seem to fall along the same line.
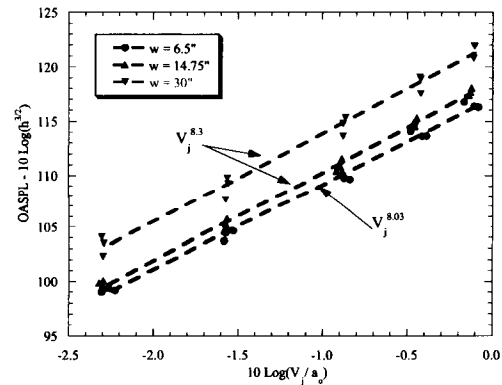


Figure 12: OASPL versus jet velocity for constant w, $\Theta$ = 90o.

Figure 13 shows the OASPL data plotted versus the width. Unfortunately there is not a distinct relationship that immediately appears from the plot, however a curve fit of the data does show a relationship following $w^{1/2}$ in the average.
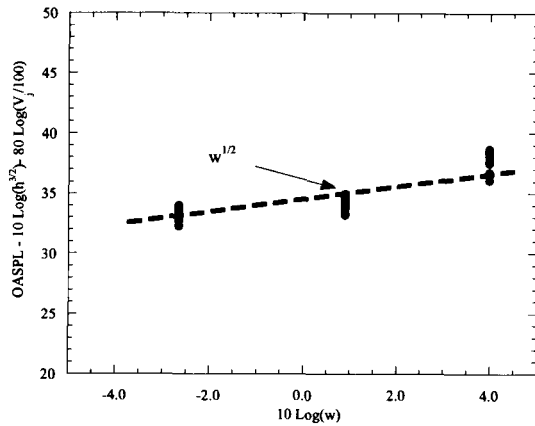
C-10

Figure 13: OASPL versus width, $\Theta = 90°$.



Figure 14: OASPL adjusted for jet velocity plotted versus equivalent diameter, $\Theta = 90°$

As was mentioned earlier, low aspect-ratio rectangular jet noise data is usually collapsed using an equivalent diameter.[7-9, 24-27] Now that the relationship for jet velocity is known, it can be used to derive a relationship for the equivalent diameter. Figure 14 shows OASPLs for a range of nozzle heights and widths plotted against equivalent diameter. This plot is similar to that shown in figure 10, except now the velocity component of the OASPL is subtracted out. There are some points that can be ascertained from this plot. Notice that there appear to be three sets of data points, each associated with a different nozzle width. It also should be noted that the OASPL is dependent on roughly the $4^{th}$ power of $D_{eq}$ for constant w. This is contrary to typical scaling done for low aspect-ratio rectangular jets, which typically use the square of the equivalent diameter. If this were an appropriate way to scale the data, the data would have collapsed into one curve with the slope proportional to $D_{eq}^2$. Since this is not the case, the equivalent diameter is not an appropriate way to scale acoustic data for nozzles with aspect ratios as large as the HARN.

Several different schemes for collapsing jet noise data were used to try to determine an appropriate scaling. The HARN data does seem to follow the same trend as round jet noise does for jet velocity. However, the equivalent diameter does not satisfactorily collapse the data. A final attempt was made to collapse the data by simply using the data to determine relationships between the OASPL and nozzle width and height. No exact relationship can be extracted from figures 11 and 13 , however, a best fit to the data was found to be OASPL $\sim h^{3/2}w^{1/2}$. Incorporated into this determination was the desire to observe the noise intensity proportional to the square of a lengthy scale as derived by Lighthill, namely that I $\sim L^2$ for all else constant. Thus, to stay consistent with the length squared dimension, an equivalent length $L_{eq}$ was defined as $L_{eq} = (h^{3/2}w^{1/2})^{1/2}$. Hence, OASPL $\sim L_{eq}^2$ for the HARN. Figure 15 shows the "best fit" to within +/- 1 dB for the HARN data and as expected the data collapses more tightly than any of the other schemes examined.
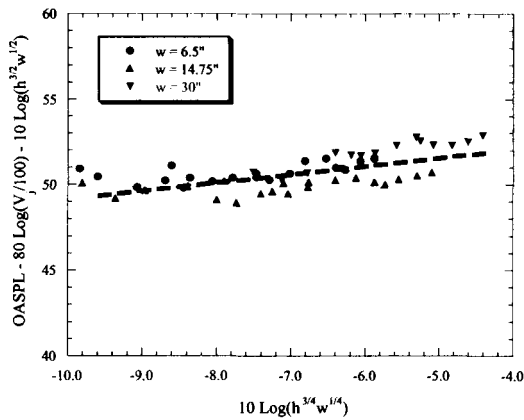
Figure 15: OASPL adjusted for area based on the "best fit" results found in the HARN study, $\Theta = 90°$

In addition to the simple collapse using $L_{eq}$, an attempt was made to collapse the data using sliding exponents for h and w as the aspect-ratio changes. This was based on the expected relationships one would encounter at the extremes of the aspect-ratio range. At an aspect ratio of 1, one would expect the height and width to have equal contribution to the acoustic emissions. However, at extremely high aspect ratios, the height would be expected to dominate the acoustic emissions since the jet is essentially 2-dimensional. This sliding exponents of h and w relationship would better relate to the physical geometry of the flow, whereas the equivalent length defined here is more of an average length scale based on a wide range of geometric configurations. Unfortunately, a reasonable relationship using sliding exponents of h and w could not be found using only the three widths tested in the HARN experiments. Further exploration of this topic is left to future work.

In this short investigation of the OASPL of the HARN acoustic data several insights have been gained. It was found that the HARN noise intensity was not proportional to the square of $D_{eq}$ as lower aspect-ratio rectangular nozzle data indicates. It was also found that the OASPL amplitude was proportional to $V_j{}^8$. This agrees with some of the research for rectangular nozzles as well as with the well-established results for round nozzles. In order to account for the discrepancy between the HARN data and low aspect-ratio data that is proportional to $D_{eq}$, the independent effects of h and w on the OASPL were sought. It was found that h and w appear to independently affect the OASPL data for the HARN.

The OASPL appears to be proportional to $h^{3/2}$ and $w^{1/2}$.

The previous figures have all dealt with data at $\Theta = 90°$. It is worthwhile to examine the relationships developed using the data at $\Theta = 90°$ between the OASPL and h and w for different polar angles. Figure 16 shows data for several different geometric conditions at the same jet velocity scaled using the parameters found from the earlier figures. Notice that the corrected OASPL values tend to vary from one polar angle to another, but the points for a particular angle tend to collapse for many of the polar angles. Thus, it appears that the relationships for h and w are not functions of polar angle.
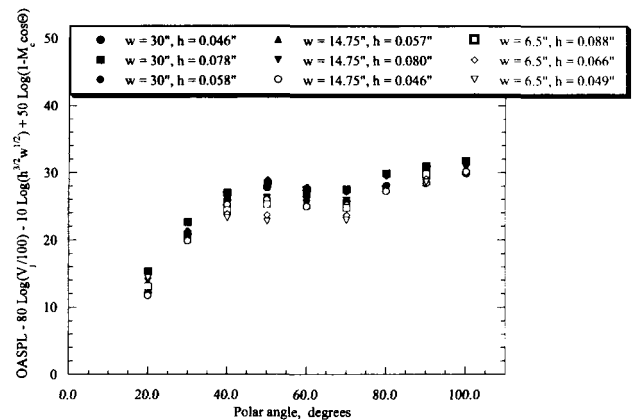


Figure 16: Directivities of HARN OASPL for several w and h combinations for constant $V_j = 1020$ ft/s.

Figure 16 showed that the OASPL relationships to h and w were consistent over most of the polar angles for a fixed jet exit velocity. Figure 17 shows a similar plot but now the jet velocity also varies. Notice that the spread of the data points, particularly at the lower angles, has increased. This indicates that OASPL $\sim V^8(1-M_c\cos\Theta)^{-5}$ is not the correct parameter for collapsing the data for all polar angles. This was somewhat expected since this result is similar to the round jet case, where this discrepancy is believed to be due to refraction and scattering of high frequency jet noise away from the low polar angles.[5]

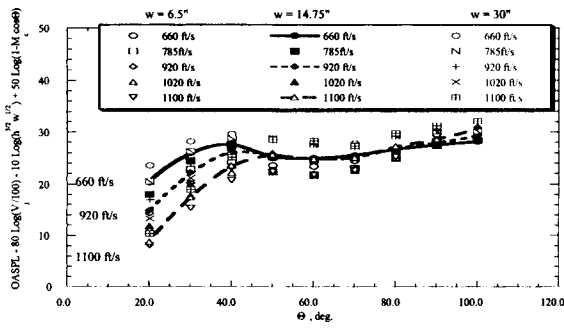Figure 17: Directivities of HARN OASPL for various test conditions.

Although these figures have shown that the data does collapse to some extent using the equivalent diameter as a scaling parameter, it definitely appears that it is not the best way to scale high aspect-ratio rectangular jet noise. The OASPL indicated that h and w have different relationships to the OASPL. This is contrary to $D_{eq}$ which is proportional to $(hw)^{1/2}$. Figure 19 is the same data shown in the previous figures, however it has now been scaled using the previously defined $L_{eq}$. As can be seen from the figure, the data collapses reasonably well over much of the frequency range. Notice that $L_{eq}$ is used to collapse the amplitude of the spectra (OASPL $\sim L_{eq}^{2}$) and also to non-dimensionalize the frequency ($f L_{eq}/V_{j}$) for different conditions.
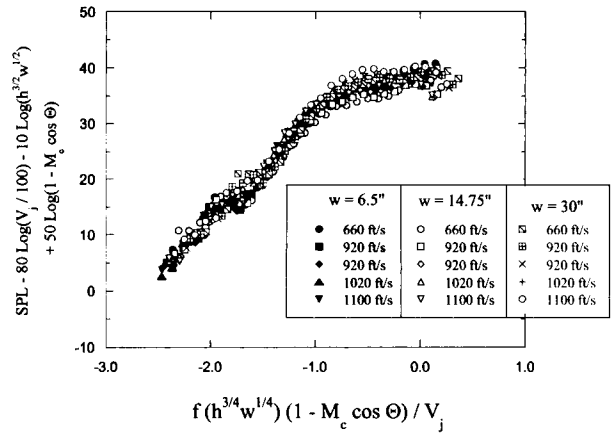
These same trends are evident not just in the OASPL for the HARN data, but also for the entire spectrum. Figure 18 shows several of the HARN spectra scaled by the jet velocity and the equivalent diameter. The frequency is also scaled by $D_{eq}$ and by the Doppler term commonly used to account for the frequency shift due to the convecting eddies. Notice that this does not satisfactorily collapse the data, and in some frequency regions the spread is over 10 dB. It should be noted that this is the scaling found to be appropriate for round jets (at polar angles greater than $30°$) and some low aspect-ratio rectangular jets. However, it is clearly not the proper choice for collapsing HARN data. Recall from figure 14 that the OASPL scaled with the amplitude corrected by $D_{eq}^{4}$ for constant width. Similar results are obtained if the spectra are examined, however, $D_{eq}^{4}$ again is not appropriate for collapsing spectra for different widths as was the case with the OASPL.



Figure 19: HARN acoustic spectra scaled by "best fit" to OASPL data, SPL $\sim V^{8}Leq^{2}(1 - Mc\cos\Theta)^{-5}$, $L_{eq} = h^{3/4}w^{1/4}$, $\Theta = 90°$

In figure 19 the frequency is non-dimensionalized into a Strouhal number based on $L_{eq}$. This is contrary to other researchers who have non-dimensionalized the frequency based on $D_{eq}$ or h. Larsen performed an extensive adaptation of round jet noise theories to 2-d rectangular jets.[32, 33] He stated that h is the appropriate length scale for the axial and normal directions (x and y directions for the HARN) for a rectangular jet with AR $>30$. Tam and his colleagues[9, 26-27] state that $D_{eq}$ is appropriate for the wide range of non-axisymmetric nozzles they have tested, including rectangular nozzles with aspect ratio up to about 10. The defined $L_{eq}$ is not supported by any literature found by the authors, it is simply a combination of the trends seen in the data and the desire to stay dimensionally consistent with Lighthill's derivation where $I \sim L^{2}$. A theoretical basis for $L_{eq}$ was explored in the references [29, 35, and 36] where attempts were made to develop a prediction scheme for rectangular jet noise based on



Figure 18: HARN acoustic spectra scaled using SPL $\sim V^{8}Leq^{2}(1 - Mc\cos\Theta)^{-5}$, $L_{eq} = h^{3/4}w^{1/4}$, $\Theta = 90°$.

fluid dynamic experimental data and jet noise theories.

As in the case with OASPL, the previous few figures have shown data only for the Θ = 90° case. This was done to be able to examine the effects of jet velocity, height and width on the spectra without the added complication of any effects due to convective amplification and refraction that is present at other polar angles. However, it is appropriate at this point to examine the data for polar angles other than 90°.

Figure 20 is an example of round jet data taken from reference [6]. Notice that there is large scatter at high frequencies. This is due to the differences seen between the data and Lighthill's prediction when examining the OASPL. Figure 21 shows similar results for the HARN data.

A further examination of the HARN noise data at various polar angles is warranted. Figure 22 shows data for the same test points as shown in figure 21 at some other polar angles. At Θ = 20° there is very little collapse of the data except at the extremely low frequencies. As the jet velocity is increased, there is increasing scatter amongst the conditions. However, notice that data for similar velocities and polar angles tend to be grouped together. This indicates that at Θ = 20° the relationship for $L_{eq}$ is reasonable for constant jet velocity and polar angle. The data at Θ = 40° shows a similar result, however to a lesser degree, and the 60° data shows reasonable collapse for each set of points of constant width, however there is some difference for different widths. Also, as expected, there is some scatter at lower frequencies caused by the low frequency peak that is believed to be due to internal noise.
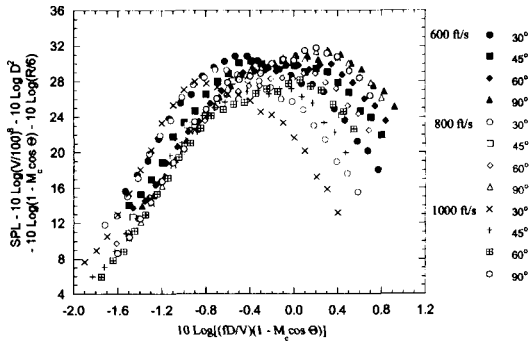


Figure 20: Round jet SPL spectra scaled according to Round jet theory for D = 2.4" from reference [6].


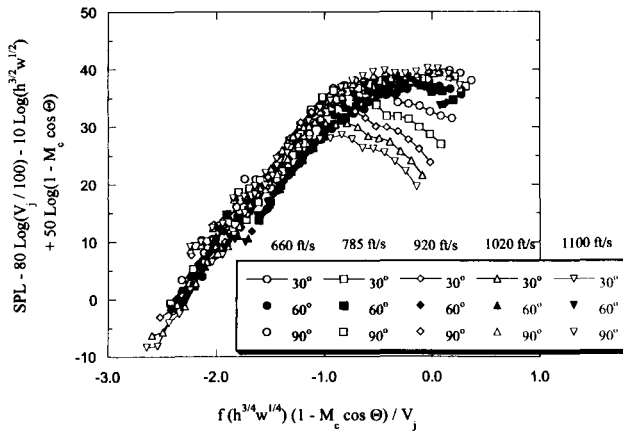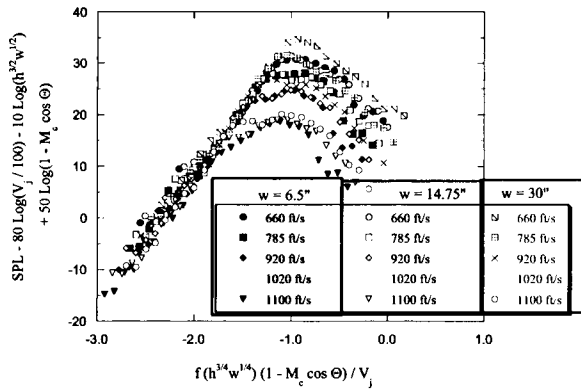
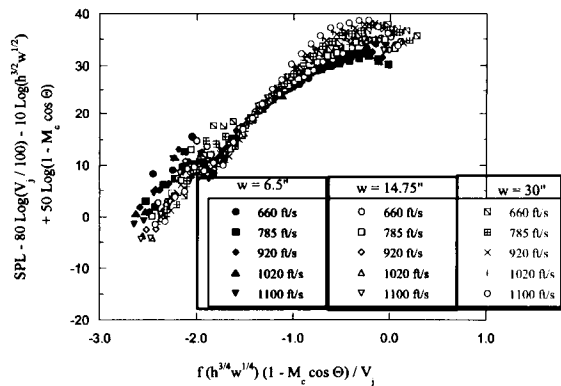Figure 21: HARN SPL spectra scaled according to parameters developed

## Summary and Conclusions

A large amount of acoustic data was collected for the HARN. This included a range of aspect ratios from 100 to 3000, well above the range of rectangular jet noise data found in the literature. The jet velocities tested ranged from 400 to 1100 ft/s and data were recorded at 9 different polar angles.

The HARN acoustic data were compared with trends expected from Lighthill's theoretical predictions and those that are commonly used to collapse and scale round jet noise data and low-aspect-ratio rectangular jet noise data. An initial comparison of sample HARN and round nozzle data showed some general similarities, but also some distinct differences. The general shape of the spectra at various polar angles seemed to be similar. The directivity of the HARN noise seems to have a peak at about $\Theta = 20°$, similar to what has been found for round jets. The HARN data also appeared to have a significant amount turbulent absorption and scattering of high frequency noise at low polar angles evidenced by lower SPL levels at high frequencies and higher SPLs at low frequencies for low polar angles.

From the HARN acoustic data, parameters for scaling acoustic data from a high aspect-ratio nozzle were found. The largest width data was found to vary with $h^2$ while the data for the two smaller nozzle widths were proportional to $h^{3/2}$. The width had only a moderate effect on the jet noise. Although no exact scaling relationship was extracted from the data, a best fit to the data was found to be $I \sim V_j^8 L_{eq}^2$, where $L_{eq} = h^{3/4} w^{1/4}$. The frequency was found to be weakly dependent on the nozzle height and width. Again, using a best-fit approach, and using the defined equivalent length as a normalizing parameter, the frequency was converted to Strouhal number by $f L_{eq}/V_j$. This definition came from the examination of the data and determining a best fit scaling law, while consistency with round jet noise theories and prediction schemes were used as a constraint, i.e., the sound intensity had to remain proportional to a characteristic length squared.

No direct relationship was found that provided reasonable scaling as a function of the polar angle. A first attempt to scale the data as a function of polar angle as it appears in the convective amplification term in Lighhill's formulation and subsequently modified by Ffowcs-Williams. This formulation did not work well at smaller polar angles. However, this result was similar to what other researchers have found when applying it to round jet noise data. It is believed that this is due to scattering and absorption of turbulence that must pass through the shear layer of the jet on its path to a microphone at a low polar angle.



Figure 22: HARN SPL scaled according to parameters found using OASPL, (a) $\Theta = 20°$, (b) $\Theta = 40°$, (c) $\Theta = 60°$.

# APPENDIX C

## References

1. Lighthill, M.J. "On sound Generated Aerodynamically. I. General Theory," Proceedings of the Royal Society A 211, pp 564-578, 1952.
2. Lighthill, M.J. "On sound Generated Aerodynamically. II. Turbulence as a Source of Sound," Proceedings of the Royal Society A 222, pp 1-21, 1954.
3. Lighthill, M.J. "Jet Noise," North Atlantic Treaty Organization Advisory Group for Aeronautical Research and Development, Report 448, 1963.
4. Lush, P. A., "Measurements of Subsonic Jet Noise and Comparison with Theory," Journal of Fluid Mechanics, Vol. 46, part 3, pp.477-500,1971.
5. Ahuja, K.K. "Correlation and Prediction of Jet Noise," Journal of Sound and Vibration, 29 (2), pp 155-168, 1973.
6. Ahuja, K.K., and Bushell, K.W. "An Experimental Study of Subsonic Jet Noise and Comparison with Theory," Journal of Sound and Vibration, 30 (3), pp 317-341. 1973.
7. Tam, Christopher K.W., Auriault, Laurent, "Jet Mixing Noise from Fine Scale Turbulence." AIAA Paper 98-2354, 1998.
8. Tam, C.K.W., Golebiowski, M., and Seiner, J.M., "On the Two components of turbulent Mixing Noise from Supersonic Jets." AIAA Paper 96-1716, 1996.
9. Tam, Christopher K. W., and Pastouchenko, Nikolai, "Noise from the Fine Scale Turbulence of Nonaxisymmetric Jets." AIAA Paper 2001-2187, May 2001.
10. Tam, Christopher K. W., "On the Failure of the Acoustic Analogy theory to Identify the Correct Noise Sources." AIAA Paper 2001-2117, May 2001.
11. Tyler, J. M., Sofrin, T. G., Davis, J. W., "Rectangular Nozzles for Jet Noise Suppression," SAE National Aeronautic Meeting, April 1959.
12. Capone, F. J., and Maiden, D. L., "Performance of Twin Two-Dimensional Wedge Nozzles Including Thrust Vectoring and Reversing Effects at Speeds up to Mach 2.20," NASA TN D-8449, 1977.
13. Capone, F. J., Hunt, B. L., and Path, G. E., "Subsonic/Supersonic Nonvectored Aeropropulsive Characteristics of Nonaxisymmetric Nozzles Installed on an F-18 Model." AIAA Paper 81-1445. 1981.
14. Seiner, John M., Ponton, Michael K., Manning, James C., "Acoustic Properties Associated with Rectangular Geometry Supersonic Nozzles," AIAA Paper 86-1472, 1986.
15. Kouts, C. A., and Yu, J. C., "Far Noise Field of a Two-Dimensional Subsonic Jet." AIAA Journal Vol. 3, No. 8, pp. 1031 – 1035. August 1975.
16. Maglieri, D. J., and Hubbard, H. H., "Preliminary Measurements of the Noise Characteristics of Some Jet Augmented Flap Configurations." NASA Memo 12-4-58L, 1958.
17. Coles, W. D., "Jet Engine Exhaust from Slot Nozzles." NASA TN D-60, 1959.
18. Maestrello, L., and McDaid, E., "Acoustic Characteristics of a High-Subsonic Jet." AIAA Journal, Vol. 9, No. 6, pp. 1058-1066, 1971.
19. Gruschka, H. D., and Schrecker, G. O., "Aeroacoustic Characteristics of Jet Flap Type Exhausts." AIAA Paper 72-130, 1972.
20. Schrecker, G. O., and Maus, J. R., "Noise Characteristics of Jet Flap Type Exhaust Flows." NASA Grant, NGR 43-001-075, 1975.
21. Olsen, W. A., Butierrez, O., and Dorsch, R. G., "The Effect of Nozzle Inlet Shape, Lip Thickness, and Exit Shape and Size on Subsonic Jet Noise." AIAA Paper 73-187, 1973.
22. Ffowcs-Williams, J. E., "Some Open Questions on the Jet Noise Problem." Boeing Science research Lab. Doc., DL-82-0730, 1968.
23. von Glahn, U. H., "Rectangular Nozzle Plume Velocity Modeling for use in Jet Noise Prediction." AIAA Paper 89-2357, 1989.
24. Tam, Christopher K. W., and Zaman, K. B. M. Q., "Subsonic Jet Noise from Nonaxisymmetric and Tabbed Nozzles." AIAA Journal, Vol. 38, No. 4, pp. 592-599, April 2000.
25. Tam, Christopher K. W., "Influence of Nozzle Geometry on the Noise of High-Speed Jets." AIAA Journal, Vol. 36, No. 8, pp. 1396-1400, August 1998.
26. Tam, C.K.W. and Zaman, K.B.M.Q., "Subsonic Jet Noise from Non-Axisymmetric and Tabbed Nozzles." AIAA Paper 99-0077, 1999.
27. Tam, Christopher K.W., "Influence of Nozzle Geometry on the Noise of High Speed Jets." AIAA paper 98-2255, 1998.
28. Munro, Scott E., Ahuja, K. K., and Englar R. J., "Airframe Noise Reduction Through Pneumatic Technology: Experiments." Submitted for

Publication to Journal of Aircraft, February, 2002.

29. Munro, Scott Edward, "Jet Noise of High Aspect-Ratio Rectangular Nozzles with Application to Pneumatic High-Lift Devices." Georgia Institute of Technology, PhD thesis, January, 2002.

30. Pope, Alan, Wind Tunnel Testing. 2nd Ed. John Wiley & Sons, NY, pp 31-80, 1964.

31. Ahuja, K.K., Tanna, H.K., and Tester, B.J. "An experimental Study of Transmission, Reflection and Scattering of Sound in A Free Jet Flight Simulation Facility and Comparison with Theory," Journal of Sound and Vibration, 75 (1), pp 51-85, 1981

32. Larsen, P. N., "Noise Generated by Air Jets from a Rectangular Slit." Ph.D. Thesis, Technical University of Denmark, 1983.

33. Bjorno, L, and Larsen, P. N., "Noise of Jets from Rectangular Slits." Acoustica, Vol. 54, pp. 247 – 256, 1984.

34. Ffowcs Williams, J.E., "The Noise From Turbulence Convected at High Speed." Philosophical Transactions of the royal Society, Vol. A-255, pp. 469-503, 1963.

35. Munro, Scott E. and Ahuja, K. K., "Fluid Dynamics of a High Aspect- Ratio Jet," AIAA-2003-3129, 2003, presented at the 9th AIAA/CEAS Aeroacoustics Conference and Exhibit, Hilton Head, South Carolina, USA, 12 - 14 May 2003.

36. Munro, Scott E. and Ahuja, K. K., "Development of a Prediction Scheme for Noise of High-Aspect Ratio Jets," AIAA-2003-3255, 2003, presented at the 9th AIAA/CEAS Aeroacoustics Conference and Exhibit, Hilton Head, South Carolina, USA, 12 - 14 May 2003.

# APPENDIX D


# Fluid Dynamics of a High Aspect-Ratio Jet

# APPENDIX D

## Fluid Dynamics of a High Aspect-Ratio Jet

**Scott E. Munro** [*]
and
**K. K. Ahuja**
**Georgia Institute of Technology**
**GTRI/ATASL**
**Atlanta, GA, 30332-0844**

### Abstract

Circulation control wings are a type of pneumatic high-lift device that have been extensively researched as to their aerodynamic benefits. However, there has been little research into the possible airframe noise reduction benefits of a circulation control wing. The key element of noise is the jet noise associated with the jet sheet emitted from the blowing slot. High aspect-ratio jet acoustic results (aspect-ratios from 100 to 3,000) from a related study showed that the jet noise of this type of jet was proportional to the slot height to the 3/2 power and slot width to the 1/2 power. Fluid dynamic experiments were performed in the present study on the high aspect-ratio nozzle to gain understanding of the flow characteristics in an effort to relate the acoustic results to flow parameters. Single hot-wire experiments indicated that the jet exhaust from the high aspect-ratio nozzle was similar to a 2-d turbulent jet. Two-wire space-correlation measurements were performed to attempt to find a relationship between the slot height of the jet and the length-scale of the flow noise generating turbulence structure. The turbulent eddy convection velocity was also calculated, and was found to vary with the local centerline velocity, and also as a function of the frequency of the eddy.

### Nomenclature

A -- Area (typically of nozzle)
AR -- Aspect ratio
a -- Speed of sound
$a_o$ -- Ambient speed of sound
f -- Frequency
HARN -- High aspect-ratio nozzle
h -- Slot height or rectangular nozzle height (small dimension)
L -- Characteristic length
$L_{eq}$ -- Characteristic length for the HARN, $L_{eq} = h^{3/4}w^{1/4}$
$L_x$ -- Length scale (streamwise direction)
$L_\tau$ -- Integral time scale
$M_c$ -- Convection Mach number

$M_t$ -- Jet centerline Mach number
PIV -- Particle image velocimetry
p -- pressure
Re -- Reynolds number
$R_x$ -- Space-correlation
$R_{x\tau}$ -- Cross-correlation
w -- width of rectangular nozzle (large dimension)
V -- Velocity
    $V_c$ -- Turbulent eddy convection velocity
    $V_j$ -- Jet exit velocity (fully expanded)
    $V_t$ -- Local jet centerline velocity
x -- Streamwise dimension, typically x = 0 is nozzle exit
y -- Dimension perpendicular to major axis of nozzle, y = 0 is center of nozzle
z -- Dimension along span of nozzle (parallel to major axis), z = 0 is center of nozzle
$\Delta x$ -- Spacing between hot-wires in x-direction
$\Delta y$ -- Spacing between hot-wires in y-direction
$\rho$ -- density
$\tau$ -- Time shift, used for cross-correlation

### Introduction

In recent years airframe noise issues have become more important to the airline industry. Thus, new and innovative ways for reducing airframe noise have been investigated. A recent study investigated the possible acoustic benefits of using a circulation control wing (CCW) as a high lift device rather than conventional flaps. [1-4]

This study found that the major contributor to airframe noise associated with a CCW configuration is the jet sheet emitted from the blowing slot. More detailed acoustic results from a high aspect-ratio nozzle (HARN) found that the level of the jet noise scaled with an equivalent length, defined as $L_{eq} = h^{3/2}w^{1/2}$. The present study is an accompanying fluid dynamic study on the same nozzle configuration. The main objective of this study was to establish a relationship between the length-scale of the flow and the nozzle geometry in an effort to relate the acoustic results to the flow. In addition, the convection velocity of the turbulent eddies was also examined.

---

## Background

Although the present study dealt exclusively with fluid dynamic measurements on a high aspect-ratio jet, an accompanying study was also performed where the acoustic characteristics of the same jet were studied. References [1, 2, and 3] discuss the acoustic work. In addition, reference [3] uses results from the present study and those of reference [2] in an effort to develop a prediction scheme for the jet noise spectra of such jets. Some of the discussion in the following sections deals with jet noise issues. In the interest of brevity, the reader is referred to the references mentioned above for background on round and rectangular jet noise. Only a brief review of rectangular jet fluid dynamic characteristics is given below.

Rectangular jets, similar to round jets, are characterized by different flow regions. In general these include the core region, the transition region, and the fully mixed turbulent region.[5] The core is characterized by an unmixed region just downstream of the nozzle exit. Eventually this disappears due to the merging of the shear layers. In a round jet, this is well defined since the shear layer is axisymmetric. However, in the case of a rectangular jet the issue is somewhat clouded. If one assumes the two dimensions to be independent, there are shear layers that grow on each of the 4 edges. The two shear layers associated with the small dimension will merge at a different location downstream than the two from the large dimension. Thus, the core is typically defined as the location where the centerline velocity falls below a certain value, usually 99% of the exit velocity. Therefore, a definite length can be associated with the core. However, one must keep in mind that the shear layers are much more complex than the round jet case.

The transition region is a region of high mixing where the jet flow is still essentially considered a 2-dimensional flow. As the flow continues downstream, the mixing eventually causes the flow to become axisymmetric. This indicates the beginning of the fully mixed region. In this region, the flow has many characteristics similar to a circular jet, including the centerline velocity decay rate proportional to $x^{-1}$ (streamwise distance).[5] The length of the core region is dependent on the jet Mach number and temperature.[5] The velocity centerline decay has also been shown to be a function of the aspect-ratio.[5]

The region where the highest levels of noise are produced in a jet is in the core region.[5] This is where the shear is very high, and the associated velocities are also at their highest. Well downstream the flow evolves into a round jet flow, however the flow velocities are much lower than the exit condition and therefore do not radiate jet noise at comparable levels to the near exit region.[5] However, as with round

jets there are many theories that have been proposed. Recently, Tam et al. have investigated nozzle shapes including rectangular jets. In their studies they have limited research to low aspect-ratio nozzles. Their results indicate that rectangular jets are actually similar to round jets.[6-10] References [7-10] show Tam's fits do indeed agree well with the experimental data. This indicates that round jet noise and rectangular jet noise are actually very similar since both can be fit to one set of generic spectral curves.

As is evident by the variation in data and theories, there is still much to be investigated in the area of rectangular jet noise. The aspect-ratios considered 'high' in the above discussion are typically one or two orders of magnitude lower than the typical aspect-ratio of a CCW system. The fluid dynamic measurements presented in this paper were taken to form a complimentary set of acoustic and flow measurements on the same system in order to relate to the acoustic and fluid dynamic properties.

## Objectives

It is well established that the acoustic radiation of a jet is related to the length-scales of the flow. In a round jet, the length-scale has been found to be proportional to the diameter of the jet. However, this is not as clear with a rectangular jet flow since there are two definite dimensions and the confusion is increased by the transitioning of the flow into an axisymmetric flow far downstream.

Hot-wires were used to obtain basic information about the jet flow, including: jet profiles, turbulence intensity profiles, centerline velocity, and the associated frequency spectra. Two-wire measurements were also made in the shear layer of the jet in an attempt to find the length-scales of the flow. An attempt was also made to obtain PIV (particle image velocimetry) data. However, due to the small size of the slot, detailed velocity information could not be obtained. However, the images themselves made for high quality flow visualization.

The PIV data will be presented first to give a general view of the flow. Then single hot-wire measurements will be presented to demonstrate how the jet flow is similar to other rectangular jet data and theoretical 2-dimensional jet flow calculations. Finally, space-time correlation data will be presented along with an analysis of the length-scales to determine the relationship between the geometry and the length-scales.

### Fabrication of the High Aspect-Ratio Nozzle

The high aspect-ratio nozzle (HARN) was designed and built in order to obtain reliable jet noise data for high aspect-ratio rectangular jets as part of an investigation examining the acoustic characteristics of circulation control wing high lift devices. It was

designed to have variable height and width so that a wide range of aspect-ratios could be tested. Much care was taken to ensure low internal noise, thus providing a test article where pure jet noise could be studied.

The upstream portion of the HARN connects to a 4" diameter pipe flange, the standard connection in all the flow facilities at GTRI, via a round-to-rectangular duct section. The inlet of the HARN is 2.75" X 2.75" and expands from the inlet dimensions to 30" wide by 0.25" high over a streamwise distance of 30" as shown in figure 1. Knife-edge blades are attached to the HARN exit to provide the final contraction to the small nozzle heights. Shims can be placed under the blades to change the height. Blanking plates were also fabricated so that the width of the nozzle could be varied as well.

Initial experiments indicated that the top and bottom plates of the HARN deflected from the air pressure used to generate the flow. In order to minimize internal noise, tie-down rods were not used to prevent the deflection. Instead, stiffening beams were added on the outside of the structure to maintain an unobstructed flow path internal to the HARN. These beams can be seen in figure 1. More details of the HARN design and internal noise issues can be found in reference [1].
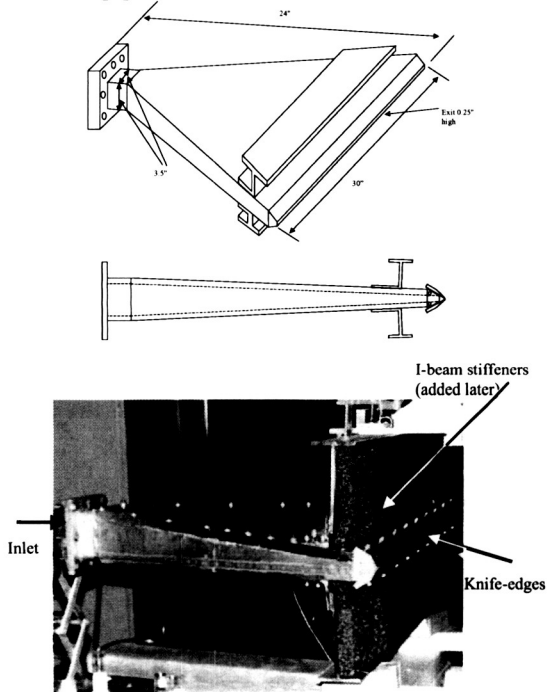


Figure 1: Harn Nozzle.

## Particle Image Velocimetry Measurements

PIV Experimental Set-Up.

A PIV system is helpful in ascertaining the general instantaneous characteristics of a flow. It provides both an overall image of the flow field and the velocity vectors for an entire plane in the flow. The PIV system used for the present investigation was a TSI Incorporated two-dimensional PIV system. The system includes two lasers, a camera and software for a PC platform to run the system and acquire the data. The lasers are positioned with lenses so that the beam is turned into a laser sheet. The sheet is positioned as desired in the flow, and the camera is positioned such that the focal plane of the camera is the same plane as the laser sheet. The lasers are synchronized so that they pulse at a set time increment. Both images are recorded by the camera. The displacement of the seed particles for the two images are compared by the software, and velocity vectors are calculated. The process is all integrated into the software, from the acquisition of the images to calculation of the velocity vectors. As with most flow visualization, acquisition of quality PIV data is not trivial and is dependent on several factors that must be adjusted, including the seeding density, the image time separation, and careful positioning of the camera and lasers.

For the HARN PIV tests, the laser sheet was positioned to align with the minor axis of the jet as depicted in figure 2. This essentially provided a flow visualization 'slice' of the jet. The camera was positioned 90° to the laser sheet such that the edge of the nozzle was visible at the upstream edge of the image. The camera was focused as close as possible to try to resolve the small core of the jet. The flow was seeded with titanium-dioxide powder by using a pressurized shaker that distributed the powder into the facility plenum chamber. PIV images were taken at several jet velocities.
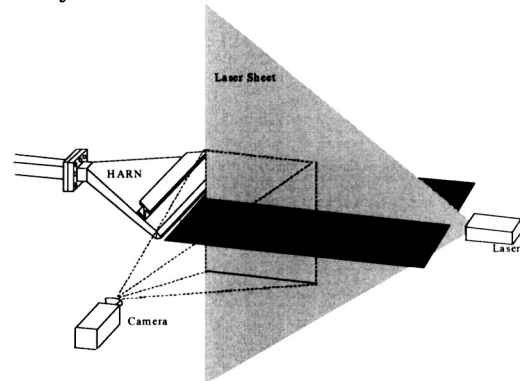


Figure 2: Schematic of PIV set-up.

## PIV Analysis and discussion

The PIV system was used to acquire general flow visualization images and to extract instantaneous flow velocity vectors from the images. In general, the size of the jet was too small to adequately extract flow velocities from the core region of the jet. The lenses available with this system were not suitable for focusing in on the extremely small potential core of the jet. However, the images were able to provide spectacular flow visualization images.

The PIV experiments were performed in the High Temperature Flow Facility (HTFF) where the PIV system is routinely used. The HTFF has a high pressure air supply and an acoustically treated plenum to absorb any upstream flow and valve noise. The HARN mounts to the downstream exit of the plenum. The PIV images were recorded at several jet exit velocities, including 10 ft/s, 60 ft/s, 450 ft/s, 700 ft/s, and 850 ft/s.

Figures 3 - 6 show some typical images for four different exit velocities: 10, 60, 460, and 720 ft/s. Some of the images' contrast and brightness were changed to make the jet visible. This does not change the content of the image, however it does brighten the background of the image revealing details that might not be visible in another image that did not need to be altered to view the jet. Also, at the higher speeds the flow could not be seeded as well as at the low speeds. This limits the detail of the image and its appearance for visual comparison from one velocity to the next. One must therefore exercise caution in drawing conclusions from one image to the next. For example, after examining figure 4 one might conclude that the jet is actually not as wide as the jet in figure 5. However, hot-wire data indicate that this is not the case and that in fact the two jets have very similar spreading characteristics.



Figure 4: Sample PIV image, Vj = 60 ft/s.
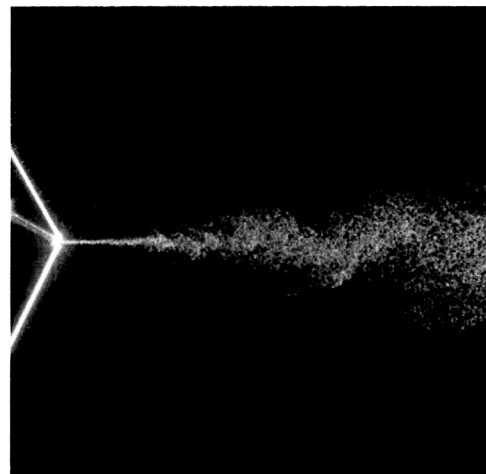


Figure 5: Sample PIV image, Vj = 460 ft/s.



Figure 6: Sample PIV image, Vj = 720 ft/s.

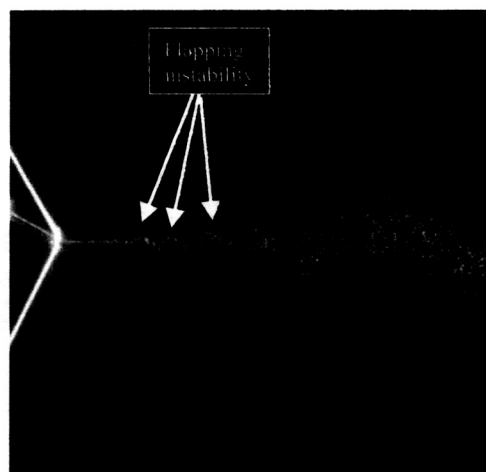

Figure 3: Sample PIV image, Vj = 10 ft/s.

Even though some caution must be exercised in drawing conclusions from these images, there are some general characteristics of the jet that can be observed. First of all, there is definitely a laminar-like region of the jet very near the jet exit. This seems to occur for all velocities tested. There is very little spreading of the jet in this region. As the jet progresses large flapping instabilities are seen in the images. This can actually be seen in at least one image presented for each velocity. This flapping developed with distance and eventually caused the jet to burst suddenly. In some cases the flapping was so strong it could be seen in the burst region as well, and even was extracted by the velocity vector extraction software. Figure 6 shows an image of this flapping in the burst region, and figure 7 shows the velocity vectors extracted by the computer where the flapping tendency of the jet can be seen quite clearly.
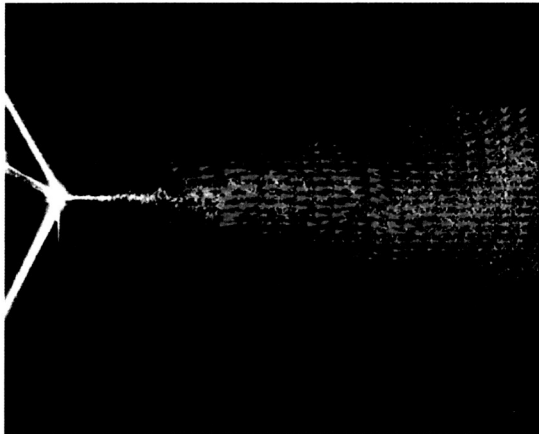


Figure 7:  Sample PIV image with velocity vectors.

The flow visualization indicated that the jet has two definite regions of flow. It was desired to determine if in fact the jet was initially laminar at the exit. However, from basic jet flow literature, and in discussions with colleagues working in the field, there does not appear to be a concrete definition of a 'laminar' jet since all jets eventually become turbulent. In general it is assumed that extremely low Reynolds number jets (Re < 30) are defined to be laminar. However, all conditions presented here would be considered turbulent (Re ~ 7,000 – 25,000 for PIV measurements). Perhaps the bursting is simply the transition mixing discussed by Dimotokis.[11] Schlichting[12] also notes that turbulent jets (2-d) have different spreading rates (laminar ~ $x^{2/3}$ and turbulent ~ x) however this trend cannot be ascertained from the PIV data. Pai[13] defines a low-speed laminar jet as one that has mixing only due to molecular transfer. It is probable that this was not the case, at least in the shear

layers of the HARN jet. However, the PIV cannot definitively answer that question. Once the bursting occurred, the jet-spread angle was approximately 7°, which is similar to that for round jets. Thus, beyond the burst region, the jet seemed to behave like any other turbulent jet.

In general, the HARN does exhibit many of the typical jet characteristics. The question of whether or not it is initially laminar or turbulent will have to wait until the discussion of the hot-wire data where hopefully more detailed tests will help clear up this issue. In any case, this was kept in mind when taking additional detailed hot-wire measurements. Since there was a good likelihood of the length-scales of these two regions of flow having somewhat independent length-scales, two sets of hot-wire data were typically taken. One set was acquired where the data points were almost assuredly in the pre-burst area of the jet, and one set where the data points were in the post-burst region of the jet.
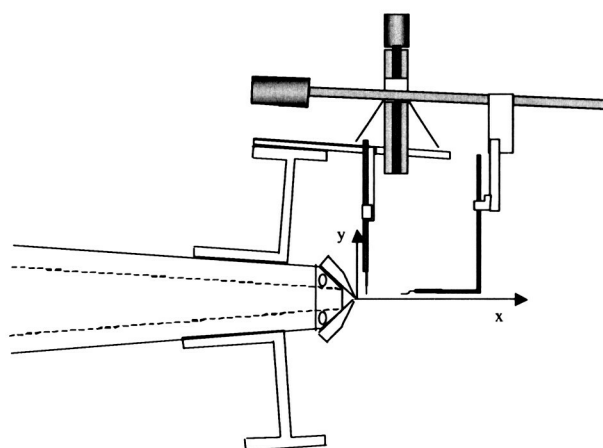
### Hot-wire Measurements
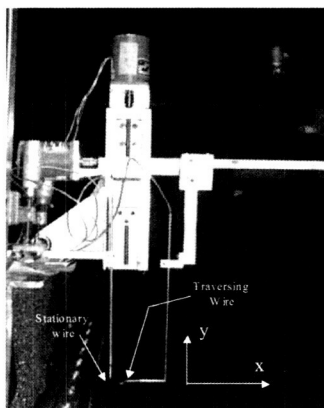
Hot-wire Experimental Set-up

The hot-wire system used was a Dantec Streamline constant temperature anemometer (CTA), model 90N10 frame and 90C10 modules. The system also has a calibration module. The software provided with the system controls the wire set-up, bridge balance, and also contains an automated calibration option, as well as real time average velocity or time signal acquisition. Due to the need for extremely high sampling rates, a separate computer and software system were used to sample and store the hot-wire signal. An HP spectra analyzer that sampled all channels simultaneously at frequencies up to 262 kHz was used to acquire the hot-wire data. This provided plenty of resolution for investigating the turbulence frequencies up to 100 kHz. The data was post-processed using Matlab® software. In-house script files were written to output a mean velocity and turbulence intensity as well as power spectral densities, cross correlations, cross powers, and coherence for the two-wire data. More details of the hot-wire data acquisition can be found in reference [1].

In order to acquire the data, one hot-wire was needed for the profile and turbulence measurements, while two were needed to acquire cross-correlation data. One of the wires in the correlation tests would need to traverse while the other remained stationary. The single wire would also need to traverse. Thus, one wire was mounted by a bar fixed to the HARN stiffening beam, while the other wire was mounted on a two axes traverse, also fixed to the HARN stiffening beam. The hot-wire mounting set-up is shown in figure 8 (a and b). For the single wire measurements, the stationary wire was simply removed from its position.

(a)



(b)

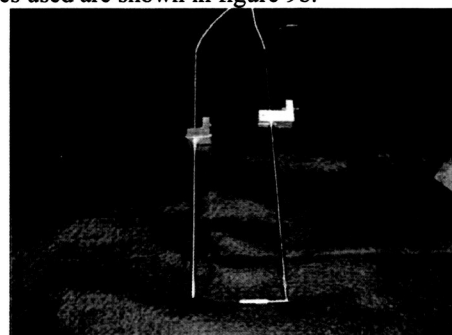Figure 8: Hot-wire measurement set-up.

wires, 1.25 mm long. Several different wire configurations were used for various measurements. The wires used are shown in figure 9b.



(a)
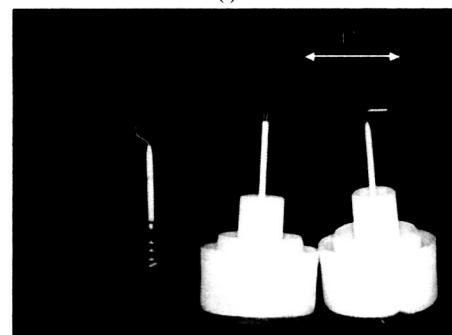


(b)

Figure 9: Hot-wire systems used in measurements. (a) probes, (b) wires.

The traversing wire was capable of traversing in the x and y directions independently. One important factor for the traverse system was that it be capable of very minute movements. This was important because the size of the jet emanating from the nozzle was very small, and accurate distances are crucial to properly calculating shear values, length and time scales, as well as the convection velocity.

For the x direction (see figure 8), the minimum traverse movement was 0.000125", while it was 0.0001965" for the y direction. More details of the traverse system and an error analysis of the hot-wire movement is contained in reference [1].

The hot-wires and probe-supports were also obtained from Dantec Measurement Technologies. Two different probe-supports were used, one completely straight (model H21), while the other had a 90° bend (model H22). These are pictured in figure 9a (and are shown installed in position in figure 8). The hot-wires were platinum-plated tungsten 5 μm diameter

The HARN was installed on GTRI's Jet Thrust Rig (JTR) for the hot-wire tests. The JTR consists of a small plenum chamber with supply air entering in on one side and a flange on the other side for mounting nozzles. The plenum is mounted to a structure fitted with load cells for thrust measurements. For the hot-wire tests on the HARN, there was no need for thrust measurements, but the facility was available and provided an air supply for the HARN. Reference [1] contains more information on the JTR and the HARN hot-wire set-up.

There was one disadvantage to using the JTR. The JTR is not an acoustic facility and therefore has no provisions for upstream noise reduction. It was feared that internal noise might become significant if there were large mass flows through the upstream piping. This would result from exit conditions that required high mass flows, either due to a large exit area or a high exit velocity. Since the acoustic data in the accompanying study[1,2] were acquired with low upstream noise, it was decided to take most of the hot-wire data at a nozzle width of 6.5" to keep the mass flow and thus any internal noise at a minimum. Basic mean flow and turbulence measurements were taken at

3 velocities. The two-wire data was mostly acquired for only one jet velocity, concentrating on the changes found when varying the slot height. In addition to keeping the internal noise low, lower exit velocities were used to help prolong hot-wire life. During the single wire tests it was found that hot-wires had a significantly shorter life in jets with exit velocities above about 600 ft/s. Thus, during the very time consuming two-wire measurements lower velocities were generally used to minimize wire breakage.

Single Hot-Wire Measurements

The main purpose of the single hot-wire measurements was to gather general information about the HARN jet flow development and compare the findings to lower aspect-ratio jet data available in literature, as well as to round jet data. These measurements mainly consisted of velocity profiles at various downstream locations, centerline velocity traces, and in some cases turbulence intensity information.

Figure 10 shows velocity profiles at several different streamwise locations. As one might expect, the flow very near the exit is nearly plug flow, and the shear layer grows as the profiles are taken father downstream. The profiles can be non-dimensionalized by simply plotting $y/h$ versus $V/V_{max}$, shown in figure 11. Again the flow starts off like a plug flow, but quickly develops into a self-similar flow. These profiles are compared with data from Schlicting[12] in the figure. Notice that the profiles are very similar to the curves from Schlicting. Different velocities are compared at the same streamwise location in figure 12. These again show that the jet is self-similar beyond the core region of the jet.
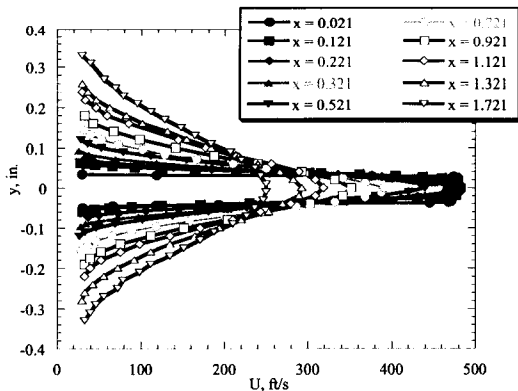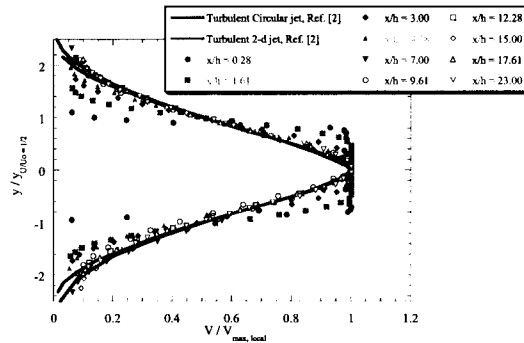


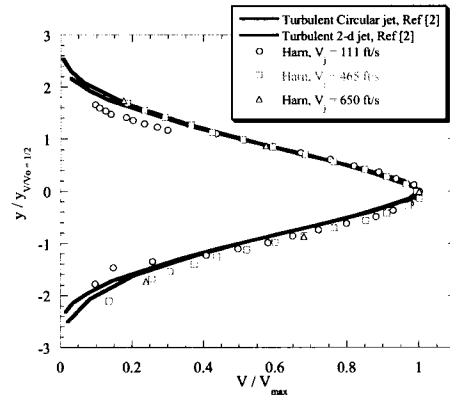Figure 11: Non-dimensionalized velocity profiles compared with theory,



Figure 12: Hot-wire velocity profiles at the same streamwise location for different jet velocities, $x/h = 37$ ($h = 0.040"$).

Turbulence intensities can also be compared for the different velocities and different locations as shown in figure 13. Near the exit, the turbulence is very low in the core, while very high in the shear layers. As one would expect, the shear layers grow and begin to merge as they progress downstream. None of the previous results were unexpected, however they do confirm that the jet is clean and behaves like a 'normal' jet, i.e., there are no obvious flow differences particular to this nozzle that might explain the different acoustic results found in references [1 and 2].



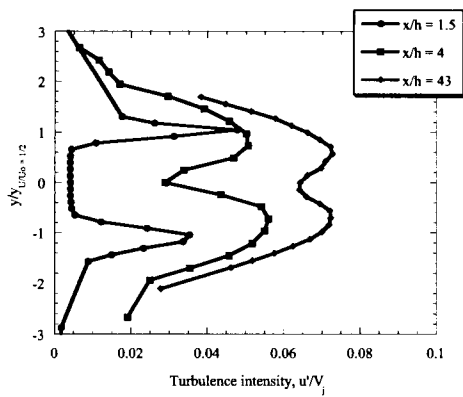Figure 10: Hot-wire velocity profiles at several downstream locations,

Figure 13: Turbulence intensity at different streamwise locations,

Velocity data were also acquired along the centerline of the jet. Due to the small size of the jet, considerable care had to be taken to verify that indeed the data were taken along the jet centerline. Figure 14 shows the centerline jet velocity for different slot heights. Notice that when velocity is normalized by the jet velocity and axial distance, x, is normalized by the slot height, h, the centerline velocity collapses for different slot heights over a wide range of x/h. Similarly, in figure 15 the centerline velocity is compared at a variety of exit jet conditions. It is worth noting that the core length appears to vary with $V_j$. There was some concern that increased internal noise of the facility where these measurements were made may have changed the mixing characteristics of the flow through acoustic excitation.[15-17]
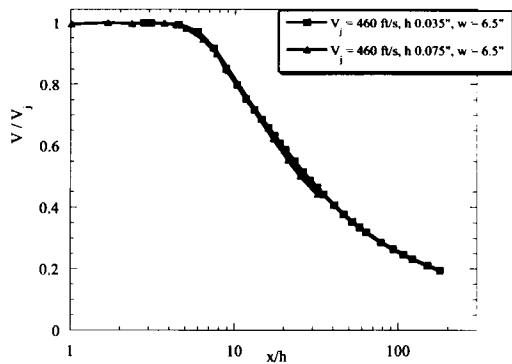


Figure 14: Centerline velocity as a function of x/h for different h.

The experiments were repeated with a muffler mounted between the flow valve and the plenum. As shown in figure 15, similar trends were obtained even with this configuration where the internal noise was reduced considerably. However, this trend has been seen by other researchers also. For example, figure 16 is data taken from Simonich.[18] Simonich noted the relationship between the jet core length and the exit Mach number. He defined the core length as the location where the velocity dropped below 99.5% of the exit velocity.[18] The current data has been plotted on top of the Simonich's data. It should be noted that the figure in reference [18] included data from several researchers, however, here all the data from the paper is shown as the same symbol to distinguish it from the present data. The HARN data falls in the middle of the previous data with a similar trend. This indicates that the change in core length may be a function of the Mach number rather than upstream noise or facility related, since even the data with a muffler installed on the JTR exhibits the same Mach number trend. There is some scatter in the core locations. This may be due to measurement errors associated with small x distances (see reference [1] for a detailed error analysis).
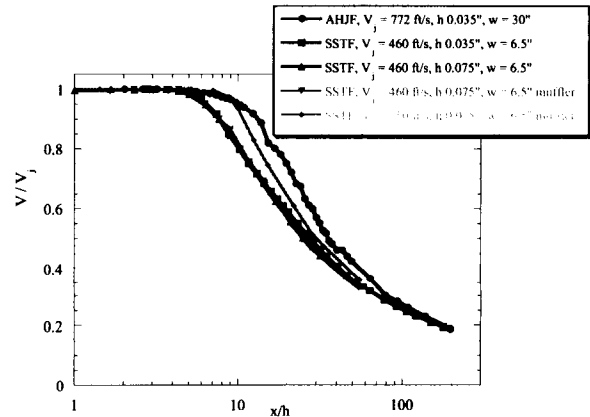


Figure 15: Centerline velocity as a function of x/h for different h, w, and Vj.

Another interesting point to note in figure 15 is the rate of decay of $V/V_j$ with x/h. Typically, for round jets, the rate of decay of the jet velocity is proportional to x/d. Here this decay rate is proportional to $(x/h)^{1/2}$ as illustrated in figure 17. Two of the curves from figure 15 have been re-plotted with a theoretical $(x/h)^{-1/2}$ curve. All of the centerline velocity data was found to be similar to $(x/h)^{-1/2}$ beyond the core. This is similar to the theoretical rate of decrease for a 2-d turbulent jet of $x^{-1/2}$ presented in reference [12]. It should also be noted

that the rate of centerline velocity decrease is $x^{1/3}$ for a 2-d laminar jet.[12] Thus, certainly downstream of the core the jet is definitely turbulent.
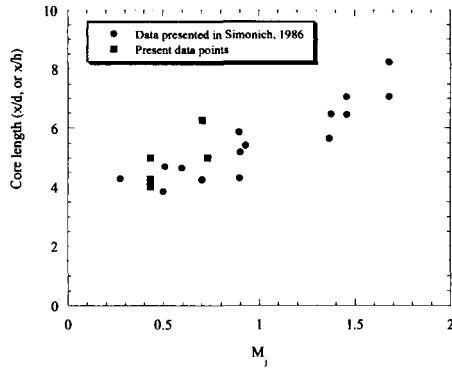


Figure 16: Variation of jet core length as a function of Mach number. Note: circles are data from reference [5], re-plotted.

Another important parameter used to evaluate jets is the spread rate. The jet half-width is commonly defined as the distance from the center of the jet to the location where the velocity is half of the centerline velocity. Using the velocity profile information, the jet half-width was found at each x location for each test condition. These data are plotted in figure 18 with a sample PIV image and the turbulence intensity along the centerline and lip line. Notice that the jet half-width data tends to have a distinct 'knee' where the spread rate (the slope of the half-width vs. x/h curve) drastically changes. This seems to coincide with the 'bursting' of the jet seen in the PIV image around x/h ~ 12. In addition, this generally coincides with higher turbulence intensities.
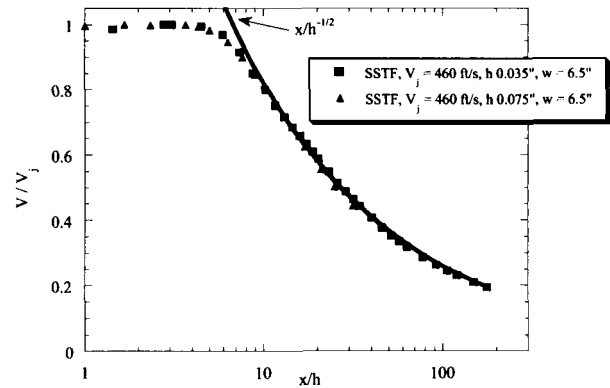


Figure 17: Centerline velocity of HARN compared to theoretical velocity variation.

As mentioned in the discussion of the PIV images, the bursting seems to come from the large instability wave that can be seen in the images just ahead of the burst region. It is not necessarily reasonable to assume that this burst region is self-similar to different slot heights and jet velocities. The instability growth and subsequent burst could be Reynolds number dependent as well as dependent on the upstream noise and turbulence. However, figure 18 indicates that indeed the bursting phenomena of the jet is self-similar since the non-dimensionalized jet half-width and the turbulence intensity tend to collapse for different jet conditions and nozzle geometries.

The single-wire data gave confidence in the hot-wire data acquisition methods. It appeared that the jet was behaving similar to other jets. This provided a background for acquiring the two-wire data in the shear layer of the jet. This initial data also supported the PIV result that there were two distinct regions associated with the flow, one before the burst region, and one after. Thus, the single wire data was a guide for determining where to position the two wires such that length-scales in both regions could be measured.

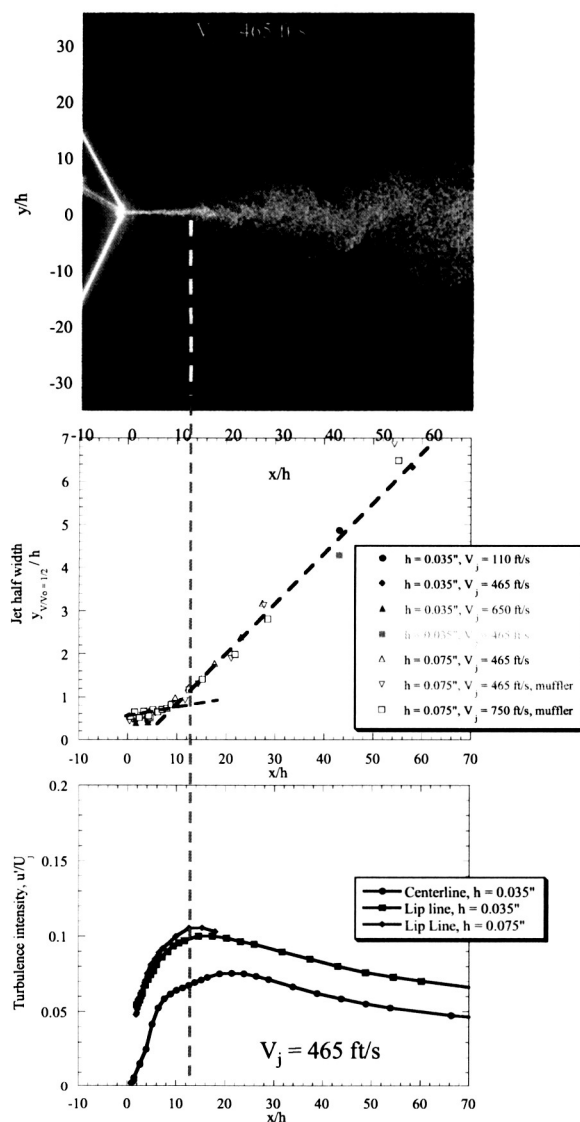Figure 18: Comparison of PIV, jet half-width, and turbulence intensity results.

## Space-Time Correlations with Two-Wire Measurements

As mentioned above, the goal of the two-wire measurements was to determine the length-scales of the HARN jet and to try to relate those length-scales back to the geometry of the nozzle. Davies, Fisher and Barratt[14] performed a study where they made careful hot-wire measurements to find length and time scales for a 1 inch diameter round jet. Using the cross-correlation of the hot-wire time signals, they found

integral length and time scales. Their methodology will be followed to calculate similar integral scales for the HARN jet.

Davies, Fisher, Barratt made two-wire measurements primarily at two streamwise locations. One wire was stationary, while the other was traversed in the x or y direction starting from directly behind or directly below the stationary wire. Figure 8 shows the set-up for similar two-wire correlation tests on the HARN. Data were recorded for both wires after moving the traversing wire by some increment. This provided a set of test points where there were two time signals to be analyzed.

Figure 19 shows a schematic of the test points for the HARN jet. Essentially two x locations were chosen, one close to the nozzle exit that would almost assuredly be upstream of the burst region, and one about 2" downstream of the nozzle exit, that was well downstream of the burst region. In order to find out how the scales of the flow varied with changes in slot height, both measurements were repeated for a second slot height. There are some differences between the current tests and those of reference [14].
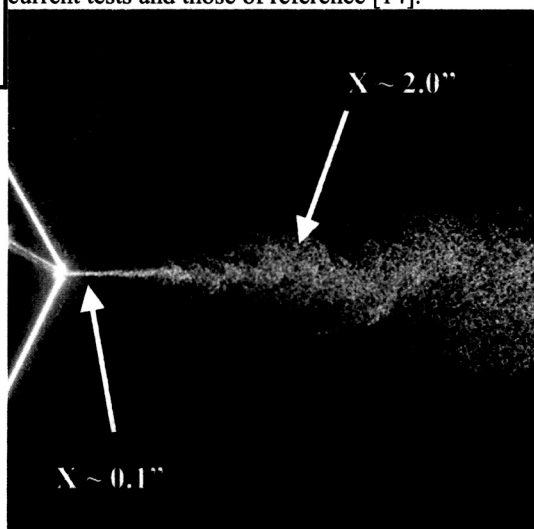


Figure 19: Jet location for cross-correlation data.

The most significant is simply a matter of the different nozzle geometries. In the case of reference [14], several radial positions were used for streamwise correlation data, however the nozzle lip-line was where most of their data were acquired and all the data was taken in the shear layer region between the core of the jet and ambient fluid (x/d = 1.5 and x/d = 4.5). Thus, the lip line was always in the region of highest mixing. In the case of the HARN, the measurement location near the nozzle exit was along the lip-line, however the downstream measurement location was well downstream of the core region. Thus, it was decided to place the downstream point at the y location that

corresponded to the jet half-width. This was done because the lip-line at that downstream location would have been considered nearly the center of the jet, since the jet is extremely large compared with the nozzle at high x/h.

At each streamwise location where data were acquired, the two wires were initially positioned as close together as possible, then the traversing hot-wire was traversed downstream, directly behind the stationary wire, or in the case of the y direction, directly below the stationary wire. Figure 20 shows some pictures of the initial wire positions. Precise initial positioning of the wire turned out to be one of the most difficult tasks of this portion of the HARN study. The initial distance between the wires ($\Delta x_o$) for a data set was measured visually. If the initial position was accurate, the following measurement points would also have accurate positions since the traverse had very fine movement capability ($\Delta x_{total} = \Delta x_o + \Delta x_{trav}$). However, if the initial position between the two wires was inaccurate, the distance between the two wires is inaccurate until the distance between the wires was such that $\Delta x_o \ll \Delta x_{trav}$. Very small errors in measuring the distances between the wires made large differences in the post-processing calculations, thus $\Delta x_o$ was an extremely important measurement. Careful measurement of the initial positions of the wires using the photos seemed to be the best method for determining their positions. They were also aligned in the y-direction in the flow by matching the measured velocity on both wires. This worked well since the velocity changed rapidly with small changes in the y-direction.
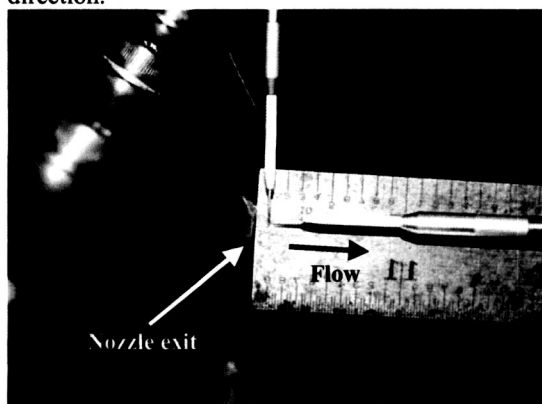


Figure 20: Sample photo of hot-wire placement.

Once the raw hot-wire time histories were taken, they were fed into Matlab where the cross-correlation, the coherence, and the cross-power between the stationary and traversing hot-wire signals were calculated. When Davies, Fisher, and Barratt wrote their paper in 1963, the available computing power was insufficient to perform cross-power spectra and coherence functions on the data, and hence most of their calculations were done using time-domain data. With the impressive capacity of the modern computers, length-scales and time-scales of the HARN flow as a function of frequency in addition to the global values from the cross-correlation can be generated. Most of the HARN data were acquired for a jet velocity of about 465 ft/s. The velocity coincided with the velocity range in reference [14] and was also one of the test points for acoustic data in the accompanying acoustic study in references [1 and 2]. However, this was also a reasonable test point because it was found that the hot-wires broke after much less use at the higher velocities. The slower velocity was also desirable because of the low internal flow rates. Increasing the exit velocity increased the internal velocities, and hence, the internal noise in the test facility used for these measurements. This was a concern since it has been shown that the flow can be excited by internal noise.[15-17] Since internal noise was known to be low for the acoustic tests in references [1 and 2], low internal noise was needed here to maintain the same flow for the hot-wire measurements.

Data were obtained for two slot heights, h ~ 0.035" and h ~ 0.075". As expected, the two hot-wire signals became uncorrelated very quickly at the location near the nozzle. This is due to the much smaller shear layer near the nozzle and therefore the resulting structures will be smaller and dissipate more quickly. However, the downstream location has highly correlated signals over a large separation distance. Since it is much easier to directly compare these data to that of reference [14], the data for the 0.075" height at x = 2.05" (x/h ~ 28) will be used to demonstrate the processing methods.

As already mentioned, there is a great wealth of information that can be extracted from the hot-wire time signals. For all the analysis shown below, the data were recorded at 262 kHz for 14.8 seconds (the maximum that could be stored on the HP analyzer system at one time). This provided ample frequency resolution up to at least 80 kHz for the frequency domain analysis, and the 14.8 seconds provided enough time for over 200 averages when taking the FFT, the coherence, and the cross-power spectra. For more details on the processing of the data, the reader is referred to reference [1].

The space correlation coefficient is defined as the cross-correlation of the time signals in space and is

$$R_x = \frac{1}{T} \int_0^T \frac{\overline{v_1(0)v_2(x)}}{v_1^2} dt, \qquad (1)$$

noting that $R_x$ is the correlation coefficient in the x direction and $v_1$ and $v_2$ are the fluctuating velocity

signals from the respective hot-wires. The integral length-scale is defined[14] as follows:

$$L_x = \int_0^\infty R_x dx. \qquad (2)$$

This is related to the longitudinal integral scale of the turbulence[14]. By introducing a time shift, $\tau$, to one of the signals, the cross-correlation can be calculated as

$$R_{x\tau} = \frac{1}{T}\int_0^T \frac{\overline{v_1(0,0)v_2(x,\tau)}}{\overline{v_1^2}}dt, \qquad (3)$$

noting that $R_{x\tau}$ is a function of both x and $\tau$. Plotting $R_{x\tau}$ versus $\tau$ allows for several observations. Each pair of signals at a given $\Delta x$ between the wires produces an $R_{x\tau}$ versus $\tau$ curve. Note from the equation for $R_{x\tau}$ that the value of $R_{x\tau}$ for $\tau = 0$ is the value of $R_x$ for that particular set of signals. Davies, Fisher and Barratt also stated that the peak of each curve represents the convection of energy-bearing turbulent eddies, and that the curve produced by taking the peak point of each curve is the auto-correlation of the energy-containing eddies of the flow in a moving frame traveling at the convection velocity.[14] The integral of this curve is referred to as the moving-axis integral time-scale, defined as

$$L_\tau = \int_0^\infty R_{\tau c} d\tau. \qquad (4)$$

This is the rate at which the turbulence changes with time.

Convection velocities can be calculated from the resulting scales, $V_c \sim L_x/L_\tau$. Alternatively, by noting the time of each cross-correlation peak and the $\Delta x$ between the wires, convection velocity for these eddies can be calculated.

The following figures and discussion will follow the methodology of reference [14], and will show the progression of the data processing for one example. Once the process has been shown using the sample data set, the resultant length scales, plus the convection velocities for all the test cases will be presented. For each data set the initial traverse increment for the hot-wire was very small to guarantee a high correlation between the signals at least for a few points. Eventually the increment between data points was increased so that the entire correlation length could be covered with a reasonable number of points. Figure 21 shows a sample distribution of data points in the x-direction. Figure 22 is the cross-correlation of the data, $R_{x\tau}$. Keep in mind that each curve represents one set of time history files. In this particular figure, only the data for every other $\Delta x$ point is plotted to reduce the clutter on the plot for demonstration purposes. Figure 23 shows only a few of the curves from figure 22 and

graphically demonstrates how $R_x$, and $R_\tau$ are pulled from the cross-correlation data. Figure 24 is the plot of $R_x$, corresponding to the data in figure 22b. This curve can be integrated numerically, resulting in $L_x = 0.15"$ for this case.
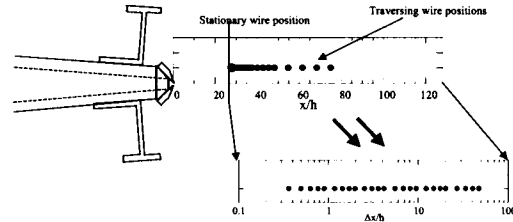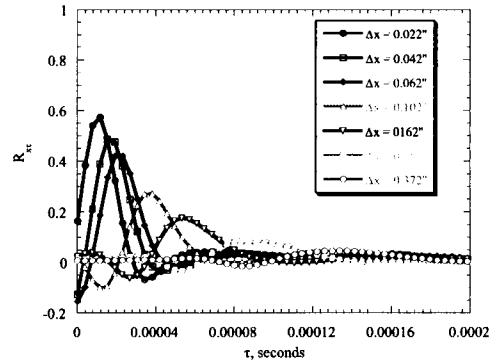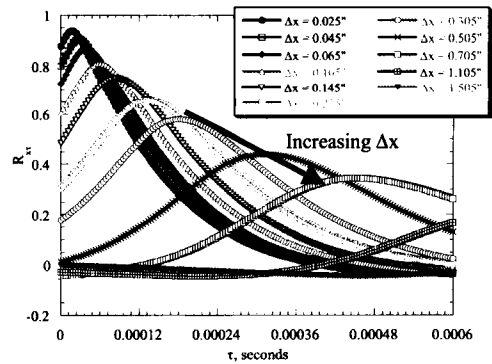


Figure 21: Distribution of data points for correlation data.



(a)



(b)

Figure 22: Cross-correlation of two hot-wires at several Dx, h ~ 0.075", Vj = 465 ft/s. (a) xstationary = 0.10", (b) xstationary = 2.10"
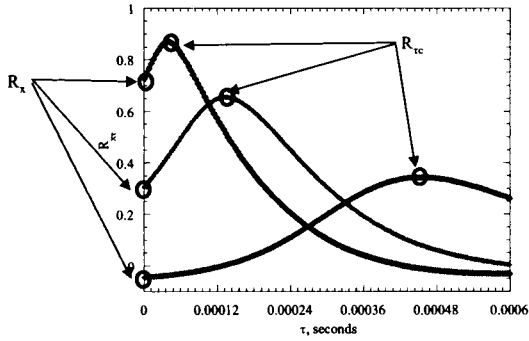
Figure 23: Illustration of how the space-correlation and auto-correlation of the energy containing eddies are found from the cross-correlation.
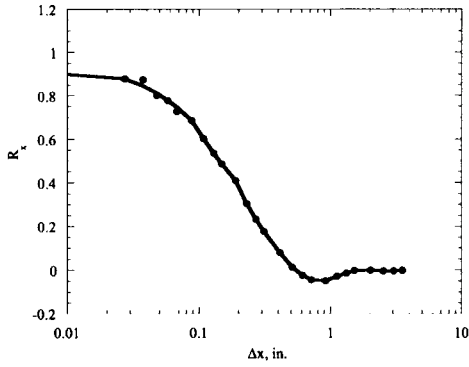


Figure 24: Space-correlation for the data in figure 24(b).

Following this process for all the data sets, the length-scale can be plotted for each condition. The length-scales are plotted versus x location in figure 25. There are only a few points to examine, but it is still worthwhile to find a relationship between the points. In reference [14] a linear relationship between $L_x$ and x was found for the round jet. In the present study, there does not appear to be a linear relationship between $L_x$ and x or $L_x/h$ and x/h. After examining several different possible relationships, it was found that the $L_x$ ~ $x(AR)^{1/4}$. This is shown in figure 26 where the x location is multiplied by the aspect-ratio factor. This is a rather unusual relationship and hence requires some closer examination.
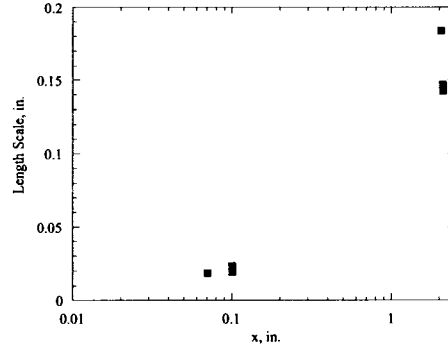


Figure 25: Global length scales calculated from the space-correlation in figure 20.

Based on relationship found in figure 26 some rather interesting observations can be made. By substituting w/h for aspect ratio and multiplying by h/h, the following re-organization can be done:

$$L_x ~ x(AR)^{1/4} \qquad (5)$$

$$L_x ~ x\left(\frac{w}{h}\right)^{1/4} \qquad (6)$$

$$L_x ~ x\frac{h}{h}\left(\frac{w}{h}\right)^{1/4} ~ \frac{x}{h}h^{3/4}w^{1/4} ~ \frac{x}{h}L_{eq}, \qquad (7)$$

Thus, it appears the length-scale is proportional to the streamwise location and the equivalent length $L_{eq}$ = $h^{3/4}w^{1/4}$ if the manipulation is appropriate. This is the same scale that was found to scale the acoustic spectra in references [1 and 2].
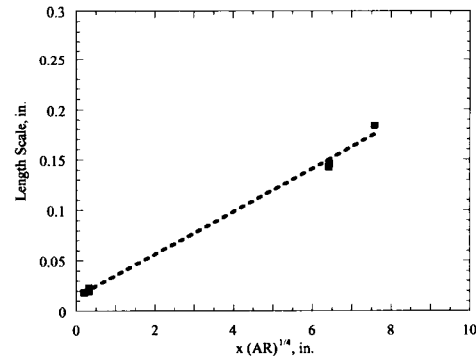


Figure 26: Global length scales plotted as a linear function of location and aspect-ratio.

It is generally accepted that different frequencies are radiated from different locations in the

jet.[18] Typically, high frequency noise is generated very near the nozzle while low frequency noise is generated at some distance from the nozzle exit. Thus, it can be assumed that the majority of noise generated for a particular frequency is generated at a particular streamwise location, x/h. It therefore makes sense that $L_x \sim x/h$ and is reasonable to extract an x/h from the relationship. Once this is done, the equivalent length falls out of the relationship. Therefore, the length-scale for a given frequency is directly proportional to $L_{eq}$. This is an extremely important result in that it supports the scaling parameters identified in the acoustic study on the same nozzle.[1, 2] However, it must be admitted that this result was extracted from a very few number of data points, and also that w was constant for all these tests. However, the fact that the equivalent-length defined during the acoustic data analysis can be derived as the appropriate length-scale for the flow from hot-wire data is noteworthy. The reader is cautioned that this result needs more examination. However, due to time constraints and facility schedule a more detailed investigation of this will have to be left to future work. It will suffice here to state that the length-scales responsible for generating a particular frequency of noise appears to be proportional to $h^{3/4}w^{1/4}$ which was also borne out by the HARN acoustic data for the same configurations.[1, 2]

## Variation of Convection Velocity with Frequency

Another parameter important to the aeroacoustics of the HARN that can be extracted from the two-wire measurements is the convection velocity of the turbulent eddies. Convection velocity can be calculated from the information already discussed. If one again returns to figure 22 of the cross correlation of the time signals, it was noted that for each wire spacing there is a cross-correlation curve. The peak of the cross-correlation curve is associated with time it takes the convected eddies to move from the first wire to the second wire. Since the distance between the wires is known, a convection speed can be calculated. A velocity can be calculated for each spacing, producing convection speed as a function of x (wire location). Normally it is assumed that the convection speed is approximately 0.65 $V_j$. Figure 27 is a plot of the convection velocity normalized by the jet exit velocity for several data-sets. Notice that this does not correlate with the assumed value of 0.65 for the ratio $V_c/V_j$. However, notice that near the exit of the nozzle (x/h < 5) the ratio of velocities is near 0.6. Clearly the jet exit velocity is not the proper scale for the convection velocity throughout the jet.
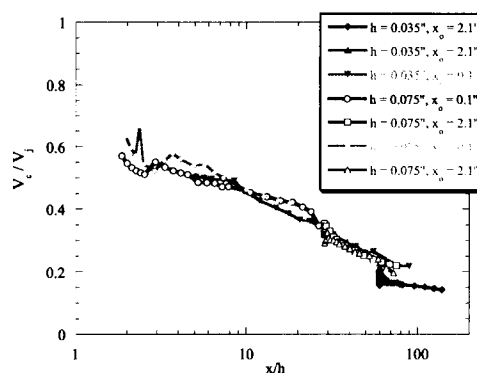


Figure 27: Convection velocity normalized by jet exit velocity.

The convection velocity drops as the local velocity drops with increasing x/h. Figure 28 is the same data normalized by the local centerline jet velocity, $V_f$. Notice that this ratio varies from 0.50 − 0.80, with an average value of 0.65. This is an important result since much of the work using a convection speed, or convection Mach number, simply uses 0.65 of the exit Velocity or Mach number. This is not strictly correct as shown in the previous figures. In fact, if one number is used to represent the convection velocity, it should be less than 0.65 $V_j$ since $V_c \sim 0.65 \ V_f$ and $V_f < V_j$ (except near the core).
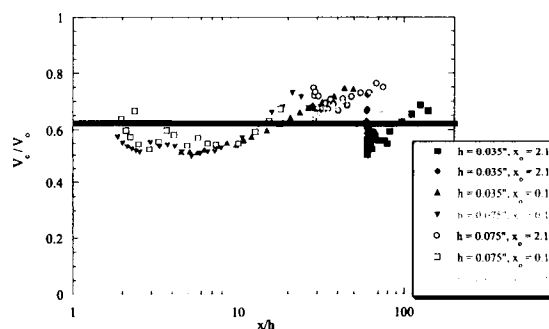


Figure 28: Convection velocity normalized by the jet centerline velocity at the appropriate x/h.

In addition to the variation of the convection speed with distance from the nozzle exit, some researchers have shown a variation of convection velocity with the frequency, or wavelength, of the eddy being convected. For example, De Belleval et al.,[20] showed this type of result, but gave no discussion on the topic, merely noting that the average was 0.65 $V_j$.

Only global convection speed can be calculated using the method in reference [14]. However, the capability now exists where the hot-wire data can easily be converted into the frequency domain, and the convection speed can be calculated for each frequency using the cross-power between the two signals. Since the cross-power is generally a complex number, it is appropriate to separate it into a magnitude and phase. The magnitude is a relative estimate of how correlated the signals are, while the phase is the relative phase between the two signals.

Figure 29 (a and b) is an example of the cross-spectra between the two wires for several values of $\Delta x$. Notice that the magnitude of the cross-power decreases as $\Delta x$ increases, particularly at frequencies greater than 500 Hz. The phase also seems to indicate that less of the spectrum is correlated as the wires separation grows. This is shown by the phase curves' smooth portion at low frequencies that eventually progresses into a random varying region as frequency is increased.

# APPENDIX E

# Development of a Prediction Scheme for High Aspect-Ratio Jet Noise

# APPENDIX E

## Development of a Prediction Scheme for High Aspect-Ratio Jet Noise

### Scott E. Munro[*]
### and
### K. K. Ahuja
### Georgia Institute of Technology
### GTRI/ATASL
### Atlanta, GA, 30332-0844

### Abstract

Circulation control wings are a type of pneumatic high-lift device that have been extensively researched as to their aerodynamic benefits. However, there has been little research into the possible airframe noise reduction benefits of a circulation control wing. The key element of noise is the jet noise associated with the jet sheet emitted from the blowing slot. This jet sheet is essentially a high aspect-ratio rectangular jet. A recent study on high aspect-ratio jet noise was performed on a nozzle with aspect-ratios ranging from 100 to 3,000. In addition to the acoustic data, fluid dynamic measurements were made as well. This paper uses the results of these two studies and attempts to develop a prediction scheme for high aspect-ratio jet noise.

### Nomenclature

A -- Area (typically of nozzle)
AR -- Aspect ratio
a -- Speed of sound
$a_o$ -- Ambient speed of sound
D -- Diameter of round jet exit
$d_{eq}$ -- Equivalent diameter, $2(A/\pi)^{1/2}$
F -- Tam's large scale turbulence generic acoustic spectrum, function of $(f/f_p)$
f -- Frequency
$f_p$ -- Peak frequency
G -- Tam's fine scale turbulence generic acoustic spectrum, function of $(f/f_p)$
HARN -- High aspect-ratio nozzle
h -- Slot height or rectangular nozzle height (small dimension)
I -- Sound intensity
L -- Characteristic length
$L_{eq}$ -- Characteristic length for the HARN, $L_{eq} = h^{3/4}w^{1/4}$
$M_c$ -- Convection Mach number
$M_o$ -- Jet centerline Mach number
P -- Sound power
$P_{ref}$ -- Reference acoustic pressure, 20 μPa
p -- pressure

q -- ½ $\rho V^2$ (dynamic pressure)
R -- Radial distance from jet exit to measurement location
SPL -- Sound Pressure Level
T -- Temperature
$T_{ij}$ -- Stress tensor, $\rho u_i u_j + p_{ij} - a_o^2 r \delta_{ij}$
w -- width of rectangular nozzle (large dimension)
V -- Velocity
    $V_c$ -- Turbulent eddy convection velocity
    $V_j$ -- Jet exit velocity (fully expanded)
    $V_l$ -- Local jet centerline velocity
x -- Streamwise dimension, typically x = 0 is nozzle exit
y -- Dimension perpendicular to major axis of nozzle, y = 0 is center of nozzle
z -- Dimension along span of nozzle (parallel to major axis), z = 0 is center of nozzle
$\Theta$ -- Angle of measurement with respect to the flow axis
$\rho$ -- density

### Introduction

This paper uses the results of a recently-completed aeroacoustics study of a High Aspect-Ratio Nozzle (HARN) performed at Georgia Tech Research Institute (GTRI) to develop an empirical noise prediction scheme of jet noise from such nozzles. Results of this studiy can be found in references 1 –3. General trends in the HARN acoustic data were examined in reference [1]. In this process, the available round jet experimental trends and theory were used as a starting point. It was found that the HARN data followed the $V_j^8$ law similar to round jets and data from low-aspect-ratio rectangular nozzles.[1]

While round jet noise follows $D^2$ and researchers have had some success scaling low aspect-ratio rectangular jet noise based on an equivalent diameter, $D_{eq} = (4hw/\pi)^{1/2}$, the HARN data did not collapse using $D_{eq}$ as the characteristic length.[1] Lighthill's estimation of jet noise developed for round jets results in the intensity of the noise being proportional to $D^2$. The use of diameter for round jets comes from the fact that the turbulent eddy volume

---

[*] Now works for the Naval Air Warfare Center, Weapons Division, China Lake, CA 93555-6100.

and frequency of the turbulence are related to the jet diameter.

In the case of the HARN, it was found that the height and width tend to affect the amplitude and frequency of the jet noise differently. The intensity of the sound was found to be proportional to $h^{3/2}$ for the lower aspect-ratio geometries and proportional to $h^2$ for the higher aspect ratios. The width was found to have little effect on the SPL for low aspect ratios, however the intensity was found to proportional to the width for the high aspect ratios.

Initially, rather than develop a complex relationship for the exponents for h and w dependent on aspect-ratio, a "best fit" relationship using constant exponents was sought. The best length scale that provided the noise intensity for the HARN proportional to the square of the length scale was found to be $L_{eq} \sim h^{3/4}w^{1/4}$. This characteristic length-scale was used to non-dimensionalize the frequency of the acoustic spectra as well as to collapse the amplitude. For constant jet velocity, this scheme collapses the data reasonably well at most polar angles.[1]

The above definition of the length-scale, namely $L_{eq} \sim h^{3/4}w^{1/4}$ and the result that the $V_j^8$ law was valid for $\Theta = 90°$ were used to collapse the HARN data at that polar angle. Figure 1 contains a sample of the unscaled and scaled data to show the reasonable effectiveness of the scaling parameters developed in reference [1]. While the data collapse is not perfect, this simple scheme does scale the data reasonably well over a wide range of nozzle conditions.

One area where this scheme, as well as prediction schemes for round jets, fails is in the prediction of the amplitude and frequency content of the noise radiated at the low polar angles. Lighthill's analogy does include a Doppler term to account for moving turbulent eddies, however it has been found that there is a significant amount of turbulence scattering of high frequency noise for polar angles below 50°.[4-5] This was found to have a large effect on the HARN data. However, as a result, the prediction schemes often used do not properly account for this effect. Tam and his colleagues contend that there is a different reason why low polar angles do not have similar noise characteristics to higher angles. They believe that there are two distinct types of noise radiating from two distinct sources within the flow.[6-13]
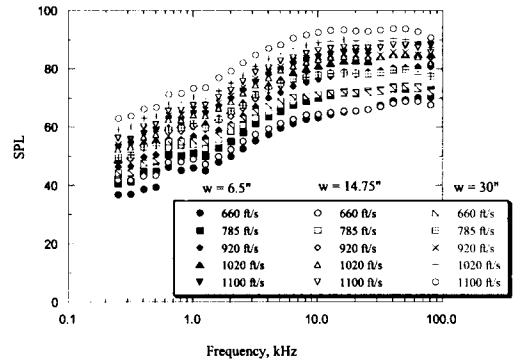


(a)
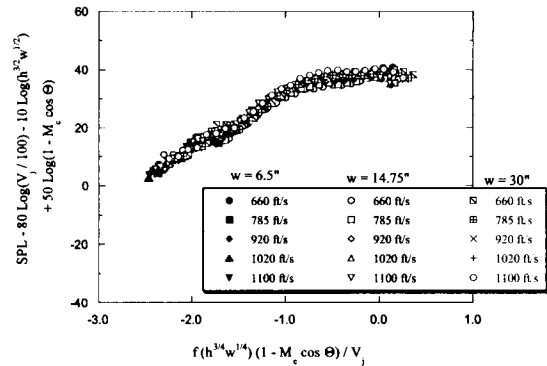


(b)

Figure 1: Typical HARN acoustic data, (a) Raw data, (b) Collapsed data.

In addition to the problems associated noise at various polar angles, the flow study (reference [2]) on the HARN revealed some interesting results that may yield some insight into the discrepancies between data and the predictions. These include the sudden bursting of the jet some distance downstream of the nozzle exit as found in our PIV and hot-wire results and the fact that convection velocity is dependent on the centerline velocity rather than the jet exit velocity. The convection velocity was also found to be a function of the frequency of the turbulence. Also, global length-scale calculations supported the $L_{eq}$ definition from the acoustic study.[2]

These results and the general jet flow characteristics are used below to enhance the prediction scheme for high aspect-ratio rectangular jet noise. Attempts are also made to relate HARN data to round data using a common prediction scheme that is relevant to all nozzles. And finally, the HARN data is compared with the predictions using schemes developed by Tam et al.[6-13]

E-2

## Review of Jet Noise Theories, Experiments, and Prediction Schemes

### Jet Noise from Round Nozzles

As soon as jet and rocket engines began making their way into the aircraft designs, the noise from these new types of engines became an issue. In some cases it was more for controlling damage, such as in the case of a rocket launch, where the launch area is subjected to a large amount of noise from the rocket motors during the launch. The other major issue came with increased jet travel and jet aircraft activity around airports. The new jet aircraft were much louder and more annoying to the surrounding population.

Thus, research into jet noise soon began to emerge. Much of the early theoretical gains in jet noise prediction came from Lighthill's work on round jets. Various versions of this work are found in references.[14-17] Lighthill derived equations for a turbulent flow including Reynolds stresses and the associated turbulent terms. He also showed that the dominant stress term was $\rho v_i v_j$ at low Mach numbers. Since turbulent fluctuations correlate well for points within a volume on the scale of the typical eddy size, Lighthill proposed that acoustic sources associated with the turbulent fluctuations at these points were coherent. Thus, the distribution of quadrupole sources in the volume radiated sound similar to a single quadrupole equal in strength to the combined distribution. Essentially the noise associated with a particular eddy is represented by a quadrupole source. Lighthill went on to assume that the jet flow was made up of a number of eddies, and thus a similar number of these point quadrupoles representing eddies. From this physical model, several relationships were derived, including 'Lighthill's eighth power law' relationships for the sound intensity and the sound power

$$: I \sim \frac{\rho_m^2 V_j^8 D^2}{\rho_0 a_0^5 R^2} \text{ and } P \sim \frac{\rho_m^2 V_j^8 D^2}{\rho_0 a_0^5}. \quad (1)$$

The derivation shown above has mostly been applied to round jets of diameter D.[14-17] Secondly, there are important relations that are shown, specifically that the sound intensity is proportional to the eighth power of velocity and inversely proportional to the square of the radius between the source and observer. The final note on these equations is that they also assume that the eddies (or quadrupoles) convected at a very low Mach number. When the eddies are convected at a higher Mach number ($M_c$) the analysis must take this into account by shifting to the reference frame of the convecting eddy. When backed out to the observer, the equations change to

$$I \sim \frac{\rho_m^2 V_j^8 D^2}{\rho_0 a_0^5 R^2} (1 - M_c \cos(\Theta))^{-5} \text{ and}$$

$$P \sim \frac{\rho_m^2 V_j^8 D^2}{\rho_0 a_0^5} \frac{(1+M_c^2)}{(1-M_c^2)^4}. \quad (2)$$

In the intensity equation, $\Theta$ is the angle of the observer with respect to the downstream jet axis. These equations predict the amplitude of jet noise, but say nothing of frequency.

However, one can again go back to the eddy which is essentially the driving force behind the noise. Near the exit of the nozzle where the mixing region is small, the turbulence is dominated by small eddies, thus higher frequency noise is associated with the small length scale. As the shear layer grows, the larger eddies further downstream are believed to be responsible for lower frequency jet noise.[4] But notice that these characteristics are dependent on the geometry and mixing characteristics of the jet. Thus, the frequencies must also scale in order to be able to predict the entire spectrum of jet noise. The frequency scaling is taken into account by non-dimensionalizing the frequency into a Strouhul number and accounting for the moving sources. This relation is

$$\frac{fD}{V}(1 - M_c \cos \Theta) \quad (3)$$

Most of Lighthill's theory has been experimentally verified for round jets. One key study in this area was performed by Ahuja, and Ahuja and Bushell.[4,5] They made careful measurements of jet noise for 3 different diameter round jets. An effort was made to eliminate all other possible sources of noise, such as valve and flow noise from upstream in the nozzle system. Ahuja verified the data by scaling all his data to the same condition, which would collapse all the data if Lighthill's theory was correct. This was a fairly straightforward process when working with sound pressure levels. Since the sound pressure level (SPL) is defined as

$$SPL = 10 \log\left(\frac{I}{I_{ref}}\right) \quad (4)$$

where $I_{ref} = 10^{-12}$ W/m². Thus, if the intensity is normalized by some "standard" intensity and a "standard" SPL is solved for, the result is[4]

$$"s\tan dard" SPL = SPL - 10\log\left(\frac{V}{V_s}\right)^8 - 10\log\left(\frac{D}{D_s}\right)^2$$

$$+ 10\log\left(\frac{R}{R_s}\right)^2 - 10\log(1 - M_c \cos\Theta)^{-5} \quad (5)$$

where the variables with an 's' subscript signify conditions of the "standard" case, i.e. $V_s$ = 100 ft/s, $D_s$ = 1", $R_s$ = 10 ft. $\Theta_s$ is typically 90°, so the reference value in the final term becomes 1 and is therefore not shown. Thus, any SPL measurement from a jet could be transformed, or scaled to the SPL for this standard case. If Lighthill's theory holds, then jet noise from experiments could all be collapsed into one curve by plotting the "standard" SPL for all data versus the normalized frequency. This is very powerful information since the reverse could be done as well. The 'Standard SPL' data could be scaled using a geometry, distance, or velocity to predict what the noise would be in that case. Ahuja's experimental data for unheated jets agreed with many of Lighthill's predictions but did not match in all cases. Even so, Lighthill's theory has until recently remained the basis for developing jet noise prediction schemes and extrapolating noise from one system to another by using the velocity, diameter, and radius factors derived in the above equations. Recently Lighthill's theory based on acoustic analogy has come under much scrutiny and some other jet noise theories have come to the forefront. One of those theories has been put forth by Tam and several other researchers.[6-8,12] Tam suggests that there are two different noise mechanisms, one that is associated with the large scale turbulence and other with the fine scale turbulence.[6,7,12] Tam and Auriault also claim that these two mechanisms dominate the acoustic jet noise spectra in different regions of the polar arc. Specifically, the large scale turbulence noise dominates the spectrum at small polar angles, while the fine-scale turbulence dominates the spectrum at higher polar angles.[6,7,12] References [6-8,12] describe two generic noise spectra, one for each type of noise. In addition to the spectra, empirical amplitude formulas have been developed that account for differences in jet velocity, temperature and diameter. These generic spectra have been applied to a wide variety of jet noise data with reasonable success.[6-8,12]

It is apparent that even in the case of the well studied round jet, there is still discussion of the appropriate theory and scaling. This is also true of jet noise rom non-round nozzles and more complex suppressor nozzles.. This is particularly true in the case of rectangular jets where there has not been nearly the focus given to round jets. The following section discusses in some detail the differences found between the round jet case and rectangular jet case.

## Jet Noise From Rectangular Nozzles

Although round nozzles dominated most of the applications where jet noise was of interest, there have always been some applications where a rectangular nozzle is more appropriate. Thus, there

has also been some work on the topic of rectangular jet noise.

Almost all work on jet noise was conducted on round jets until there were applications where a non-axisymmetric shape had advantages over an axisymmetric nozzle. The first rectangular nozzle work strictly for noise reduction appears to have been performed performed by Tyler, et al.[18] Other applications were more thrust related. Rectangular nozzles produced better performance at higher Mach numbers in military aircraft tests.[19,20] However, the rectangular nozzles in these applications typically had aspect-ratios from 2 – 7.[21] These early studies were typically also limited to higher subsonic or supersonic Mach numbers.[22] Other examples of very early studies are Maglieri and Hubbard's work on jets of different aspect-ratios,[23] and Cole's work on high aspect-ratio slot-noise.[24] Maestrello and McDaid investigated slot jets with aspect-ratios from 5 to 20.[25] Gruschka and Schrecker[26] and Schrecker and Maus[27] investigated the noise emitted from high aspect-ratio slot jets. One of the major motivations behind this work was the fact that jet velocity of rectangular jets decayed at a higher rate compared with round jets, thus resulting in a lower sound energy.[28] However, in all these works high aspect-ratio referred to aspect-ratios typically at least an order of magnitude lower (sometimes two orders of magnitude) than the HARN jet investigated in the present work.[21,26,27]

The research on rectangular nozzles has produced some differing results. The acoustic power dependence of $V_j^8$ for round circular jets has been found by some researchers[48] while $V_j^7$ has been reported by others[22,27,29] The work documented in references [25,26] found that the jet velocity dependence was actually a function of the aspect-ratio of the jet. The range of aspect-ratios tested were from 30 to 120, and the velocity scaling function ranged from $V_j^6$ to $V_j^7$.

Ffwocs-Williams suggested in reference [29] that the exit geometry can affect the noise by an additional component he termed "lip noise." The lip noise radiates as a fluctuating force dipole source. Typically, the dipole source radiates noise proportional to $V_j^6$. Reference [21] speculated that this noise combined with the turbulent mixing noise produced the $V_j^7$ relationship found in their investigation.

Kouts and Yu[22] also noted that the peak frequency of the spectra only had a week dependence on jet velocity. They also found that the rectangular jet seemed to have more high frequency content than circular jets.[22] Also, in contrast to round jets, researchers have found that the peak frequency has a weak dependence on the nozzle height.[22,26,27] This was unexpected since round jets have a strong dependence

on jet diameter and the nozzle height is the appropriate scale for the initial mixing region in rectangular jets.[22]

Since the literature has shown some differences in the acoustic characteristics of rectangular jets compared with circular jets, it is worthwhile to look at the basic fluid dynamic characteristics as well. Similar to round jets, rectangular jets are characterized by different flow regions. In general these include the core region, the transition region, and the fully-mixed turbulent region.[28] The core is characterized by an unmixed region just downstream of the nozzle exit. Eventually, this disappears due to the merging of the shear layers. In a round jet, this is well defined since the shear layer is axisymmetric. However, in the case of a rectangular jet the issue is somewhat clouded. If one assumes the two dimensions to be independent, there are shear layers that grow on each of the 4 edges. The two shear layers associated with the small dimension will merge at a different location downstream than the two from the large dimension. The core is typically defined as the location where the centerline velocity falls below a certain value, usually 99% of the exit velocity. Therefore, a definite length can be associated with the core. However, one must keep in mind that the shear layers are much more complex than the round jet case.

The transition region in a rectangular jet is a region of high mixing where the jet flow is still essentially considered a 2-dimensional flow. As the flow continues downstream, the mixing eventually causes the flow to become axisymmetric. This indicates the beginning of the fully mixed region. In this region, the flow has many characteristics similar to a circular jet, including the centerline velocity decay rate proportional to $x^{-1}$ (streamwise distance).[28] The length of the core region is dependent on the jet Mach number and temperature.[28] The velocity centerline decay has also been shown to be a function of the aspect-ratio.[28]

The region where the highest level of noise is produced in a jet is in the mixing layer around the core region.[28] This is where the shear is very high, and the associated velocities are also at their highest. Well downstream the flow evolves into a round jet flow, however the flow velocities are much lower than the exit condition and therefore do not radiate jet noise at comparable levels to the near exit region.[28] However, as with round jets there are many theories that have been proposed. In addition to studying round jets, Tam has investigated other nozzle shapes including rectangular jets. In his studies he has limited his research to low aspect-ratio nozzles. His results indicate that rectangular jets are actually similar to round jets.[7,9-12] References [7,9-12] show Tam's fits do indeed agree well with the experimental data. This indicates that round jet noise and rectangular jet noise are actually very similar since both can be fit to one set of generic spectral curves.

As is evident by the variation in data and theories, there is still much to be investigated in the area of rectangular jet noise. The aspect-ratios considered 'high' in the above discussion are typically one or two orders of magnitude lower than the typical aspect-ratio of the HARN system of the present study. Thus, there is definitely a need to generate some clean, systematic very high aspect-ratio noise data so that theories can be extended to this realm.

### Results

Adaptation of Lighthill's Acoustic Analogy for Rectangular Jets

Lighthill's analogy for aerodynamic comes from the solution of the linearized flow equations. The acoustic pressure is found to be

$$p \sim \iiint_V \frac{\partial^2}{\partial t^2} T_{ij} \partial V . \tag{6}$$

By assuming

$$\frac{\partial^2}{\partial t^2} \sim \omega^2 \sim \left(\frac{U}{L}\right)^2 \tag{7}$$

$$T_{ij} \sim \rho u_i u_j \sim \rho U^2 \tag{8}$$

$$\partial V \sim AL \tag{9}$$

It can be shown that the acoustic intensity is

$$I \sim p^2 \sim \left[\rho U^4 \frac{AL}{L^2}\right]^2 \tag{10}$$

where U is the freestream velocity and L is a characteristic length-scale of the flow in the axial direction. Typically, the differential volume is assumed to be proportional to the cross-sectional area of the nozzle and the axial length-scale, $dV \sim AL$. For a round jet, $L \sim D$ and $A \sim D^2$. In the case of the HARN, $A \sim hw$ and Larsen[30], in his adaptation of Lighthill's jet noise prediction scheme, stated that the axial and cross-direction length-scales were both proportional to nozzle height, $L \sim h$. Thus, substituting these values into the differential volume definition, $dV \sim h^2 w$. The resulting proportionality for the intensity of the jet noise becomes

$$I \sim p^2 \sim \left[\rho U^4 \frac{h^2 w}{h^2}\right]^2 \sim \rho^2 U^8 \frac{h^4 w^2}{h^4} \sim \rho^2 U^8 w^2 . \tag{11}$$

Interestingly, the sound intensity appears to be proportional to the square of the width and not proportional to the nozzle height at all. This is not what has been found in the HARN data or by others.

Thus, the adaptation of Lighthill's scaling equation to rectangular jet noise is not as simple as it initially appeared.

Rather than attempting to completely re-evaluate the terms in the acoustic pressure equation to achieve an adapted intensity relationship, we will assume that the eddy volume and length scale will produce a relationship similar to that for the round jet noise case, in that $I \sim L^2$. Using the OASPL data $L_{eq}$ can be defined as it was in reference [1]. This seems as though it is an ad-hoc way of resolving the problem, however its validity can be checked by using the defined length scale in the Strouhal number and examining how well the spectra collapse. Figure 1(b) shows typical HARN acoustic spectra scaled according to the defined equivalent length. It is noted that the relationship collapses the data reasonably well, although there it can be seen that the scaling has not completely removed the effect of nozzle width.

To further examine the differences between the noise data at different widths, the OASPL is plotted verses the aspect-ratio of the nozzle in figure 2. The data for all three widths appear to have similar trends, with slopes varying from 1.6 to 2.1. However, perhaps a more direct comparison is to remove the change in SPL due to the nozzle area. Round jet noise has been found to scale with nozzle area. Similarly, figure 3 shows the same HARN data from figure 2 with an additional factor subtracted out to account for the change in noise due to change in area. This produces an interesting result.
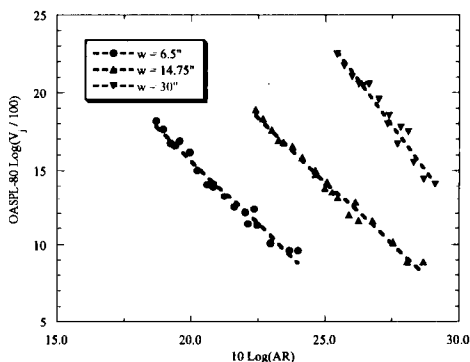


Figure 2: HARN OASPL data versus aspect-ratio, AR = (w / h).

Rather than having three independent curves based on different widths, the two smaller widths appear to fall along the same trend-line in the plot. The largest width, w = 30", however does not collapse in the same manner. Two possible scenarios exist: (1) there is a significant change in the jet flow between w = 15" and

w = 30", or (2) there is a consistent error in the w = 30" data. All aspects of the experiments were examined to verify the quality of the data. No error, or inconsistency was found in the experiment, or the data. One possible problem that may have affected the data was the relatively short distance between the nozzle exit and the jet collector in the chamber. Due to the size of the HARN, the distance from the HARN exit and the collector inlet was only 7 ft. Thus, the location of the collector was only at x/w = 2.8 for w = 30". In the width dimension, the collector is only 4' wide. Thus, it was possible that the jet may have impacted the sides of the collector inlet. How much noise might be produced in this case is unknown, however the collector is covered in acoustic foam. For the other two nozzle widths the x/w was about 6 and 13, respectively. This could be a possible cause of the different trend for the w = 30" case.
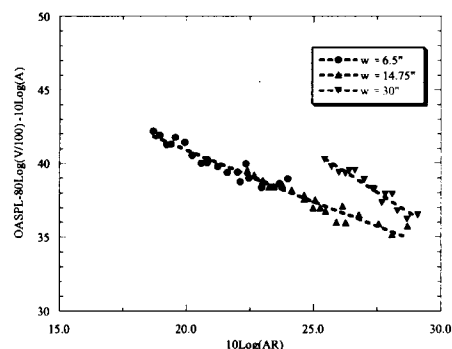


Figure 3: HARN OASPL corrected for jet velocity and nozzle area versus aspect-ratio.

An attempt at obtaining the best fit for the effect of aspect ratio showed that the OASPL was proportional to $AR^{-1/2}$. The data is shown in figure 4 corrected using all the parameters discussed thus far. This collapses the OASPL data at $\Theta = 90°$ to within +/- 2 dB. For the two smaller widths, the scheme improves, collapsing the data to within +/- 1 dB.
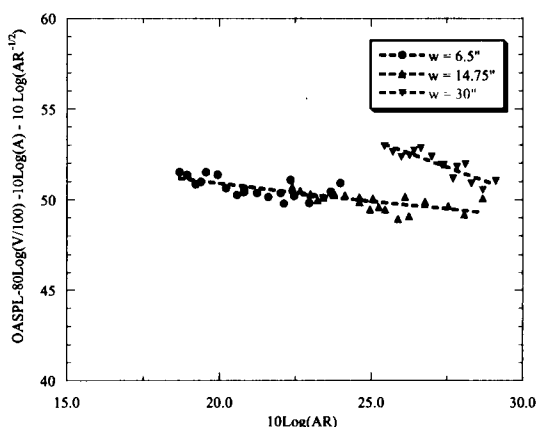
Figure 4: Best fit scaling to OASPL data based on aspect-ratio.

## Improvements to Prediction of Jet-Noise at Low Polar Angles

It has been well documented that at low polar angles the high frequency sound undergoes refraction, scattering, and absorption by mixing layer turbulence.[5] This is because the high frequency noise is generated very close to the nozzle exit and then must pass through a large portion of the turbulent jet in order to arrive at the microphone. If the turbulence scale is on the order of the wavelength of the noise there can be significant amounts of absorption and scattering.[5] Thus, when compared to prediction schemes that do not account for this effect, the data does not coincide with what is expected from the prediction.

Referring to the prediction scheme based upon Lighthill's theory for round jets, the sound intensity is given by

$$I \sim \frac{\rho_m^2 V_j^8 D^2}{\rho_o a_o^5 R^2} (1 - M_c \cos(\Theta))^{-5}. \quad (12)$$

Notice that the only term that varies with polar angle is the convection amplification term, $(1 - M_c \cos \Theta)^{-5}$. This involves the convection Mach number of the turbulent eddies. Typically most researchers assume $M_c \sim 0.65 \; M_j$. However, it was shown by the present authors in reference [2], that the convection velocity decreased with increased distance from the nozzle. It was found that the convection velocity was generally in the range of $0.65 V_j$. It was also shown in reference [2] that $V_\ell/V_j \sim (x/h)^{-1/2}$ beyond the core.

This information can be used to calculate a more accurate convection Mach number for the entire noise-producing region of a jet. Given that

$$M_c = \frac{V_c}{a}, \quad (13)$$

and multiplying by $\dfrac{V_\ell}{V_\ell}\dfrac{V_j}{V_j}$, the convection Mach number can be re-arranged into the form

$$M_c = \frac{V_c}{a}\frac{V_\ell}{V_\ell}\frac{V_j}{V_j} = \frac{V_c}{V_\ell}\frac{V_\ell}{V_j}\frac{V_j}{a} \sim 0.65\frac{V_\ell}{V_j}M_j, \quad (14)$$

since $V_c/V_\ell \sim 0.65$. The maximum is 0.65 due to the fact that $V_\ell/V_j < 1$ beyond the core region of the jet. Since the noise producing region of a jet is on the order of 20 x/h and the core length is on the order of 4 x/h, a constant value of $M_c = 0.65 \; M_j$ is not a representative value for the entire noise producing region. Unfortunately, the form of the convection Mach number shown in equation (14) is not implemented easily into most prediction schemes that assume a constant convection Mach number for agiven jet exoit Mach number. However, an average $M_c$, over the entire noise producing region, can easily be calculated and used in prediction schemes that only allow a constant $M_c$. In the case of the HARN, it was shown $V_\ell/V_j \sim (x/h)^{-1/2}$. Taking the average of $V_\ell/V_j$ from x/h = 0 to x/h = 20 results in $[V_\ell/V_j]_{ave} \sim 0.55$. Thus, an improved constant value convection Mach number (for a fixed $M_j$ for the HARN, based on equation (14) is $M_c = (0.65)(0.55)M_j = 0.36M_j$.

Figure 5 shows some comparisons between using the original and new values of $M_c$. There is an obvious improvement in the data, however it has still not collapsed into one curve that could be used for prediction. One might think that this type of correction would only improve the low frequency portion of the spectrum, since much of the low frequency noise is produced downstream of the tip of the potential core. On the other hand, the high frequency noise is presumed to be produced near the nozzle exit and upstream of the tip of the potential core Thus, the convection velocity for high frequencies should be on the order of $0.65M_j$. However, there is a vast improvement in the collapse of the data from using the lower convection Mach number.

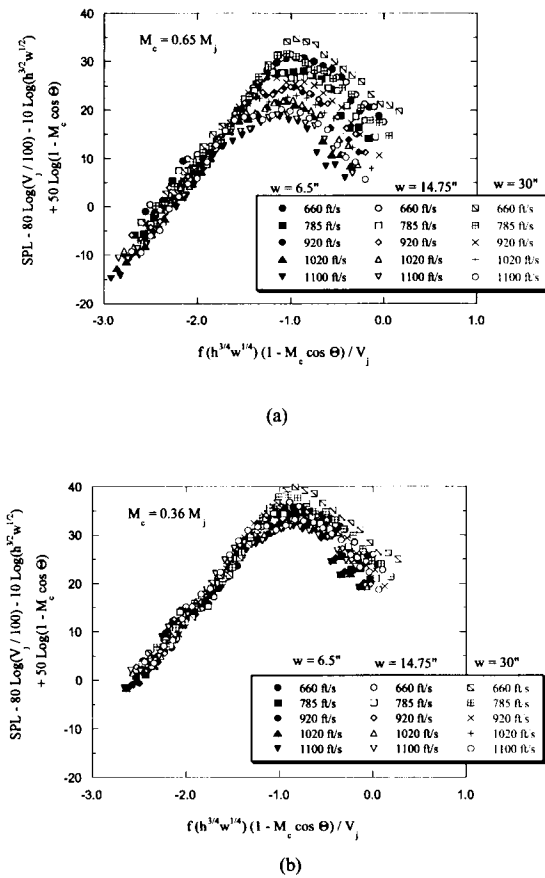were calculated to determine a general range of Strouhal number for the HARN tests. Strouhal numbers for the HARN ranged from $fh/V_j = 0.0002$ to $1.02$ ($f_{min} h_{min} / V_{max}$ to $f_{max} h_{max}/V_{min}$). From the data in reference [31] and recent low aspect-ratio rectangular nozzle source location data, it was determined that even the frequencies with the highest Strouhal numbers were associated with sources at at least 5 nozzle heights downstream from the nozzle exit, and therefore beyond the core region of the jet.

Larsen[30] also reported results for his nozzle at Strouhal numbers, $fh/V_j$ of 0.5 and 0.1. He showed that most of the noise was generated at downstream distances $> 5h$, and in the case of the lower Strouhal number the noise producing region was significant as far away from the nozzle as $x/h \sim 25$. This tends to indicate that the majority of the high frequency HARN noise is produced downstream of the core. Thus, even the high frequency noise that was measured needs the convection velocity adjustment described earlier. Hence, this could be a reason why the $M_c$ adjustment improves the data at the higher frequencies. Thus it is assumed that $M_c = 0.36M_j$. It is a reasonable average convection Mach number when all frequency sources are considered, and explains the improved collapse seen in figure 5. It should be pointed out that it is likely, that in our case, the noise produced very near the nozzle exit is at frequencies beyond the measurement capability of the microphone system used. The data acquisition system used in the experiments was only able to acquire data up to 100 kHz. This in combination with the lowest velocity tested of 660 ft/s and the largest slot height of 0.080" only produces a Strouhal number of 1.02 for a frequency of 100 kHz. Thus, the highest frequency sources recorded are located around $x/h > 5$. This tends to indicate that all the noise generated from sources located at $x/h < 5$ will have higher frequencies and are therefore are not recorded in the data. This is supported by examining the HARN data at $\Theta = 90°$. Notice that the spectra are very flat, and never tend to roll-off at high frequency as one might expect based on other jet noise data. Therefore, it is probable that the recorded spectra and the actual spectra should actually extend well beyond the 100 kHz limit of the frequency analyzer as depicted in figure 6. Because of this fact, it should be noted that the OASPL data for the HARN maybe somewhat lower than it should be. Therefore data from a larger nozzle, where the entire frequency spectrum is recorded, will most likely have a higher OASPL value when compared to HARN data. In the example shown in figure 6, this difference is small, only by about 1 dB. There could be a more pronounced difference in the OASPL values if the peak value of the HARN spectrum at a particular



Figure 5: HARN acoustic data at $\Theta = 20°$, (a) $M_c = 0.65 M_j$, (b) $M_c = 0.36 M_j$.

Possible explanation for these observations can be explained using the source location data by others of both the round and rectangular nozzles. The source locations of the HARN were examined using available data in the literature to better estimate the value for convection Mach number. In their effort to develop a new source location methodology, Ahuja, Massey, and D'Agostino performed a study for round nozzles[31] to determine the streamwise source locations of different frequencies as a function of $fD/V_j$. Like a number of earlier studies on jet noise source location, they found that high frequency noise tended to be generated near the nozzle, while lower frequency noise was generated further downstream.[31] It should also be noted that similar trends were found in recent (unpublished at the time of writing of this paper) source location results on low aspect-ratio rectangular nozzles obtained at GTRI using $fh/V_j$ as the Strouhal number.

For comparison, the maximum and minimum values for Strouhal number for all the HARN data

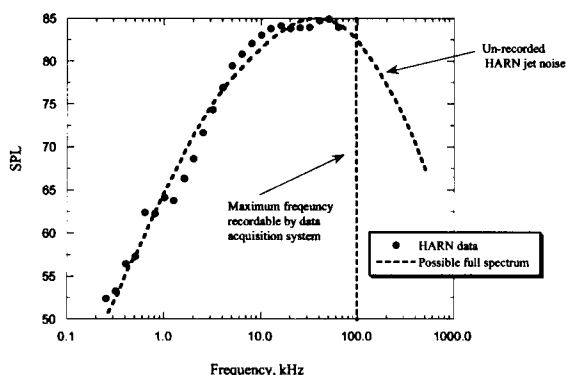condition was at a frequency higher than the maximum recorded frequency.



Figure 6: Depiction of possible HARN jet noise beyond the frequency range capabilities of the data acquisition system.

Based on the HARN acoustic and fluid dynamic data, a reasonable collapse of the OASPL and the frequency spectra has been obtained. For high aspect-ratio rectangular jet noise, it has been found that the sound intensity is given by

$$I \sim \frac{\rho_m^2 V_j^8 L_{eq}^2}{\rho_o a_o^5 R^2}(1 - M_c \cos(\Theta))^{-5} \quad (15)$$

where $M_c$ is a function of frequency and $x/h$; and $L_{eq}$ $= (h^{3/4} w^{1/4})$. The basic form of the equation is similar to the equation for sound intensity developed for round jets. Other researchers have used equivalent diameter as the characteristic length scale, however, the HARN data did not follow $I \sim D_{eq}^2$ where $D_{eq} = (4hw/\pi)^{1/2}$. Finally, it was found that some simple improvements to the estimation of the convection Mach number also improved the prediction of the noise at low polar angles.

Although this prediction scheme collapsed the high aspect-ratio data quite well, it is still desirable to develop a prediction scheme that can relate round jet noise and rectangular jet noise. This would enable the wealth of data for round jet noise to be used for jet noise prediction for rectangular jets. Thus, in the following section, HARN jet noise will be compared with round jet noise data and an attempt will be made to develop one set of scaling parameters that predict noise levels for either geometry.

Comparison of HARN Jet Noise with Round Jet Noise.

Since most of the available experimental data and literature concerning jet noise is associated with round nozzles, it is desirable to compare and scale the HARN results with those for round nozzles. If a relationship between the two types of jet-noise could be established, all the theory and correlations used for round jet noise could be applied to rectangular jet noise using this relationship as a bridge.

Ahuja and Bushell[4] and Lush[16] were some of the first experimenters that made an attempt to verify the relationships developed by Lighthill. Ahuja and Bushell tested 3 different diameter round nozzles at several different jet velocities and made acoustic measurements at several different polar angles.[4] Ahuja found mixed results when trying to compare his data with Lighthill's theory.[5] At high polar angles he was able to collapse data for different velocities and nozzle diameters using Lighthill's relationships. However, at small polar angles, the data did not collapse at high frequency. Figures 7 and 8 are representative figures from reference [4] and are typical results. Figure 7 shows that the jet noise does indeed scale for polar angles above 60°. However, figure 8 shows that there is relatively poor collapse at the lower polar angles, particularly at higher frequencies. Ahuja suggested that this was due to absorption and scattering of the high frequency noise by the turbulent eddies of the shear layer, through which sound arriving at a microphone at a low polar angle would have to travel.[5] Using his data, Ahuja developed two prediction schemes, one for low frequencies below the peak frequency and a different prediction scheme for frequencies higher than the peak value.
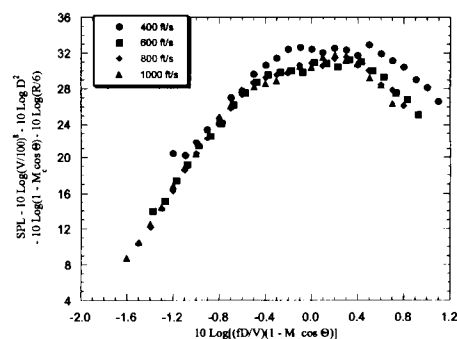


Figure 7: Ahuja round jet data from reference [4], D = 2.84", high polar angles.

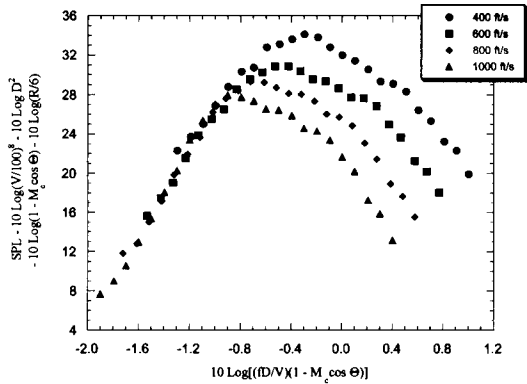Figure 8: Ahuja round jet data from reference [4], D
= 2.40", Θ = 30°.

Similar scaling parameters have been found for the HARN and collapsing the data showed similar results. In the previous sections the noise prediction scheme was improved by using observations from the HARN data and by using results from fluid dynamic measurements. Some easy to implement improvements were made that drastically improved the prediction and the scaling of the HARN data. Lighthill's scaling for the HARN with the length-scale replaced by $L_{eq}$ is

$$I \sim \frac{\rho_m^2 V_j^8 L_{eq}^2}{\rho_o a_o^5 R^2}(1 - M_c \cos(\Theta))^{-5}, \qquad (16)$$

where the convection Mach number is a function of the frequency and the location of the source of the sound in the flow. Equation (11) can be re-arranged into a more convenient form using the area and the aspect ratio rather than $L_{eq}$,

$$I \sim \frac{\rho_m^2 V_j^8 A(AR)^{-1/2}}{\rho_o a_o^5 R^2}(1 - M_c \cos(\Theta))^{-5},$$

where AR = w/h. (17)

Since the adapted equation is a better prediction of the noise for the HARN jet, it stands to reason that this new equation may improve round jet noise results as well. The round jet data used for the comparison will be the data of Ahuja and Bushell from reference [4]. It is easiest to use equation (17) since substituting $A \sim D^2$ and AR = 1 for a round jet reduces equation (17) to the well-known sound intensity relationship for round jets.

The same source location data was used to determine the locations associated with the different frequencies for the round jet data. Figure 9 is the data from figure 8 with the modified $M_c$. As it turns out, the addition of the improved convection Mach number

does not improve the scaling of the round jet data. Since it has shown to produce a significant improvement in the case of the HARN, it requires further examination.
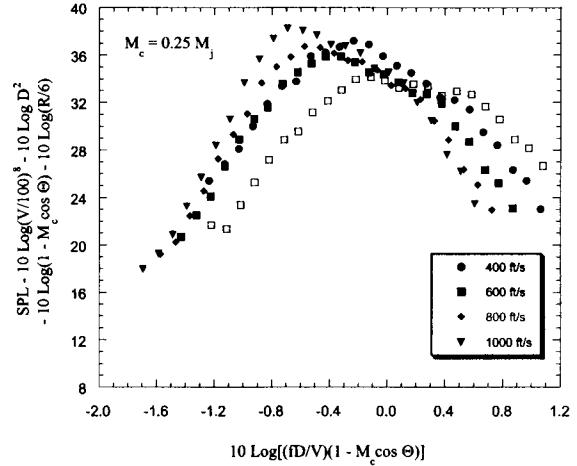


Figure 9: Round jet noise data scaled using modified convection Mach number.

Figure 10 shows sample calculated source locations for the jet noise for the round nozzle data and the HARN based on the data from reference [31]. Notice that the HARN range of Strouhal numbers indicates that the noise sources are well downstream of the nozzle exit while the round jet has a significant number of the sources in its frequency range located in the region of the jet core. In the fluid dynamic study of the HARN, it was found that the convection velocity decreased as distance from the nozzle increased. Thus, since sources of different frequencies are located at different streamwise locations, different frequencies will have different convection velocities. Figure 11 shows the convection velocity of the noise sources based on their location. Notice that the sources for the round jet noise data span a wide range of streamwise locations from the nozzle exit to several diameters downstream of the core. This would possibly explain the different results between the HARN and the round jet.
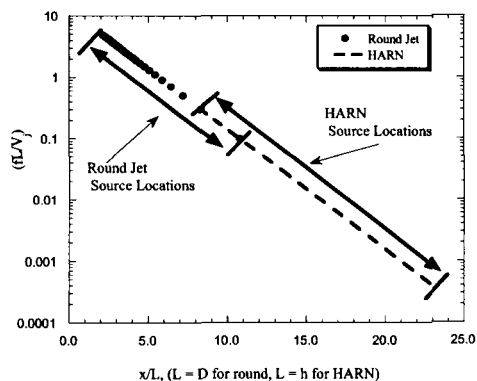
Figure 10: Source locations for HARN and round jet noise based on data from reference [31].
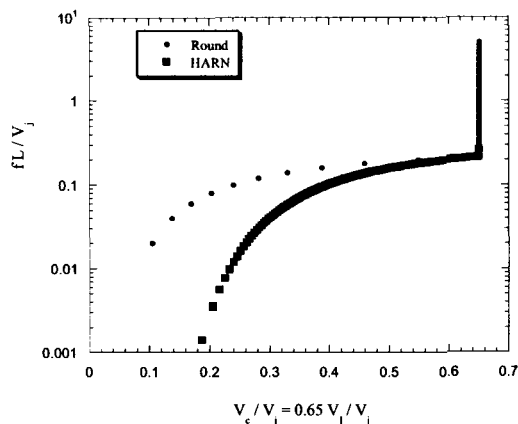


Figure 11: Convection velocities of turbulent eddies based on source location.

Since the round jet data has sources in the region near the nozzle exit, modifying the convection Mach number may not improve the data collapse. However, in the case of the HARN, where much of the noise generated near the nozzle exit appears to be at frequencies beyond the capability of the data acquisition system, the sources associated with the recorded data are located mostly downstream of the core. Therefore, there was a major benefit to modifying the convection Mach number to a value more appropriate for the sources.

Figure 12 shows both the HARN and round nozzle jet noise data scaled according equation (17). The frequency has been normalized by the respective length scale for each set of data, i.e., $L = D$ for the round data, and $L = L_{eq}$ for the HARN data. Thus, one scaling equation has been used to collapse both sets of

data. Notice that the data sets are similar, however, they do not have similar peak frequencies and levels. It is apparent that the two configurations do not completely collapse into one curve using the parameters discussed. This figure also supports the argument that a significant portion of the HARN data is not recorded by the data acquisition system since the HARN spectra appear to be similar to half of a round jet noise spectra.
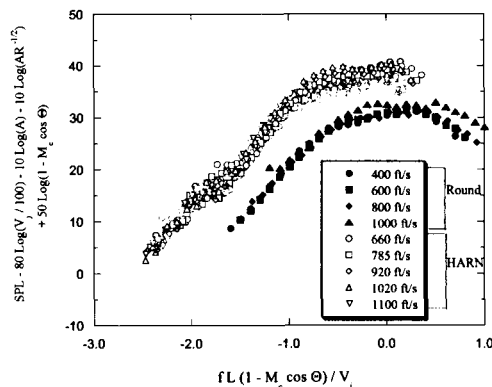


Figure 12: HARN and round nozzle data scaled using the same parameters.

The HARN and the round nozzle curves have similar shapes, but appear to be shifted. This indicates that the two types of jet noise may be related, but that the particular scaling parameters used here are not completely appropriate for collapsing the two data sets. More work will have to be done in this area to improve this result. In particular, systematic data examining the aspect-ratio contribution to jet noise may help clarify the relationship.

In summary, scaling from Lighthill's equation was adapted to estimate the noise levels of the HARN acoustic data. Some modifications were also made to the convection Mach number term based upon the findings from the fluid dynamic portion[2] of the present study. This new prediction scheme was then applied to HARN and classic round jet noise data. The new prediction scheme was found to improve the collapse of only the HARN data at lower polar angles, but the modified convection Mach number did not improve the collapse of the round jet noise data. The two sets of data were then directly compared using a common scaling equation. It was found that the common scaling equation did not quite collapse both sets of data to one curve. Since the spectral shapes are similar, it does appear possible to collapse the two types of jet noise data with an improved scaling relationship.

## Comparison of HARN Data to Tam's Generic Jet Noise Spectra.

Although Lighthill's theory has been around for many years, there is still a great amount of controversy as to whether or not the theory based on acoustic analogy is in fact valid. The $V_j^8$ law and the relationship between the noise and the diameter of a round jet have been well documented in experiments. However, the Doppler shift term remains questionable since data scaled by this term does not seem to collapse with varying polar angle.

Recently, Tam et al. have suggested some reasoning behind the discrepancy.[6-13] They suggested that the reason high polar angles and low polar angles do not collapse is because they are associated with different types of noise.[6-13] Tam et al. broke down the jet noise into two components: one associated with the large-scale structures and from the other associated with the fine-scale turbulence.[10-13] He contends that the large-scale structures radiate predominately in the downstream direction, i.e., low polar angles, while the fine-scale turbulence noise dominates at the higher polar angles.[10-13] Tam et al argue that since there are two mechanisms generating the noise at the different angles, there is no reason why they should scale in the same manner, and hence there should be two distinct spectra associated with the different mechanisms.

This argument was backed up by Tam by generating curve fits to several sets of experimental data under many different conditions.[10-13] These empirical fits are generic jet noise spectra that are particular to the direction of radiation. One curve represents jet noise radiated at low polar angles and is associated with the large-scale turbulence of the jet flow, while the other is valid for higher polar angles, and hence is the result of fine-scale turbulence noise. ]

Tam has expanded his theory beyond round jets.[9, 11, 12, 13] Tam contends that the shape of the jet noise spectra will not change even for varying geometry.[9] He has with some success been able to show that his generic spectra fit experimental data for nozzle geometries other than round. He does however qualify this extension only to "reasonable" geometries that include geometries that would not create a significant thrust loss compared with a round nozzle.[11]

Since Tam has had success in comparing his generic jet noise spectra to many types of jet noise data, it is useful to compare Tam's generic jet noise spectra with the HARN data. This can help support Tam's case that the jet noise spectrum shape is independent of nozzle configuration.[11] It would also expand this theory to an extreme geometric case where he has not yet attempted to apply his generic spectra.

The generic spectra functions are generated as a function of $f/f_p$ ($f_p$ = peak frequency) and can be found in several of Tam's references.[9-13] The

functions were programmed into a Matlab script file and are presented in figure 13. Notice that the peak is at a non-dimensional frequency of $f/f_p = 1$ and that the peak amplitude is normalized to zero. It should also be noted that Tam generated these curves from narrowband data reduced to the power spectral density (PSD, $\Delta f = 1$ Hz). This fit cannot be generated by simply using $f/f_p$ based on 1/3-octave bands and be expected to be appropriate. In fact in references [6-13], for comparison to experimental data the generic curves were left in narrowband frequencies and 1/3-octave jet noise data was converted back to narrowband for comparison.
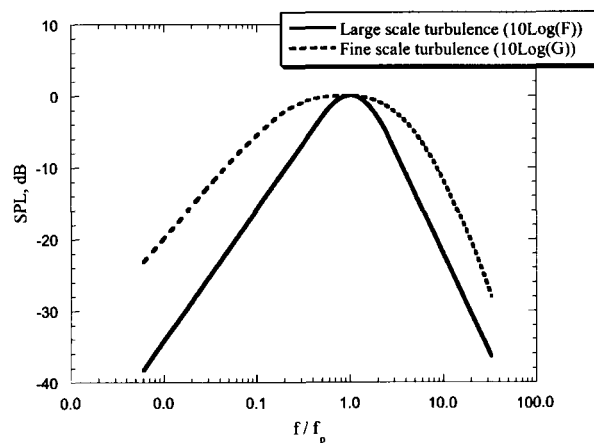


Figure 13: Tam's generic jet noise spectra (reproduced from equations in reference[9]).

In the case of the HARN, narrowband data was available, however significant effort had already been taken to compare all data in 1/3-octave bands so it could be readily compared with older classic experiments. Suddenly switching to comparing data in narrowband would change the peak amplitude, frequency, and shape of the spectra that have already been presented and discussed. Thus it was decided to transform Tam's generic curve fits to 1/3-octave spectra.

Figure 14 shows Tam's curves converted to 1/3-octave bands with the frequencies $f_p = 1000$ Hz. The equations can be re-scaled and at this point these generic curves can be compared with experimental data in 1/3-octave bands. Initially Tam's curves will be compared with HARN data by simply shifting HARN data by subtracting off the peak amplitude and dividing the frequency by the peak frequency. Once this general comparison has been performed, an attempt will be made to use an empirical prediction fit to predict the peak frequency and amplitude of HARN spectra.
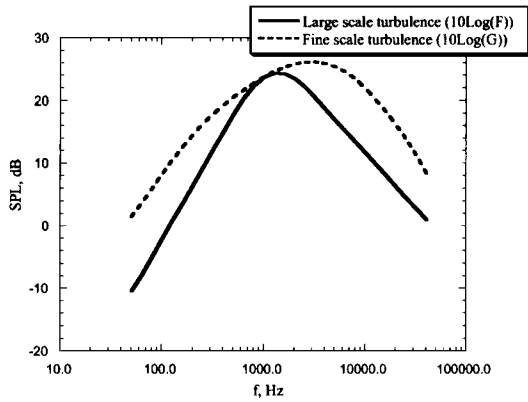
Figure 14: Tam's generic jet noise spectra converted to 1/3 octave bands from the PSD with $f_p = 1000$ Hz.

For the HARN data, the large-scale generic spectrum will be compared with experimental data at polar angles at $\Theta = 30°$ while the fine-scale turbulence generic spectrum will be compared with HARN data for $\Theta = 90°$. Figure 15 shows a comparison between Tam's curves and HARN data. Several HARN spectra are shown in the figure normalized by their peak SPL and frequency. Thus, several HARN curves can be directly compared to the generic spectra on one plot.

The large-scale curve is used to compare with the 30° data, while the fine-scale curve is used to compare with 90° data. A combination of both curves is used to examine 60° data. In general, it appears that the curves do tend to represent the shape of the spectra at high and low polar angles, and the mid-range angles appear to be a combination of both curves. These results are in agreement with Tam's conclusions.



(a)



(b)



(c)
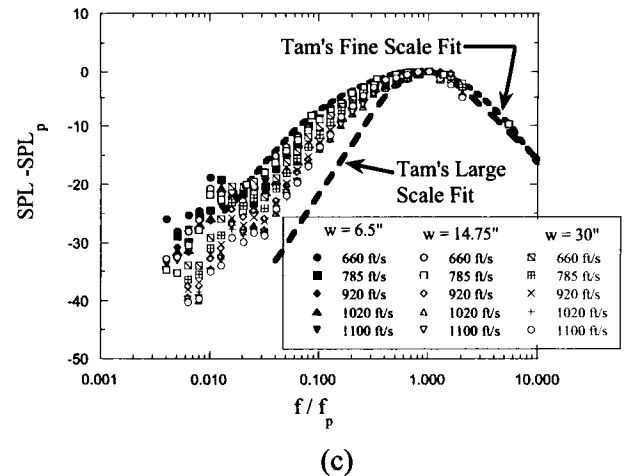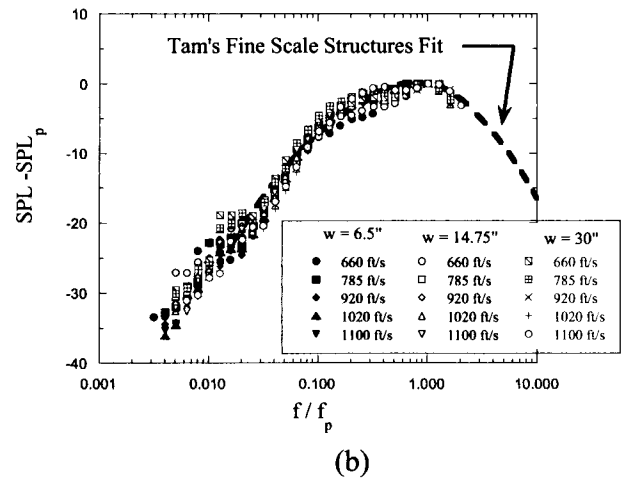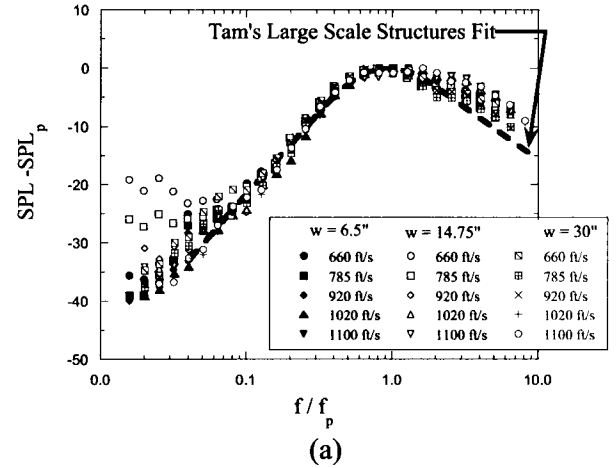
Figure 15: Typical HARN data compared to Tam's corresponding curves, (a) $\Theta = 30°$, (a) $\Theta = 90°$, (c) $\Theta = 60°$.

E-13

## Summary

From the HARN acoustic and fluid dynamic data there were some basic trends that had been identified. The acoustic data was found to vary with $V_j^8$. An equivalent length was also defined to parallel round jet scaling based on Lighthill's equation, which contains a length dimension squared. No direct relationship was immediately apparent between $L_{eq}$ and h and w. A "best-fit" to the data was used to define $L_{eq}$ making the sound intensity proportional to $L_{eq}^2$. The relationship found was $L_{eq} = h^{3/4}w^{1/4}$.

Since this was a rather unlikely scaling-parameter, a more in-depth examination of the OASPL data's variation with h and w was carried out. The prediction scheme was re-arranged into a form containing area and aspect ratio rather than $L_{eq}$ ($I \sim (A \cdot (AR)^{-1/2}$, note $A(AR)^{-1/2} = L_{eq}^2$). This provided a direct way of scaling both round jet noise and HARN jet noise using the same scaling equation.

In addition to the scaling parameter associated with the geometry, the fluid dynamic data revealed that the convection Mach number was not necessarily $0.65 M_j$. In fact, $M_c$ varied with distance downstream of the nozzle and actually was found to be proportional to the local centerline velocity of the jet, $V_l$. Thus, over much of the noise-producing region of the jet, the average $M_c$ is much lower than $0.65M_j$.

In addition, it was found that $M_c/M_l$ was also a function of frequency. Other researchers have shown that different frequencies are generated at different downstream locations in the jet flow. These facts were used to generate an improved convection Mach number estimation. These changes to the estimates from Lighthill's equation improved the collapse of HARN acoustic data, particularly at low polar angles where the convection Mach number has the greatest effect.

This data was also compared with classic round jet acoustic data using the same modifications in order to make the comparison using a common prediction scheme. The two very different nozzles produced similar results in many ways. Both jets follow the $V_j^8$ law and have a similar spectral shape and were found to have similar amplitudes when scaled by the developed prediction scheme. The amount of agreement was surprising since the geometries were so vastly different. However, the modified convection Mach number did not improve the collapse of the round jet data used in the comparison. This is believed to be due to the fact that the high frequency noise from the round jet is produced near the jet exit, thus a significant portion of the spectra actually is associated with a convection Mach number of $0.65 M_j$. However, in the case of the HARN, collapse was improved because it is believed that the noise generated close to the exit of the HARN had such high frequencies that it was beyond the capabilities of the data acquisition system. Thus, the majority of the noise recorded in the spectra is associated with turbulence with much lower convection Mach numbers downstream of the core region of the jet.

The HARN acoustic data was also compared with Tam's generic jet noise spectra. Tam's generic curves predicted the shape of the spectra quite well. In general, the HARN data was found to collapse using a modified version of the round jet scaling parameters derived from Lighthill's equation.

## References

1. Munro, Scott E. and Ahuja, K. K., "Aeroacoustics of a High Aspect- Ratio Jet," AIAA-2003-3323, 2003, presented at the 9th AIAA/CEAS Aeroacoustics Conference and Exhibit, Hilton Head, South Carolina, USA, 12 - 14 May 2003.

2. Munro, Scott E. and Ahuja, K. K., "Fluid Dynamics of a High Aspect- Ratio Jet," AIAA-2003-3129, 2003, presented at the 9th AIAA/CEAS Aeroacoustics Conference and Exhibit, Hilton Head, South Carolina, USA, 12 - 14 May 2003.

3. Munro, Scott Edward, "Jet Noise of High Aspect-Ratio Rectangular Nozzles with Application to Pneumatic High-Lift Devices." Georgia Institute of Technology, PhD thesis, January, 2002.

4. Ahuja, K.K., and Bushell, K.W., "An Experimental Study of Subsonic Jet Noise and Comparison with Theory." Journal of Sound and Vibration, Vol. 30, No. 3, pp. 317-341, 1973.

5. Ahuja , K.K., "Correlation and Prediction of Jet Noise." Journal of Sound and Vibration, Vol 29, No. 2, pp. 155-168, 1973.

6. Tam, C.K.W., Golebiowski, M., and Seiner, J. M., "On the Two Components of turbulent Mixing Noise from Supersonic Jets." AIAA Aeroacoustics Conference, AIAA paper 96-1716, May 1996.

7. Tam, Christopher K.W., "Influence of Nozzle Geometry on the Noise of High-Speed Jets." AIAA Journal, Vol. 36, No. 8, pp. 1396 – 1400, August 1998.

8. Tam, Christopher K.W., and Laurent, Auriault, "Jet Mixing Noise from Fine Scale Turbulence." AIAA paper 98-2354.

9. Tam, Christopher K.W., "Influence of Nozzle Geometry on the Noise of High-Speed Jets." AIAA paper 98-2255, 1998.

10. Tam, C.K.W., and Zaman, K.B.M.Q., "Subsonic Jet Noise from Non-Axisymmetric and Tabbed Nozzles." AIAA Aerospace Sciences Meeting, AIAA paper 99-0077, January 1999.

11. Tam, Christopher K.W., and Zaman, K.B.M.Q., "Subsonic Jet Noise from Nonaxisymmetric and Tabbed Nozzles." AIAA Journal, Vol. 38, No. 4, pp. 592 – 599, April 2000.

12. Tam, Christopher K.W., and Pastoouchenko, Nikolai, "Noise from the Fine Scale Turbulence of Nonaxisymmetric Jets." AIAA Aeroacoustics Conference, AIAA paper 2001-2187, May 2001.

13. Tam, Christopher K.W., "On the Failure of the Acoustic analogy Theory to Identify the Correct Noise Sources." AIAA Aeroacoustics Conference, AIAA paper 2001-2117, May 2001.

14. Lighthill, M.J. "On sound Generated Aerodynamically. I. General Theory," Proceedings of the Royal Society A 211, pp 564-578, 1952.

15. Lighthill, M.J. "On sound Generated Aerodynamically. II. Turbulence as a Source of Sound," Proceedings of the Royal Society A 222, pp 1-21, 1954.

16. Lighthill, M.J. "Jet Noise," North Atlantic Treaty Organization Advisory Group for Aeronautical Research and Development, Report 448, 1963.

17. Lighthill, M.J. "Jet Noise," AIAA Journal, Vol. 1 Number 7, pp. 1507-1517, 1963.

18. Tyler, J. M., Sofrin, T. G., Davis, J. W., "Rectangular Nozzles for Jet Noise Suppression," SAE National Aeronautic Meeting, April 1959.

19. Capone, F. J., and Maiden, D. L., "Performance of Twin Two-Dimensional Wedge Nozzles Including Trhust Vectoring and Reversin Effects at Speeds up to Mach 2.20," NASA TN D-8449, 1977.

20. Capone, F. J., Hunt, B. L., and Path, G. E., "Subsonic/Supersonic Nonvectored Aeropropulsive Characteristics of Nonaxisymmetric Nozzles Installed on an F-18 Model." AIAA Paper 81-1445. 1981.

21. Seiner, John M., Ponton, Michael K., Manning, James C., "Acoustic Properties Associated with Rectangular Geometry Supersonic Nozzles," AIAA Paper 86-1472, 1986.

22. Kouts, C. A., and Yu, J. C., "Far Noise Field of a Two-Dimensional Subsonic Jet." AIAA Journal Vol. 3, No. 8, pp. 1031 – 1035. August 1975.

23. Maglieri, D. J., and Hubbard, H. H., "Preliminary Measurements of the Noise Characteristics of Some Jet Augmented Flap Configurations." NASA Memo 12-4-58L, 1958.

24. Coles, W. D., "Jet Engine Exhaust from Slot Nozzles." NASA TN D-60, 1959.

25. Maestrello, L., and McDaid, E., "Acoustic Characteristics of a High-Subsonic Jet." AIAA Journal, Vol. 9, No. 6, pp. 1058-1066, 1971.

26. Gruschka, H. D., and Schrecker, G. O., "Aeroacoustic Characteristics of Jet Flap Type Exhausts." AIAA Paper 72-130, 1972.

27. Schrecker, G. O., and Maus, J. R., "Noise Characteristics of Jet Flap Type Exhaust Flows." NASA Grant, NGR 43-001-075, 1975.

28. Olsen, W. A., Butierrez, O., and Dorsch, R. G., "The Effect of Nozzle Inlet Shape, Lip Thickness, and Exit Shape and Size on Subsonic Jet Noise." AIAA Paper 73-187, 1973.

29. Ffowcs-Williams, J. E., "Some Open Questions on the Jet Noise Problem." Boeing Science research Lab. Doc., DL-82-0730, 1968.

30. Larsen, P. N., "Noise Generated by Air Jets from a Rectangular Slit." Ph.D. Thesis, Technical University of Denmark, 1983.

31. Ahuja, K. K., Massey, K. C., D'Agostino, M. S., "A Simple Technique of Locating Noise Sources of a Jet Under Simulated Forward Motion." 4th AIAA/CEAS Aeroacoustics Conference, AIAA 98-2359, 1998.

32. Lush, P. A., "Measurement of Subsonic Jet Noise and Comparison with Theory." Journal of Fluid Mechanics, Vol. 46, pp. 477-500, 1971.

# APPENDIX F

# Computational Evaluation of the Steady and Pulsed Jet Effects on the Performance of a Circulation Control Wing Section

# APPENDIX F

# Computational Evaluation of the Steady and Pulsed Jet Effects on the Performance of a Circulation Control Wing Section

Yi Liu, Lakshmi N. Sankar, Robert Englar, K. Ahuja, R. Gaeta
Georgia Institute of Technology, Atlanta, GA 30332-1150

## Introduction

Circulation Control Wing (CCW) technology is a very effective way of achieving very high lift coefficients needed by aircraft during take-off and landing. This technology can also be used to directly control the flow field over the wing. Compared to a conventional high-lift system, a Circulation Control Wing (CCW) can generate the required values of lift coefficient $C_{L,max}$ during take-off/ landing with fewer or no moving parts and much less complexity.

Earlier designs of CCW configurations used airfoils with a large radius rounded trailing edge to maximize the lift benefit. However, these designs also produced very high drag [1]. These high drag levels associated with the blunt, large radius trailing edge can be prohibitive under cruise conditions when Circulation Control is no longer necessary. To overcome this difficulty, an advanced CCW section, i.e., a circulation hinged flap [2, 3], was developed to replace the original rounded trailing edge CC airfoil. This concept developed by Englar is shown in Figure 1. The upper surface of the CCW flap is a large-radius arc surface, but the lower surface of the flap is flat. The flap could be deflected from 0 degrees to 90 degrees. When an aircraft takes-off or lands, the flap is deflected as in a conventional high lift system. Then this large radius on the upper surface produces a large jet turning angle, leading to high lift. When the aircraft is in cruise, the flap is retracted and a conventional sharp trailing edge shape results, greatly reducing the drag. This kind of flap does have some moving elements that increase the weight and complexity over an earlier CCW design. But overall, the hinged flap design still maintains most of the Circulation Control high lift advantages, while greatly reducing the drag in cruising condition associated with the rounded trailing edge CCW design.

In the present work, an unsteady three-dimensional Navier-Stokes analysis procedure has been developed and applied to this advanced CCW configuration. The solver can be used in both a 2-D and a 3-D mode, and can thus model airfoils as well as finite wings. The jet slot location, slot height, and the flap angle can all be varied easily and individually in the grid generator and the flow solver. Steady jets, pulsed jets, the leading edge and trailing edge blowing can all be studied with this solver.

# APPENDIX F

## Objectives of the Present Research

The objectives of the present research effort are to:

a) Develop a numerical analysis method to simulate the aerodynamics of advanced Circulation Control wing sections

b) Investigate the effects of blowing coefficient, angle of attack, free-stream velocity and jet slot height on the performance of the CC airfoil with steady jets

c) Evaluate the effects of pulsed jets on the performance of the CC airfoil, and assess the effects of the frequency of the pulsed jets on its performance

## Mathematical and Numerical Formulation

### Governing Equations

The Reynolds-averaged Navier-Stokes equations were solved in the present simulation. An unsteady three-dimensional compressible Navier-Stokes solver is being used. The solver can model the flowfield over isolated wing-alone configurations. Some applications of this solver on finite wings have been done by Kwon et al [4] and Bangalore et al [5]. Modifications of this solver have been made to model circulation control jets. Both 3-D finite wings and 2-D airfoils may be simulated with the same solver. Two turbulence models have been used: the Baldwin-Lomax [6] algebraic model and Spalart and Allmaras [7] one equation model.

### Computational Grid

The construction of a high-quality grid about the CCW airfoil is made difficult by the presence of the vertical jet slot. In this solver, the jet slot is treated as a grid boundary as done by Shrewsbury[8, 9] and Williams and Franke[10]. A hyperbolic three-dimensional C-H grid generator is used in all the calculations. The three-dimensional grid is constructed from a series of two-dimensional C-grids with an H-type topology in the spanwise direction. The grid is clustered in the vicinity of the jet slot and the trailing edge to accurately capture the jet behavior over the airfoil surface.

The grid generation and the surface boundary condition routines are general enough so that one can easily vary the slot location, slot size, blowing velocity and direction of blowing.

# APPENDIX F

## Boundary Conditions

In CCW studies, the driving parameter is the blowing momentum coefficient, $C_\mu$, defined as follows.

$$C_\mu = \frac{\dot{m}V_{jet}}{\frac{1}{2}\rho_\infty V_\infty^2 S}$$ (1)

Here, the jet mass flow rate is given by:

$$\dot{m} = \rho_{jet}V_{jet}A_{jet}$$ (2)

Conventional airfoil boundary conditions are applied everywhere except at the jet slot exit. Non-reflection boundary conditions are applied at the outer boundaries of C grid, and on the airfoil surface, adiabatic and no-slip boundary conditions are applied.

At the jet slot exit, the jet is set to be subsonic, and the following boundary conditions are specified at the slot exit: the total temperature of the jet, the momentum coefficient $C_\mu$ as a function of time, and the flow angle at the exit. In this simulation, the jet was tangential to the airfoil surface at the exit. All other parameters were computed using ideal gas law, and through an extrapolation of the latest solution static pressure distribution to the slot exit.


## Results and Discussions

The advanced CCW airfoil studied with the body fitted grid is shown in Figure 2. The CCW flap setting may be varied both in the experiments and the simulations. The studies presented here are all for the 30 degree flap setting. In these studies, the free stream velocity was approximately 94.3 ft/sec at a dynamic pressure of 10 psf and an ambient pressure of 14.2 psia. The free stream density is about 0.00225 slugs/ft$^3$. These conditions have been chosen to closely match the experiments done by Englar et al [2]. These conditions translate into a free-stream Mach number 0.0836 and a Reynolds Number of 395,000.


## Steady Jet Results:

Figure 3 shows the variation of lift coefficient with respect to $C_\mu$ at a fixed angle of attack ($\alpha$=0 degree) for the CC airfoil with a 30-degree flap. Excellent agreement with measured data from experiment by Englar [2] is evident. It is seen that very high lift can be achieved by Circulation Control technology with a relatively low $C_\mu$. A lift coefficient as high as 4.0 can be obtained at a $C_\mu$ value of 0.33, and the lift augmentation $\Delta C_l/\Delta C_\mu$ is greater than 10 for this 30-degree flap configuration.

# APPENDIX F

Figure 4 shows the computed $C_l$ variation with the angle of attack, for a number of $C_\mu$ values, along with measured data. It is found that the lift coefficient increases linearly with angle of attack until stall, just as it does for conventional sharp trailing edge airfoils. However, the increase of lift with angle of attack breaks down at high enough angles. This is due to static stall, and is much like that experienced with a conventional airfoil, but occurs at very high $C_{l,max}$ values, thanks to the beneficial effects of Circulation Control. The calculations also correctly reproduce the decrease in the stall angle observed in the experiments at high momentum coefficients. Unlike conventional airfoils, this is a leading edge stall. Figure 5 shows the streamlines around the CC airfoil at an angle of attack of 6 degrees, and $C_\mu$ = 0.1657. In this case, a leading edge separation bubble forms, that spreads over the entire upper surface resulting in a loss of lift. However, the flow is still attached at the trailing edge because of the strong Coanda effect.

Based on the above baseline results, a simulation was also to study the effects of the free-stream velocities on the lift and drag coefficients of the CC airfoil. In this case, the jet momentum coefficient, $C_\mu$, is fixed at 0.1657, and the jet slot height is also fixed at 0.015 inch. However, the free-stream velocities are varying from 0.5 to 1.8 times of the experimental free-stream velocity, which is equal to 94.3 ft/sec, thus the jet velocity will vary with the free-stream velocity to keep a constant $C_\mu$. As shown in Figures 6 and 7, for a given momentum coefficient, the lift coefficient and drag coefficient do not vary significantly with the change of the free-stream velocity except at the very low free-stream velocities. The reason for the production of low lift and high drag at low free-stream velocities is that the jet velocity is too low to generate a sufficiently strong Coanda effects that eliminates separation and the vortex shedding. It can be concluded that the performance of CC airfoils is independent of the free-stream velocity and the Reynolds number under the fixed $C_\mu$ and fixed jet slot height conditions, and that $C_\mu$ is an appropriate driving parameter for CC blowing if the slot-height is fixed.

## Pulsed Jet Results:

The present computational studies were aimed at answering the following questions: Can pulsed jets be used to achieve desired increases in the lift coefficient at lower mass flow rates relative to a steady jet? What are the effects of the pulsed jet frequency on the lift enhancement at a given time-averaged $C_\mu$? What is the optimum wave shape for the pulsed jet, i.e. how should it vary with time?

In the calculations below, the angle of attack was set at zero, and the dual-radius CC airfoil flap angle was fixed at 30 degrees. The shape of the CC airfoil, free-stream Mach number, slot height, chordwise location of the slot, and Reynolds number were all, likewise, held fixed as in the steady jet studies. In the present studies, the following variation of the momentum coefficient with time was assumed:

$$C_\mu(t) = C_{\mu,0}[1 + F(t)] \tag{3}$$

where, $C_{\mu,0}$ is the time-averaged momentum coefficient, which is also the value of the steady jet used for comparison. *F(t)* is a function of time, which varies from $-1$ to $1$, and determines the temporal variation of the pulsed jet.

The sinusoidal pulsed jet is found not very effective compared to a square wave form pulsed jet due to higher mass flow rates required with sinusoidal jets. For square wave pulsed jets, Figures 8 and 9 show the variation of the time-averaged incremental lift coefficient $\Delta C_l$ over and above the base-line unblown configuration at three frequencies, 40 Hz, 120 Hz and 400 Hz. Figure 8 shows the variation with the average momentum coefficient $C_{\bar\mu}$, and Figure 9 shows the variation with the average mass flow rate. For a given value of $C_{\mu,0}$, a steady jet gives a higher value of $\Delta C_l$ compared to a pulsed jet as shown in Figure 8. This is to be expected because the pulsed jet is operational only half the time during each cycle as where the steady jet is continuously on. The benefits of the pulsed jet are more evident in Figure 9. At a given mass flow rate, it is seen that the time-averaged values of lift are higher for the pulsed jet compared to the steady jet, especially at higher frequencies. Figures 10 show the variation of the average lift coefficient with the frequency. It is seen that higher frequencies are, in general, preferred over lower frequencies. For example, as shown in Figure 10, when the frequency is equal to 400 Hz, the square form pulsed jet only requires 73% of the average steady jet mass flow rate while it can achieve 95% of the lift achieved with a steady blowing.

For aerodynamic and acoustic studies, the frequency is usually expressed as non-dimensional quantity called the Strouhal number. A simulation has been done to calculate the average lift generated by the pulsed jet at fixed Strouhal numbers, which is defined as follows:

$$Str = \frac{f\,L_{ref}}{U_\infty} \tag{4}$$

In the present study, for the baseline case, the $L_{ref}$ is 8 inches, and the $U_\infty$ is equal to 94.3 ft/sec. For a 200 Hz pulsed jet, the Strouhal number is equal to 1.41.

From above equation, besides the frequency, there are other two parameters that could affect the Strouhal number, which are the free-stream velocity and $L_{ref}$ (Chord of the CC airfoil). Thus, three cases have been studied. In the first case, as shown in Table 1, the free-stream velocity and the Chord of the CC airfoil are fixed, and the Strouhal number is varied with the change of frequency. In the second case, as shown in Table 2, the Strouhal number is fixed at 1.41 and the chord of the CC airfoil is also fixed. The frequency is varied along with the free-stream velocity to achieve the same Strouhal number. In the third case, as shown in Table 3, the Strouhal number is fixed at 1.41 and the free-stream velocity is also fixed, while the frequency is varied along with the chord of the CC airfoil. The Mach number and Reynolds number are also functions of the free-stream velocity and the airfoil chord, and were changed appropriately.

# APPENDIX F

The time-averaged momentum coefficient, $C_{\mu,0}$, is fixed at 0.04 in these studies. Figure 11 shows the lift coefficient variation with the frequency for these three cases.

From tables 2 and 3, it is seen that the computed time-averaged lift coefficient varies less than 2% when the Strouhal number is fixed. Table 2 indicates that the same $C_l$ can be obtained at a much lower frequency with a smaller free-stream velocity as long as the Strouhal number is fixed. Table 3 shows that for a larger configuration, the same $C_l$ can be obtained at a lower frequency provided the Strouhal number is fixed. Table 1, on the other hand, shows that varying the frequency and Strouhal number while holding the other variables fixed can lead to a 12% variation in $C_l$. Thus, it can be concluded the Strouhal number has a more dominant effect on the average lift coefficient of the pulsed jet than just the frequency.

### Additional Results and Discussions to be included in the full paper

In the full paper, the effects of the jet slot height on the performance of steady jets will be added. More detailed explanation and discussion about some results will also be included, especially an explanation for the improved performance for high frequency pulsed jets over steady jets.

### References

1. Englar, R. J. and Huson, G. G., "Development of Advanced Circulation Control Wing High Lift Airfoils," AIAA paper 83-1847, presented at AIAA Applied Aerodynamics Conference, July, 1983.

2. Englar, Robert J., Smith, Marilyn J., Kelley, Sean M. and Rover, Richard C. III., "Application of Circulation Control to Advanced Subsonic Transport Aircraft, Part I: Airfoil Development," Journal of Aircraft, Vol.31 No.5, pp. 1160-1168, Sep. 1994.

3. Englar, Robert J., Smith, Marilyn J., Kelley, Sean M. and Rover, Richard C. III., "Application of Circulation Control to Advanced Subsonic Transport Aircraft, Part II: Transport Application," Journal of Aircraft, Vol.31, No.5, pp. 1169-1177, Sep. 1994.

4. Kwon, J. and Sankar, L.N., "Numerical Study of the Effects of Icing on Finite Wing Aerodynamics," AIAA Paper 90-0757.

5. Bangalore, A., Phaengsook, N. and Sankar, L. N., "Application of a Third Order Upwind Scheme to Viscous Flow over Clean and Iced Wings," AIAA Paper 94-0485.

6. Baldwin, B. S., and Lomax, H., "Thin Layer Approximation and Algebraic Model for Separated Turbulent Flows," AIAA Paper 78-257, Jan. 1978.

## APPENDIX F

7. Spalart, P. R., and Allmaras, S. R., "A One-Equation Turbulence Model for Aerodynamic Flows," AIAA Paper 92-0439, Jan. 1992.

8. Shrewsbury, G. D., "Numerical Evaluation of Circulation Control Airfoil Performance Using Navier-Stokes Methods," AIAA paper 86-0286, January 1986.

9. Shrewsbury, G. D., "Numerical Study of a Research Circulation Control Airfoil Using Navier-Stokes Methods," Journal of Aircraft, Vol. 26, No. 1, pp.29-34, 1989.

10. Williams, S. L. and Franke, M. E., "Navier-Stokes Methods to Predict Circulation Control Airfoil Performance," Journal of Aircraft, Vol. 29, No.2, pp.243-249, March-April 1992.
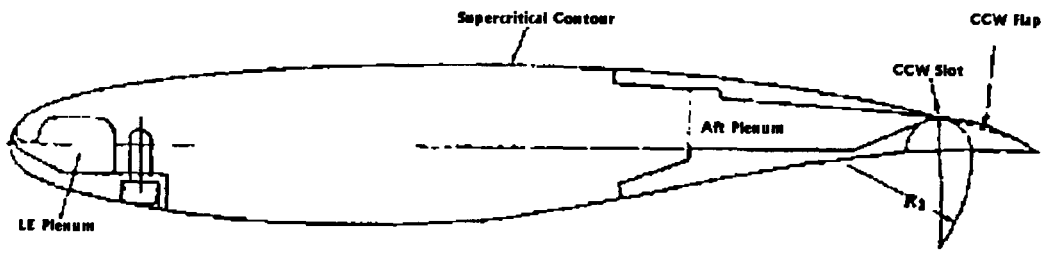
**Figure 1.** Dual Radius CCW Airfoil with LE Blowing [2]
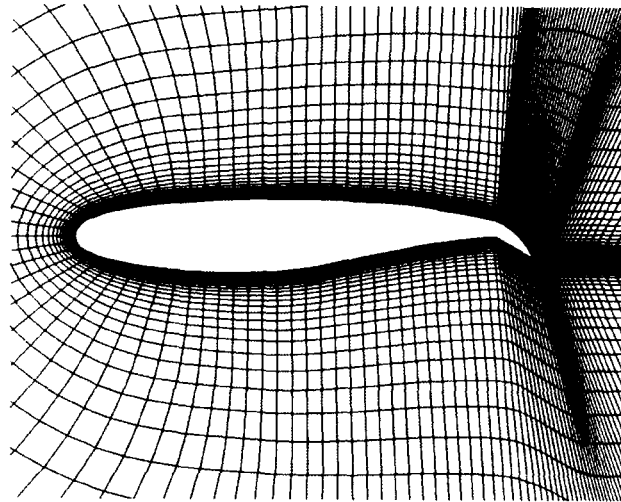


**Figure 2.** The Body-fitted C Grid near the CC Airfoil Surface.
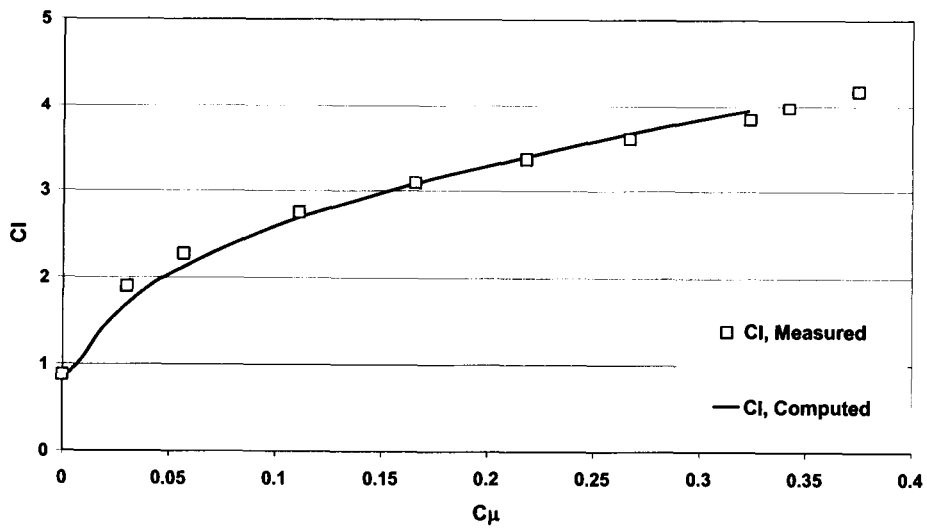


**Figure 3.** Variation of the Lift Coefficient with Momentum Coefficients at α=0°
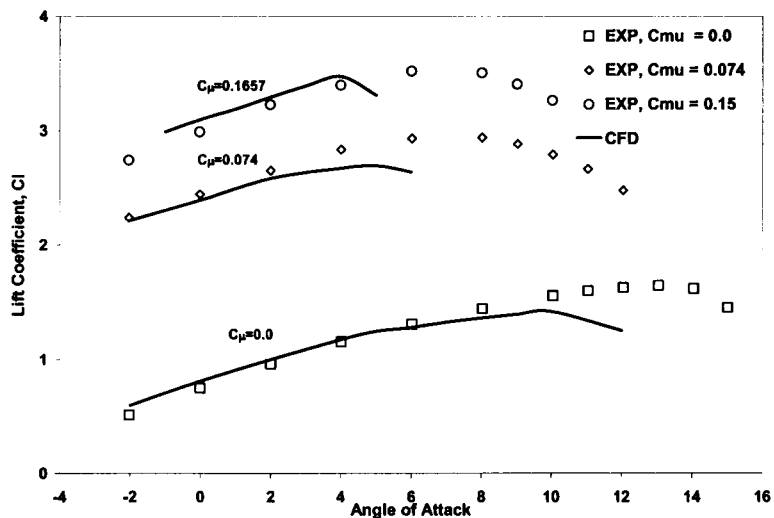
**Figure 4.** The Variation of the Lift Coefficient with Angle of Attack
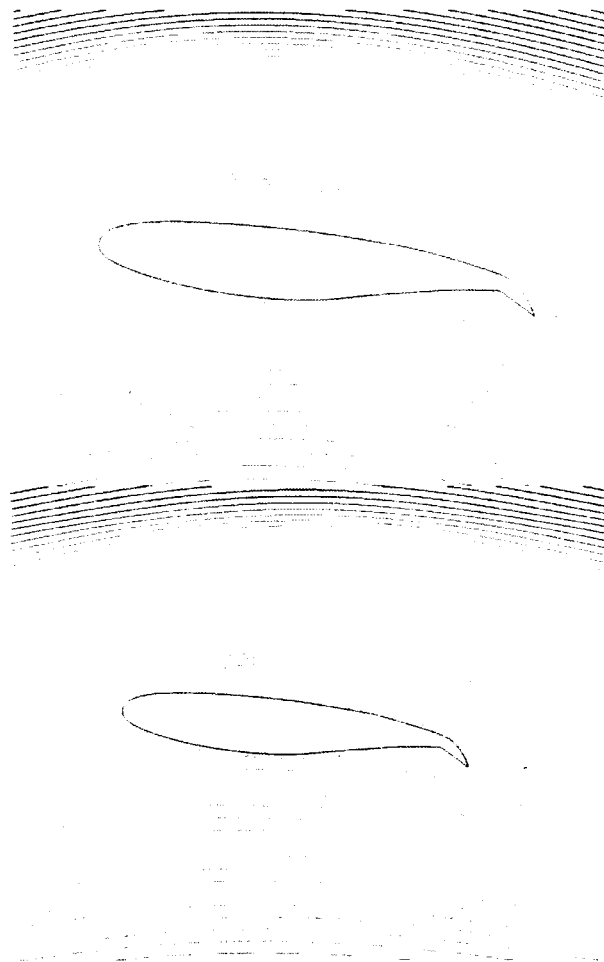


**Figure 5.** The Streamlines over the CC airfoil at Two Instantaneous Time Step
$(C_\mu = 0.1657,$ Angle of Attack $= 6^0)$
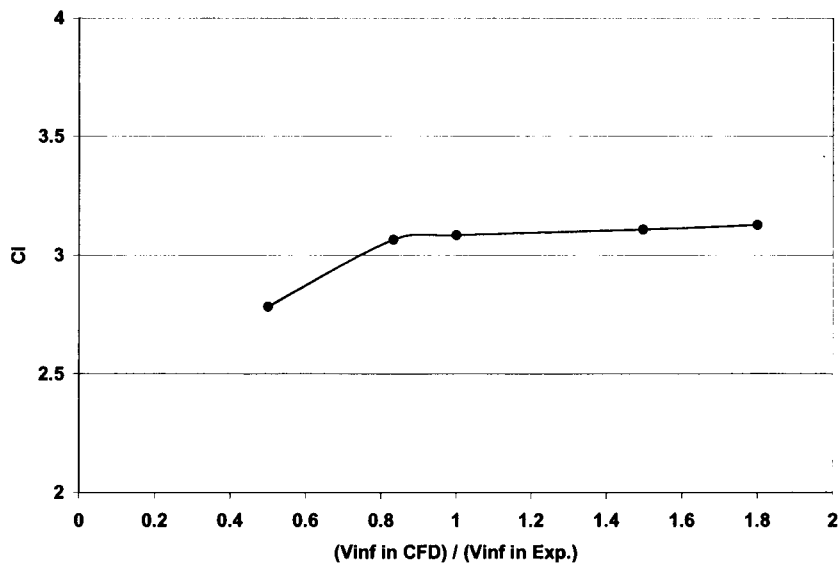
**Figure 6.** Lift Coefficient vs. Free-stream Velocity
($C_\mu = 0.1657$, h = 0.015 inch and $V_{\infty,\,exp} = 94.3$ ft/sec)
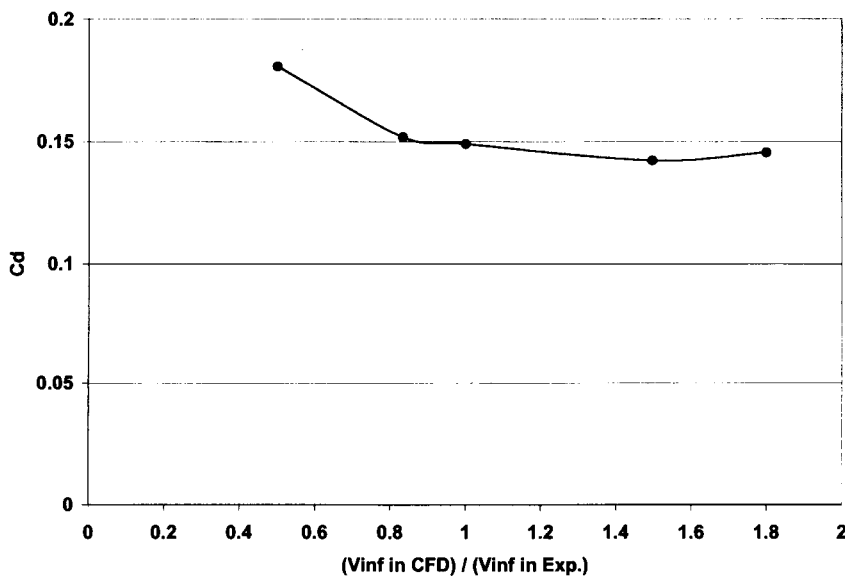


**Figure 7.** Drag Coefficient vs. Free-stream Velocity
($C_\mu = 0.1657$, h = 0.015 inch and $V_{\infty,\,exp} = 94.3$ ft/sec)
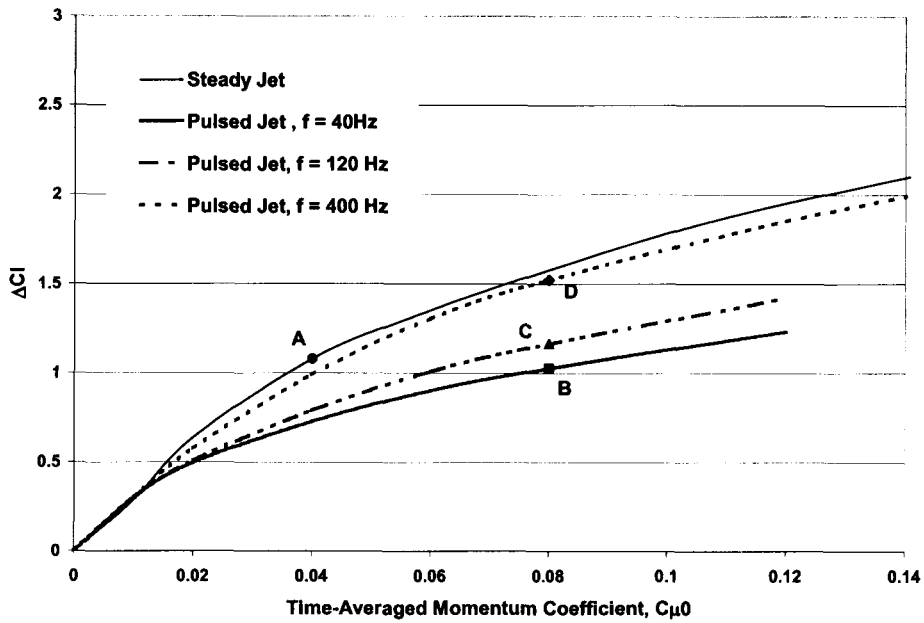
**Figure 8.** The Incremental Lift Coefficient vs. Time-averaged Momentum Coefficient
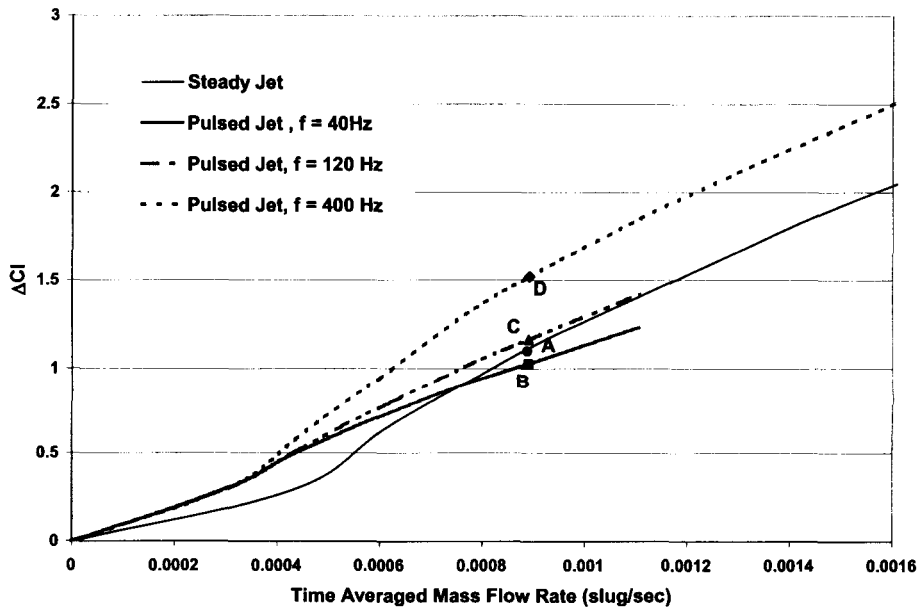


**Figure 9.** The Incremental Lift Coefficient vs. Time-averaged Mass Flow Rate
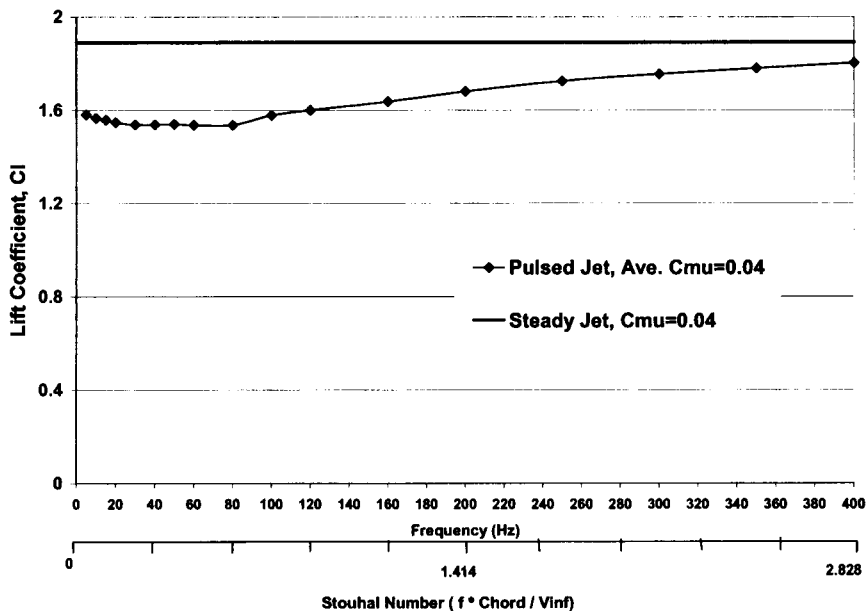
**Figure 10.** Time-averaged Lift Coefficient vs. Frequency & Strouhal Number
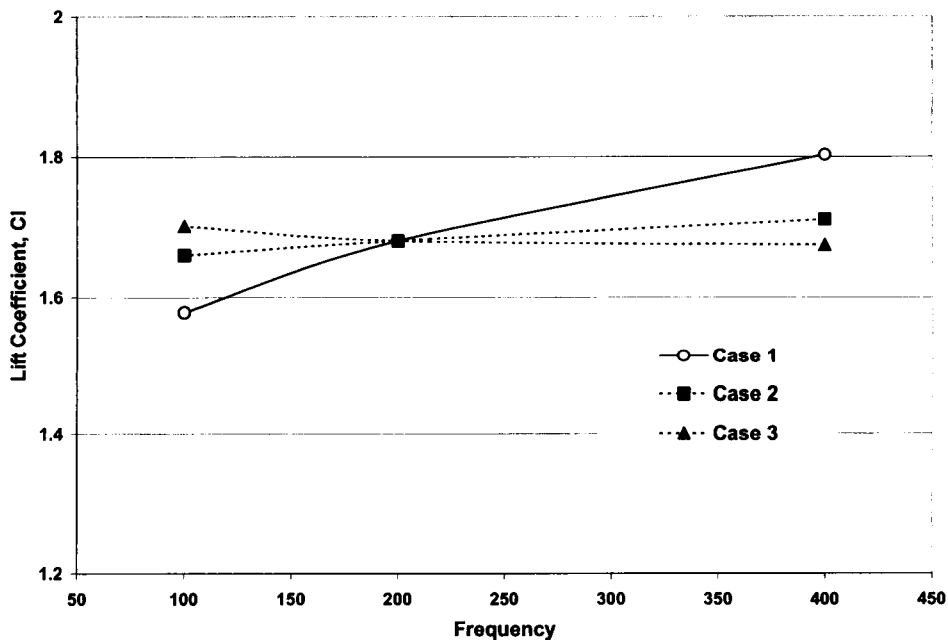
**Figure 11.** Time-averaged Lift Coefficient vs. Frequency

(Case 1. Strouhal number was not fixed; $U_\infty$ and $L_{ref}$ were fixed)
(Case 2. Strouhal number and $L_{ref}$ were fixed; $U_\infty$ was not fixed)
(Case 3. Strouhal number and $U_\infty$ were fixed; $L_{ref}$ was not fixed)

**Table 1.** The Computed Time-averaged Lift Coefficient for the Case one
($U_\infty$ and $L_{ref}$ fixed, the Strouhal number varying with the frequency)

|  | Baseline | Half Frequency | Double Frequency |
|---|---|---|---|
| Frequency (Hz) | 200 | 100 | 400 |
| Free-Stream Velocity $U_\infty$ (ft/sec) | 94.3 | 94.3 | 94.3 |
| Chord of the Airfoil $L_{ref}$ (inch) | 8 | 8 | 8 |
| Strouhal Number | **1.41** | **0.705** | **2.82** |
| Computed Average Lift Coefficient $(C_l)$ | **1.6804** | **1.5790** | **1.8026** |

**Table 2.** The Computed Time-averaged Lift Coefficient for the Case Two
(Strouhal number and $L_{ref}$ fixed, the $U_\infty$ varying with the frequency)

|  | Baseline | Half Velocity | Double Velocity |
|---|---|---|---|
| Frequency (Hz) | 200 | 100 | 400 |
| Free-Stream Velocity $U_\infty$ (ft/sec) | 94.3 | 47.15 | 118.6 |
| Chord of the Airfoil $L_{ref}$ (inch) | 8 | 8 | 8 |
| Strouhal Number | **1.41** | **1.41** | **1.41** |
| Computed Average Lift Coefficient $(C_l)$ | **1.6804** | **1.6601** | **1.7112** |

**Table 3.** The Computed Time-averaged Lift Coefficient for the Case Three
(Strouhal number and $U_\infty$ fixed, the $L_{ref}$ varying with the frequency)

|  | Baseline | Double Chord | Half Chord |
|---|---|---|---|
| Frequency (Hz) | 200 | 100 | 400 |
| Free-Stream Velocity $U_\infty$ (ft/sec) | 94.3 | 94.3 | 94.3 |
| Chord of the Airfoil $L_{ref}$ (inch) | 8 | 16 | 4 |
| Strouhal Number | **1.41** | **1.41** | **1.41** |
| Computed Average Lift Coefficient $(C_l)$ | **1.6804** | **1.7016** | **1.6743** |

# APPENDIX G

# Effect of Pulsed Blowing on Farfield Noise

# *Effect of Pulsed Blowing on Farfield Noise*

by
R. J. Gaeta, K. K. Ahuja, B. Hellman, and R. Combier

Georgia Institute of Technology
Atlanta, Georgia 30332-0844

# APPENDIX G

## Executive Summary

This portion of the report documents the results of an experimental program, which focused on pulsed blowing from the trailing edge of a CCW. The main objective of this study was to assess whether pulsed blowing resulted in more, less, or the same amount of radiated noise to the farfield. *Results show that a reduction in farfield noise of up to 5 dB is measured when pulse flow is compared to steady flow for an equivalent lift configuration.* This reduction is in the spectral region associated with the trailing edge jet noise. This result is due to the unique advantage that pulsed flow has over steady flow. For a range of frequencies, more lift is experienced with the same mass flow as the steady case. Thus, for an equivalent lift and slot height, the pulsed system can operate at lower jet velocities, and hence lower jet noise.

At low frequencies (below 1 kHz), the pulsed flow configuration generated more noise in the farfield. This is most likely due to the pulsing mechanism itself. Since the high pressure air feeding the pulsing mechanism was first passed through a high performance muffler, it is likely that this increase in not due to upstream valve noise. Most likely, the impulsive component of the air that periodically fills the plenum causes a broadband source that reaches the farfield. Although the benefit of a pulse trailing edge jet is evident from a mass flow usage and jet noise perspective, attention should be paid towards the design of a viable pulsing system. Future research program in this area should concentrate on the development of a "quiet" pulsing device.

# APPENDIX G

## Table of Contents

| Description | Page |
|---|---|

**APPENDIX G**

## List of Figures

## 1.0    Introduction

The first year of this grant focused on the farfield acoustic ramifications of steady blowing from the trailing edge of a two-dimensional wing[1]. By replacing a convention flap system with a rounded Coanda surface, a powerful high-lift device is produced. Studies have shown[2] that this type of circulation control can outperform the high lift capability of conventional flaps. The purpose of examining this type of high lift system is the expected acoustic benefit resulting from the removal of a flap system, which is believed to be a significant contributor to airframe noise on approach. Results from the first year of this grant showed that for an equivalent lift, the Circulation Control Wing (CCW) produced less noise than a wing with a conventional flap system. It was also found that proper design of the internal blowing plenum can be crucial in trying to minimize farfield noise.

The positive results of the steady blowing lead to the following question: Since compressed air for the blowing is expensive (typically, a parasitic bleed of a gas turbine), can the amount of air required be reduced by pulsing the air? Ideally, by using a square-wave pulse, half of the mass flow would be needed produce the same performance. This begs a second, more important question: Would a pulsing flow produce more, less, or about the same radiated noise to the farfield. The experimental program documented here attempts to answer this question.

Among the pertinent results presented in this report, one finding became obvious. The development of a pulsing actuation system that simultaneously provides adequate frequency response, pulse quality, and *quiet* operation is a significant challenge. Indeed, much of the work for this part of the grant was driven by this challenge. While an actuation device was ultimately used that performed adequately, a separate program to develop an actuator with the unique design requirements is needed. The challenge to produce an adequate pulse actuator was documented previously in the second year's report[3]. Among other issues, the frequency response (or lack thereof) of the actuator plays a crucial role. If the actuator pulse train quality deteriorates in the frequency range of interest, equivalent comparisons are difficult. Furthermore, actuator self-noise or related noise can interfere with the measurement of the jet noise from the trailing edge slot. Steps taken to address these concerns were outlined in the second year's report and included flow-straightening foam in the slot plenum and a reduction of

the plenum volume. The latter measure was undertaken to minimize the capacitive effect (damping) of the plenum on the pulse shape.

Solenoid valves were used initially; however, they had a very small frequency range over which a reliable, quality pulse could be generated. This limit was below 20 Hz. This was primarily due to the relatively large mass flow being used. The solenoid performance degraded with high line pressures. Moreover, the solenoids tended to overheat and fail complete after many hours of operation. Because of these drawbacks to the use of solenoids, a new type of actuator was employed for testing. A torque-motor device was used to create a pulsing flow that could be brought into the wing's blowing plenum. The torque-motor is an electro-mechanical device that takes air at high pressure as input and distributes the air alternately through two output ports. A shuttle valve is used to open and close each port. The frequency of the opening and shutting of a port is dictated by an electronic signal input to the device. Figure 1.1 shows the torque-motor. Each output from the torque-motor is $180^0$ out of phase with each other. It is with this device that pulsed air is ejected from the 2D airfoil used in the present program.



**Figure 1.1. Electro-Mechanical torque-motor.**

  
## 2.0 Technical Approach

### Farfield Acoustic Measurements and Pulse Blowing

The test article for the pulse blowing study was the same 2D airfoil used in the steady blowing
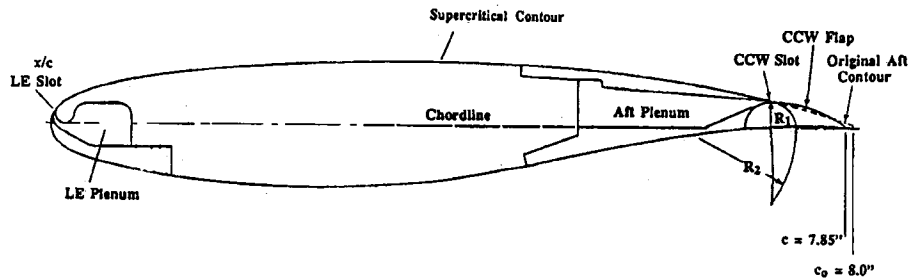


**Figure 2.1. Cross section view of 2D wing used for blowing tests.**

program reported earlier. Figure 2.1 shows a cross-sectional drawing of the basic airfoil. In an effort to reduce the trailing edge slot plenum volume, the wing was modified so only the middle 12 inches of the span would be used for air flow. The reduction in plenum volume would help reduce the damping of the pulsed velocity amplitude. Figure 2.2 shows the basic airflow path of the control air. Since the plenum volume would be reduced, it is imperative that velocity be as uniform as possible through the slot exit. At the back of the plenums, a strip of aluminum foam was installed to evenly distribute the slot exit velocity. Previous work[3] established this and Figure 2.3 shows the results of the addition of aluminum foam.

Since the torque-motor output is $180^0$ out of phase, two torque-motors were used for each 6-inch
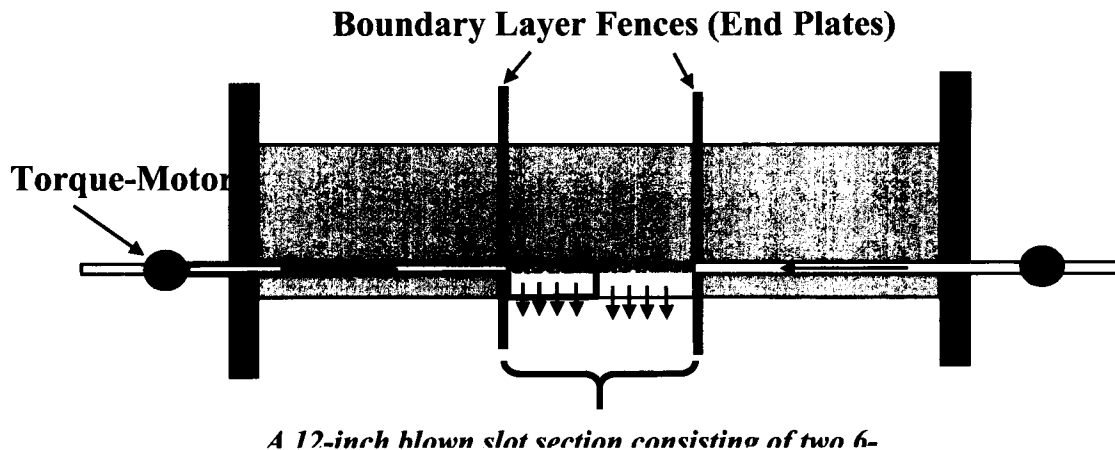


**Figure 2.2. Modified internal flowpath for CC Wing for pulsed slot blowing tests.**

section of the slot plenum. This meant that one output leg of each torque-motor was "dumped overboard". That is, the out of phase leg was allowed to exhaust into the ambient air. In order to avoid certain jet noise contamination, these outputs were run through 25 feet of copper tube coil and exhausted into a foam lined muffler.

### Steady Jet Measured with Hot-Wire
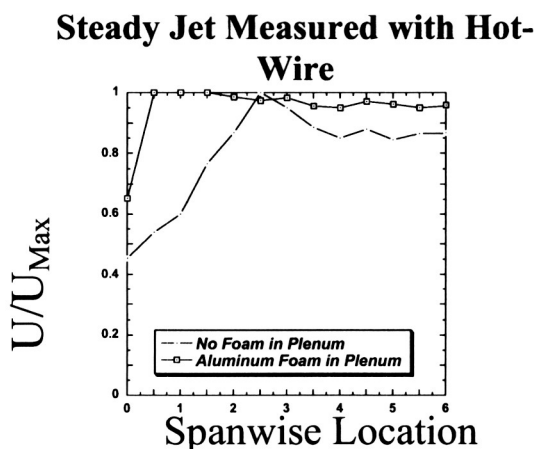


**Figure 2.3. Improved flow uniformity with Aluminum foam in**

The 2D wing was installed in GTRI's Anecohic Flight Simulation Facility (AFSF). The wing was exposed to freestream velocity by installing it in the exhaust region of a 28-inch diameter nozzle issuing into the anechoic room. Farfield microphones record noise levels in the farfield for several freestream velocities, slot exit velocities, and pulsing frequencies. All tests were conducted with the wing at zero angle of attack. Figure 2.4 shows this test set-up in the AFSF.

There are essentially two ways to assess the acoustic performance of a pulsing Circulation Control wing.

1) Compare the farfield spectra of a steady blowing case versus a pulsed blowing case where the averaged $C_\mu$ of the pulsed case is equivalent to steady $C_\mu$ value.

2) Compare the farfield spectra of a steady blowing case versus a pulsed blowing case where the peak $C_\mu$ of the pulsed case is equivalent to the steady $C_\mu$ value.
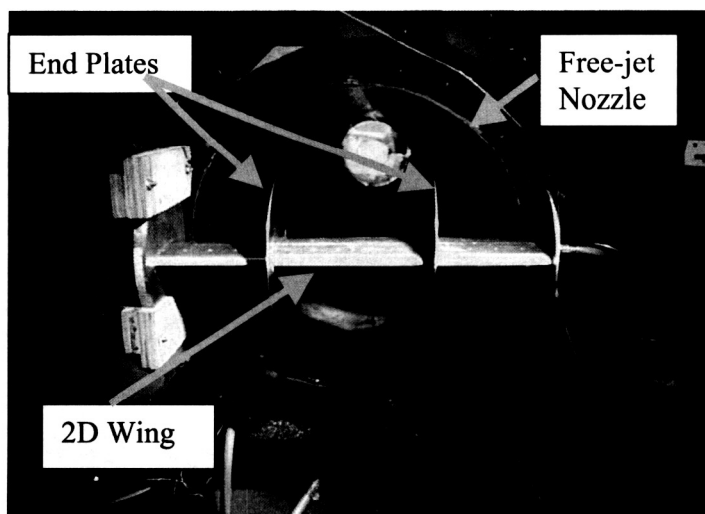


**Figure 2.4 Blown 2D wing installation in Anechoic Flight Simulation Facility.**

Figure 2.5 shows schematically what ideal $C\mu$ time histories would correspond to cases 1 and 2 above.
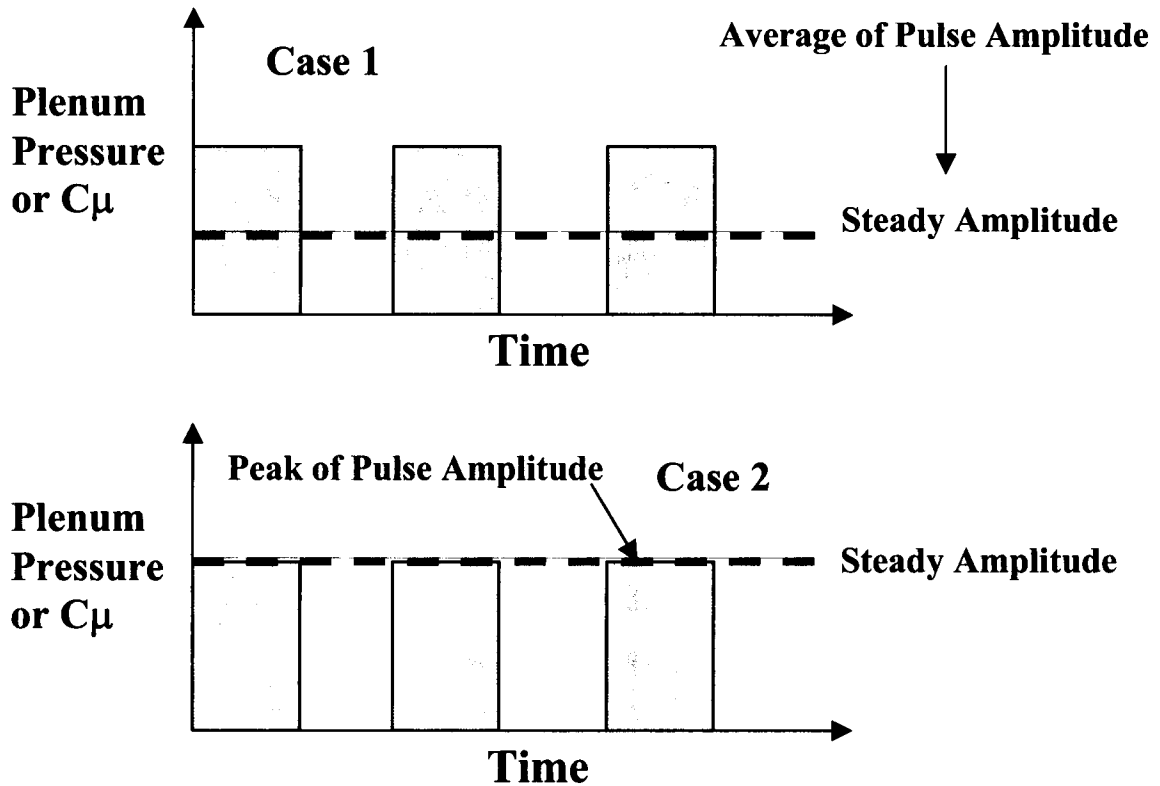


**Figure 2.5. Schematic of two possible cases for comparing steady to pulsed blowing in assessing farfield acoustic performance.**

It would appear that the first case above is relevant if one assumes that aerodynamically the response of the airfoil to a steady $C_\mu$ is equivalent to the response of an unsteady $C_\mu$. Simply put, if the average $C_\mu$ (and thus $C_L$) the wing experiences is the same, then the lift generated should be the same.

## Aerodynamic Benefits of Pulsed Trailing Edge Blowing

Work performed at GTRI under NASA LaRC Grant[4] demonstrates that case 1 is not necessarily desirable. This grant evaluated the identical wing configuration in a wind tunnel. The wing was installed on a balance and lift was measured for a variety of pulsing and steady blowing conditions. Results confirmed earlier findings by Rockwell[5] that over a certain range of $C_\mu$ or

MTF 061, Unsteady Pulsed Blowing, Straight Trapeze Tares.
α=0°, q=10 psf, h=0.014"
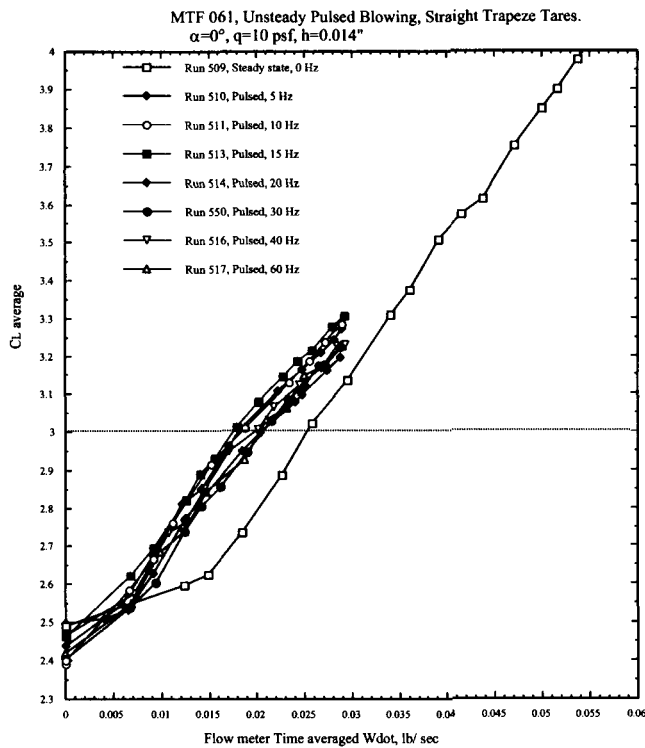
Figure 2.6. Effect of pulse blowing on lift as a
function of blowing mass flow (from ref. 4).

mass flows, pulse blowing produces *higher* lift than steady blowing. Figure 2.6 shows this remarkable result by showing mass flow vs. lift coefficient for a range of frequencies. There is an effect of the pulse frequency. It appears that the increase in lift seen when pulsing diminishes somewhat as the frequency increases. It is not known exactly why this is the case, but the quality (or lack thereof) of the pulse at high frequency is most likely the reason. To understand why a benefit is realized, one needs to consider the two type of pulsing comparisons outlined above in Figure 2.5. Consider the pulse train shown for case 1. The averaged momentum ratio, $C\mu$, is the same in both the steady and pulsing conditions. Thus, for a constant slot height, this means that the mass flow rates are equivalent. However, for at least half of the time, the momentum ratio is roughly twice as high as the steady condition. This means that the airfoil has higher lift during this time. Averaged over some period, the pulsed blowing case experiences a higher lift as demonstrated by the results in Figure 2.6. Another way to look at it is that for equivalent lift, less momentum ratio and hence less mass flow is required for the pulsing case. The implication of this improved aerodynamic benefit is positive. For an equivalent lift system, less mass flow is needed for the pulsing case, implying therefore that (for a fixed slot height) the slot jet velocity will be lower. This should lead to a lower contribution from jet noise in the farfield relative to a steady blown case.

## 3.0    Test Facilities, Instrumentation, and Data Acquisition

The farfield acoustic measurements were acquired in GTRI's Anechoic Flight Simulation Facility. This is an open jet wind tunnel housed in an anechoic chamber. The interior of this facility is shown in Figure 3.1. The flow for simulating flight is generated through the working section in the anechoic room by the operation of a jet ejector and/or a diesel driven fan. Air is drawn into the intake at the left through the honeycomb and screens to the
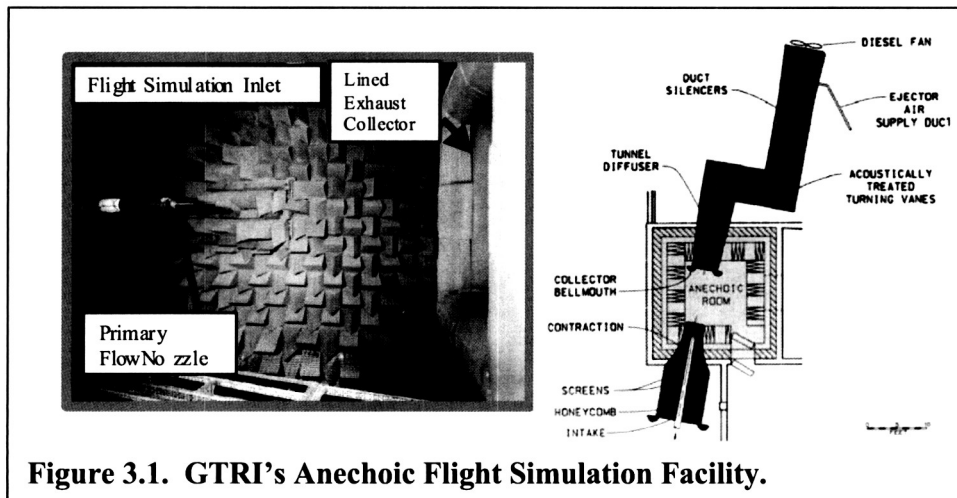


**Figure 3.1.  GTRI's Anechoic Flight Simulation Facility.**

contraction (see Figure 3.1), across the anechoic room to the collector, through the diffuser, the two right angle corners with acoustically treated turning vanes, the duct silencers, and the transition section to the powered exhaust section. The facility is capable of providing continuous free jet velocities up to 100 m/s with a circular test section diameter of 0.71 m. It is possible to make acoustic measurements on a circular arc of 3 m radius, centered on the model, in the range 30° to 100° with respect to the tunnel axis. The angular range may be increased by reducing the arc radius for a few measurement locations at the higher angles.

Auxilliary air used for the trailing edge blowing was supplied from a 125 psig source. The flow rate was measured with a venturi flow meter and then allowed to pass through a large muffler designed to significantly reduce any upstream valve noise. The flow was split and each leg was fed into a torque-motor. Figure 3.2 shows a schematic of this set up.
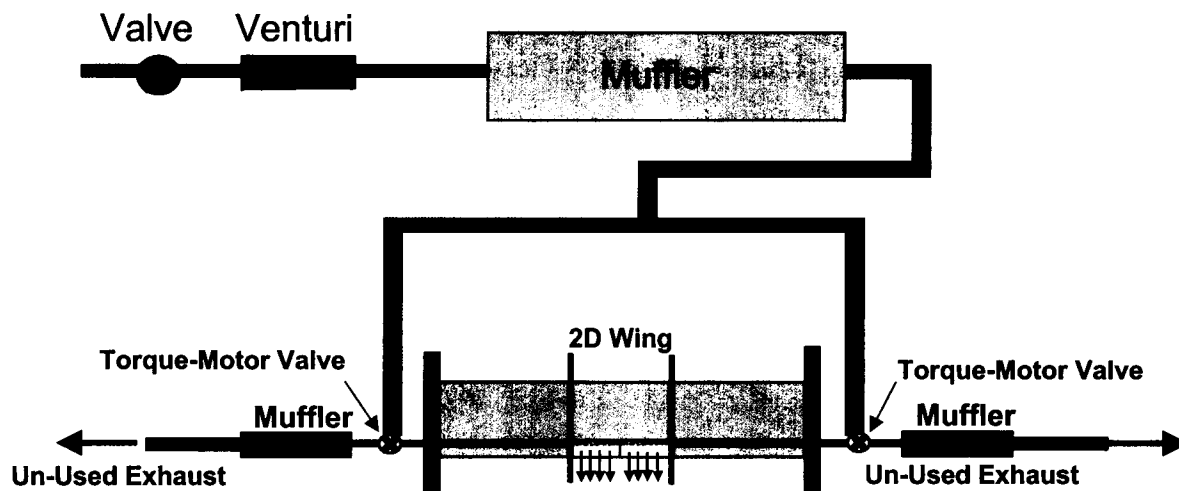
**Figure 3.2. Test set up for pulsed blown wing.**

## Data Acquisition

*Flow Data*

Unsteady pressure transducers (Kulite and Endevco) were used to measure the venturi pressures as well as the plenum pressure in the trailing edge of the wing. These transducers were powered by a battery and input into a computer A/D board. Facility ambient pressure and temperature were monitored. The simulated freestream velocity was computed from static pressure measurements made around the circumference of the nozzle bringing air into the facility. A Labview data acquisition program was written on a Windows platform to collect the pressures from the venturi and the wind tunnel. Mass flow to the wing was computed via venturi flow analysis. Steady tunnel pressures were acquired with a PSI multi-channel pressure transducer. All flow data was stored in retrievable files on the computer.

*Acoustic Data*

Acoustic data were acquired with 1/4-inch B&K condenser microphones using B&K Nexus power supplies and amplifiers. These microphones were placed on a polar arc directly beneath the wing model. Using the facility's jet exhaust axis as the $0^0$ polar angle, eight microphones were placed $10^0$ apart from $100^0$ to $30^0$. Figure 3.3 shows this set up. All microphones except

the $100^0$ and the $30^0$ were located 10 feet. The data from the $100^0$ and $30^0$ microphones were corrected to a distance of 10 feet. Furthermore, all acoustic data was corrected for atmospheric absorption, free-field response, and the microphone grid effect. Pressure time histories were acquired on an HP 3667A Multi-Channel Signal Analyzer for FFT analysis running on a Pentium-based Windows computer platform.
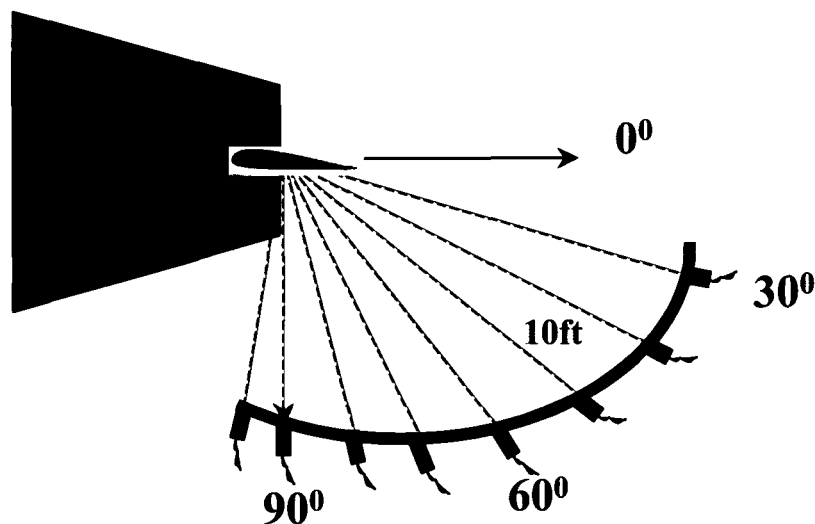


**Figure 3.3. Farfield microphone set-up in Anechoic Flight Simulation Facility.**

## 4.0 Pulse Actuator Performance

The torque-motor used in the present pulsed blowing experiments produced slot exit velocity characteristics that were, in general, more repeatable than the problematic solenoid valves. While the ideal goal of perfect square waves (as shown above in Figure 2.5) is unobtainable, reasonable pulse quality was obtained from the device. Figure 4.1 shows typical slot exit velocity time histories measured with a hot wire. A Kulite pressure transducer installed in the slot plenum was also used to gauge the pulsing velocity. Figure 4.2 shows a typical plenum pressure history.
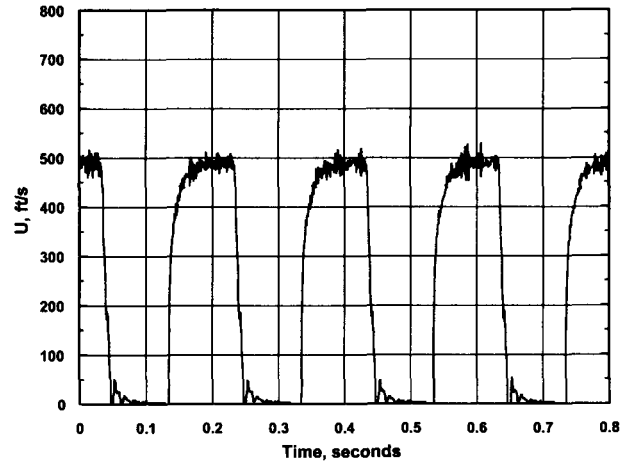
**Figure 4.1. Slot exit velocity time history for 5 Hz pulse, measured with hot wire.**
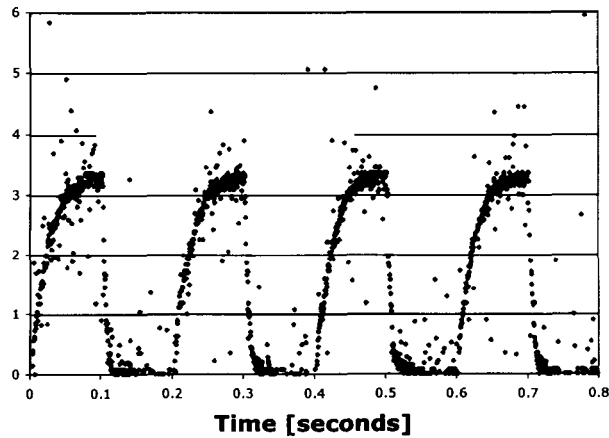


**Figure 4.2. Plenum pressure time history during 5 Hz pulsing.**

It is noted that there is a rounded ramp-up to the maximum pressure before a relatively sharp drop to near zero pressure. It is believed that this is due to finite time needed to fill the plenum with air. The DC offset was nearly zero for low frequencies but was on the order of 0.2 psig above 30 Hz.

## 5.0    Farfield Acoustic Results

The main objective of this study was to discern the differences (if any) in the farfield acoustic spectra of a Circulation Control wing under steady trailing edge blowing from unsteady (pulsed) blowing conditions. While microphones in the farfield were stationed from $110^0$ to $30^0$ at 10-degree increments along the chord-line axis, data presented here will consist mostly of the 30, 60, and 90-degree locations. It is the noise from the jet issuing from the trailing edge slot, which is of interest. Most of the noise generated from a high-lift wing employing circulation control in this way will be attributed to this jet noise. Thus, it is important that the farfield acoustic measurements indicate this jet noise component. There will be contributions from the free-jet issuing into the anechoic room, the wing itself, and it mounting hardware. Due to the characteristic dimension of the high-speed jet exiting the trailing edge (approximately 0.014 inches), it is expected that the noise generated by this jet will be at frequencies exceeding 20 kHz.

Verification that the slot exit noise is discernable in the farfield spectra can be observed in Figure 5.1. This figure shows spectra for five cases: background ambient, wing mounted with NO blowing, and wing mounted with steady blowing at three separate mass flow conditions. Since slot height is constant, each mass flow case represents a different jet
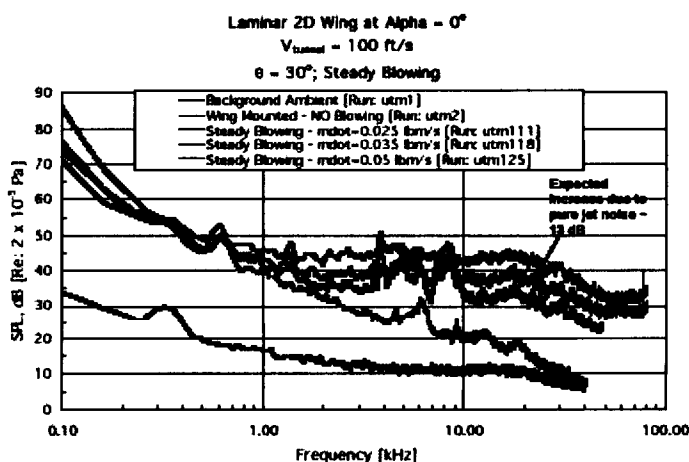


Figure 5.1  Presence of slot jet noise in measured farfield spectra.

velocity. It is clear that the noise at the lower frequencies is due to the free jet and the wing alone (any contribution of the slot jet is too low to impact spectra at these frequencies). However, it can be seen that above approximately 10 kHz, the noise from the jet operation is distinct. Furthermore, jet noise theory predicts that the amplitude should increase by 80Log(Jet Velocity). It is estimated that the increased mass flow case should increase the jet noise by approximately 13 dB. The data show that this is roughly the case above 10 kHz. Thus,

examining the farfield spectra above 10 kHz reveals noise generated by the trailing edge blowing slot.

## Comparison with Equivalent Blowing Ratio

When comparing spectra for steady and pulsed blowing that represent a condition similar to Case 1 in Figure 2.5, it is expected that the averaged slot exit velocity should be equivalent to the steady jet velocity. Hence, the jet noise radiating to the farfield should be similar. Figure 5.2 shows a slot plenum pressure time history for a steady and pulse blowing case representing this case. Figure 5.3 shows the resulting farfield acoustic spectra at 30, 60, and 90 degrees. It is clear that the noise generated from the pulsed blowing case [in the region identified as noise due to the blowing jet, > 10 kHz] is on the order of the steady case, as expected.

**Instantaneous Plenum Pressure**
**f =30 Hz Time History**
**[$V_{tunnel}$ = 100 ft/s; $m_{dot}$ = 0.07 $lb_m$/s]**
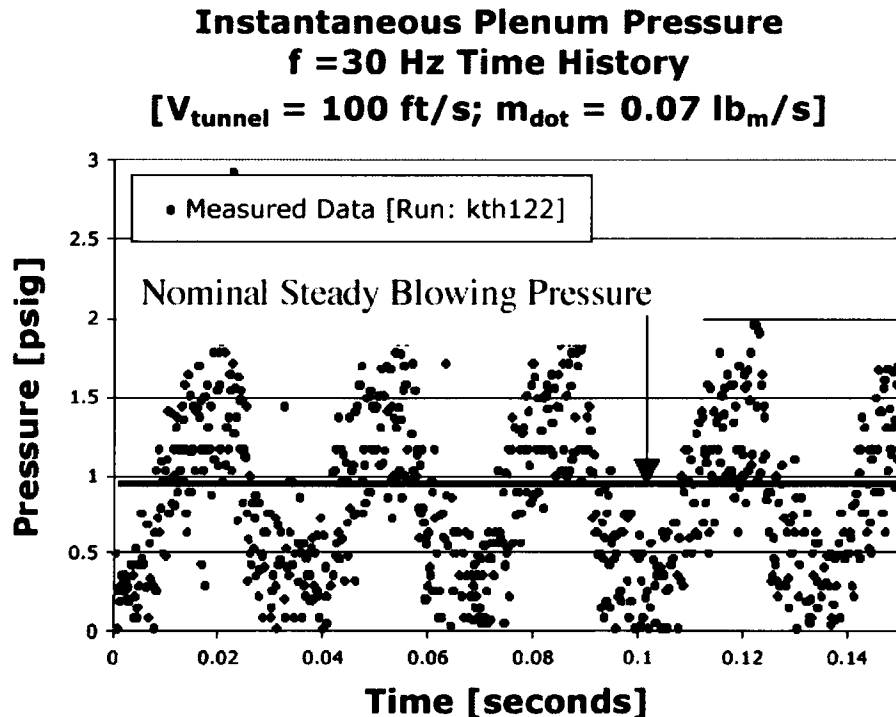


**Figure 5.2  Slot plenum pressure time history for "equivalent lift" case.**

It is also clear that noise levels below 1 kHz for the pulse blowing case are 5 – 10 dB higher than the steady blowing case. This suggests that part of the pulsing mechanism could be contributing to the noise in this region. Care was taken to place acoustic foam around the torque-motor, but the impulsive opening of the valve might be contributing to a wide-band noise below 1 kHz. In
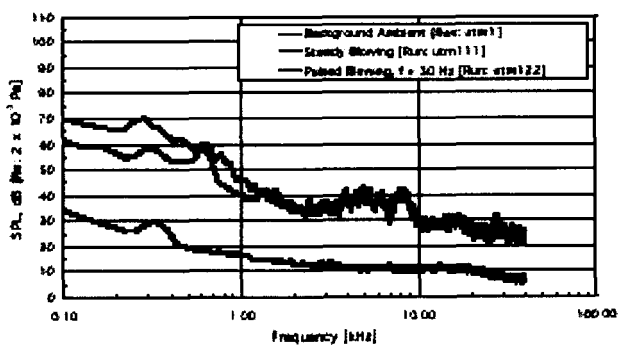
assessing whether a pulsing system would be viable for full scale use on an aircraft, the pulsing mechanism would have to be carefully designed to minimize its farfield radiated noise contribution. For the present study, focusing on the noise generated above 10 kHz is relevant for assessing the noise generated by a pulsed slot-jet at the wing trailing edge.
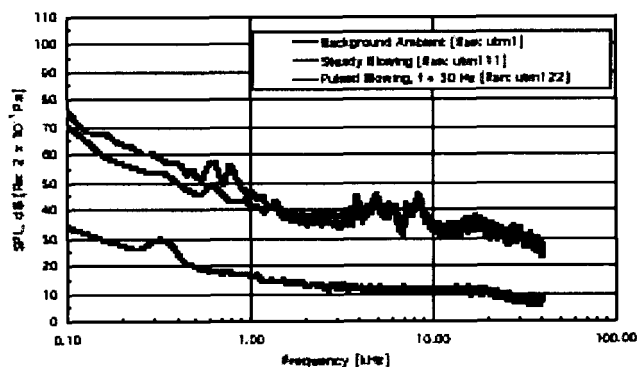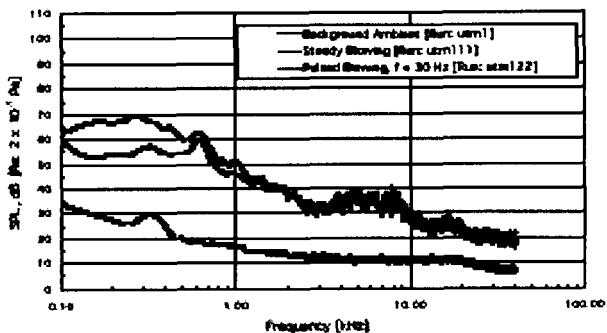
**Figure 5.3 Comparison of farfield acoustic spectra for steady vs. pulsed blowing [V=100 ft/s, f = 30 Hz]**

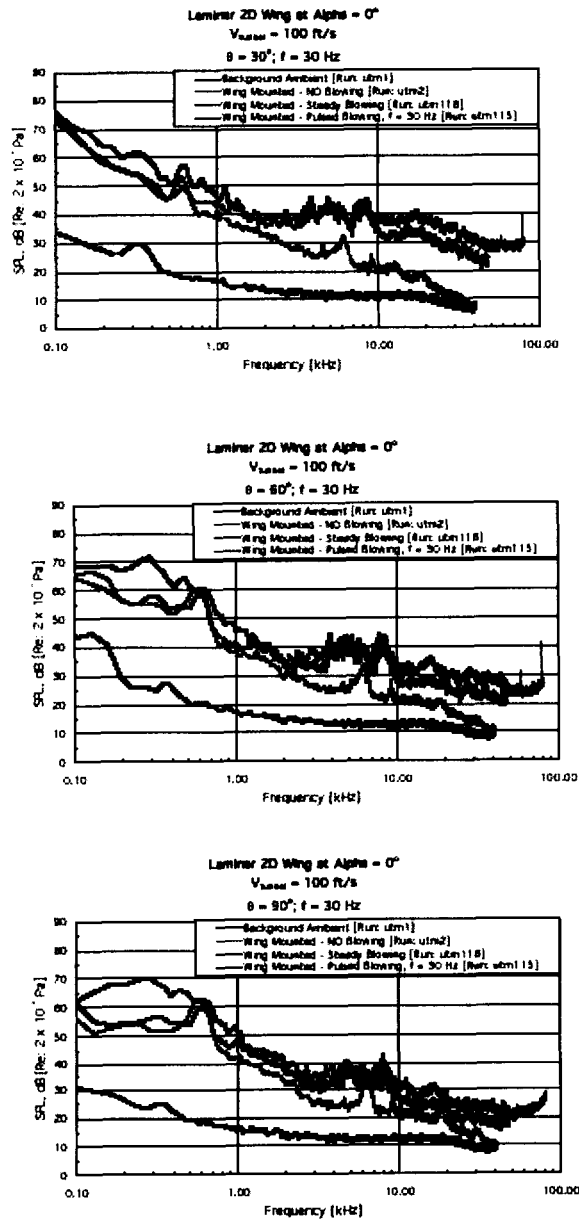## Comparison with Equivalent Lift

Using Figure 2.6 as a guide, one can see that for a case of equivalent lift, less mass flow is needed for the pulsing condition. Choosing a set of data at which the pulsed blowing mass flow is roughly 70% of the steady mass flow, a comparison can be made of the farfield jet noise. Figure 5.4 shows the farfield noise spectra of just such a case. Here it is observed that indeed a modest acoustic benefit is obtained with the pulsed blowing case at higher frequencies. At 30 degrees, it is as much as 5 –6 dB above 20 kHz. This reduction in jet noise is due to the fact that the average slot jet exit velocity is lower that the steady jet. This is a result of the unique aerodynamic benefit of pulse blowing, that is, not as much mass flow is required when pulsing.

## 6.0 Conclusions

In an effort to enhance the viability of the Circulation Control wing, pulsed rather than steady blowing has been investigated as a means of reducing the total amount of air needed for such a system. Indeed there is an aerodynamic benefit that can be realized with pulsing trailing edge flow. Within a certain range of blowing ratios, an increased amount of lift can be obtained for a given mass flow (See Figure 2.6). *The experimental results presented in this report suggest that there is potential to reduce the noise associated with a pulsed jet that issues from the trailing edge, if the noise in question is associated with the issuing jet only.* It is evident from the data that a quieter delivery system needs to be pursued if any serious attempt is made to integrate this concept on a large system.

A further important result from this program is the general lack of a robust, aeroacoustically designed, pulsing mechanism that could be used for this type of application. The field of active flow control in general, where pulsing flow is a very popular concept, is in need of devices that can pulse flow with good frequency response, amplitude, and quiet operation.

**Figure 5.4 Comparison of farfield acoustic spectra for steady vs. pulsed blowing; "Equivalent Lift"** |V=100 ft/s, f = 30 Hz|

# APPENDIX G

## 7.0 References

1.  1st year CCW NRA Grant Annual Report.

2.  Englar, Robert J. *Circulation Control Pneumatic Aerodynamics: Blown Force and Moment Augmentation and Modification; Past, Present & Future*  AIAA 2000-2541, Presented at the Fluids 2000 Conference, Denver, CO.  19-22 June, 2000.

3.  2nd Year CCW NRA Grant Annual Report

4.  Englar, R. J., Gaeta, R. J., and Kabo, E. M. *Evaluation of Pulsed Unsteady Blowing Applied to Circulation Control Wing Configurations*. Final Report, NASA Grant NAS1-00087-A003, Georgia Tech Research Institute, March, 2002.

5. Oyler, T. E., and Palmer, W. E., Exploratory Investigation of Pulse Blowing for Boundary Layer Control, Columbus Aircraft Div., North American Rockwell Corp., Report NR72H-12, January 15, 1972.

# APPENDIX H

# Flap-Edge Blowing Experiments

# APPENDIX H

## Flap-Edge Blowing Experiments

By
R. J. Gaeta, R. J. Englar, and K. K. Ahuja
Georgia Tech Research Institute
Atlanta, Georgia, 30332-0844

This Appendix documents the salient results from an effort to mitigate the so-called flap-edge noise generated at the split between a flap edge that is deployed and the un-deployed flap. Utilizing a Coanda surface installed at the flap edge, steady blowing was used in an attempt to diminish the vortex strength resulting from the uneven lift distribution. The strength of this lifting vortex was augmented by steady blowing over the deployed flap. It documents the salient results from an effort to mitigate the so-called flap-edge noise generated at the split between a flap edge that is deployed and the un-deployed flap. Utilizing a Coanda surface installed at the flap edge, steady blowing was used in an attempt to diminish the vortex resulting from the uneven lift distribution. The strength of this lifting vortex was augmented by steady blowing over the deployed flap.

The test article for this study was the same 2D airfoil used in the steady blowing program reported earlier (also used in pulsed blowing tests, see Appendix G), however its trailing edge geometry was modified. An exact duplicate of the airfoil shape was made out of fiberglass with no flap, and in the "clean" configuration. It was attached to the existing airfoil to make an airfoil that has half of its flap deployed and half un-deployed. Figure 1 shows a schematic of the planform showing the two areas where steady blowing was introduced. The flap-edge blowing or the auxiliary blowing was in the direction normal to the freestream velocity vector. Slot heights for the blowing chambers were on the order of 0.014 inches.
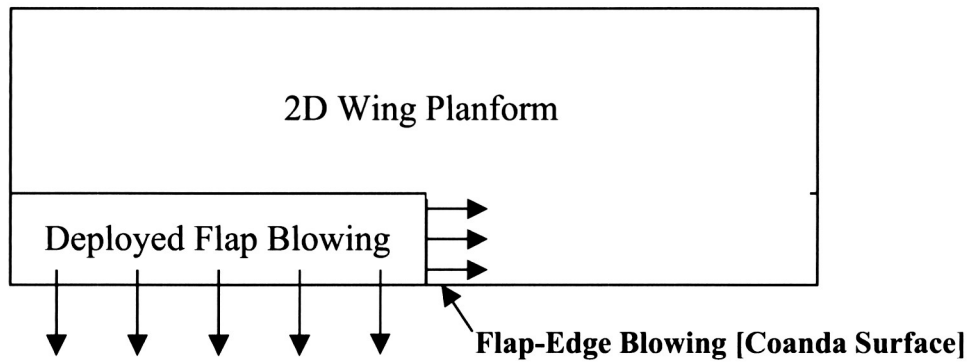
**Figure 1. Schematic of Flap-Edge Blown 2D airfoil.**

Figure 2 shows this airfoil installed in GTRI's Anechoic Free Simulation Facility.
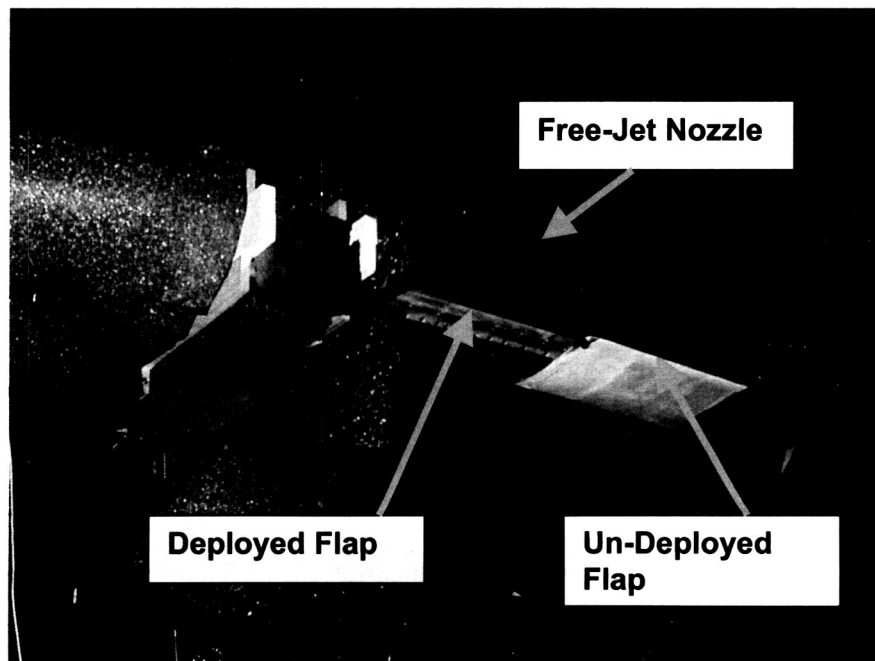


**Figure 2. Test article installed in Anechoic Flight Simulation Facility.**

## Data Acquisition

*Flow Data*

Total pressures in the blowing plenums were recorded with Kulite pressure transducers. Facility ambient pressure and temperature were monitored. The simulated freestream velocity was computed from static pressure measurements made around the

circumference of the nozzle bringing air into the facility. A Labview data acquisition program was written on a Windows platform to collect the pressures from the venturi and the wind tunnel. All flow data was stored in retrievable files on the computer.

*Acoustic Data*

Acoustic data were acquired with 1/4-inch B&K condenser microphones using B&K Nexus power supplies and amplifiers. These microphones were placed on a polar arc directly beneath the wing model. Using the facility's jet exhaust axis as the $0^0$ polar angle, eight microphones were placed $10^0$ apart from $100^0$ to $30^0$. Figure 3 shows this set up. All miccropones, except the $100^0$ and the $30^0$, were located 10 feet. The data from the $100^0$ and $30^0$ microphones were corrected to a distance of 10 feet. Furthermore, all acoustic data was corrected for atmospheric absorption, free-field response, and the microphone grid effect. Pressure time histories were acquired on a Multi-Channel Signal Analyzer for FFT analysis running on a Pentium-based Windows computer platform.
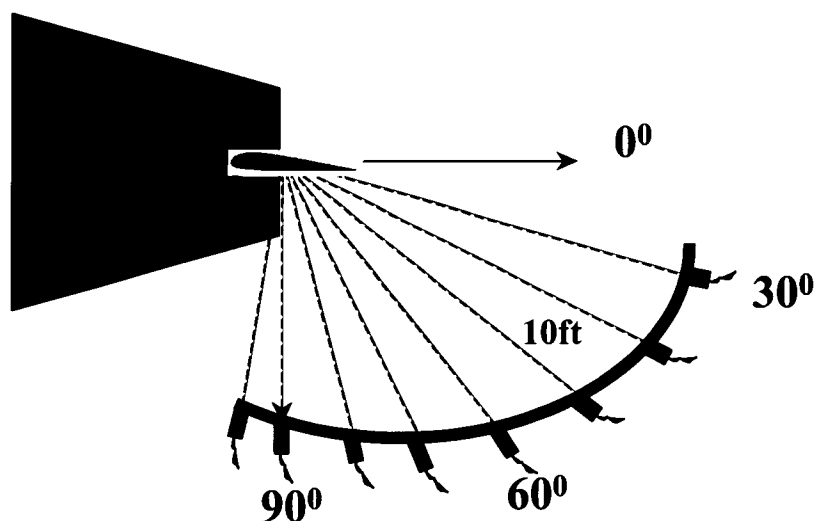


**Figure 3. Farfield microphone set-up in Anechoic Flight Simulation Facility.**

## Test Conditions

Test conditions concentrated on a freestream condition of 100 ft/s. Two levels of blowing were tested for both the main flap and the flap-edge blowing slot. These were approximately 1 and 3 psig. Combinations of these blowing levels were used as acoustic test points. Note that data presented here does not account for the free jet shear layer effects or atmospheric absorption. Furthermore, the data has not been corrected for the microphone grid and free-field effects. This is of small consequence since we are examining differences of configurations tested in the same facility in the same time period.

## Results

With a freestream velocity of 100 ft/s and no blowing operating, the radiated farfield noise character of the wing is dominated by noise below 1000 Hz. Figure 4 shows the SPL (Sound Pressure Level) spectrum at a polar angle of 90 degrees of such a case.
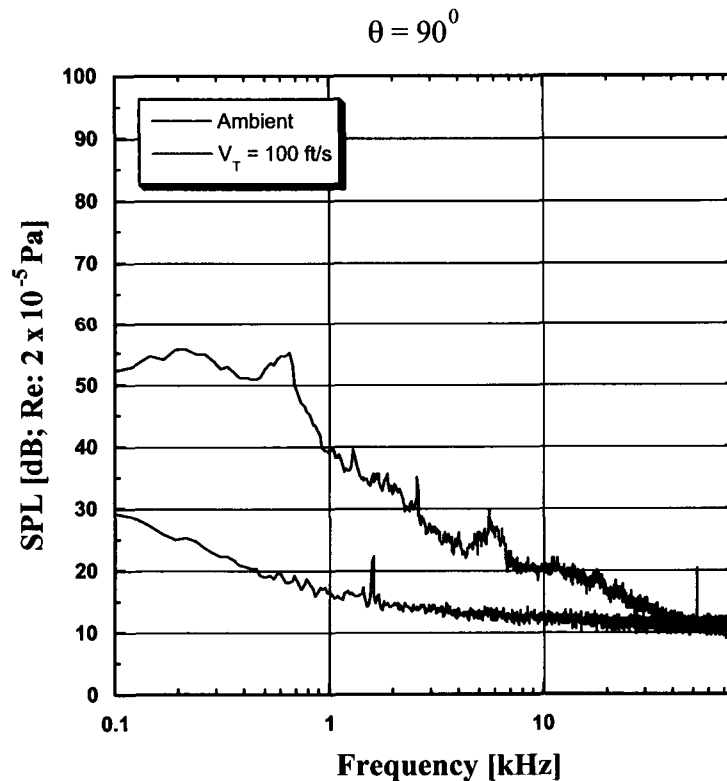
$$\theta = 90^0$$



**Figure 4. Farfield noise of wing with no blowing at freestream velocity of 100 ft/s, $\theta = 90^0$.**

A tuft placed at the flap edge (at the midspan location of the trailing edge), was visualized with a strobe light and the lift vortex due to the increased lift of the flap, was clearly visible. Figure 5 shows a photograph of this effect.



**Figure 5. Lift vortex visualized with tuft at midspan trailing edge**.

The effect of the flap-edge blowing was first examined without any main flap blowing operating. At a freestream velocity of 100 ft/s, the auxiliary or flap-edge blowing was operated at 0, 1 and 3 psig total pressure conditions. Figure 6 shows the resulting farfield acoustic SPLs at polar angles of 30, 60, and 90 degrees, respectively. Clearly, the small jet over the Coanda surface has an impact on the radiated noise above 6000 Hz in the 1 psig case and 1000 Hz in the 3 psig case. At $\theta = 90^0$, the intermediate pressure of 1 psig seems to reduce the noise peak around 600 Hz, but it is elevated again at a pressure of 3 psig.

Figure 7 shows spectra for several flap-edge blowing pressures with a main flap blowing pressure of 1 psig for polar angles of 30, 60, and 90 degrees. The low frequency peak noise at roughly 600 Hz with no blowing is shifted to a higher frequency when the main blowing is turned on and is now at approximately 1500 Hz. This is most likely due to the increased lift caused by the main flap blowing. The increased amount of jet blowing from the trailing edge increases the high frequency noise (above 1000 Hz) substantially. These results were similar to results found at the higher main flap blowing pressure.

## APPENDIX H

Flow visualization of the vortex indicated that the effect of increasing the main flap blowing was a "strengthening" of the lift vortex. The strengthening was only assumed and not quantified. The vortex became more "vigorous" and intuitively, wing lift was increasing on the deployed flap, the vortex should have become more intense. The effect of blowing on the flap edge was observed to "push" the vortex further towards the trailing edge span. This was observed clearly with tufts. This can be seen clearly in Figure 8. This picture was taken with the camera pointed at the underneath of the wing/flap system. With no blowing from the flap edge, the tuft at the flap edge follows the vigorous motion of the tip vortex. As soon as the flap edge blowing is turned on, the vortex moves to the right in the picture from tuft labeled 1 to tuft labeled 2. The strength of the shifted vortex was not quantified but the effect on the farfield acoustics was to increase the high frequency content of the radiated noise, most likely due to the issuing air jet, while mildly affecting the low frequency content. Thus no noise benefits were observed. Additional work needs to be done on the effect of tip blowing on flap-edge noise.

# APPENDIX H

Effect of Main Flap and Flap Edge Blowing ;
$V_{Tunnel}$ = 100 ft/s
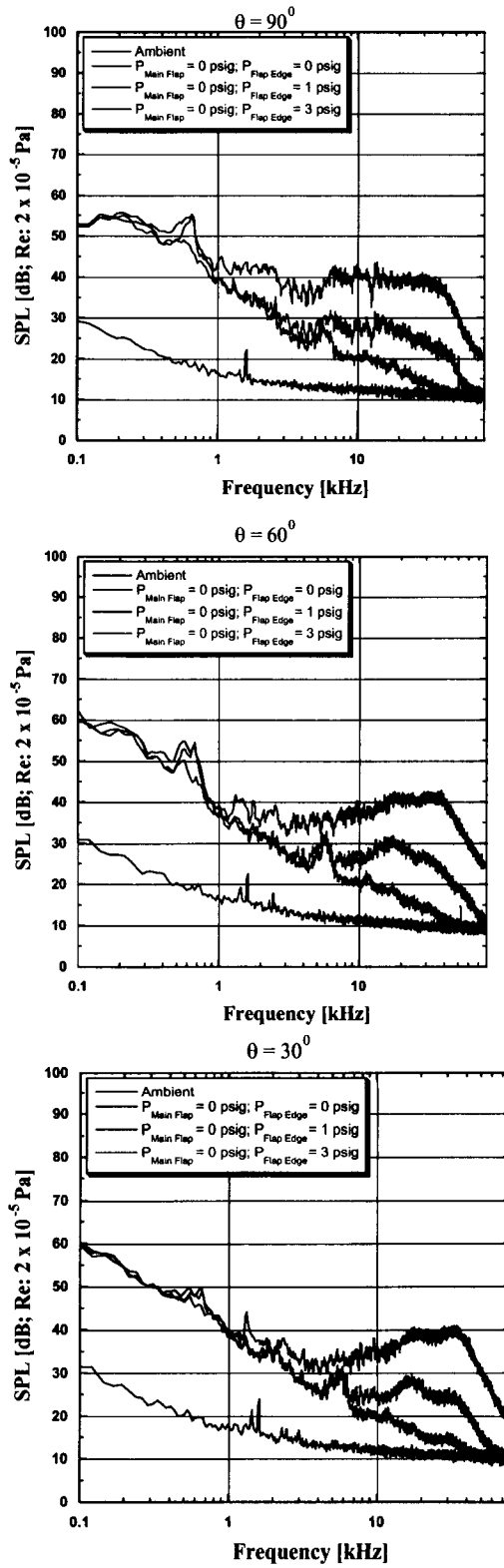
$\theta = 90^0$



$\theta = 60^0$



$\theta = 30^0$



**Figure 6.  Effect of Flap-Edge blowing on farfield noise.**

## APPENDIX H
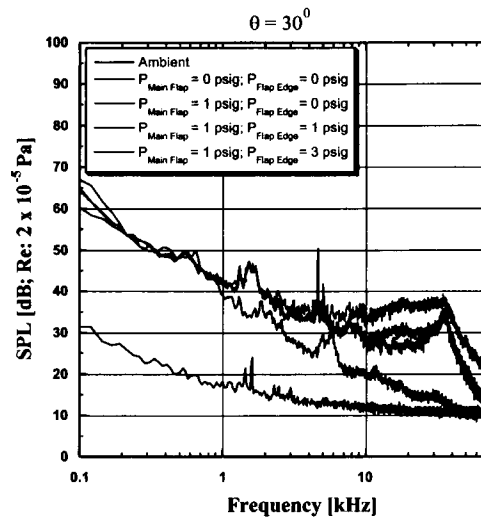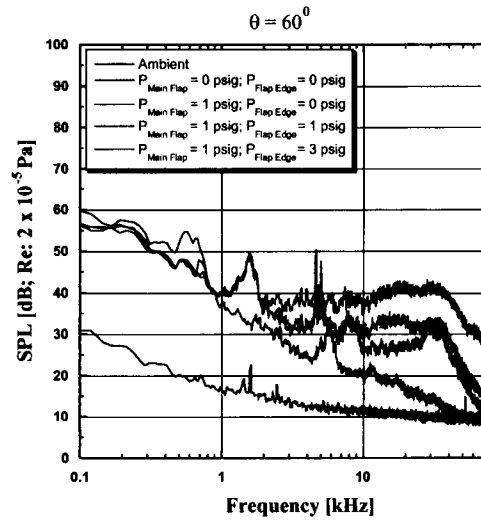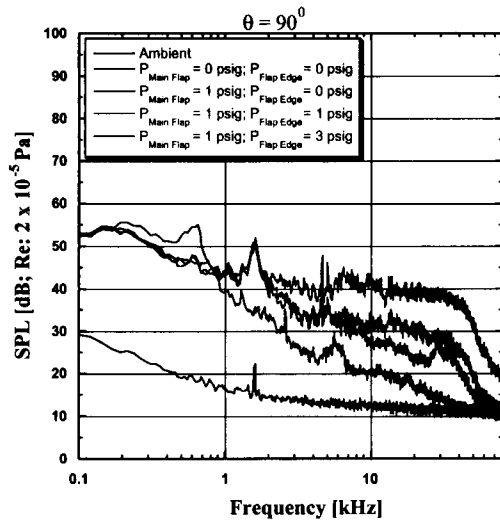Effect of Main Flap and Flap Edge Blowing ;
$$V_{Tunnel} = 100 \text{ ft/s}$$

$\theta = 90^0$

$\theta = 60^0$

$\theta = 30^0$

**Figure 7. Effect of Flap-Edge blowing on farfield noise with main flap blowing.**

Lift vortex    Tufts    Undeployed
                        Flap

2

Flap-Edge    Freestream
             Direction

1

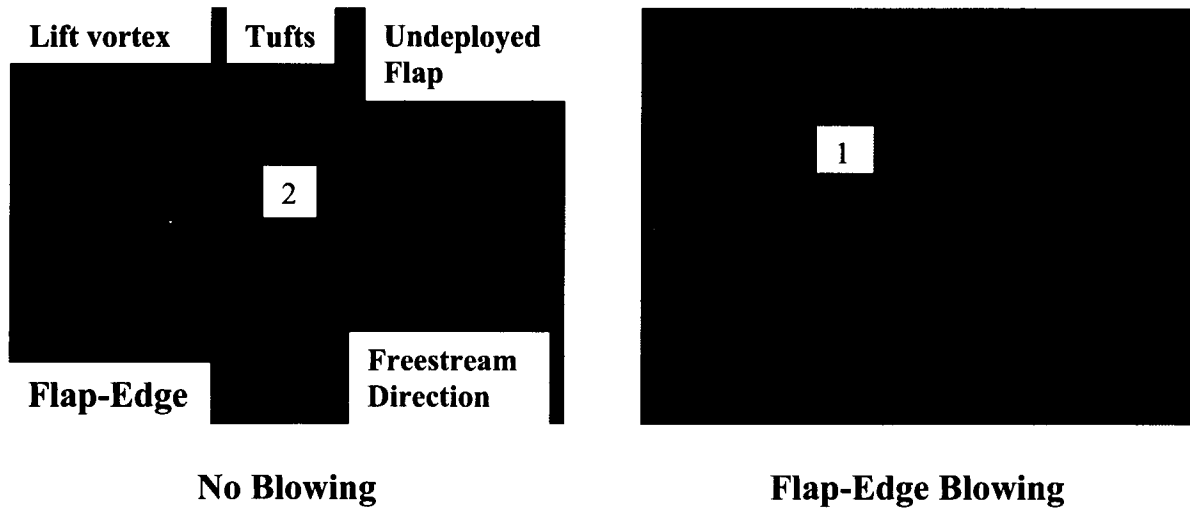**No Blowing**                **Flap-Edge Blowing**

Figure 8. Vortex moves from tuft 1 to tuft 2 on blowing from the tip of the flap edge.